Bulk Electric System Reliability Evaluation Incorporating Wind Power and Demand Side Management

A Thesis Submitted to the College of Graduate Studies and Research

In Partial Fulfillment of the Requirements

For the Degree of

Doctor of Philosophy

In the

Department of Electrical and Computer Engineering

University of Saskatchewan

Saskatoon

By

Dange Huang

PERMISSION TO USE

The author has agreed that the Libraries of the University of Saskatchewan may make this thesis freely available for inspection. The author has further agreed that permission for copying of this thesis in any manner, in whole or in part, for scholarly purposes may be granted by the professor or professors who supervised the thesis work recorded herein or, in their absence, by the Head of the Department or the Dean of the College in which the thesis work was done. It is understood that any copying or publication or use of this thesis or parts thereof for financial gain shall not be allowed without approval by the University of Saskatchewan and the author's written permission. It is also understood that due recognition shall be given to the author and to the University of Saskatchewan in any scholarly use which may be made of any material in this thesis.

Requests for permission to copy or to make other use of material in this thesis in whole or part should be addressed to:

Head of the Department of Electrical and Computer Engineering
University of Saskatchewan
Saskatoon, Saskatchewan
Canada S7N 5A9

ABSTRACT

Electric power systems are experiencing dramatic changes with respect to structure, operation and regulation and are facing increasing pressure due to environmental and societal constraints. Bulk electric system reliability is an important consideration in power system planning, design and operation particularly in the new competitive environment. A wide range of methods have been developed to perform bulk electric system reliability evaluation. Theoretically, sequential Monte Carlo simulation can include all aspects and contingencies in a power system and can be used to produce an informative set of reliability indices. It has become a practical and viable tool for large system reliability assessment technique due to the development of computing power and is used in the studies described in this thesis. The well-being approach used in this research provides the opportunity to integrate an accepted deterministic criterion into a probabilistic framework. This research work includes the investigation of important factors that impact bulk electric system adequacy evaluation and security constrained adequacy assessment using the well-being analysis framework.

Load forecast uncertainty is an important consideration in an electrical power system. This research includes load forecast uncertainty considerations in bulk electric system reliability assessment and the effects on system, load point and well-being indices and reliability index probability distributions are examined. There has been increasing worldwide interest in the utilization of wind power as a renewable energy source over the last two decades due to enhanced public awareness of the environment. Increasing penetration of wind power has significant impacts on power system reliability, and security analyses become more uncertain due to the unpredictable nature of wind power. The effects of wind power additions in generating and bulk electric system reliability assessment considering site wind speed correlations and the interactive effects of wind power and load forecast uncertainty on system reliability are examined. The

concept of the security cost associated with operating in the marginal state in the well-being framework is incorporated in the economic analyses associated with system expansion planning including wind power and load forecast uncertainty. Overall reliability cost/worth analyses including security cost concepts are applied to select an optimal wind power injection strategy in a bulk electric system. The effects of the various demand side management measures on system reliability are illustrated using the system, load point, and well-being indices, and the reliability index probability distributions. The reliability effects of demand side management procedures in a bulk electric system including wind power and load forecast uncertainty considerations are also investigated. The system reliability effects due to specific demand side management programs are quantified and examined in terms of their reliability benefits.

ACKNOWLEDGMENTS

The author would like to express her sincere gratitude and appreciation to her supervisor, Dr. Roy Billinton, for his guidance during the course of this research work. The support, encouragement, criticism, assistance and discussions during this process are highly appreciated. The author would also like to acknowledge Dr. Billinton's time, effort, patience and helpful suggestions in the preparation of this thesis. It is a great opportunity for the author to study under Dr. Billinton's guidance and what she has learned will be very helpful in her life and career in the future.

The author would like to thank the advisory committee members for their support, encouragement and suggestions throughout this research work. The author would also like to thank Wijarn Wangdee for his support during the process of modifying the RapHL-II program.

The author would also like to thank her parents, Pinlan Zhan and Jinsheng Huang, her brothers Xiaoxia and Dongyang, for their love and consistent encouragement. Appreciation also goes to all her friends, both inside and outside the Department of Electrical and Computer Engineering.

Financial assistance provided by Dr. Roy Billinton in the form of research support from the Natural Sciences and Engineering Research Council (NSERC) of Canada and by the University of Saskatchewan in the form of a Graduate Scholarship is thankfully acknowledged.

TABLE OF CONTENTS

PERMISSION TO USE i
ABSTRACT ii
ACKNOLEDGEMENTS iv
TABLE OF CONTENTS v
LIST OF TABLES viii
LIST OF FIGURES xiv
LIST OF ABBREVIATIONS xix
1. INTRODUCTION 1
1.1. Power System Reliability Evaluation 1
1.2. Bulk Electric System Reliability Evaluation 5
1.3. Scope and Objectives of the Thesis 9
2. BULK ELECTRIC SYSTEM RELIABILITY EVALUATION 12
2.1. Introduction 12
2.2. Sequential Monte Carlo Simulation 14
2.2.1. Basic Methodology 14
2.2.2. Random Variate Generation 16
2.2.3. System Analysis and Reliability Index Calculations 17
2.2.4. Stopping Rules 23
2.3. Well-being Analysis Framework 24
2.4. Existing Programs 27
2.5. Study Systems 27
2.5.1. RBTS Results 31
2.5.2. IEEE-RTS Results 33
2.6. Conclusion 36
3. EFFECTS OF LOAD FORECAST UNCERTAINTY 37
3.1. Introduction 37
3.2. Incorporating Load Forecast Uncertainty in the Simulation Process 38
3.2.1. Methodology 38
3.2.2. Modification of the HLI and RapHL-II programs 40
3.3. Effects of Load Forecast Uncertainty on HLI Reliability Evaluation 43
3.3.1. Effects on HLI system indices 43
3.3.2. Effects on HLI reliability index probability distributions 44
3.4. Effects of Load Forecast Uncertainty on HLII Reliability Evaluation 47
3.4.1. Effects on HLII system indices 47
3.4.2. Effects on HLII reliability index probability distributions 49
3.4.3. Effects of LFU with increase in the peak load 53
3.4.4. Effects of LFU on HLII load point indices 56
3.5. Effects of Bus Load Correlation on HLII Reliability Evaluation 63
3.5.1. Effects on the HLII system indices 64

3.5.2. Effects on the HLII load point indices 66
3.6. Effects of Load Forecast Uncertainty on HLII Reliability Evaluation with Different Network Configurations 71
3.6.1. Study Cases 71
3.6.2. RRBTS Results 72
3.6.3. IEEE-RTS Results 76
3.7. Conclusion 79
4. EFFECTS OF WIND POWER 81
4.1. Introduction 81
4.2. Methodology to Incorporate Wind power 82
4.2.1. Methodology 83
4.2.2. Wind speed correlation considerations 85
4.2.3. Modification of the HLI and HLII programs 86
4.3. Effects of Wind Power Additions on HLI Reliability Evaluation 87
4.3.1. Effects of wind power addition on HLI reliability indices 88
4.3.2. Increases in peak load carrying capability due to adding wind power to the RBTS 89
4.4. Effects of Wind Power on Conventional HLII Reliability Evaluation 93
4.4.1. Effects of wind speed correlation on HLII reliability evaluation 93
4.4.2. Interactive effects of wind and LFU on conventional HLII reliability evaluation 97
4.5. Effects of Wind power on the HLII Well-being Analysis Framework 103
4.5.1. Effects of wind power additions 104
4.5.2. Effects of wind power on a wind replaced conventional generating unit system in the HLII well-being analysis framework 106
4.5.3. Interactive effects of wind power and load forecast uncertainty in the well-being analysis framework 115
4.5.4. Effects of wind power in the well-being analysis framework for the IEEE-RTS 122
4.6. Planning Studies Incorporating Wind Power and Load Forecast Uncertainty 126
4.6.1. Planning studies 126
4.6.2. Reliability cost/worth studies for different system reinforcement alternatives 130
4.6.3. Reliability cost/worth study for different system reinforcement alternatives incorporating security cost 134
4.7. Conclusion 144
5. EFFECTS OF DEMAND SIDE MANAGEMENT 147
5.1. Introduction 147
5.2. Incorporating Demand Side Management in HLII Reliability Evaluation 148
5.2.1. Methodology 148
5.2.2. Programs and results 150
5.3. Effects of Peak Clipping in the Well-being Analysis Framework 156
5.3.1. RRBTS Results 156
5.3.2. IEEE-RTS Results 159
5.4. Effects of Load Shifting on the Well-being Analysis Framework 161
5.4.1. Load shifting on all buses 161
5.4.2. Effects on load carrying capability 170

5.4.3. Load shifting on the residential load sector 171
5.4.4. Interactive effects of residential load shifting and LFU 177
5.5. Effects of Off-peak Load Addition in the Well-being Analysis Framework ... 178
5.5.1. Effects of load addition on HLI reliability evaluation 178
5.5.2. Effects of load addition on HLII reliability evaluation 180
5.6. Effects of Distributed Generation in the Well-being Analysis Framework 184
5.6.1. Wind power added as distributed generation 184
5.6.2. Conventional generation added as distributed generation 191
5.6.3. Increase in the peak load 194
5.6.4. Interactive effects of distributed generation and LFU 196
5.6.5. Interactive effects of wind power and LFU considering load shifting 197
5.7. Conclusion 199
6. SUMMARY AND CONCLUSIONS 203
REFERENCES 210
APPENDIX A: BASIC SYSTEM DATA FOR THE RBTS AND THE IEEE-RTS 221
APPENDIX B: CUSTOMER SECTOR LOAD DATA 226

LIST OF TABLES

Table 2.1: The RBTS customer sector peak loads at the load buses 30
Table 2.2: The IEEE-RTS customer sector peak loads at the load buses 30
Table 2.3: The HLI system indices for the RBTS base case using the two load models 31
Table 2.4: The well-being indices for the RBTS base case at HLI using the different load models 32
Table 2.5: The HLII system and load point indices for the RBTS base case using the modified load model 32
Table 2.6: The HLII system and load point indices for the RRBTS base case using the modified load model 33
Table 2.7: The HLII well-being indices for the RRBTS base case using the modified load model 33
Table 2.8: The HLI system indices for the IEEE-RTS base case using the two load models 33
Table 2.9: The HLI well-being indices for the IEEE-RTS base case using the two load models. 34
Table 2.10: The HLII system and load point indices for the IEEE-RTS base case using the modified load model. 35
Table 2.11: The well-being indices for the IEEE-RTS base case at HLII using the modified load model. 35
Table 3.1: The HLI reliability indices for the RBTS with LFU 43
Table 3.2: The HLI reliability indices for the IEEE-RTS with LFU 44
Table 3.3: The HLII system indices for the RBTS with various LFU 47
Table 3.4: The HLII system indices for the IEEE-RTS with various LFU 48
Table 3.5: The HLI system indices for the RBTS with LFU, peak load increased by 10% 54
Table 3.6: The HLII system indices for the RBTS with LFU, peak load increased by 10% 54
Table 3.7: The HLI system indices for the IEEE-RTS with LFU, peak load increased by 10% 55
Table 3.8: The HLII system indices for the IEEE-RTS with LFU, peak load increased by10% 55
Table 3.9: Case B bus load correlation for the RBTS 64
Table 3.10: Case B bus load correlation for the IEEE-RTS 64
Table 3.11: The system indices for the RBTS Cases A, B and C with LFU 64
Table 3.12: The system indices for the IEEE-RTS Cases A, B and C with LFU 65
Table 3.13: The modified RBTS Cases 71
Table 3.14: The modified IEEE-RTS Cases 71
Table 3.15: The system indices for the RRBTS with LFU, peak load = 179.28 MW 72

Table 3.16: The increase in the system indices for the RBTS and the RRBTS with LFU, peak load =179.28 MW 72
Table 3.17: The system indices for the RRBTS with LFU, peak load = 188.24 MW 73
Table 3.18: The system indices for the RRBTS with LFU, peak load = 197.21 MW 73
Table 3.19: The system indices for RBTS Case 2 with LFU, peak load = 197.21 MW . 74
Table 3.20: The increase in the system indices for the RRBTS and RBTS Case 2 with LFU, peak load = 197.21 MW 75
Table 3.21: The system indices for RBTS Cases 3 and 4 with LFU, peak load = 215.14 MW 75
Table 3.22: The increases in the system indices for RBTS Cases 3 and 4 with LFU, peak load = 215.14 MW 76
Table 3.23: The IEEE-RTS Case 1 system indices with LFU, peak load = 4132.13 MW 77
Table 3.24: The reliability index increases for the IEEE-RTS and IEEE-RTS Case 1 with LFU, peak load = 4132.13 MW 77
Table 3.25: The IEEE-RTS Case 2 reliability indices with LFU, peak load = 4132.13 MW 78
Table 3.26: The increase in the system indices for the IEEE-RTS Cases 1 and 2 with LFU, peak load = 4132.13 MW 78
Table 4.1: The RBTS Wind Capacity Credit (CC) with sequential wind power additions based on the LOLE 91
Table 4.2: The RBTS Wind Capacity Credit (CC) with sequential wind power additions based on the LOEE 91
Table 4.3: HLII indices for the RBTSW at various wind speed correlation levels 94
Table 4.4: HLII indices for the RRBTSW with wind speed correlation 94
Table 4.5: HLII reliability indices for RRBTSW at various peak load levels 95
Table 4.6: HLII reliability indices for the RBTSW at an LFU of 5% 99
Table 4.7: Reliability indices for the RRBTS with different wind additions 104
Table 4.8:The system probability in hrs/yr of each state for the RRBTS with different wind additions 104
Table 4.9: The system frequency in occ/yr of each state for the RRBTS with different wind additions 105
Table 4.10: The average residence duration in hrs/occ of each state for the RRBTS with different wind additions 105
Table 4.11: The HLII system indices for the three study systems 107
Table 4.12: The HLII system indices for the RRBTS with changing peak loads 108
Table 4.13: The HLII system indices for the WRRBTS-1 with changing peak loads .. 108
Table 4.14: The HLII system indices for the WRRBTS-2 with changing peak loads .. 108
Table 4.15: The system probability in hrs/yr of each operating state for the different systems 110
Table 4.16: The system frequency in occ/yr of each operating state for the different systems 111
Table 4.17: The average residence duration in hrs/occ of each operating state for the different systems 111
Table 4.18: The HLII system indices for the RRBTS with LFU 115
Table 4.19: The HLII system indices for the WRRBTS-1 with LFU 116

Table 4.20: The HLII system indices for the WRRBTS-2 with LFU 116
Table 4.21: The system probability in hrs/yr of each state for the RRBTS with LFU at HLII 117
Table 4.22: The system frequency in occ/yr of each state for the RRBTS with LFU at HLII 117
Table 4.23: Average duration in hrs/occ of each state for the RRBTS with LFU at HLII 118
Table 4.24: The system probability in hrs/yr of each state for the WRRBTS-1 with LFU at HLII 118
Table 4.25: The system frequency in occ/yr of each state for the WRRBTS-1 with LFU at HLII 119
Table 4.26: The average duration in hrs/occ of each state for the WRRBTS-1 with LFU at HLII 119
Table 4.27: The system probability in hrs/yr of each state for the WRRBTS-2 with LFU at HLII 119
Table 4.28: The system frequency in occ/yr of each state for the WRRBTS-2 with LFU at HLII 119
Table 4.29: The average duration in hrs/occ of each state for the WRRBTS-2 with LFU at HLII 120
Table 4.30: The HLII system indices for the IEEE-RTS with peak load 123
Table 4.31: The HLII system indices for the IEEE-WRTS with peak load 123
Table 4.32: Well-being indices for the IEEE-RTS and IEEE-WRTS 124
Table 4.33: The system probability in hrs/yr of each state for the IEEE-RTS and the IEEE-WRTS with LFU at HLII 124
Table 4.34: The system frequency in occ/yr of each state for the IEEE-RTS and the IEEE-WRTS with LFU at HLII 125
Table 4.35: The average duration in hrs/occ of each state for the IEEE-RTS and the IEEE-WRTS with LFU at HLII 125
Table 4.36: The system indices for the IEEE-WMRTS with different wind speed correlations 127
Table 4.37: The system indices for the IEEE-WMRTS1 and IEEE-WMRTS2 with the three reinforcement alternatives 128
Table 4.38: The system indices for the IEEE-WMRTS1 and IEEE-WMRTS2 with the three reinforcement alternatives considering LFU 129
Table 4.39: The system indices for the IEEE-WMRTS with different transmission network reinforcement alternatives 132
Table 4.40: The system indices for the IEEE-WMRTS with different transmission network reinforcement alternatives considering LFU 132
Table 4.41: The ACP, ECOST and TOC for the IEEE-WMRTS cases with LFU 133
Table 4.42: The responding energy, security cost and average security cost for the RRBTS with LFU 137
Table 4.43: The responding energy, security cost and average cost for the RRBTS with various peak loads 138
Table 4.44: HLII Well-being indices for the IEEE-MRTS with LFU 138
Table 4.45: HLII Well-being indices for the IEEE-WMRTS7 Case 1 with LFU 139
Table 4.46: HLII Well-being indices for the IEEE-WMRTS7 Case 2 with LFU 139

Table 4.47: HLII Well-being indices for the IEEE-WMRTS7 Case 4 with LFU 140
Table 4.48: HLII Well-being indices for the IEEE- WMRTS8 Case 6 with LFU..... 141
Table 4.49: HLII Well-being indices for the IEEE-WMRTS8 Case 10 with LFU 141
Table 4.50: Responding energy and security cost for the IEEE-WMRTS Cases with LFU 142
Table 4.51: The ECOST, TOC and TOC+Security Cost for the IEEE-WMRTS Cases with LFU 143
Table 5.1: The DSM programs used in this research 152
Table 5.2: HLII system reliability indices for the RRBTS with peak clipping..... 156
Table 5.3: HLII system probability of each operating state for the RRBTS with peak clipping 158
Table 5.4: HLII system frequency of each operating state for the RRBTS with peak clipping 158
Table 5.5: HLII average duration of each operating state for the RRBTS with peak clipping 159
Table 5.6: HLII system reliability indices for the IEEE-RTS with peak clipping 160
Table 5.7: HLII load point indices for the IEEE-RTS with the PC80 procedure..... 160
Table 5.8: HLII system reliability indices for the RRBTS with load shifting 162
Table 5.9: HLII system probability of each operating state for the RRBTS with load shifting..... 165
Table 5.10: HLII system frequency of each operating state for the RRBTS with load shifting..... 165
Table 5.11: HLII average duration of each operating state for the RRBTS with load shifting..... 165
Table 5.12: HLII system reliability indices for the IEEE-RTS with load shifting..... 166
Table 5.13: The HLII IEEE-RTS load point indices with LS80 167
Table 5.14: HLII system probability of each operating state for the IEEE-RTS with load shifting..... 169
Table 5.15: HLII system frequency of each operating state for the IEEE-RTS with load shifting..... 169
Table 5.16: HLII average duration of each operating state for the IEEE-RTS with load shifting..... 170
Table 5.17: HLII system reliability indices for the RRBTS with load shifting applied to the residential sector..... 171
Table 5.18: The EDLC (hrs/yr) at each bus for the RRBTS with load shifting applied to the residential sector..... 172
Table 5.19: HLII system probability of each operating state for the RRBTS with load shifting applied to the residential sector..... 173
Table 5.20: HLII system frequency of each operating state for the RRBTS with load shifting applied to the residential sector. 173
Table 5.21: HLII system average duration of each operating state for the RRBTS with residential sector load shifting 173
Table 5.22: HLII system reliability indices for the IEEE-RTS with residential sector load shifting..... 174
Table 5.23: HLII load point indices for the IEEE-RTS with residential sector load shifting..... 175

Table 5.24: The IEEE-RTS system reliability indices with residential sector load shifting and LFU 177
Table 5.25: HLI system reliability indices for the RBTS with load addition 179
Table 5.26: The HLI well-being indices for the RBTS and the RBTS with LA60 179
Table 5.27: HLI system reliability indices for the IEEE-RTS with load addition 179
Table 5.28: HLI well-being indices for the IEEE-RTS with load addition 180
Table 5.29: The number of off-peak hours in a year and the added energy for the RRBTS 181
Table 5.30: HLII system reliability indices for the RRBTS with the load additions 181
Table 5.31: HLII well-being indices for the RRBTS with load addition. 182
Table 5.32: HLII system reliability indices for the IEEE-RTS with load addition. 183
Table 5.33: HLII well-being indices for the IEEE-RTS with load addition..... 183
Table 5.34: HLII system reliability indices for the RRBTS with the 20 MW of wind added at different buses and extra generation not transmitted to the BES.. 185
Table 5.35: HLII system reliability indices for the RRBTS with the 20 MW of wind power added at different buses and the extra capacity transmitted to the BES..... 186
Table 5.36: The load bus EDLC (hrs/yr) for the RRBTS with the 20 MW wind power added as distributed generation at different buses 187
Table 5.37: The load bus EENS (MWh/yr) for the RRBTS with the 20 MW wind power added as distributed generation at different buses 187
Table 5.38: The load bus EFLC (occ/yr) for the RRBTS with the 20 MW wind power added as distributed generation at different buses 188
Table 5.39: The load bus ECOST (k$/yr) for the RRBTS with the 20 MW wind power added as distributed generation at different buses 188
Table 5.40: HLII system probability of each operating state for the RRBTS with the 20 MW wind power added as distributed generation..... 189
Table 5.41: HLII system frequency of each operating state for the RRBTS with the 20 MW wind power added as distributed generation..... 189
Table 5.42: HLII average duration of each operating state for the RRBTS with the 20 MW wind power added as distributed generation..... 190
Table 5.43: HLII system reliability indices for the IEEE-RTS with the 100 MW of wind power added as distributed generation 190
Table 5.44: HLII load point indices for the IEEE-RTS with the 100 MW of wind power added as distributed generation 191
Table 5.45: HLII system reliability indices for the RRBTS with the 5 MW conventional generation added as distributed generation at different buses..... 191
Table 5.46: The load bus EDLC (hrs/yr) for the RRBTS with the 5 MW conventional..... generation added as distributed generation at different buses..... 192
Table 5.47: The load bus EENS (MWh/yr) for the RRBTS with the 5 MW conventional generation added as distributed generation at different buses..... 192
Table 5.48: HLII system indices for the RBTS with the 5 MW conventional generation added as distributed generation at different buses 193
Table 5.49: HLII load point indices for the RBTS with the 5 MW conventional generation added as distributed generation at bus #3..... 193

Table 5.50: HLII system indices for the RBTS with the 5 MW conventional generation added as distributed generation at bus #6 194
Table 5.51: HLII system reliability indices for the RRBTS with the 20 MW of wind power added at bus #3 as distributed generation considering LFU 196
Table 5.52: The load point indices for the RRBTS with the 20 MW of wind power added at bus #3 as distributed generation considering LFU 197
Table 5.53: HLII system well-being indices for the RRBTS with the 20 MW of wind ..... power added at bus #3 as distributed generation considering LFU 198
Table 5.54: HLII system reliability indices for the RRBTS with the 20 MW of wind power added at bus #3 as distributed generation considering LFU with Res-LS80 198
Table A.1: The bus data for the RBTS 221
Table A.2: The line data for the RBTS 221
Table A.3: The generating unit reliability data for the RBTS 222
Table A.4: The bus data for the IEEE-RTS 223
Table A.5: The line data for the IEEE-RTS 224
Table A.6: The generating unit reliability data for the IEEE-RTS 225
Table B.1: Weekly Residential Sector Allocation 226
Table B.2: Daily percetnage of the sector peak load for all sectors. 227
Table B.3: Hourly percentage of the sector peak load for all sectors 227
Table B.4: Hourly percentage of the sector peak load for all sectors (continued). 228

LIST OF FIGURES

Figure 1.1: Basic aspects of system reliability 2
Figure 1.2: Hierarchical levels 2
Figure 1.3: Model for system well-being analysis 5
Figure 2.1: Block diagram of the sequential Monte Carlo simulation process 15
Figure 2.2: Two state model 17
Figure 2.3: Block diagram to conduct well-being analysis using sequential Monte Carlo simulation 26
Figure 2.4: Bounded network 26
Figure 2.5: Single diagram of the RBTS 28
Figure 2.6: Single diagram of the IEEE-RTS 29
Figure 2.7: System load duration curves for the RBTS and the IEEE-RTS based on the original and modified load models 31
Figure 3.1: M intervals representation for the normal cumulative probability distribution function 38
Figure 3.2: The block diagram for incorporating LFU in the HLI program using the tabulating technique 41
Figure 3.3: The block diagram for incorporating LFU in the RapHL-II using the tabulating technique. 42
Figure 3.4: Probability distributions of the HLI LOL for the RBTS with LFU 45
Figure 3.5: Probability distributions of the LOE for the RBTS with LFU 46
Figure 3.6: Probability distributions of the FLC for the RBTS with LFU 46
Figure 3.7: Probability distributions of the LOL for the IEEE-RTS with LFU 47
Figure 3.8: Changes in the reliability indices in the HLI and HLII evaluations for the RBTS with LFU 48
Figure 3.9: Changes in the reliability indices in the HLI and HLII evaluations for the IEEE-RTS with LFU 49
Figure 3.10: Probability distributions of the DLC at HLII for the RBTS with LFU 49
Figure 3.11: Probability distributions of the ENS at HLII for the RBTS with LFU 50
Figure 3.12: Probability distributions of the FLC at HLII for the RBTS with LFU 51
Figure 3.13: Probability distributions of the DLC at HLII for the IEEE-RTS with LFU 52
Figure 3.14: Probability distributions of the ENS at HLII for the IEEE-RTS with LFU 52
Figure 3.15: Probability distributions of the FLC at HLII for the IEEE-RTS with LFU 53
Figure 3.16: Relative changes in the reliability indices in the HLI and HLII evaluations with LFU for the RBTS, peak load increased by 10% 54
Figure 3.17: Relative changes in the reliability indices in the HLI and HLII evaluations with LFU for the IEEE-RTS, peak load increased by 10% 55
Figure 3.18: Load bus indices with LFU at HLII for the RBTS using the Pass-I criterion 57
Figure 3.19: The EDLC with LFU at HLII for the RBTS using the Pass-II criterion 57

Figure 3.20: The load bus indices with LFU at HLII for the RBTS using the Priority Order criterion 58
Figure 3.21: The EDLC for the RBTS with different load shedding philosophies 59
Figure 3.22: The IEEE-RTS load bus indices with LFU at HLII using the Pass-I criterion 60
Figure 3.23: The IEEE-RTS load bus indices with LFU at HLII using the Pass-II criterion 61
Figure 3.24: The IEEE-RTS load bus indices with various LFU at HLII using the Priority Order criterion 62
Figure 3.25: The EDLC for the IEEE-RTS with LFU and different load shedding philosophies 63
Figure 3.26: The system indices for the RBTS Cases A, B and C with LFU 65
Figure 3.27: The system indices for the IEEE-RTS Cases A, B and C with LFU 66
Figure 3.28: The load bus indices for the RBTS cases with LFU, using the Pass-I criterion 67
Figure 3.29: The EDLC for the RBTS cases with LFU, using the Pass-II criterion 68
Figure 3.30: The load bus indices for the RBTS cases with LFU using the Priority Order criterion 68
Figure 3.31: The load bus indices for the IEEE-RTS Cases A, B and C, LFU=5%, using the Pass-II criterion 69
Figure 3.32: The load bus indices for the IEEE-RTS Cases A, B and C, LFU=10%, using the Pass-II criterion 70
Figure 3.33: Increase in the EDLC for the RRBTS considering LFU and bus load correlation 74
Figure 4.1: Wind turbine generator power curve 84
Figure 4.2: Block diagrams to incorporate wind power in the HLI and HLII sequential simulation program 87
Figure 4.3: The RBTS LOLE and LOEE with successive wind power additions 88
Figure 4.4: The RBTS LOEE as a function of the peak load with successive wind power additions 89
Figure 4.5: The RBTS IPLCC as a function of the added capacity based on LOLE and LOEE 90
Figure 4.6: The RBTS IPLCC as a function of the added conventional capacity based on the LOLE and LOEE 92
Figure 4.7: The ELCC based on the EDLC for the RRBTSW considering wind speed correlation 96
Figure 4.8: The ELCC based on the EFLC for the RRBTSW considering wind speed correlation 96
Figure 4.9: The system indices versus LFU for the RBTS with different wind injection options 98
Figure 4.10: The increase in the EDLC and EENS attributable to the LFU with different wind injection options 98
Figure 4.11: The ELCC based on the EDLC for the RBTSW with different wind speed correlations, LFU = 5%. 99
Figure 4.12: The ELCC based on the EENS for the RBTSW with different wind speed correlations, LFU=5% 100

Figure 4.13: The ELCC based on the EFLC for the RBTSW with different wind speed correlations, LFU = 5% 100
Figure 4.14: The ELCC based on the EDLC for the RBTSW with different wind speed correlations, LFU=10% 101
Figure 4.15: The ELCC based on the EENS for the RBTSW with different wind speed correlations, LFU=10% 101
Figure 4.16: The ELCC based on the EFLC for the RBTSW with different wind speed correlations, LFU = 10% 102
Figure 4.17: The EDLC for the RBTS with different LFU and generation unit addition options 103
Figure 4.18: The system frequency of each state for the RRBTS with different wind additions 105
Figure 4.19: The average residence duration of each state for the RRBTS with different wind additions 106
Figure 4.20: The EDLC for the RRBTS, WRRBTS-1 and WRRBTS-2 versus peak load 109
Figure 4.21: The EENS for the RRBTS, WRRBTS-1 and WRRBTS-2 versus peak load 110
Figure 4.22: The probability of the healthy state with changing peak loads for the three systems 112
Figure 4.23: The probability of the marginal state with changing peak loads for the three systems 113
Figure 4.24: The frequency of the healthy state with peak load for the three systems . 113
Figure 4.25: The frequency of the marginal state with peak load for the three systems 114
Figure 4.26: The average duration of the healthy state with peak load for the three systems 114
Figure 4.27: The average duration of the marginal state with peak load for the three systems 115
Figure 4.28: The average duration of the at risk state with peak load for the three systems 115
Figure 4.29: The system probabilities of the three operating states for the RRBTS and the WRRBTS-1 with LFU 120
Figure 4.30: The system frequencies of the three operating states for the RRBTS and the WRRBTS-1 with LFU. 121
Figure 4.31: The average durations of the three operating states for the RRBTS and the WRRBTS-1 with LFU 122
Figure 4.32: The EDLC for the IEEE-RTS and IEEE-WRTS versus peak load..... 124
Figure 4.33: The EDLC for the IEEE-WMRTS1 reinforcement alternatives with LFU 130
Figure 4.34: The DPUI for the IEEE-WMRTS1 reinforcement alternatives with LFU 130
Figure 4.35: The ECOST of the IEEE-WMRTS cases with LFU..... 133
Figure 4.36: The TOC for the IEEE-WMRTS cases with LFU 134
Figure 4.37: The TOC based on the ascending order at a LFU of 0% for the IEEE-WMRTS cases with LFU 134
Figure 4.38: The security cost for the IEEE-WMRTS cases with LFU..... 142

Figure 4.39: The TOC and TOC+Security Cost for the IEEE-WMRTS at the LFU of 0% 144
Figure 4.40: The TOC and TOC+Security Cost for the IEEE-WMRTS at the LFU of 5% 144
Figure 5.1: The process to incorporate DSM in sequential Monte Carlo simulation.... 151
Figure 5.2: A 48-hour load profile at bus #3 of the RBTS with various DSM programs 153
Figure 5.3: A 48-hour residential load profile at bus #3 of the RBTS with various DSM programs 154
Figure 5.4: A 48-hour system load profile of the RBTS with various DSM programs. 154
Figure 5.5: A 48-hour load profile at bus #18 of the IEEE-RTS with the various DSM programs..... 155
Figure 5.6: A 48-hour residential load profile at bus #18 of the IEEE-RTS with the various DSM programs 156
Figure 5.7: The load point indices for the RRBTS with peak clipping..... 157
Figure 5.8: The load point EENS for the IEEE-RTS with the various peak clipping programs..... 161
Figure 5.9: Differences in the reliability indices between peak clipping and load shifting for the RRBTS at the various pre-specified peak loads 162
Figure 5.10: The load point EDLC and EENS for the RRBTS with the application of peak clipping and load shifting at the various pre-specified peak load 163
Figure 5.11: The difference in the load point EENS in percent for the RRBTS with the application of peak clipping and load shifting 163
Figure 5.12: The DLC probability distribution for the RRBTS base case and the RRBTS with LS80 and LS90..... 164
Figure 5.13: The ENS probability distribution for the RRBTS base case and the RRBTS with LS80 and LS90..... 164
Figure 5.14: Differences in the reliability indices between peak clipping and load shifting for the IEEE-RTS at various pre-specified peak load..... 166
Figure 5.15: The load point EDLC and EENS for the IEEE-RTS with the application of peak clipping and load shifting at the various pre-specified peak loads... 167
Figure 5.16: The DLC probability distribution for the IEEE-RTS base case and the RRBTS with LS80 and LS90..... 168
Figure 5.17: The ENS probability distribution for the IEEE-RTS base case and the RRBTS with LS80 and LS90..... 168
Figure 5.18: The EDLC and EENS versus peak load for the RRBTS with load shifting 170
Figure 5.19: Decreases in the RRBTS load point EENS and ECOST with Res-LS procedures 172
Figure 5.20: The IEEE-RTS DLC distribution with residential sector load shifting 176
Figure 5.21: The IEEE-RTS ENS distribution with residential sector load shifting..... 176
Figure 5.22: The IEEE-RTS EDLC and EENS with residential sector load shifting and LFU 177
Figure 5.23: The 48-hour system load for the IEEE-RTS with load addition..... 178
Figure 5.24: The load point EDLC and EENS for the RRBTS and RRBTS with LA60 181

Figure 5.25: The load point EDLC and EENS for the IEEE-RTS and IEEE-RTS with LA60 183
Figure 5.26: The EENS for the RRBTS with 20 MW of wind power added at different buses with increase in the peak load 194
Figure 5.27: The EENS for the RRBTS with the 20 MW wind power added at different buses with increase in the peak load 195
Figure 5.28: The EENS for the RRBTS with the 20 MW wind power addition with or without Res-LS80..... 199
Figure 5.29: The ECOST for the RRBTS with the 20 MW wind power addition with or without Res-LS80..... 199

LIST OF ABBREVIATIONS

$	Dollars
AC	Alternating Current
ACP	Annual Capital Payment
AR	Auto-Regressive
ARMA	Auto-Regressive and Moving Average
BES	Bulk Electric System
CEA	Canadian Electricity Association
CG	Conventional Generation
COPT	Capacity Outage Probability Table
CTU	Combustion Turbine Unit
DC	Direct Current
DG	Distributed Generation
DLC	Duration of Load Curtailment (hrs/year)
DPUI	Delivery Point Unavailability Index (Sys.Min)
DSM	Demand Side Management
Dur{H}	Average residence duration in the healthy state (hrs/occ)
Dur{M}	Average residence duration in the marginal state (hrs/occ)
Dur{R}	Average residence duration in the at risk state (hrs/occ)
ECOST	Expected Customer Interruption Cost ($/year)
EDLC	Expected Duration of Load Curtailment (hrs/year)
EENS	Expected Energy Not Supplied (MWh/year)
EFLC	Expected Frequency of Load Curtailment (occ/year)
ELCC	Effective Load Carrying Capability
ENS	Energy Not Supplied (MWh/year)
FLC	Frequency of Load Curtailment (occ/year)
Freq{H}	Frequency of the healthy state (occ/year)
Freq{M}	Frequency of the marginal state (occ/year)
Freq{R}	Frequency of the at risk state (occ/year)
HL	Hierarchical Level
HLI	Hierarchical Level I
HLII	Hierarchical Level II
HLIII	Hierarchical Level III
hr	hour
hrs	hours
IEAR	Interrupted Energy Assessment Rate ($/kWh)

IEEE	Institute of Electrical and Electronic Engineers
IEEE-MRTS	Modified IEEE-RTS
IEEE-RTS	IEEE Reliability Test System
IEEE-WMRTS	Wind assisted IEEE-MRTS
IEEE-WRTS	Wind assisted IEEE-RTS
Int	Interruption
IPLCC	Increased Peak Load Carrying Capability
LA	Load Addition
LFU	Load Forecast Uncertainty
LM	Load Management
LOE	Loss of Energy (MWh/year)
LOEE	Loss of Energy Expectation (MWh/year)
LOL	Loss of Load (hrs/year)
LOLE	Loss of Load Expectation (hrs/year)
LOLF	Loss of Load Frequency (occ/year)
LS	Load Shifting
MA	Moving Average
MCS	Monte Carlo Simulation
MW	Megawatt
MWh	Megawatt hour
No.	Number
occ	occurrences
OPF	Optimal Power Flow
PC	Peak Clipping
PI	Performance Index
PLC	Probability of Load Curtailment (/year)
Prob{H}	Probability of the healthy state (/year)
Prob{M}	Probability of the marginal state (/year)
Prob{R}	Probability of the at risk state (/year)
RapHL-II	Reliability Analysis Program for HLII
RBTS	Roy Billinton Test System
Res-LS	Residential Load Shifting
RRBTS	Reinforced RBTS
Std. Dev.	Standard Deviation
SVC	Static VAR Compensator
sys. min	system. minutes
TOC	Total Cost
WECS	Wind Energy Conversion System
WRRBTS	Wind assisted RRBTS

WTG	Wind Turbine Generator
yr	year

CHAPTER 1

INTRODUCTION

The primary function of a power system is to supply its customers with electrical energy as economically as possible with an acceptable reliability and quality [1]. Dramatic changes are taking place throughout the world in electric power systems with respect to structure, operation and regulation. Demand for electricity continues to increase due to industrial load growth and increases in population. The infrastructure investment required to meet the increasing demand is expected to be very expensive. Electric power utilities also face increasing pressure due to environmental and societal constraints. There is increasing interest in the development and use of renewable energy sources as substitutes for more conventional energy because of their huge potential and minimum impact on the environment. In the new competitive environment, electric utilities face the challenging task of minimizing capital investments and operating and maintenance expenditures in order to hold down electricity rates while maintaining the reliability at an acceptable level.

Power system reliability is an important consideration during the planning, design and operating phases of an electric power system. Power system reliability can be improved by increasing the investment in the system. This does not mean that power systems should be designed to be as reliable as possible as the associated cost may be unacceptable. The economic and the reliability constraints are therefore often in conflict and can lead to difficult managerial decisions [2]. These issues create new concerns in power system reliability evaluation.

1.1. Power System Reliability Evaluation

Power system reliability is generally defined as the ability of a power system to adequately supply its customers. Two basic aspects of power system reliability are system adequacy and system security [2]. This division is shown in Figure 1.1.

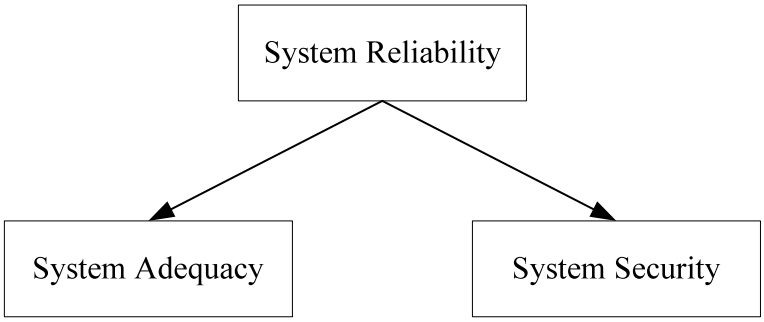

Figure 1.1: Basic aspects of system reliability

System adequacy involves the existence of sufficient facilities in the system to satisfy the customer demand. These facilities include the generating capacity required to generate enough energy and the transmission and distribution elements needed to transfer the generated energy to the customer load points. Adequacy involves static system conditions rather than system disturbances and is affected by many factors such as the installed capacity, unit sizes, unit availabilities, maintenance requirements, interconnections and so on. System security, however, concerns the ability of the system to respond to disturbances. Power systems have to maintain certain levels of static and operating reserves in order to achieve a required level of adequacy and security.

A power system consists of the three basic functional zones of generation, transmission and distribution [2] as shown in Figure 1.2.

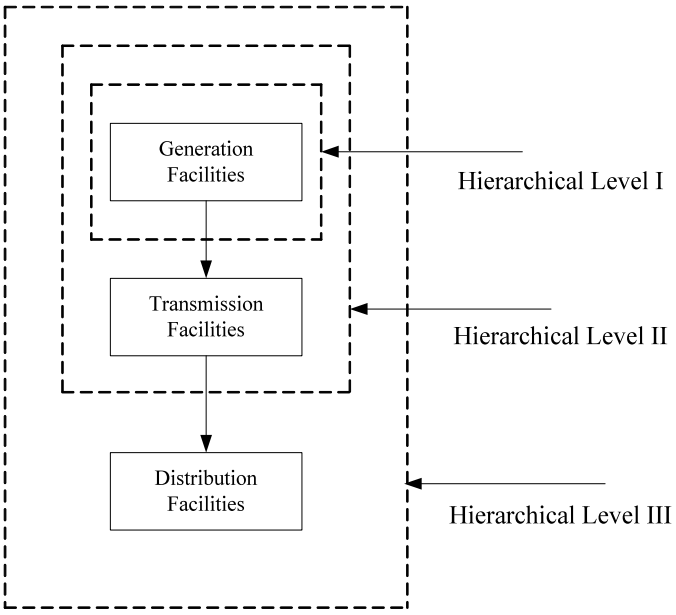

Figure 1.2: Hierarchical levels

The three functional zones shown in Figure 1.2 can be combined to form hierarchical levels. Hierarchical Level I (HLI) is concerned with only the generation facilities, while Hierarchical Level II (HLII) includes both the generation and transmission facilities and is designated as the composite generation and transmission system or bulk electric system, Hierarchical Level III (HLIII) includes all the three functional zones to provide a complete system. Studies at HLI and HLII are performed regularly. It is difficult to perform HLIII studies in an actual system due to the scale of the problem. Functional zone studies are usually performed without including the zones above them.

A considerable number of methods have been developed to perform power system reliability evaluation [3-11]. These methods can be categorized into two types, analytical techniques and simulation techniques [1, 2]. Analytical methods represent the system by mathematical models and evaluate the reliability indices using direct numerical solutions. Simulation methods estimate the reliability indices by simulating the actual process and random behavior of the system.

Both methods have their own merits and demerits. Analytical techniques can usually provide the expected index values in relatively short computation times. Assumptions are sometimes needed to simplify the problem, particularly when the system and the operating procedures are complex. Simulation methods generally require longer computing times and more computational resources, but theoretically, can include all aspects and contingencies in the power system. There is increasing interest in modeling the system behavior more comprehensively and in producing a more informative set of reliability indices. The development of increased computing power has made the use of simulation methods a practical and viable tool for large system reliability assessment.

Criteria and techniques have been developed and utilized by utilities and systems for many years [2, 12-15]. Deterministic criteria were first used in virtually all practical applications and some of them are still in use today. The deterministic criterion commonly applied is known as the N-1 approach, which requires the system to remain secure under the loss of any one generating unit or transmission line. Probability methods have also been applied in power system reliability evaluation for many years

and particularly in the area of generating system planning. The utilization of these techniques in actual transmission applications, however, is not as extensive as in the generation planning area, and most utilities utilize a deterministic approach to transmission planning. Deterministic approaches are relatively simple and direct and the results are easily interpreted by planners and operators. The essential weakness of deterministic criteria is that they do not respond to the stochastic nature of system behavior, customer demands or component failures. Probabilistic methods, on the other hand, are able to respond to the actual factors that influence the reliability of the system and some basic probabilistic criteria are now widely used by electric power utilities [1, 2]. There is growing interest in combining deterministic criteria with probabilistic assessment in an integrated approach to composite system reliability evaluation. This approach has the potential to create a bridge between the deterministic and probabilistic methods and create an effective adequacy and security assessment framework.

As noted earlier, there are two domains in composite system reliability evaluation, adequacy and security. Adequacy describes a state of a system without considering the physical entry and the departure conditions. Security is related to the dynamic process occurring during system state transitions. There are two types of security analyses, transient and steady-state. Steady state analysis, on the other hand, considers if there is a new steady-state in which the system can reside after a contingency. Most of the research in references 3-10 are related to adequacy problems. In reality, however, system transitions are fundamental in the determination of whether a state can be static or just very temporary.

A concept to address system security in the form of system operating states is formulated in [16, 17] and quantified in [18]. The total power network can be divided into the operating states of normal, alert, emergency, extreme emergency, and restorative conditions. The operating state framework is simplified in [19] and the resulting process designated as system well-being analysis. Figure 1.3 shows the simplified model for well-being analysis.

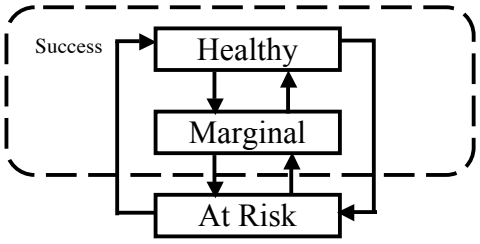

Figure 1.3: Model for system well-being analysis

The system states shown in Figure 1.3 are categorized as healthy, marginal and at risk. In the healthy state, there is sufficient generation and transmission capacity to serve the total system demand and to meet the N-1 criterion. The system is operating without violation in the marginal state, but there is not enough margin to satisfy the pre-defined deterministic criterion. In the at risk state, system operating constraints are violated and load may be curtailed.

The well-being indices related to the three operating states can be included in a composite system reliability evaluation to provide more insight on the system reliability. Those indices include the system probability, frequency and average duration of the healthy, marginal and at risk states.

Reference 20 extends the application of the well-being framework to large composite systems using a non-sequential Monte Carlo simulation method. Reference 21 incorporates steady-state, transient stability and voltage stability considerations in composite system reliability evaluation. The well-being analysis presented in [22] incorporates static security considerations based on a sequential Monte Carlo model.

This thesis is focused on HLII evaluation, which involves the determination of the total system generation required to satisfy the total load requirement and the ability of the transmission system to deliver the generated energy to the delivery points.

1.2. Bulk Electric System Reliability Evaluation

Bulk electric system or composite generation and transmission system performance depends on many factors [23] including the installed generating capacity, generating unit sizes, transmission line load carrying capabilities, switching facility arrangements, facility availabilities and system load etc. Two basic approaches used to evaluate composite system reliability are the contingency enumeration technique, which is an analytical method, and Monte Carlo simulation techniques. Monte Carlo

simulation can be categorized into non-sequential and sequential techniques [12]. AC load flow calculations are usually used to examine system deficiencies such as voltage and overload problems and to assess the effect of remedial actions. The application of analytical methods for HLII reliability evaluation appears to have been started in North America, while the application of the Monte Carlo simulation technique appears to have been started in Europe, and extended later in Brazil [13].

Considerable debate has occurred regarding the merits and demerits of the two approaches. The results in [24] indicate some of the conceptual differences in the two methods regarding modeling and problem perception in composite system reliability assessment. The major difference between the two methods is in the process of selecting states and the way the probability and system adequacy indices are evaluated. Research has also been conducted on the use of combined analytical and simulation techniques to perform evaluations [25-27]. Analytical approaches are ideally suited for composite systems with relatively limited operating constraints. In cases where large-scale composite systems are to be evaluated, or information such as index standard deviations and probability distributions in addition to the expected values are required, simulation becomes necessary. Inherent operating complications and chronological behavior make the use of sequential simulation, almost mandatory [23]. There has been a growing interest and increasing trend in applying Monte Carlo simulation to composite system reliability assessment in the last decade.

A wide range of research has been conducted on reliability assessment in composite generation and transmission systems involving generation and transmission outages, reliability equivalents, the impact of station-initiated outages and other considerations [17-42]. The two main sets of indices used to assess composite system reliability are system indices and load point indices [2, 12, 15]. The two sets of indices serve entirely different purposes and are complementary. System indices provide the power system operators and planners with information on the whole system while the load point indices provide additional insight into local system performance.

Load Forecast Uncertainty

It is an important requirement to accurately forecast the load in electric power system planning and operating. It is impossible, however, to exactly forecast the load at

some future time and therefore some degree of load forecast uncertainty will always exist. This is particularly true in the case of long range planning which looks into conditions extending over the next decade. Considerable work has been done on the incorporation of load forecast uncertainty in generating capacity adequacy evaluation [43-46]. Load forecast uncertainty can have a significant effect on the calculated reliability indices in a generating capacity study and in general it requires a higher capacity reserve to satisfy a future uncertain load than it does to meet a future known load at a specified level of reliability. The recognition of load forecast uncertainty also creates increases in the inadequacy indices in composite system reliability studies and the effect increases as the uncertainty increases [29]. The increased competition in the electric utility industry resulting from deregulation has created a need for more comprehensive risk evaluation procedures [45]. There has been relatively little work on incorporating load forecast uncertainty in HLII analyses relative to that done at HLI. The inclusion of load forecast uncertainty in bulk electric system reliability evaluation is of practical importance and it is necessary to consider both the system load forecast uncertainty and the correlation between the individual buses in security constrained adequacy assessment [29].

Load forecast uncertainty can be described by a probability distribution whose parameters can be estimated from past experience and future considerations. It is difficult to obtain sufficient historical data to determine the distribution type and the most common practice is to describe the uncertainty by a normal distribution with a given standard deviation [2]. The distribution mean is the forecast peak load. The load forecast uncertainty represented by a normal distribution can be approximated using the discrete interval method, or simulated using the tabulating technique of sampling [29]. The tabulating approach and the bus load correlation sampling technique are both utilized in this research work to incorporate load forecast uncertainty and bus load correlation in bulk electric system reliability evaluation.

Wind Power

Wind is an important energy source and is regarded as an important alternative to more traditional electric power generating sources [47]. The reliability aspects of using wind energy in electric power systems have been generally ignored in the past

because of the relatively insignificant contributions of wind power and the lack of appropriate techniques. There is an increasing interest in the development and use of wind energy as a substitute for conventional energy because of its huge potential and minimum impact on the environment for the last two decades. The initial development of wind energy technologies in the 1980's has resulted in wind turbines with high availability at a relatively low price [48]. Wind energy is one of the lowest-priced renewable energy technologies available today. The Canadian Wind Energy Association (CanWEA) has committed itself a specific target of 10,000 MW of wind power capacity by 2010, which requires an annual growth rate of 60% [49]. The installed wind capacity grew from a mere 4 MW in 1990 to 567 MW by the end of 2003 in China and it is expected to reach 5,000 MW and 20,000 MW by 2010 and 2020 respectively [50]. In India, wind energy installation was around 1340 MW as of March 31, 2001. The Indian program has a gross wind potential of around 45, 000 MW and the technical potential is estimated at 13,000 MW [51]. The increasing penetration of wind power can have significant impacts on power system reliability and cost [52]. The variation in wind speeds and the nonlinear relationship between wind turbine generator power output and the wind velocity can create considerable variability in system reliability performance that is quite different from that due to conventional energy sources. A large number of studies incorporating wind power or load forecast uncertainty in generating system reliability evaluation (HLI) assessment have been conducted. Relatively little work has been done on composite generation and transmission system (HLII) reliability assessment incorporating wind power and particularly using the well-being framework. Wind power considerations in the HLII well-being analysis framework are a major area of study in the research described in this thesis.

Demand Side Management

Demand side management (DSM) refers to initiatives that can be implemented by an electric power utility to encourage consumers to adopt energy efficient practices that are beneficial from both customer and system viewpoints [53-63]. DSM initiatives are utility sponsored programs to influence the amount or timing of customer energy use and modify the total system load curve. These initiatives involve the joint control of electricity supply and electrical demand. Demand side management includes a wide

range of techniques and objectives, one of which is load shaping or management (LM). A variety of LM techniques such as peak clipping, valley filling, load shifting, energy conservation, etc, have been proposed and studied. DSM activities are beneficial to utilities, electric customers and society [56, 63-69] in that these initiatives can improve power system reliability and reduce network congestion, maintenance and equipment replacement costs, delay the need for generation, transmission and distribution upgrading, reduce customers' electricity bills and air pollution, and greenhouse gas emissions.

The demand for electricity is generally increasing throughout the world, including both the developing and developed countries, due to industrial load growth and increases in population. The International Energy Agency forecasts that the electricity demand throughout the world in 2030 will be over 50% higher than the current demand [70]. The infrastructure investment required to meet the increasing demand is going to be very expensive. Power utilities are also faced with an increasing awareness of environment conditions [53, 54, 64]. It is expected that existing and new DSM programs will therefore play an important practical role in meeting the challenges faced by electric power utility companies.

The results in [53-56] show that DSM programs can have considerable reliability and economic impacts on electric power systems. References 53-70 cover a wide range of issues and applications. The research described in this thesis show that both the system and load point reliability indices can be impacted and improved by implementing DSM activities and that these improvements can be quantified using a probabilistic approach.

1.3. Scope and Objectives of the Thesis

This research work is an investigation of important factors that impact bulk electric system adequacy evaluation and security constrained adequacy assessment using the well-being analysis framework. The sequential Monte Carlo simulation method was utilized to conduct the research in the following main areas.

1. An examination of the effects of load forecast uncertainty on system and load point reliability indices, adequacy index probability distributions in adequacy evaluation

and well-being analysis of bulk electric systems.

2. An examination of the impacts on reliability indices and reliability cost/worth assessment in the HLII security constrained framework due to wind power injections in a bulk electric system.
3. A detailed investigation of the effects on system reliability and reliability worth of demand-side management programs using HLII adequacy evaluation and well-being analysis.

The basic concepts of the sequential Monte Carlo simulation technique utilized in this research are discussed in Chapter 2 together with the system reliability indices produced using this approach. The concept of well-being analysis is also introduced. The two study systems used throughout the thesis are introduced together with a set of base case load point and system reliability indices for each test system.

Chapter 3 introduces the tabulating and sampling methods used to incorporate load forecast uncertainty in bulk electric system reliability evaluation. A range of load forecast uncertainty levels and bus load correlation are considered. The system reliability indices, load point indices and system well-being indices are used to examine the effects of load forecast uncertainty. The resulting reliability index probability distributions are also studied in this chapter.

The method used to incorporate wind power in the simulation process is presented in Chapter 4. The impacts of wind power additions on bulk electric system reliability evaluation in the well-being framework are shown. The effects of wind site speed correlation and the impacts of wind power at different peak load levels are illustrated. The system reliability indices, load point indices, well-being indices and system load carrying capability under different wind power conditions are presented. The interactive effects on the system reliability of load forecast uncertainty and wind power are also investigated. Planning studies incorporating wind power are presented in this chapter. Security cost, which is related to the marginal state in the well-being

analysis is introduced. Overall reliability cost/worth including marginal cost concepts are applied to select an optimal wind power injection strategy in a bulk electric system.

The inclusion of demand side management in the sequential Monte Carlo simulation is described in Chapter 5. Different demand side management programs such as peak clipping, load shifting, valley filling and distributed generation are considered. Various DSM programs are applied to all buses, one bus or one customer load sector. The reliability impacts are shown using system indices, load point indices and well-being indices. Wind power and conventional generation are used as distributed generation.

Chapter 6 presents a summary and the conclusions.

CHAPTER 2

BULK ELECTRIC SYSTEM RELIABILITY EVALUATION

2.1. Introduction

A wide range of research work has been done on generating capacity adequacy assessment (HLI). Relatively little work has been done on composite generation and transmission system reliability evaluation (HLII). There are considerable differences in the techniques and procedures used in generating capacity adequacy assessment and composite system reliability evaluation. The ability of the transmission network to deliver the generated energy is an important consideration in bulk electric system reliability evaluation and its analysis involves load flow calculations, emergency state selections, overload alleviation, generation rescheduling, load shedding policy, etc. The analyses at HLII are more complicated than at HLI.

Two basic techniques are used in power system reliability evaluation and can be generally designated as analytical and simulation methods. The state enumeration method is a widely used analytical method in bulk electric system reliability evaluation. The general approach is to list all contingencies up to a given order, usually the second order, and then calculate the reliability indices from the probabilities of the contingencies [2, 12]. Simulation is a more sophisticated procedure that treats the problem as a series of experiments [2, 12, 27]. The simulation techniques used in reliability evaluation are loosely referred to as Monte Carlo simulation (MCS). In this approach, component states are simulated and analyzed to determine the system state, which is then considered in terms of its ability to serve the required load. The simulation is conducted over a long period of time. The Monte Carlo simulation technique can be divided into the two categories of non-sequential and sequential Monte Carlo simulation. The most basic non-sequential technique is the state sampling approach, in which each component state is determined by sampling the probability that the component exists in that state [2, 12]. A system state is an aggregation of all the

component states. The state duration sampling approach, which is sequential MCS, is based on the probability distributions of the component state durations. A chronological component operating history for all the components in the system is simulated and the chronological system operating history is created by aggregating the state transition processes of all the components.

There are advantages and disadvantages in each method. The advantage of the state enumeration technique is that it is relatively simple and it gives the same results every time. A disadvantage in using the state enumeration method is that the higher order contingencies not included in the evaluation can have a non-negligible contribution to the system reliability [28]. It is also difficult to accurately estimate the required frequency and duration indices as this involves recognition of the transitions between the no load curtailment states and the failure states [30, 36, 37]. The state sampling MCS technique is relatively simple compared to the state duration sampling approach as it only needs to generate uniformly distributed random numbers between [0, 1] to represent the component states and it is not necessary to sample a distribution function. The basic required reliability data to perform an evaluation are the component state probabilities. The process can be used to sample not only component failure states but also other power system reliability parameters such as load data, weather states, hydrological conditions, etc. One main disadvantage is that it cannot provide an accurate estimate of the system failure frequency index.

The advantages of sequential MCS are that frequency indices can be easily calculated, any kind of state duration distribution can be considered and reliability index probability distributions can be obtained in addition to the expected index values. Sequential MCS can incorporate a wide range of relevant factors in composite generation and transmission system reliability evaluation. The main disadvantages of sequential Monte Carlo simulation are that it requires more computation time and storage compared to the state sampling approach and requires more reliability data.

These methods have complementary features. Some research work has been conducted on developing hybrid techniques which combine the state enumeration method with Monte Carlo simulation techniques in order to reduce the number of

simulation samples while still utilizing the flexibility of the simulation technique [25-27, 40-41].

Simulation techniques are generally considered to be more attractive compared to enumeration methods for large scale power system reliability studies [71, 72]. There has been an increasing interest in using sequential Monte Carlo simulation over the last two decades. The research conducted on this thesis uses sequential Monte Carlo simulation to perform bulk electric system reliability evaluation. The process of sequential Monte Carlo simulation is described in detail in this chapter. Well-being analysis is used as a basic reliability framework in this thesis. The concepts and process used to perform well-being analysis in bulk electric system reliability evaluation are also described in this chapter.

Two existing programs using sequential Monte Carlo simulation for HLI [73] and HII [22] reliability evaluation were modified and extended to incorporate factors that are examined in this thesis. These two programs were applied to two study systems. The calculated reliability indices for these base case studies are shown in this chapter and used as reference values in the following chapters.

2.2. Sequential Monte Carlo Simulation

2.2.1. Basic Methodology

The basic procedure of applying sequential Monte Carlo simulation in composite generation and transmission system reliability evaluation [2, 12] is as follows.

Step 1: Specify the initial state of each component (including all generating unit and transmission lines) in the study system. It is assumed that all components are initially in a successful state.

Step 2: Sample the duration of each component residing in its present state using the relevant probability distribution. The inverse transform method described in detail in Section 2.2.2 is applied in the developed simulation program.

Step 3: Repeat Step 2 in a given time span, usually a one year period, for all components and record the chronological state transition process of each component. The chronological system state transition history in the given time span is created using the component histories.

Step 4: Conduct system analysis for each system state in the given time period and calculate the required reliability indices. This is described in detail in Section 2.2.3.

Step 5: Check to see if the coefficient of variation of a designated reliability index is less than a pre-specified tolerance value. If so, then the simulation is considered to have converged, otherwise repeat Step 2 to 5. The stopping criterion and the calculation of the coefficient of variation are discussed in Section 2.2.4.

The block diagram of the simulation process is shown in Figure 2.1.

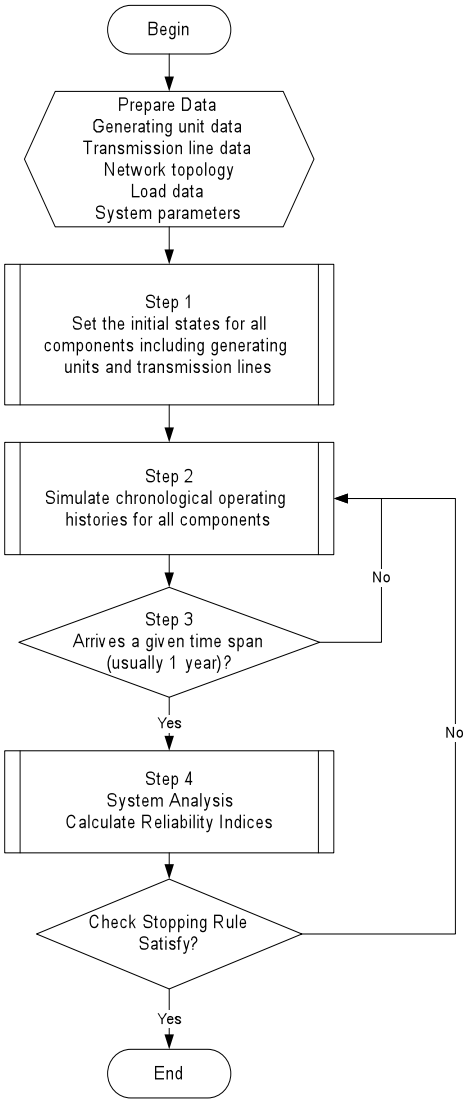

Figure 2.1: Block diagram of the sequential Monte Carlo simulation process

A block diagram of the HLI reliability evaluation process using sequential Monte Carlo simulation is shown in [73]. The basic sequential simulation processes for HLI and HLII assessment are similar. The difference is mainly in Step 4, where the

system analysis for HLII is much more complicated due to the addition of the transmission network and the required load flow calculations. The analysis at HLI only compares the total generation with the total load at each time interval.

2.2.2. Random Variate Generation

A random variate is a random variable that follows a given distribution. Usually the development software environment includes a random number generator that can generate a random variate uniformly distributed between [0, 1]. The procedure used to generate a random variate using the inverse transform method is as follows [12, 74]:

Step 1: Generate a uniformly distributed random number U between [0,1].

Step 2: Calculate the random variate X which has the cumulative probability distribution function F(x) using

$$X = F^{-1}(U) \tag{2.1}$$

Given that the variate X follows an exponential distribution, the probability density function for the exponential distribution is,

$$f(x) = \lambda e^{-\lambda x} \tag{2.2}$$

where $\frac{1}{\lambda}$ is the mean value of the distribution. The cumulative probability distribution function is:

$$F(x) = 1 - e^{-\lambda x} \tag{2.3}$$

Using the inverse transform method:

$$U = F(x) = 1 - e^{-\lambda x}$$

$$X = F^{-1}(U) = -\frac{1}{\lambda}\ln(1-U) = -\frac{1}{\lambda}\ln(U) \tag{2.4}$$

U is a uniformly distributed random number and therefore (1-U) distributes uniformly in the same way as U in the interval [0,1].

Figure 2.2 shows a basic two state component representation. When the component is in the up state (success state), the sample duration at this state is $T = -\frac{1}{\lambda}\ln(U)$, where λ is the failure rate. When the component is in the down state (failure state), the sample duration is $T = -\frac{1}{\mu}\ln(U)$, where μ is the repair rate. The

operating history of each component in the system can be created using a series of samples.

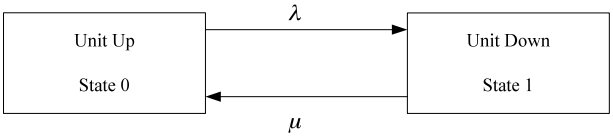

Figure 2.2: Two state model

2.2.3. System Analysis and Reliability Index Calculations

System analysis is required to examine the conditions in each sampled system state and to determine whether loads need to be curtailed to satisfy operating constraints. Various techniques can be used to perform the required load flow calculations. The three basic techniques are the network flow method [75, 76], the DC load flow method [77, 78] and the AC load flow method [78-80]. It is important to select an appropriate technique to meet the designated objectives of the analysis.

Load Flow Calculation

The network flow method is one of the simplest techniques and looks at the system as a transportation model. It is based on the movement of a particular commodity from a number of sources to a number of demand centers. The network flow model maintains the power balance of each bus of the network but does not satisfy Kirchhoff's Law. The DC load flow method is an approximate technique, which estimates the line power flows without considering the bus voltages and the generating unit reactive power limits. It is a simple and fast technique. Both the network flow method and the DC load flow method have been used in bulk system reliability evaluation.

More accurate AC load flow techniques are required when voltage levels and generating unit MVar limits are to be considered. Two basic AC load flow techniques are the Newton-Raphson and Gauss-Seidel methods. These two basic techniques require large computer storage and are computationally expensive. A load flow calculation must be performed at each hourly time interval when the chronological hourly load model is used in an HLII reliability evaluation. The Newton-Raphson approach has been modified [80, 81] to provide a fast AC load flow technique. The fast decoupled AC load flow technique is used in this thesis to perform load flow calculations because it is a

good compromise between the basic AC and DC load flow techniques in regard to storage requirements and computation time. It can be used to check the continuity of a power system and important power flow requirements involving reactive power and voltage constraints. The fast decoupled load flow technique is briefly described in the following.

The general equation for the power system mismatch at all system buses except the swing bus can be obtained using the Newton-Raphson load flow technique [81]. The fast decoupled load flow technique neglects the weak coupling between the changes in real power and voltage magnitude, and the changes in reactive power and phase angle. Equations (2.5) and (2.6) express the mismatches of active power and reactive power.

$$[\Delta P] = [J_\delta][\Delta\delta] \tag{2.5}$$

$$[\Delta Q] = [J_v][\Delta V / V] \tag{2.6}$$

where: ΔP_i is the active power mismatch at Bus i,

ΔQ_i is the reactive power mismatch at Bus i,

$\Delta\delta_i$ is the increment in phase angle of the voltage at Bus i,

ΔV_i is the increment in magnitude of the voltage at Bus i,

J_δ, J_v are the substances of the Jocobian matrix [81],

δ_i is the phase angle of the voltage at bus i,

V_i is the magnitude of the voltage at bus i.

These two equations can be further simplified as shown in (2.7) and (2.8).

$$[\Delta P / V] = [B'][\Delta\delta] \tag{2.7}$$

$$[\Delta Q / V] = [B''][\Delta V] \tag{2.8}$$

This simplification is based on the following assumptions, which are normally valid in a practical power system.

$$Cos(\delta_i - \delta_j) \approx 1.0$$

$$g_{ij} \times \sin(\delta_i - \delta_j) << b_{ij}$$

$$Q_i << b_{ij} \times V_i^2$$

where: $(g_{ij} - j b_{ij})$ is the series admittance of the line connecting Buses i and j,

Q_i is the reactive power at Bus i.

The matrices [B'] and [B''] in (2.7) and (2.8) are real, sparse and contain only network admittances. They only need to be inverted or factorized once at the beginning of the iterative process. The voltage magnitude at each load bus and the phase angle at each bus except the swing bus are modified in each iteration as shown in (2.9) and (2.10).

$$[\delta]_{new} = [\delta]_{old} + [\Delta\delta] \tag{2.9}$$

$$[V]_{new} = [V]_{old} + [\Delta V] \tag{2.10}$$

The power mismatches ΔP and ΔQ are calculated for each new value of bus angle and bus voltage. Equations (2.7) and (2.8) are iterated until the power mismatches are less than the pre-specified tolerance. In the case of transmission or transformer outages, the Sherman-Morrison correction formula [82] is used to reflect the outages without rebuilding the matrices [B'] and [B''].

The changes in the voltage magnitude are neglected in a DC load flow method. The linear model in Equation (2.11) is used to calculate the voltage phase angle.

$$[P] = [B'][\delta] \tag{2.11}$$

where: [P] is the vector of bus power injection,

[B'] is the system susceptance matrix,

$[\delta]$ is the vector of voltage phase angle in radians.

The calculated voltage phase angles can be used to determine the power flow in each transmission line or transformer.

$$P_{ij} = \frac{\delta_i - \delta_j}{X_{ij}} \tag{2.12}$$

where: P_{ij} is the real power flowing from Bus i to Bus j,

δ_i, δ_j are the phase angles at Bus i and Bus j respectively,

X_{ij} is the reactance of the line between Bus i and Bus j.

Voltage and reactive power constraints and transmission line losses cannot be calculated using the DC load flow method. This method is, however, fast and free of convergence problems. This method is used when the fast decoupled load flow technique is not able to converge under infrequent ill-conditioned network situations.

Operating Constraints

The operating constraints including voltage magnitude constraints, branch flow constraints, real power generation constraints and reactive power generation constraints are examined. All operating constraints need to be satisfied for normal operation of a bulk electric system. The operating constraints considered in this research are as follows [12]:

Voltage magnitude constraints: $V^{\min} \le V \le V^{\max}$, where $V^{\min}$ and $V^{\max}$ represent the minimum and maximum voltage limits respectively.

Branch flow constraints: $|T| \le T^{\max}$, where T is the power flow on a branch, $T^{\max}$ is the maximum capacity limit of a transmission line or a transformer.

Real power (MW) generation constraints: $P^{\min} \le P \le P^{\max}$, where $P^{\min}$ and $P^{\max}$ represent the minimum and maximum power generation at each generator bus respectively.

Reactive power (MVar) generation constraints: $Q^{\min} \le Q \le Q^{\max}$, where $Q^{\min}$ and $Q^{\max}$ represent the minimum and maximum reactive power generation at each generator bus respectively.

When any constraint is violated, corrective actions must be taken to alleviate the situation and to restore the system to normal operation.

Corrective Actions

The corrective actions normally included in bulk system assessment include [12, 79, 83, 84] generation rescheduling when there is not sufficient capacity in the system, alleviation of transmission line overloads, correction of MVar limit violations and voltage problems, bus isolation and system splitting and load curtailment.

An optimal power flow (OPF) approach is used to conduct corrective action to alleviate operating constraints. A linear programming model used for load curtailment, generation rescheduling, voltage adjustment and reactive load curtailment is described in [12, 22]. A dual simplex algorithm [85, 86] is used for generation rescheduling and to minimize load curtailment. A primal simplex algorithm [85, 87] is used for voltage adjustment and reactive load curtailment. When the system network configuration changes due to outages of lines or transformers, the network may be split into two or more smaller networks. An approximate technique used in this research to solve split

network situations represents the outaged lines as lines in service with infinite impedance and very low power flow capacity. The power flow through these lines will be very small due to the high impedances. In the case of an ill-conditioned network, caused by line or transformer outages, the AC load flow method may not converge due to high values of mismatch in the reactive power that exceed the permissible tolerance limit. The DC load flow method is used to resolve the operating constraints under these circumstances. Load must be curtailed when the operating constraints are still violated after all possible corrective actions have been taken.

Load Shedding Policies

A wide range of load shedding policies can be formulated to meet different requirements. The three policies adopted in this thesis are designated as the Pass-I, Pass-II and Priority Order policies [22]. In the Pass-I approach, loads are curtailed at the delivery points that are closest to (or one line away from) the element(s) on outage. This policy minimizes the number of delivery points affected by a specific event. The Pass-II policy is an extension of the Pass-I policy. Loads are curtailed at the delivery points which are one line away and two lines away from the outaged element. Interruptible loads at the delivery points that are one line away are curtailed first, and if not enough, followed by those at the delivery points that are two lines away. The firm loads at the delivery points one line away from the outaged element are only curtailed when the interruptible load curtailments at the delivery points one line away and two lines away are not sufficient to meet the operating constraints. The Priority Order policy is based on a reliability worth index such as the Interrupted Energy Assessment Rate (IEAR) in $/kWh [2]. The delivery points with lower IEAR values will be curtailed first.

Reliability Index Calculations

Adequacy indices are calculated when load curtailments occur. The load point and system indices are calculated as follows [2, 12].

HLII Load Point Indices

Expected Duration of Load Curtailment (EDLC) at Bus k:

$$EDLC_k = \frac{\sum_{i=1}^{NS}\left(\sum_{j=1}^{N_{i,k}} d_{j,i,k}\right)}{NS} \qquad (hours/year) \tag{2.13}$$

where: $N_{i,k}$ = Number of interruptions occurring in year i, at Bus k,

$d_{j,i,k}$ = Duration of the j^{th} interruption (hours) in year i at Bus k,

NS = Number of simulation years.

Probability of Load Curtailment (PLC) at Bus k:

$$PLC_k = \frac{EDLC_k}{8760} \qquad (/year) \tag{2.14}$$

Expected Frequency of Load Curtailment (EFLC) at Bus k:

$$EFLC_k = \frac{\sum_{i=1}^{NS} N_{i,k}}{NS} \qquad (occurrences/year) \tag{2.15}$$

Expected Energy Not Supplied (EENS) at Bus k:

$$EENS_k = \frac{\sum_{i=1}^{NS}\left(\sum_{j=1}^{N_{i,k}} BusENS_{j,i,k}\right)}{NS} \qquad (MWh/year) \tag{2.16}$$

where $BusENS_{j,i,k}$ = Energy not supplied in MWh for the j^{th} interruption, in year i at Bus k.

HLII System Indices

Expected Duration of Load Curtailment (EDLC) for the overall system:

$$EDLC = \frac{\sum_{i=1}^{NS}\left(\sum_{j=1}^{N_i} d_{j,i}\right)}{NS} \qquad (hrs/year) \tag{2.17}$$

where: N_i = Number of interruptions occurring in year i for the system,

$d_{j,i}$ = Duration of the j^{th} interruption (hours) in year i for the system.

Probability of Load Curtailment (PLC) for the system:

$$PLC = \frac{EDLC}{8760} \qquad (/year) \tag{2.18}$$

Expected Frequency of Load Curtailment (EFLC) for the system:

$$EFLC = \frac{\sum_{i=1}^{NS} N_i}{NS} \qquad (occ/year) \tag{2.19}$$

Expected Energy Not Supplied (EENS) for the system:

$$EENS = \frac{\sum_{i=1}^{NS}\left(\sum_{j=1}^{N_i} SysENS_{j,i}\right)}{NS} \qquad (MWh/year) \tag{2.20}$$

where $SysENS_{j,i}$ = Energy not supplied in MWh for the j^{th} interruption, in year i for the system.

Delivery Point Unavailability Index (DPUI) is a measure of overall bulk electric system performance in terms of a composite index of unavailability in System Minutes (sys. min).

$$DPUI = \frac{Total\ Unsupplied\ Energy\ (MW\ -\ minutes)}{System\ Peak\ Load\ (MW)} \tag{2.21}$$

HLI Reliability Indices

Similar HLI reliability indices used and calculated in this thesis are as follows.

Loss of Load Expectation (LOLE):

$$LOLE = \frac{\sum_{i=1}^{N} LLD_i}{N} \qquad (hrs/year) \tag{2.22}$$

The unit of the LOLE depends on the load model used. If the daily peaks are used, the unit is days/yr. If the hourly values are used, the unit is hrs/yr.

$$LOEE = \frac{\sum_{i=1}^{N} ENS_i}{N} \qquad (MWh/year) \tag{2.23}$$

$$LOLF = \frac{\sum_{i=1}^{N} LLO_i}{N} \qquad (occ/year) \tag{2.24}$$

Where N is the total number of sampling years, LLD_i, ENS_i, LLO_i respectively are the loss of load duration, energy not supplied and loss of load occurrence for sampling year i.

2.2.4. Stopping Rules

Stopping rules are used to decide when to stop a simulation. The objective of a stopping rule is to facilitate a compromise between accuracy and computation time.

Two stopping rules:

Rule 1: The simulation stops when the coefficient of the variation is less than a specified tolerance value.

Rule 2: The simulation stops at a specified number of sampling years.

The coefficient of variation of an index is:

$$\alpha = \frac{s}{E(x)\sqrt{N}} \tag{2.25}$$

E(x) is the expected value of an index.

s is the standard deviation of the index.

The index with the slowest speed of convergence should be used as the convergence criterion when multiple indices are determined. The EENS index normally has the lowest rate of convergence and the coefficient of variation of the EENS is used as the convergence criterion in this research.

2.3. Well-being Analysis Framework

Probability methods have been applied in power system reliability evaluation for many years and particularly in the area of generating system planning. The utilization of these techniques in actual transmission system applications, however, is not as extensive as in the generation planning area, and most utilities utilize a deterministic approach to transmission planning. Deterministic approaches are relatively simple and direct and the results are easily interpreted by planners and operators. The deterministic criterion commonly applied is known as the N-1 approach, which requires the system to remain secure under the loss of any one generating unit or transmission line. Deterministic approaches are not consistent [89] and do not provide an accurate basis for comparing alternative equipment configurations and performing economic analyses. There is growing interest in combining deterministic criteria with probabilistic assessment in an integrated approach to composite system reliability evaluation [89-91]. This approach

has the potential to create a bridge between the deterministic and probabilistic methods and create an effective adequacy and security assessment framework.

The N-1 concept is used as the deterministic criterion in the well-being analysis described in this thesis. The system is divided into three states as shown in Figure 1.3. The well-being indices include the probabilities, frequencies and average durations of the healthy, marginal and at risk states [22].

Prob{H} = Probability of the healthy state (/year)

Prob{M} = Probability of the marginal state (/year)

Prob{R} = Probability of the at risk state (/year)

Freq{H} = Frequency of the healthy state (occ/year)

Freq{M} = Frequency of the marginal state (occ/year)

Freq{R} = Frequency of the at risk state (occ/year)

Dur{H} = Average residence duration in the healthy state (hrs/occ)

Dur{M} = Average residence duration in the marginal state (hrs/occ)

Dur{R} = Average residence duration in the at risk state (hrs/occ)

The average duration of each operating state can be calculated by dividing the probability by the frequency of each state.

The at risk state in a well-being analysis is simply designated as the risk state in conventional bulk system reliability assessment. The at risk state probability and frequency are the same as the system PLC and EFLC calculated in a conventional assessment. The basic sequential simulation process to conduct well-being analysis is shown in Figure 2.3.

In order to satisfy the N-1 criterion, each component must be removed and the system examined to see if it meets the operating constraints. This is very time consuming especially for a large power system. A contingency selection process embedded in the well-being analysis is used to reduce the number of outaged components to be considered and to speed up the simulation.

In the case of generation facilities, the largest generating unit in each generating station is selected. The selection procedure for transmission elements is as follows.

Step 1: Transmission facilities are ranked using a scalar performance index (PI) [86] that measures how much a transmission component failure might affect the system.

Step 2: During each simulation hour, a bounding technique [86, 91] is used to select critical components to add to the contingency list. The basic principle is that transmission network outages tend to have a local effect. As shown in Figure 2.4, if a line between buses m and n fails, the lines connected to buses m and n, lines # 1-4 in this case, are added to the contingency list.

Step 3: Add the most critical transmission components to the contingency list according to the calculated PI values in Step 2, if they are not yet included.

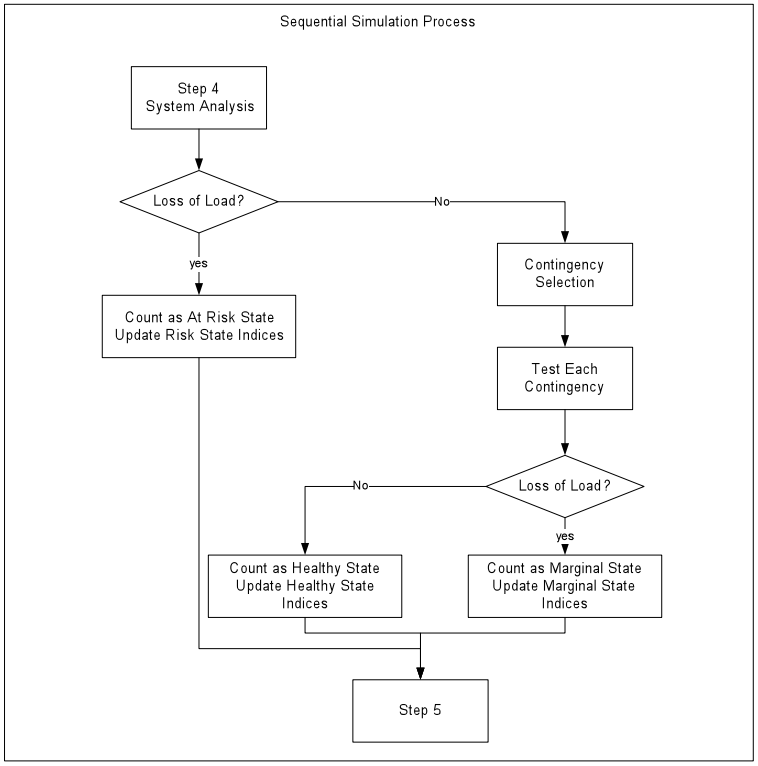

Figure 2.3: Block diagram to conduct well-being analysis using sequential Monte Carlo simulation

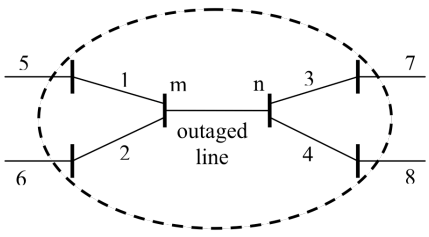

Figure 2.4: Bounded network

The system can then be examined by removing one component at a time in the contingency list and see if the system is able to supply the load at each simulation hour.

In HLI reliability evaluation, the procedure used to incorporate well-being analysis is to check if the total system capacity is able to satisfy the total system load and the required operating reserve with the removal of the largest unit at each time interval when there is no actual loss of load in the simulation process.

2.4. Existing Programs

Two existing programs developed to conduct HLI and HLII reliability evaluations were used in this research. Both programs use sequential Monte Carlo simulation as stated in Section 2.2.

The HLI program [73] was first developed using Visual C++ .Net 2003 to perform generating capacity adequacy evaluation including factors such as generating unit derated states, various state residence time distributions, peaking unit considerations and so on. The program was extended to incorporate the concept of well-being analysis, as stated in Section 2.3. The HLI program can accommodate different load models such as a daily peak load model, and constant load or hourly load model. The hourly load model is used throughout this thesis.

The HLII program now designated as RapHL-II was first developed by A. Jonnavithula [42] utilizing Fortran. The chronological load model is utilized in the program. It was then modified and extended by W. Wangdee [22] to include wind power and well-being analysis separately. The program was further modified in the research described in this thesis to include load forecast uncertainty, wind power and demand side management combining well-being analysis. The incorporations of these factors are described in the following chapters.

The two programs are the basic tools used to conduct the studies in this research work. The results obtained using these two programs for the two study system base cases are shown in Section 2.5.

2.5. Study Systems

Two study systems are used in this thesis. The Roy Billinton Test System (RBTS) is a small test system [92]. It is a six-bus system with nine transmission lines

and a total installed capacity of 240 MW in eleven generating units. The system peak load is 185 MW. The other system is the IEEE-Reliability Test System (IEEE-RTS) [93]. It is a twenty-four-bus system with thirty-eight transmission lines and a total installed capacity of 3405 MW in thirty-two generating units. The basic system data for the two study systems are shown in Appendix A. The original load model for both the RBTS and the IEEE-RTS is given in [93]. This model formulation can be used to create the annual load profile on an hourly basis for a given peak load. This load representation is designated as the Original Load Model in this research.

The single diagram of the RBTS is shown in Figure 2.5.

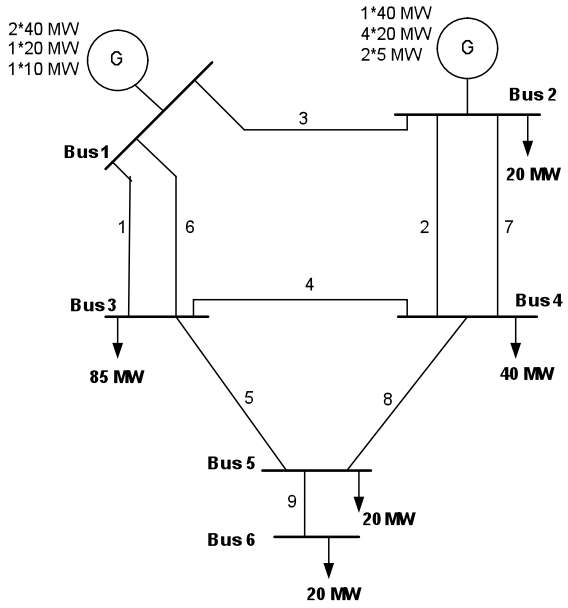

Figure 2.5: Single diagram of the RBTS

It is noticeable in Figure 2.5 that there is only one transmission line between buses 5 and 6 and the load at bus 6 will lose power supply when transmission line 9 fails. In this case, the RBTS is not able to satisfy the N-1 criterion. The RBTS was reinforced by adding a transmission line (#10) between buses 5 and 6 and the reinforced system is designated as the RRBTS.

The IEEE-RTS is a transmission strong system and the generation is mainly in the northern part of the system. The single diagram of the IEEE-RTS is shown in Figure 2.6.

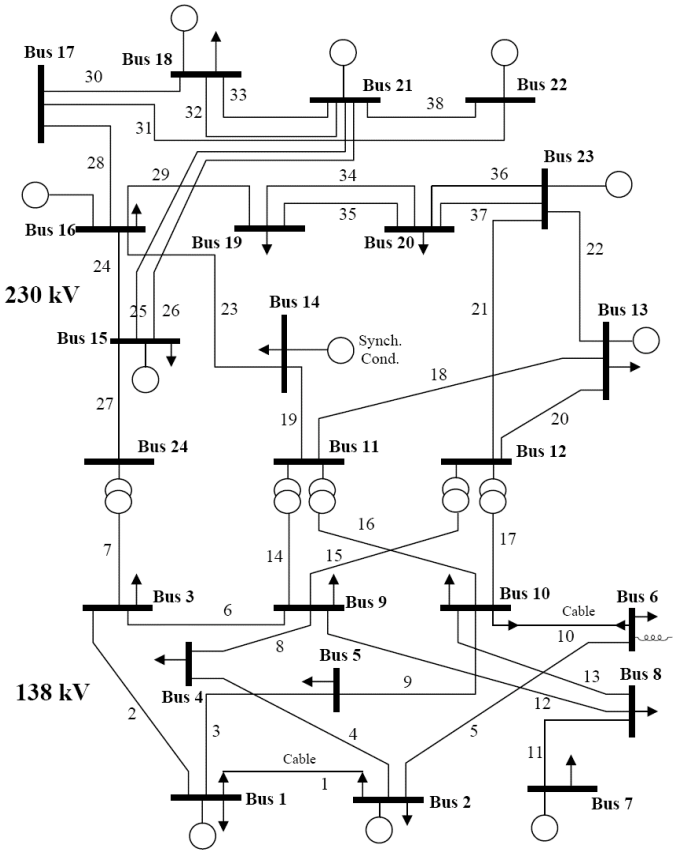

Figure 2.6: Single diagram of the IEEE-RTS

In order to conduct customer interruption cost research, the aggregate load at each bus was decomposed into customer sector loads [22, 35, 94], and each load point in the RBTS and the IEEE-RTS is then composed of a number of customer sectors. The load model at a bus is therefore obtained by summing the customer load sector data at that bus. This load representation is designated as the Modified Load Model in this research. There are seven customer load sectors: Residential, Commercial, Industrial, Government, Office, Large Users and Agricultural. The customer sector allocations at the different buses for the RBTS and the IEEE-RTS are shown in Tables 2.1 and 2.2 respectively. The customer sector load data are shown in Appendix B. The system peak loads for the RBTS and the IEEE-RTS are 179.28 MW and 2754.75 MW respectively.

Table 2.1: The RBTS customer sector peak loads at the load buses

Bus No.	Resid. (MW)	Comm. (MW)	Indus. (MW)	Govern. (MW)	Office (MW)	Lrg U. (MW)	Agri. (MW)	Total (MW)
2	7.25	3.70	3.50	5.55	0	0	0	20
3	19.90	4.70	3.05	0	1.85	55.50	0	85
4	19.00	4.70	16.30	0	0	0	0	40
5	8.90	3.70	0	5.55	1.85	0	0	20
6	7.85	1.70	3.05	0	0	0	7.40	20

where: Agri. = Agricultural, Lrg U. = Large Users, Res. = Residential,

Govt. = Government and Institution, Ind. = Industrial,

Com. = Commercial, Offic. = Office and Building.

Table 2.2: The IEEE-RTS customer sector peak loads at the load buses

Bus No.	Res. (MW)	Com. (MW)	Ind. (MW)	Govt. (MW)	Offic. (MW)	Lrg. U. (MW)	Agri. (MW)	Total (MW)
1	36.85	14.25	39.90	17.00	0.00	0.00	0.00	108
2	48.45	14.25	0.00	34.30	0.00	0.00	0.00	97
3	94.50	14.25	59.80	0.00	0.00	0.00	11.45	180
4	25.55	14.25	0.00	34.20	0.00	0.00	0.00	74
5	36.85	14.25	19.90	0.00	0.00	0.00	0.00	71
6	67.50	14.25	39.95	0.00	2.85	0.00	11.45	136
7	48.10	14.25	39.95	0.00	0.00	0.00	22.70	125
8	94.05	28.55	19.90	0.00	2.85	0.00	25.65	171
9	41.50	8.50	0.00	0.00	5.70	85.50	33.80	175
10	80.15	14.25	39.95	0.00	0.00	42.75	17.90	195
13	80.15	28.55	59.80	25.65	11.40	42.75	16.70	265
14	62.98	5.60	39.95	0.00	0.00	85.47	0.00	194
15	54.50	34.50	0.00	0.00	14.25	213.75	0.00	317
16	25.90	14.25	0.00	17.10	0.00	42.75	0.00	100
18	62.40	22.55	39.90	0.00	19.95	188.20	0.00	333
19	55.78	14.25	0.00	0.00	0.00	110.97	0.00	181
20	53.79	14.25	0.00	17.10	0.00	42.86	0.00	128

The original and modified system load duration curves for the two study systems are shown in Figure 2.7.

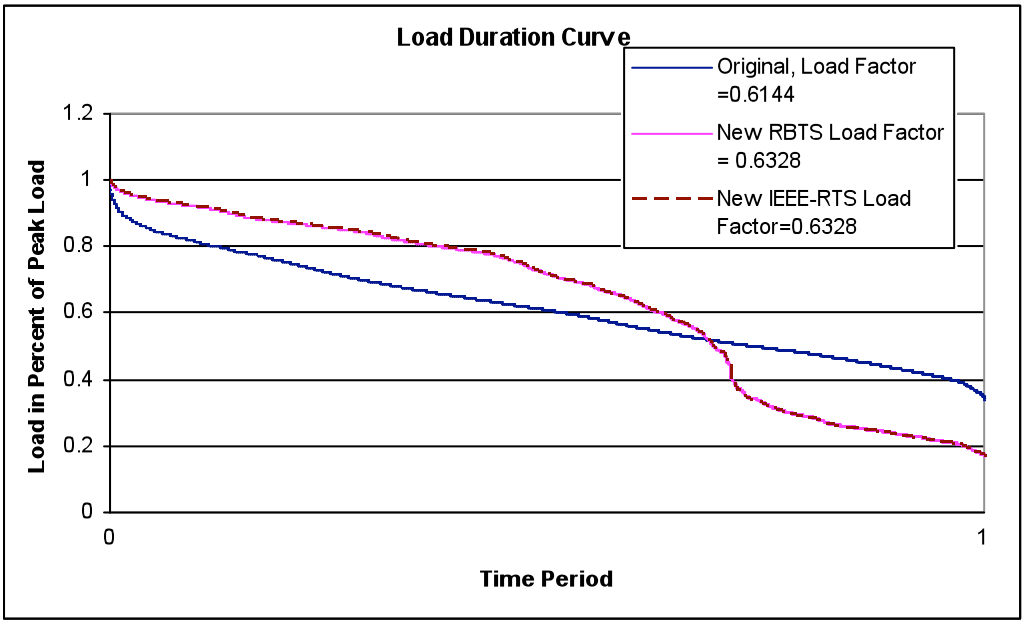

Figure 2.7: System load duration curves for the RBTS and the IEEE-RTS based on the original and modified load models

The basic reliability indices for the RBTS and the IEEE-RTS are shown in the following.

2.5.1. RBTS Results

The HLI program was applied to the RBTS base case. The sample size is 200,000 years. The system indices are shown in Table 2.3.

Table 2.3: The HLI system indices for the RBTS base case using the two load models

Load Model	Coefficient of Variation	LOLE (hrs/year)	LOEE (MWh/year)	LOLF (occ/year)
Original Load Model	0.0125	1.09	9.85	0.22
Modified Load model	0.0063	3.59	34.06	0.71

It can be seen from Figure 2.7 that the modified load model has a slightly larger load factor. The profile of the modified load model is significantly higher than that of the original load model [93] for a large portion of the year. It can be seen from Table 2.3 that the indices for the RBTS base case are larger when the modified load model is used.

Table 2.4 shows the HLI well-being indices for the RBTS using the two different load models.

Table 2.4: The well-being indices for the RBTS base case at HLI using the different load models

State	Using the original load model		
	System Probability (hrs/year)	System Frequency (occ/year)	Average Duration (hrs/occ)
Healthy	8693.11	7.37	1179.57
Marginal	41.80	7.57	5.52
At Risk	1.09	0.22	5.00
State	Using the modified load model		
	System Probability (hrs/year)	System Frequency (occ/year)	Average Duration (hrs/occ)
Healthy	8604.44	22.67	379.49
Marginal	127.97	23.33	5.49
At Risk	3.59	0.71	5.06

The HLII sequential Monte Carlo simulation program incorporates the individual load profiles at the different load buses. The system and load point indices for the RBTS base case using the modified load model are shown in Table 2.5. The sampling size is 10,000 years and the coefficient of variation is 0.0129.

Table 2.5: The HLII system and load point indices for the RBTS base case using the modified load model

Bus #	PLC(/year)	EDLC (hrs/year)	EENS (MWh/year)	EFLC (occ/year)	ECOST (k$/year)
2	0.000065	0.56	1.64	0.21	12.95
3	0.000374	3.27	29.54	0.76	79.27
4	0.000291	2.55	17.60	0.58	110.49
5	0.000031	0.27	1.43	0.10	10.55
6	0.000065	9.65	102.07	0.92	392.21
System Indices	0.001521	13.28	152.23	1.71	605.47

As noted earlier, the RBTS does not satisfy the N-1 criterion and therefore the RRBTS is used in the well-being analysis framework.

The system, load point and well-being indices for the RRBTS are shown in Tables 2.6 and 2.7. A sampling period of 8,000 years was used for the well-being analysis.

Table 2.6: The HLII system and load point indices for the RRBTS base case using the modified load model

Bus #	EDLC (hrs/year)	EENS (MWh/year)	EFLC (occ/year)	ECOST (k$/year)
2	0.55	1.57	0.17	12.25
3	3.22	27.41	0.72	72.43
4	2.64	18.22	0.54	113.63
5	0.07	0.25	0.02	1.95
6	0.03	0.11	0.01	0.48
System Indices	3.92	47.55	0.85	200.73

Table 2.7: The HLII well-being indices for the RRBTS base case using the modified load model

State	System Probability (hrs/year)	System Frequency (occ/year)	Average Duration (hrs/occ)
Healthy	8541.66	39.13	218.30
Marginal	190.41	39.93	4.77
At Risk	3.92	0.85	4.59

2.5.2. IEEE-RTS Results

The HLI program was applied to the IEEE-RTS using a sampling period of 50,000 years. The HLI system indices for the IEEE-RTS using the two load models are shown in Table 2.8.

Table 2.8: The HLI system indices for the IEEE-RTS base case using the two load models

Load Model	Coefficient of Variation	LOLE (hrs/year)	LOEE (MWh/year)	LOLF (occ/year)
Original Load Model	0.0112	9.46	1191.68	1.92
Modified Load model	0.0060	30.93	3872.98	8.19

The HLI well-being indices for the IEEE-RTS using the two load models are shown in Table 2.9.

Table 2.9: The HLI well-being indices for the IEEE-RTS base case using the two load models.

State	Using the original load model		
	System Probability (hrs/year)	System Frequency (occ/year)	Average Duration (hrs/occ)
Healthy	8612.87	20.30	424.31
Marginal	113.67	22.17	5.13
At Risk	9.46	1.92	4.93
State	Using the modified load model		
	System Probability (hrs/year)	System Frequency (occ/year)	Average Duration (hrs/occ)
Healthy	8386.02	73.34	114.35
Marginal	319.06	79.97	3.99
At Risk	30.93	8.19	3.78

The HLII system indices for the IEEE-RTS using the modified load model are shown in Table 2.10. The sampling size is 8,000 years and the coefficient of variation is 0.0202 in this case.

It can be seen that the HLII system indices are relative close to those of the HLI system indices for the IEEE-RTS. This is due to the fact that the IEEE-RTS is a transmission strong system. The generation contingencies cause the bulk of the load curtailments.

Table 2.10 shows that the reliability indices at bus 18 are the largest, followed by those at bus 13. The load shedding philosophy used is that loads are curtailed at the delivery points that are closest to (or one line away from) the element(s) on outage. A 400 MW generating unit is connected at bus 18 and another 400 MW unit connected at bus 21, which is one line away from bus 18. Both units have failure and repair rates of 7.96 occ/year and 58.4 occ/year respectively. The forced outage rate for these two units is 0.12. The failure of these two large units will cause load curtailment at bus 18. Three 197 MW generating units are connected at bus 13, with failure and repair rates of 9.22 occ/year and 175.2 occ/year respectively and a forced outage rate of 0.05. A 350 MW unit is connected at bus 23 which is one line away from bus 13. The failure, repair and forced outage rates for this unit are 7.62 occ/year, 87.6 occ/year and 0.08 respectively.

The forced outage rates for the noted units are relatively large compared to the other units. The peak loads at buses 13 and 18 are 265 MW and 333 MW respectively, and are larger than those of the other buses. These are the two main reasons why the EDLC and EENS at buses 13 and 18 are larger than those of the other load buses.

Table 2.10: The HLII system and load point indices for the IEEE-RTS base case using the modified load model.

Bus #	PLC(/year)	EDLC (hrs/year)	EENS (MWh/year)	EFLC (occ/year)	ECOST (k$/year)
1	0.000081	0.71	23.08	0.22	168.52
2	0.000229	2.00	56.65	0.62	357.98
3	0.000213	1.86	86.58	0.60	437.05
4	0.000203	1.77	41.48	0.56	331.79
5	0.000287	2.50	56.73	0.79	450.07
6	0.000334	2.92	115.39	0.90	644.53
7	0.000236	2.07	67.85	0.71	404.78
8	0.000353	3.09	149.87	0.87	897.18
9	0.000004	0.04	2.11	0.01	5.48
10	0.000007	0.06	4.07	0.02	16.90
13	0.000924	8.07	637.06	2.02	3474.46
14	0.000012	0.11	5.63	0.03	16.38
15	0.000350	3.06	236.95	0.87	920.83
16	0.000610	5.33	175.33	1.51	931.62
18	0.003009	26.29	2544.78	6.30	9004.02
19	0.000505	4.41	255.15	1.23	754.68
20	0.000175	1.53	53.75	0.64	251.60
System Indices	0.004112	35.92	4514.39	9.29	19070.46

Table 2.11 shows the HLII well-being indices for the IEEE-RTS base case using the modified load model.

Table 2.11: The well-being indices for the IEEE-RTS base case at HLII using the modified load model

State	System Probability (hrs/year)	System Frequency (occ/year)	Average Duration (hrs/occ)
Healthy	8207.15	103.43	79.35
Marginal	492.93	110.87	4.45
At Risk	35.92	9.29	3.87

The reliability indices for the RBTS, RRBTS and the IEEE-RTS are the base case system values used to compare with the calculated indices when different factors such as load forecast uncertainty, wind power addition and demand side management are considered later in this thesis.

2.6. Conclusion

The basic concept and methodology of the sequential Monte Carlo simulation technique and the well-being analysis framework are described in this chapter. The load flow calculation techniques used in this research are briefly described and the formulation of various HLI and HLII system and well-being indices are illustrated.

Two existing programs utilizing sequential Monte Carlo simulation for HLI and HLII reliability evaluation are briefly introduced. Load forecast uncertainty, wind power and demand side management were incorporated in the two existing programs and the information on the procedures used to are given in the following chapters. These factors can be performed on the well-being analysis framework. The two programs are basic tools in this research and are used to conduct a wide range of system studies.

The two study systems used in this research are introduced in this chapter and the system, load point and well-being indices for the base cases are presented. The indices presented in this chapter are the base case values used in the following chapters to investigate the impacts of load forecast uncertainty, wind power and demand side management in HLII reliability evaluation.

CHAPTER 3

EFFECTS OF LOAD FORECAST UNCERTAINTY

3.1. Introduction

Load forecast uncertainty is an important consideration in an electrical power system. Published results [95] show that system load forecast uncertainty has a significant effect on generating system reliability indices. The recognition of load forecast uncertainty also creates increases in the inadequacy indices in composite system reliability studies and the effect increases as the uncertainty increases [29]. Increased competition in the electric utility industry requires more comprehensive risk evaluation [29, 45, 46]. The inclusion of load forecast uncertainty in bulk electric system reliability evaluation is of practical importance and it is necessary to consider both the system load forecast uncertainty and the correlation between the individual buses in security constrained adequacy assessment [29, 96-98].

Load forecast uncertainty (LFU) can be described by a probability distribution whose parameters can be estimated from past experience and future considerations. It's difficult to obtain sufficient historical data to determine the distribution type and the most common practice is to describe the uncertainty as a normal distribution with a given standard deviation [2]. The distribution mean is the forecast peak load. The LFU represented by a normal distribution can be approximated using the discrete interval method, or simulated using the tabulating technique of sampling [29].

The tabulating technique and the bus load correlation sampling technique are utilized in this research work to incorporate LFU and bus load correlation in bulk electric system reliability evaluation. The existing computer programs for HLI evaluation [73] and for HLII evaluation [22], were modified and extended to include LFU considerations.

The reliability indices and the reliability index probability distributions change with variation in the LFU, the configuration of the system, the operating policies, etc.

The incorporation of LFU considerations in bulk electric system reliability evaluation provides a realistic and comprehensive appraisal of future system reliability. This research work examines the effects of LFU and bus load correlation on composite system reliability indices and index probability distributions. Impacts of the LFU and bus load correlation on different network configurations are also examined.

3.2. Incorporating Load Forecast Uncertainty in the Simulation Process

3.2.1. Methodology

Bus LFU can be modeled using a normal distribution [2]. Normally distributed random numbers are therefore required in order to incorporate LFU in the simulation process. The tabulating technique and the bus load correlation sampling technique used in this research are described as follows. Assume the mean value of the load is μ and the standard deviation is σ.

Tabulating technique of normal distribution sampling

There are two steps in the tabulating technique of Normal distribution sampling. The first one is tabulating, the second one is sampling.

In the tabulating process, the cumulative probability distribution function is divided into M equal subintervals as shown in Figure 3.1.

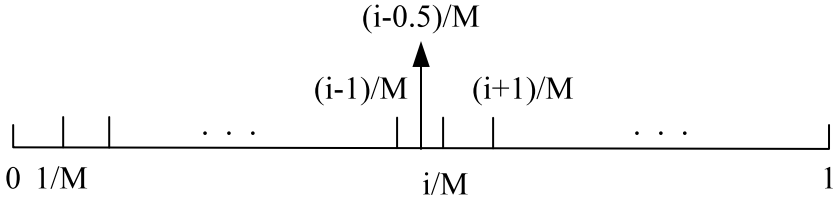

Figure 3.1: M intervals representation for the normal cumulative probability distribution function

The mid-point value of a subinterval is used to represent all values of the normal cumulative probability function F in this subinterval. Therefore,

$$F(X_i) = \frac{i - 0.5}{M} \qquad (i = 1,2...,M) \tag{3.1}$$

X_i is a normal distributed random number with a mean of 0 and standard deviation of 1. X_i can be calculated using inverse transform method as follows.

$$X_i = F^{-1}(X_i) = F^{-1}(\frac{i-0.5}{M}) \qquad (i = 1,2...,M) \tag{3.2}$$

X_i can be calculated using the following approximate formulas [29, 99] from the value of the normal cumulative probability distribution function $F(X_i)$.

$$X_i = \begin{cases} -z & 0 \le F(X_i) < 0.5 \\ 0 & F(X_i) = 0.5 \\ z & 0.5 < F(X_i) \le 1.0 \end{cases} \qquad (i = 1,2...,M) \tag{3.3}$$

$$z = w - \frac{\sum_{j=0}^{2} C_j w^j}{1 + \sum_{j=1}^{3} D_j w^j} \tag{3.4}$$

where $w = \sqrt{-2\ln(Q)}$, $Q = \begin{cases} F(X_i) & 0 \le F(X_i) < 0.5 \\ 1 - F(X_i) & 0.5 < F(X_i) \le 1.0 \end{cases}$

$C_0 = 2.515517 \qquad C_1 = 0.802853 \qquad C_2 = 0.010328$

$D_1 = 1.432788 \qquad D_2 = 0.189269 \qquad D_3 = 0.001308$

i is the subinterval number, i=1,2,…,M.

A table of the value of the cumulative probability function $F(X_i)$ with the corresponding normally distributed random number X_i can be formed using the above equations. This table can be designated as Table D.

The sampling process can be described in the following steps.

a) Generate a uniformly distributed random number Y between [0,1].

b) Select the corresponding X from the formed Table D.

c) Calculate the load. $NewPeakLoad = X * \sigma + \mu$.

The tabulating technique is actually a discretization technique. The discretization error is relatively small when the subinterval number is large. Normally M equal to 500 is sufficient.

Bus load correlation sampling technique

Assume there are N load buses. If all bus loads are completely dependent, then only one normally distributed random number is needed to determine all the bus loads.

If the bus loads are 100% independent, then N normally distributed random numbers should be generated. In a practical power system, the bus loads are not completely dependent or independent and there is some correlation between the bus loads. Bus load correlation can be sampled as follows.

Assume R is an N dimensional normally distributed random vector with mean B and covariance matrix C. Let G be a N dimensional normally distributed random vector. The components in G are independent of each other and have a mean of 0 and variance of 1. R can be represented by:

$$R = AG + B \tag{3.5}$$

The covariance matrix C can be calculated by:

$$C = E[(R-B)(R-B)^T] = E(AGG^TA^T) = E(AA^T) = AA^T \tag{3.6}$$

Matrix A is a lower triangular matrix and can thus be calculated by the following equations according to the covariance matrix C.

$$A_{i1} = \frac{C_{i1}}{(C_{11})^{1/2}} \qquad (1 \le i \le N) \tag{3.7}$$

$$A_{ii} = (C_{ii} - \sum_{k=1}^{i-1} A_{ik}^2)^{1/2} \qquad (1 < i \le N) \tag{3.8}$$

$$A_{ij} = (C_{ij} - \sum_{k=1}^{j-1} A_{ik}A_{jk})/A_{jj} \qquad (1 < j < i \le N) \tag{3.9}$$

The steps in bus load correlation sampling are as follows.

a) Generate an independent N dimensional normally distributed random vector G as in 3.2.1.

b) Calculate matrix A.

c) Create the correlative normally distributed N dimensional random vector R which has a covariance matrix C.

3.2.2. Modification of the HLI and RapHL-II programs

Both the Monte Carlo simulation program for HLI evaluation [73] and the RapHL-II program [22] were extended to incorporate LFU using the tabulating technique. The processes involved in including the tabulating technique in the two programs are shown in Figures 3.2 and 3.3.

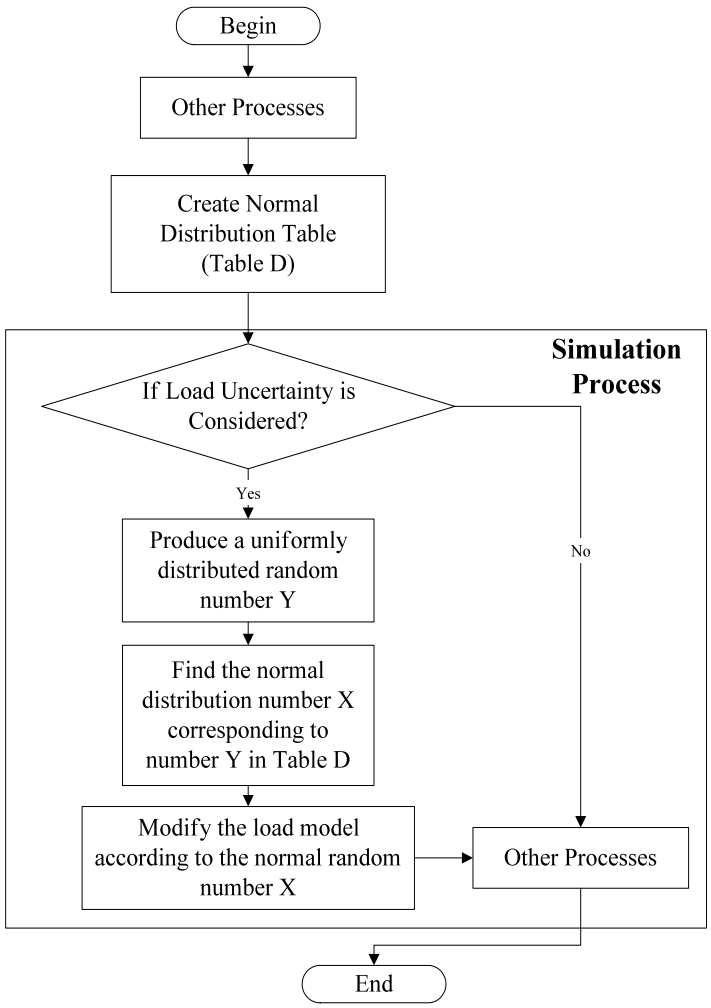

Figure 3.2: The block diagram for incorporating LFU in the HLI program using the tabulating technique

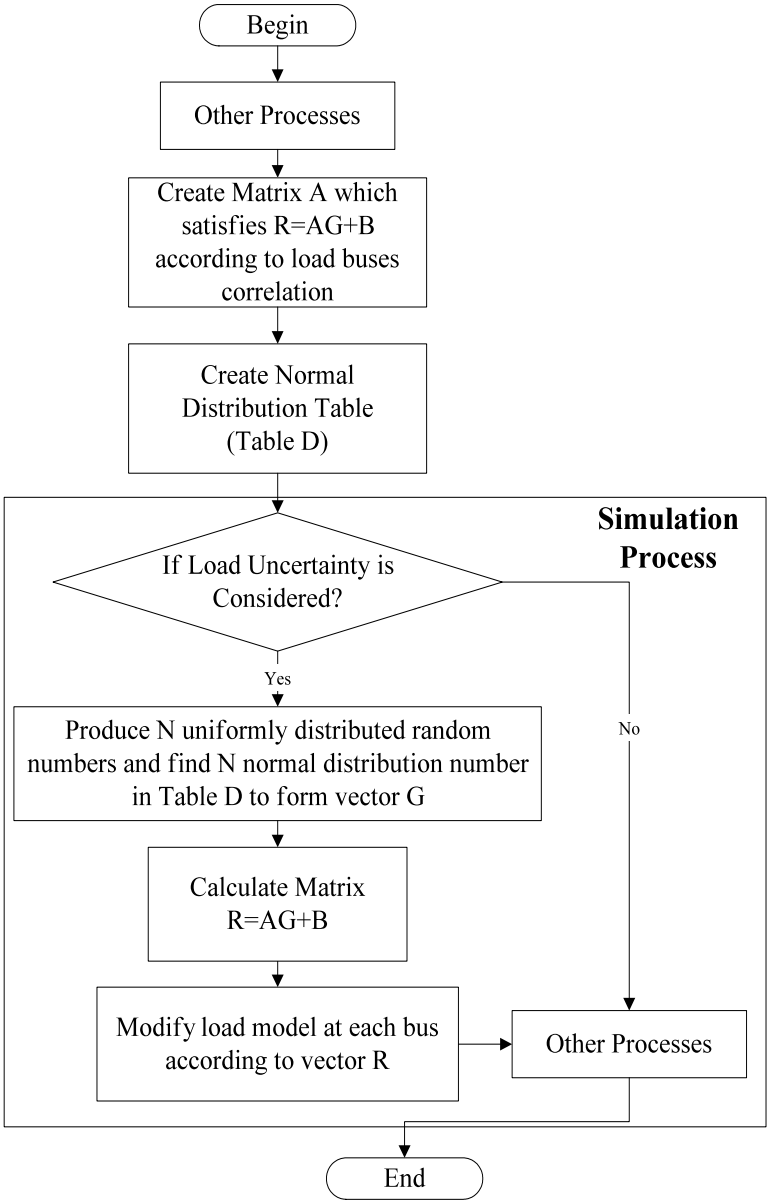

Figure 3.3: The block diagram for incorporating LFU in the RapHL-II using the tabulating technique.

Tables D, Y, X, R, A, G, B in Figure 3.2 and 3.3 are described in Sections 3.2.1.

The effects of LFU on composite system reliability evaluation are shown in the following sections by applying the HLI and RapHL-II programs to the study systems described in Chapter 2.

3.3. Effects of Load Forecast Uncertainty on HLI Reliability Evaluation

The HLI simulation program was applied to the RBTS and the IEEE-RTS. The RBTS has 240 MW of installed capacity in 11 generating units. The peak load of the RBTS is 179.28 MW. The sample size is 20,000 years for the RBTS. The IEEE-RTS has 3405 MW of installed capacity in 32 generating units. The peak load is 2754.75 MW. The sample size is 10,000 years for the IEEE-RTS. The modified hourly load model described in Chapter 2 was used in both the RBTS and the IEEE-RTS.

The LFU was considered by assuming the standard deviation describing the uncertainty to be 5% and 10% of the forecast peak load in this study. The designating LFU is used to indicate the standard deviation of the LFU in the discussion in this thesis. The bus load correlation is considered to be 100% dependent. The number of subintervals is 500.

3.3.1. Effects on HLI system indices

RBTS results

The reliability indices for the RBTS when the LFU is 0%, 5% and 10% are shown in Table 3.1. It can be seen that the reliability indices increase with increase in the LFU. The changes in the reliability indices for the LFU of 0% and 5%, and 0% and 10% are also shown in Table 3.1. The index changes are the differences between the index at a certain LFU level and that of the LFU of 0% divided by the index at the LFU of 0%.

Table 3.1: The HLI reliability indices for the RBTS with LFU

LFU	LOLE (hrs/yr)	LOLE Change (%)	LOEE (MWh/yr)	LOEE Change (%)	LOLF (occ/yr)	LOLF Change (%)
0%	3.56	0	33.49	0	0.74	0
5%	4.40	23.49	43.73	30.57	1.08	46.35
10%	9.36	162.66	101.93	204.36	2.33	217.19

It can be seen that the reliability indices increase significantly when the LFU increases from 5% to 10%.

IEEE-RTS results

The reliability indices for the IEEE-RTS when the LFU is 0%, 5% and 10% are shown in Table 3.2. It can be seen that the reliability indices increase with increase in the LFU. The reliability index standard deviations for the IEEE-RTS at the LFU of 0%, 5%, and 10% are also shown in Table 3.2.

Table 3.2: The HLI reliability indices for the IEEE-RTS with LFU

LFU	LOLE (hrs/yr)	LOL Std. Dev.	LOEE (MWh/yr)	LOE Std. Dev.	LOLF (occ/yr)	FLC Std. Dev.
0%	31.44	29.74	3950.84	5341.00	8.70	6.61
5%	42.60	55.28	5862.90	9644.30	10.68	12.00
10%	87.10	165.56	14684.04	35165.14	19.58	31.89

Where: Std. Dev.- Standard Deviation

It can be seen that the reliability index standard deviations increase significantly when the LFU increases, especially when the LFU increases to 10%.

3.3.2. Effects on HLI reliability index probability distributions

RBTS results

The loss of load (LOL) probability distributions for the RBTS with various LFU are shown in Figure 3.4. The class interval width is 1.5 (hrs/yr) and the last interval in each case shows the cumulative relative frequency of loss of load from 45 to 78 (hrs/yr), 144 (hrs/yr) and 473 (hrs/yr) respectively. The relative frequency of encountering no loss of load is 62.15%, 57.63%, and 55.67% for the three cases respectively. The relative frequency of encountering no loss of load is not shown in Figure 3.4.

It can be seen from Figure 3.4 that the loss of load distributions change with change in the LFU. The range of the loss of load increases with increasing LFU. The relative frequencies for larger loss of load intervals increase with increase in the LFU.

The loss of energy (LOE) probability distributions for the RBTS with different LFU are shown in Figure 3.5. The standard deviations of the LOE for the three LFU levels are 7.38 (MWh/yr), 24.95 (MWh/yr) and 331.08 (MWh/yr) respectively. The range of the LOE increases significantly with increase in the LFU.

The LOLF for the three LFU levels are shown in Table 3.1. The standard deviations of the frequency of load curtailment (FLC) are 1.24 (occ/yr), 1.85 (occ/yr) and 5.54 (occ/yr) for the three cases respectively.

The relative frequency of the FLC for the first 15 intervals is shown in Figure 3.6. The relative frequency of the FLC drops faster when the LFU is smaller. The cumulative relative frequency of the FLC from 10 (occ/yr) to 11 (occ/yr), 27 (occ/yr) and 81 (occ/yr) for the LFU of 0%, 5% and 100% is 0.01%, 0.41% ad 5.90% respectively and is not shown in Figure 3.6. The range of the FLC increases significantly with increase in the LFU.

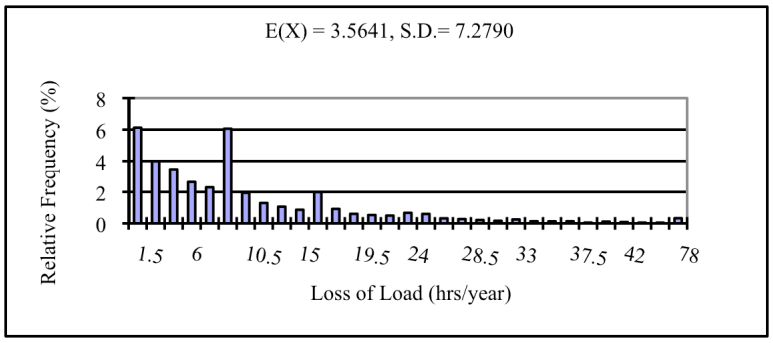

(a) LFU=0%

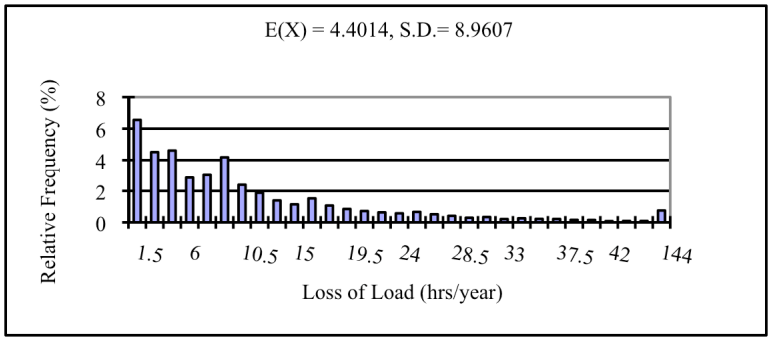

(b) LFU=5%

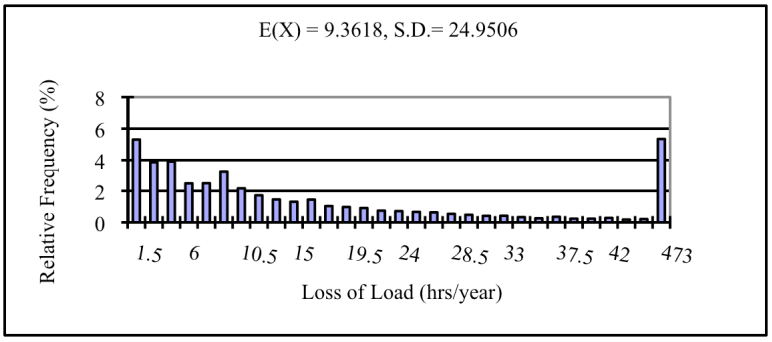

(c) LFU=10%

Figure 3.4: Probability distributions of the HLI LOL for the RBTS with LFU

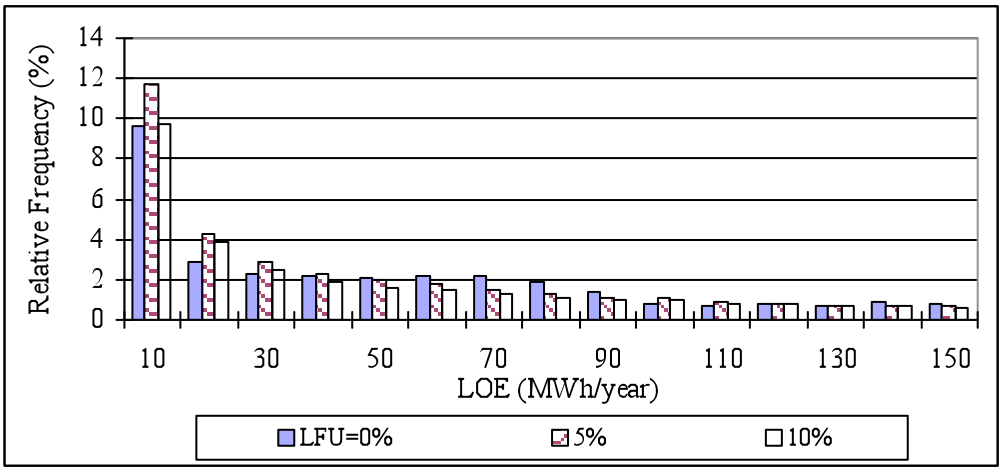

Figure 3.5: Probability distributions of the LOE for the RBTS with LFU

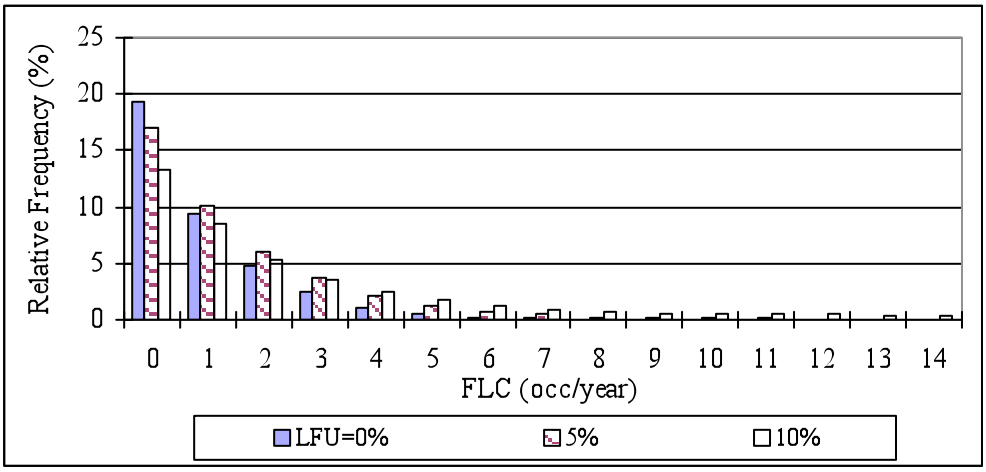

Figure 3.6: Probability distributions of the FLC for the RBTS with LFU

IEEE-RTS results

The LOL probability distributions for the IEEE-RTS with LFU are shown in Figure 3.7. The class interval width is 4 (hrs/yr). The relative frequency of encountering no loss of load is 8.73%, 11.74%, and 21.77% for the three cases respectively and is not shown in this figure.

The LOE and the FLC distributions change in a similar manner to the LOL distribution with increasing LFU and are not shown here.

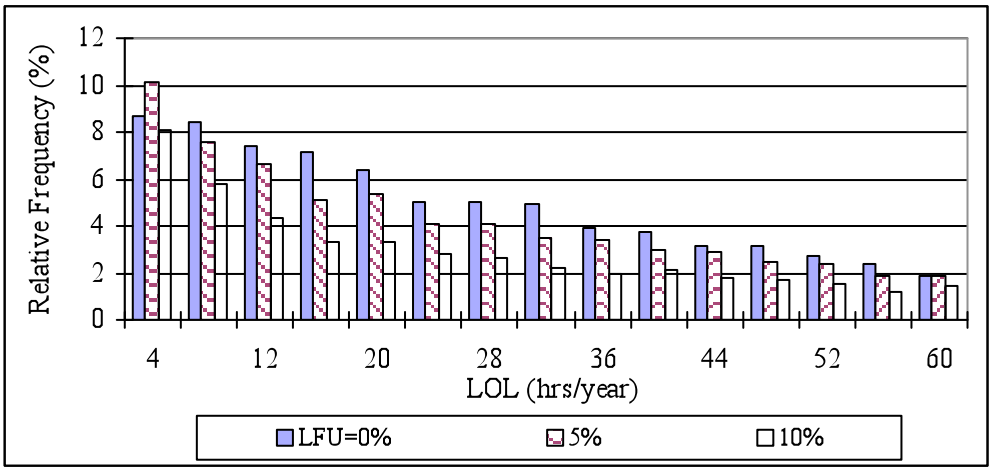

Figure 3.7: Probability distributions of the LOL for the IEEE-RTS with LFU

3.4. Effects of Load Forecast Uncertainty on HLII Reliability Evaluation

The RapHL-II program was applied to the RBTS and the IEEE-RTS. The load shedding philosophy is the Pass-I criterion. Both generation and transmission contingencies are considered. The bus load is considered to be 100% dependent in this section. The sample size is 8,000 years and 6,000 years for the RBTS and the IEEE-RTS respectively.

3.4.1. Effects on HLII system indices

RBTS results

The system indices and the index changes with increasing LFU for the RBTS in the HLII reliability evaluation are shown in Table 3.3.

Table 3.3: The HLII system indices for the RBTS with various LFU

LFU	PLC	EDLC (hrs/yr)	EDLC Change (%)	EENS (MWh/yr)	EENS Change (%)	EFLC (occ/yr)	EFLC Change (%)
0%	0.001525	13.36	0	152.92	0	1.72	0
5%	0.001642	14.38	7.67	168.80	10.38	2.02	17.36
10%	0.002198	19.25	44.13	248.19	62.3	3.25	88.46

The changes in the reliability indices for the RBTS due to the LFU in both the HLI and HLII evaluations are shown pictorially in Figure 3.8.

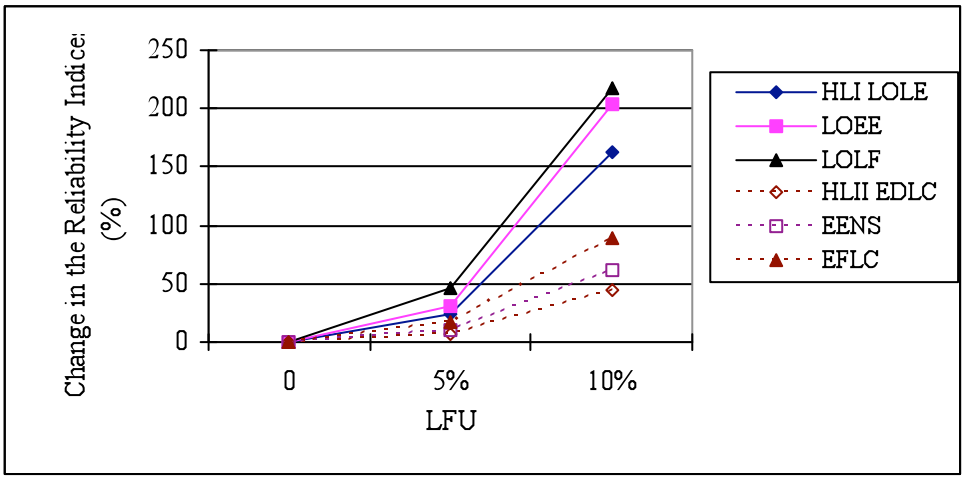

Figure 3.8: Changes in the reliability indices in the HLI and HLII evaluations for the RBTS with LFU

It can be seen from Figure 3.8 that the changes in the reliability indices at HLII are not as great as those at HLI for the RBTS cases. The differences in the LOLE, LOEE and LOLF at HLI when the LFU is 10% are over 150%, while in the HLII evaluation, the differences are between 50% and 100%. This is mainly due to the fact that the HLII reliability indices are dominated by the single line supply between buses #5 and #6, which masks the effects of the LFU.

IEEE-RTS results

The system indices for the IEEE-RTS in the HLII reliability evaluation are shown in Table 3.4.

Table 3.4: The HLII system indices for the IEEE-RTS with various LFU

LFU	PLC	EDLC (hrs/yr)	EDLC Change (%)	EENS (MWh/yr)	EENS Change (%)	EFLC (occ/yr)	EFLC Change (%)
0%	0.004040	35.35	0	4490.49	0	9.02	0
5%	0.005520	48.39	36.89	6859.71	52.76	11.44	26.92
10%	0.011400	100.15	183.3	16954.06	277.56	21.26	135.76

The changes in the reliability indices for the IEEE-RTS due to the LFU in both the HLI and HLII evaluations are shown in the Figure 3.9.

It can be seen from Figure 3.9 that the changes in the reliability indices at HLII are larger than those at HLI for the IEEE-RTS cases. The differences in the LOLE,

LOEE and LOLF in HLI when the LFU is 10% are over 100%, while in the HLII evaluation, the differences are between 135% and 280%. The effects of LFU at HLI and HLII are different. The effects of LFU are also different for systems having different reliability levels.

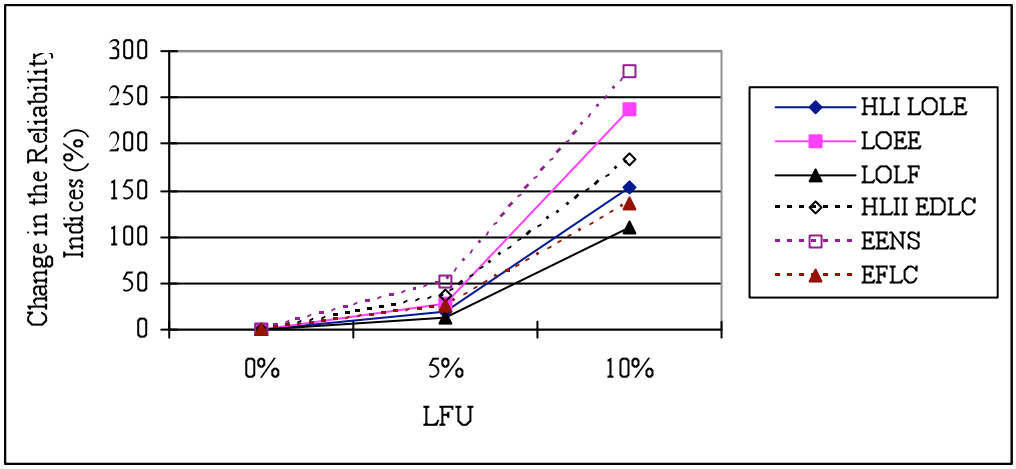

Figure 3.9: Changes in the reliability indices in the HLI and HLII evaluations for the IEEE-RTS with LFU

3.4.2. Effects on HLII reliability index probability distributions

RBTS results

The first 15 intervals of the HLII Duration of Load Curtailment (DLC) distribution for the RBTS for the selected LFU are shown in Figure 3.10.

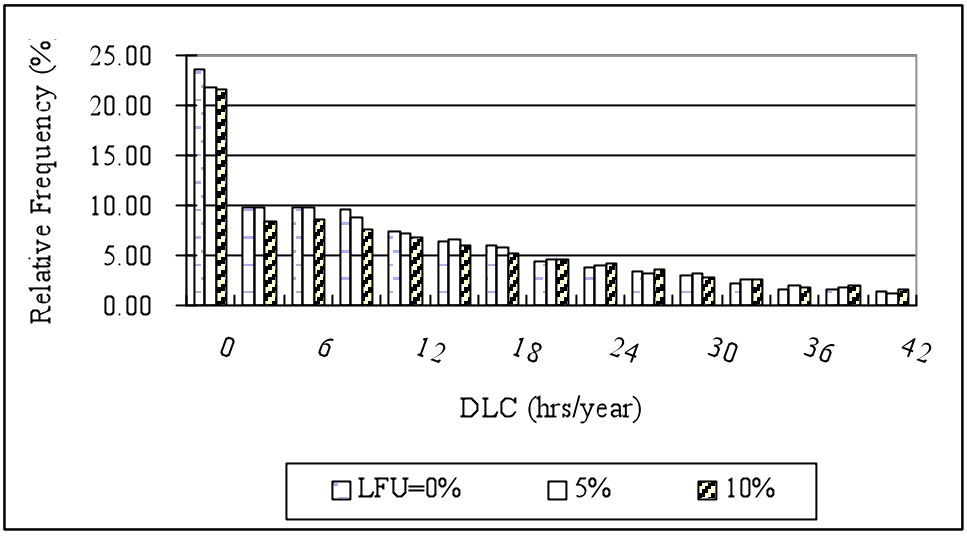

Figure 3.10: Probability distributions of the DLC at HLII for the RBTS with LFU

The class interval width for the DLC distribution is 3 (hrs/yr). The relative frequency when there is no loss of load decreases with increase in the LFU. The standard deviations of the DLC for the RBTS at the LFU of 0%, 5% and 10% are 15.76, 16.73 and 28.37 (hrs/yr) respectively. The range of the loss of load increases with the LFU. The DLC standard deviation increases by a factor of 1.9 when the LFU of 0% moves to 10%. This is not as significant as in the HLI case, where the LOL standard deviation increases by a factor of 3.4.

It can be seen from Figure 3.10 that the relative frequency of the DLC changes differently from that of the LOL at HLI shown in Figure 3.4. The transmission network is considered in the HLII reliability evaluation and the effects of LFU on the reliability index probability distribution are masked by the transmission deficiency that dominates the load curtailments.

The relative frequencies for the first 15 intervals of the HLII ENS for the RBTS are shown in Figure 3.11. The class interval width for the ENS distribution is 20 (MWh/yr). The ENS standard deviations are 198.43, 225.99 and 480.29 (MWh/yr) at the LFU of 0%, 5% and 10% respectively. The range of the energy not supplied increases with the LFU but not as great as in the HLI case. It can be seen from Figure 3.11 that the ENS distribution has a similar form to the DLC distribution.

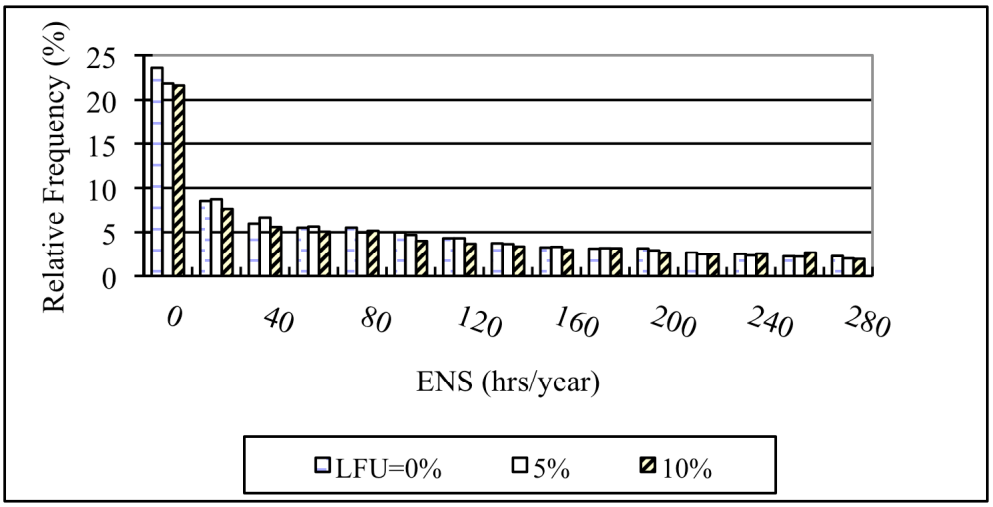

Figure 3.11: Probability distributions of the ENS at HLII for the RBTS with LFU

The relative frequency of the FLC for the first several intervals is shown in Figure 3.12. The class interval width for the FLC distribution is 1 (occ/yr). The HLII

FLC standard deviations are 1.63, 2.04 and 5.45 (occ/yr) for the LFU of 0%, 5% and 10% respectively. The HLII FLC distribution changes differently than the HLI FLC distribution. The single line between buses #5 and #6 dominates the system load curtailment and masks the effects of the LFU not only on the reliability indices, but also on the reliability index probability distributions.

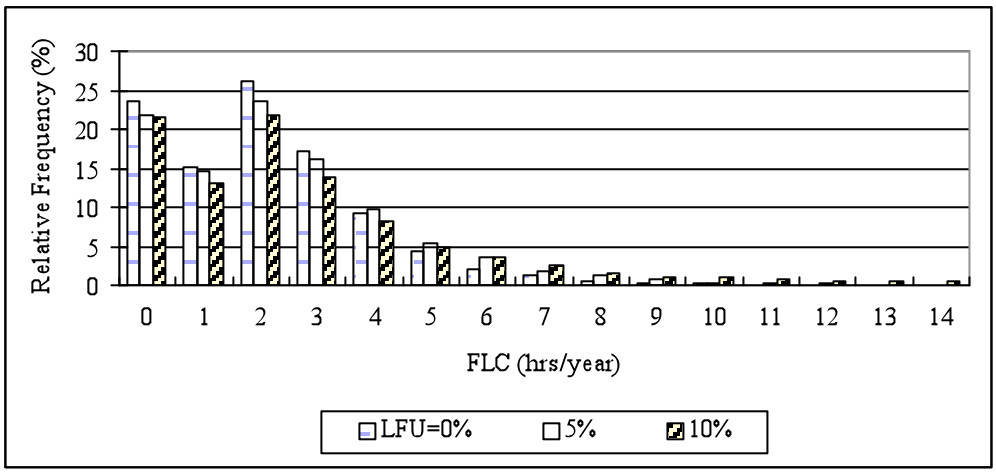

Figure 3.12: Probability distributions of the FLC at HLII for the RBTS with LFU

IEEE-RTS results

The relative frequencies for the first 14 intervals of the DLC of the IEEE-RTS are shown in Figure 3.13. The class interval width for the DLC distribution is 5 (hrs/yr). It can be noted that the relative frequency when there is no loss of load increases with increase in the LFU. This is different from the RBTS case where the relative frequency when there is no loss of load decreases with increasing LFU. The LFU has different effects on the relative frequency of no loss of load for systems with different reliability levels. The range of the loss of load increases with the LFU. The DLC standard deviations for the IEEE-RTS at the LFU of 0%, 5% and 10% are 33.16, 61.33 and 180.20 (hrs/yr) respectively. The DLC standard deviation increases by a factor of 5.45 when the LFU increases from 0% to 10%. This is similar to the HLI LOL standard deviation, which increases by a factor of 5.53. The IEEE-RTS is a transmission strong system and the load curtailment is not dominated by transmission deficiencies. The effects of the LFU on the reliability indices and the reliability index probability distributions are not masked by the transmission network.

It can be seen from Figure 3.13 that the IEEE-RTS DLC distribution has a different form to that for the RBTS. In the IEEE-RTS cases, the relative frequency of the no loss of load interval increases. The relative frequency when the DLC is between 10 (hrs/yr) and 65 (hrs/yr) decreases with increase in the LFU, while in the RBTS case, the changes in the relative frequency due to the LFU tend to fluctuate.

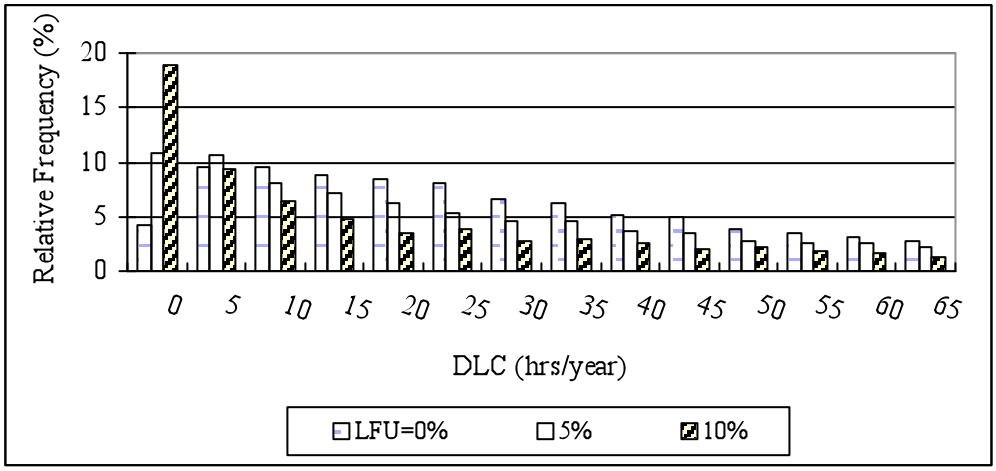

Figure 3.13: Probability distributions of the DLC at HLII for the IEEE-RTS with LFU

The first 15 intervals of the HLII ENS distributions for the IEEE-RTS with LFU are shown in Figure 3.14. The class interval width for the ENS distribution is 300 (MWh/yr). The ENS standard deviations are 5936.06, 11493.01 and 38361.28 (MWh/yr) respectively at the LFU of 0%, 5% and 10%. The increases in ENS standard deviation are similar to those of the HLI LOE.

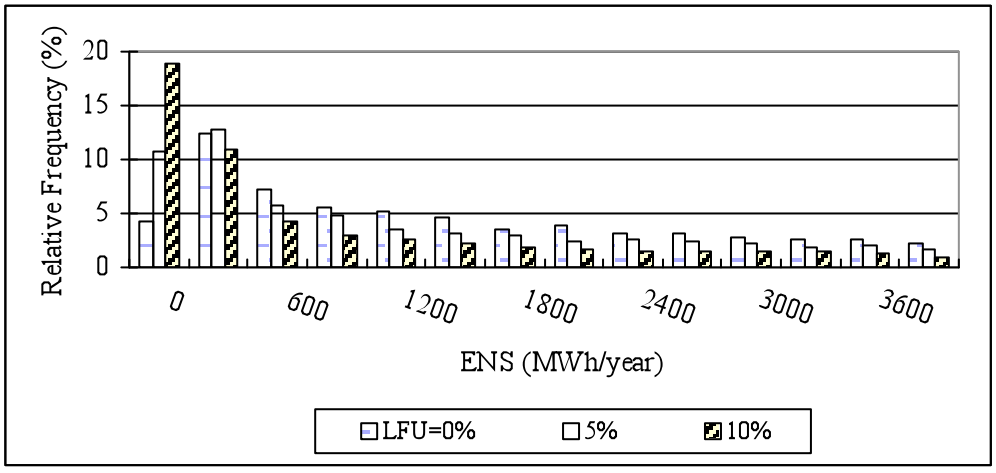

Figure 3.14: Probability distributions of the ENS at HLII for the IEEE-RTS with LFU

The range of the energy not supplied increases significantly with the LFU. The HLII ENS distributions for the IEEE-RTS have a similar form to the DLC distributions.

The class interval width in the HLII FLC distribution for the IEEE-RTS is 2 (occ/yr). The relative frequencies of the FLC for the first several intervals are shown in Figure 3.15. The FLC standard deviations are 6.90, 12.53 and 33.04 (occ/yr) at the LFU of 0%, 5% and 10% respectively. The FLC range increases significantly with increasing LFU.

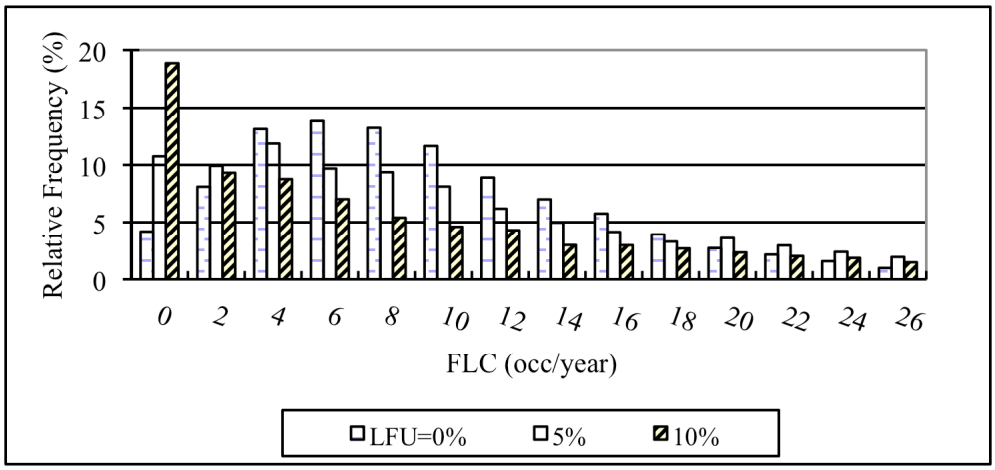

Figure 3.15: Probability distributions of the FLC at HLII for the IEEE-RTS with LFU

3.4.3. Effects of LFU with increase in the peak load

The previous sections show the effects of LFU on HLI and HLII reliability evaluation for the RBTS and IEEE-RTS. The LFU has different effects on systems with different reliability levels. The peak loads of the RBTS and the IEEE-RTS are changed in this section to show how the effects of the LFU varies with changing peak load. The peak loads in the RBTS and IEEE-RTS were increased by 10% and the reliability indices for the two systems with LFU of 0%, 5% and 10% were calculated. The results for the two systems at HLI and HLII are shown in the following.

RBTS results

The system indices for the RBTS at HLI and HLII are shown in Tables 3.5 and 3.6 respectively. The index changes are the differences between the index at a certain LFU level and that of the LFU of 0% divided by the index at the LFU of 0%.

Table 3.5: The HLI system indices for the RBTS with LFU, peak load increased by 10%

LFU	PLC	EDLC (hrs/yr)	EDLC Change (%)	EENS (MWh/yr)	EENS Change (%)	EFLC (occ/yr)	EFLC Change (%)
0%	0.001579	13.83	0	156.39	0	2.68	0
5%	0.002206	19.33	39.77	211.75	35.40	4.92	83.74
10%	0.004782	41.89	202.95	522.67	234.21	9.05	238.17

Table 3.6: The HLII system indices for the RBTS with LFU, peak load increased by 10%

LFU	PLC	EDLC (hrs/yr)	EDLC Change (%)	EENS (MWh/yr)	EENS Change (%)	EFLC (occ/yr)	EFLC Change (%)
0%	0.002822	24.72	0	336.89	0	4.12	0
5%	0.003559	31.18	26.13	435.52	29.28	6.49	57.70
10%	0.006308	55.26	123.57	920.87	173.35	10.89	164.52

The relative changes in the reliability indices for the RBTS at HLI and HLII are also shown pictorial in Figure 3.16. It can be seen that the relative changes in the HLI indices are larger than those at HLII. This is similar to the relative changes at the original peak load. The differences in the HLI and HLII reliability indices are different from those shown in Figure 3.8.

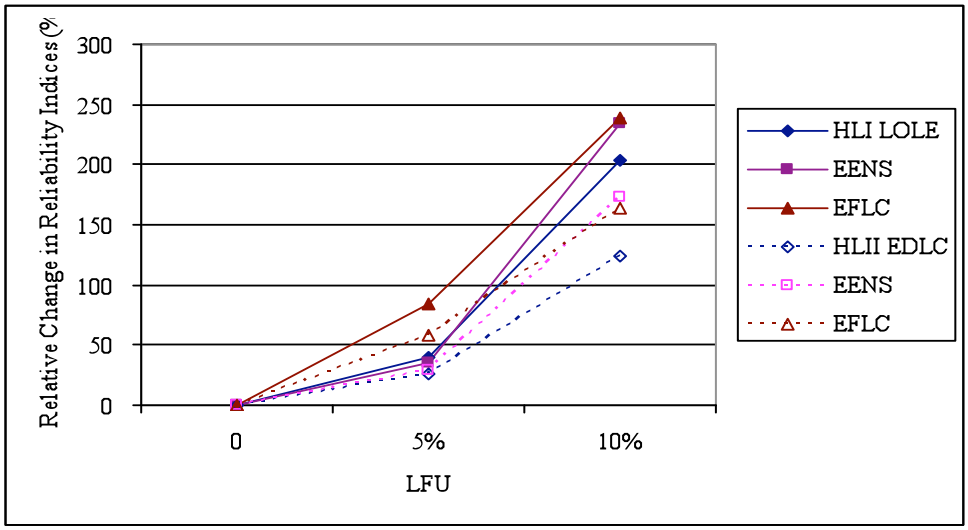

Figure 3.16: Relative changes in the reliability indices in the HLI and HLII evaluations with LFU for the RBTS, peak load increased by 10%

IEEE-RTS results

Similar studies were performed on the IEEE-RTS. The HLI and HLII system indices are shown in Tables 3.7 and 3.8 respectively.

Table 3.7: The HLI system indices for the IEEE-RTS with LFU, peak load increased by 10%

LFU	PLC	EDLC (hrs/yr)	EDLC Change (%)	EENS (MWh/yr)	EENS Change (%)	EFLC (occ/yr)	EFLC Change (%)
0%	0.017100	149.87	0	23408.46	0	33.65	0
5%	0.022600	197.74	31.94	32998.98	40.97	42.49	26.29
10%	0.035600	312.12	108.25	64339.71	174.86	58.23	73.08

Table 3.8: The HLII system indices for the IEEE-RTS with LFU, peak load increased by 10%

LFU	PLC	EDLC (hrs/yr)	EDLC Change (%)	EENS (MWh/yr)	EENS Change (%)	EFLC (occ/yr)	EFLC Change (%)
0%	0.019600	171.87	0	27200.14	0	38.62	0
5%	0.025200	221.10	28.64	37554.13	38.07	46.90	21.44
10%	0.039600	346.48	101.60	73186.04	169.06	63.59	64.64

The relative changes in the system indices at HLII and HLI for the IEEE-RTS are shown in Figure 3.17.

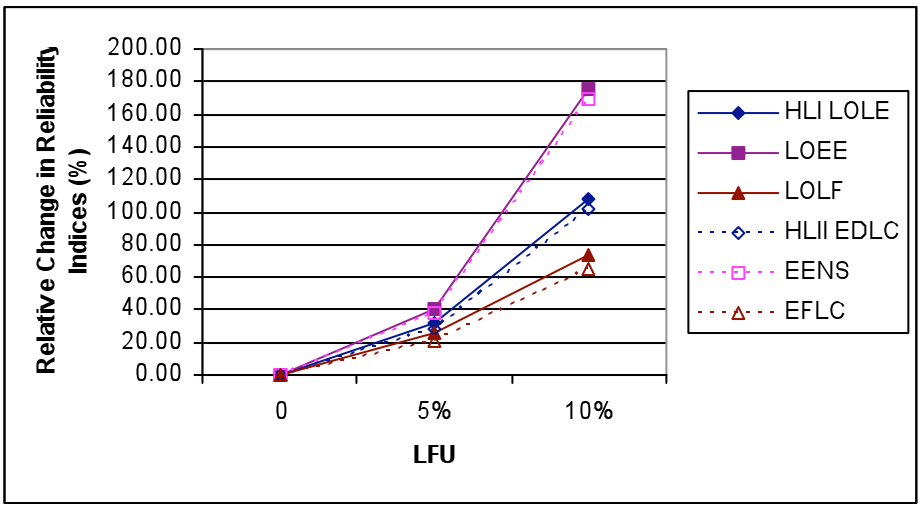

Figure 3.17: Relative changes in the reliability indices in the HLI and HLII evaluations with LFU for the IEEE-RTS, peak load increased by 10%

The reliability indices increase with increase in the LFU. The effect of LFU on HLI indices and HLII indices are different. At the original peak load, the index changes at HLI are larger than those at HLII for the RBTS, while for the IEEE-RTS, the HLII indices change more than the HLI indices with increase in the LFU. The RBTS is a transmission deficient system while the IEEE-RTS is a generation deficient system. When the peak load increases by 10% in the two systems, the relative changes in the HLI indices are larger than those in the HLII indices for both systems. The differences between the relative changes for the IEEE-RTS are, however, very small.

3.4.4. Effects of LFU on HLII load point indices

The RapHL-II program can also produce load point indices. These indices for the RBTS and the IEEE-RTS with various LFU based on the different load shedding philosophies designated as Pass-I, Pass-II and Priority Order are shown in this section.

The LFU at different buses is considered to be 100% dependent. In this study, the peak loads are 179.28 MW and 2754.75 MW for the RBTS and the IEEE-RTS respectively.

RBTS results

The load bus indices when using the Pass-I criterion for the RBTS at HLII with LFU are shown in Figure 3.18.

It can be seen in Figure 3.18 that the load bus indices increase with increase in the LFU. The increases in the load bus indices are larger at buses #3 and #4. The indices at buses #5 and #6 remain almost the same with increase in the LFU. The changes in the EDLC, EENS and EFLC indices are similar.

When the Pass-II criterion is used, the load bus indices are almost the same as the ones when the Pass-I criterion is used. The RBTS is a relatively small system and therefore the Pass-I and Pass-II criteria have similar effects on the load point indices. The EDLC (hrs/yr) for each load bus with the various LFU are shown in Figure 3.19.

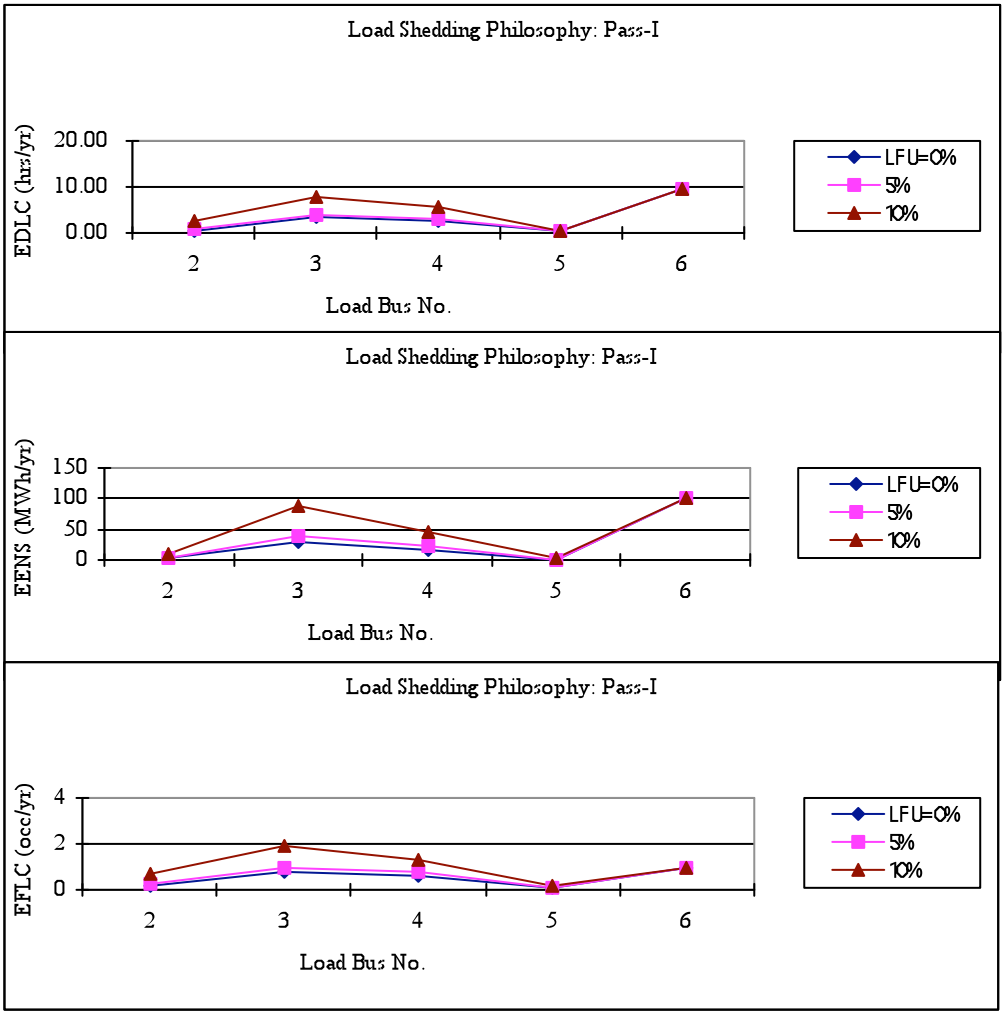

Figure 3.18: Load bus indices with LFU at HLII for the RBTS using the Pass-I criterion

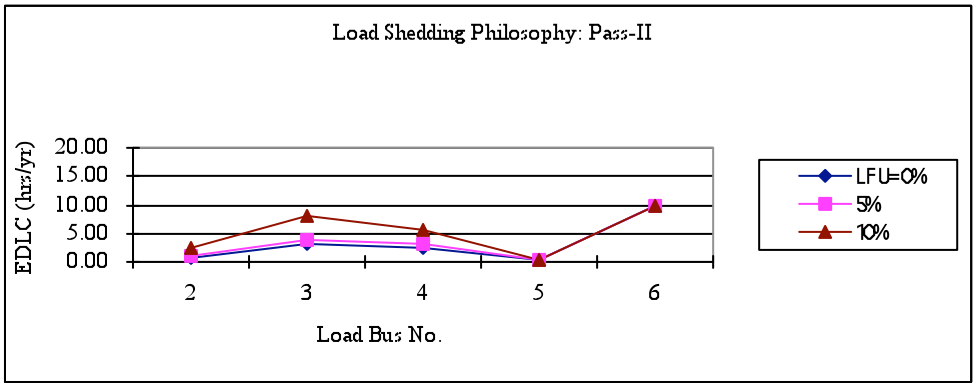

Figure 3.19: The EDLC with LFU at HLII for the RBTS using the Pass-II criterion

The load bus indices with the various LFU for the RBTS using the Priority Order criterion are shown in Figure 3.20.

The Priority Order criterion is based on the IEAR value at each bus. The buses with the lowest IEAR values are curtailed first. The buses in descending IEAR order are bus #2, #5, #4, #6 and #3, where bus #2 has the highest IEAR and bus #3 has the lowest IEAR. Load at bus #3 is curtailed first when load curtailments are required.

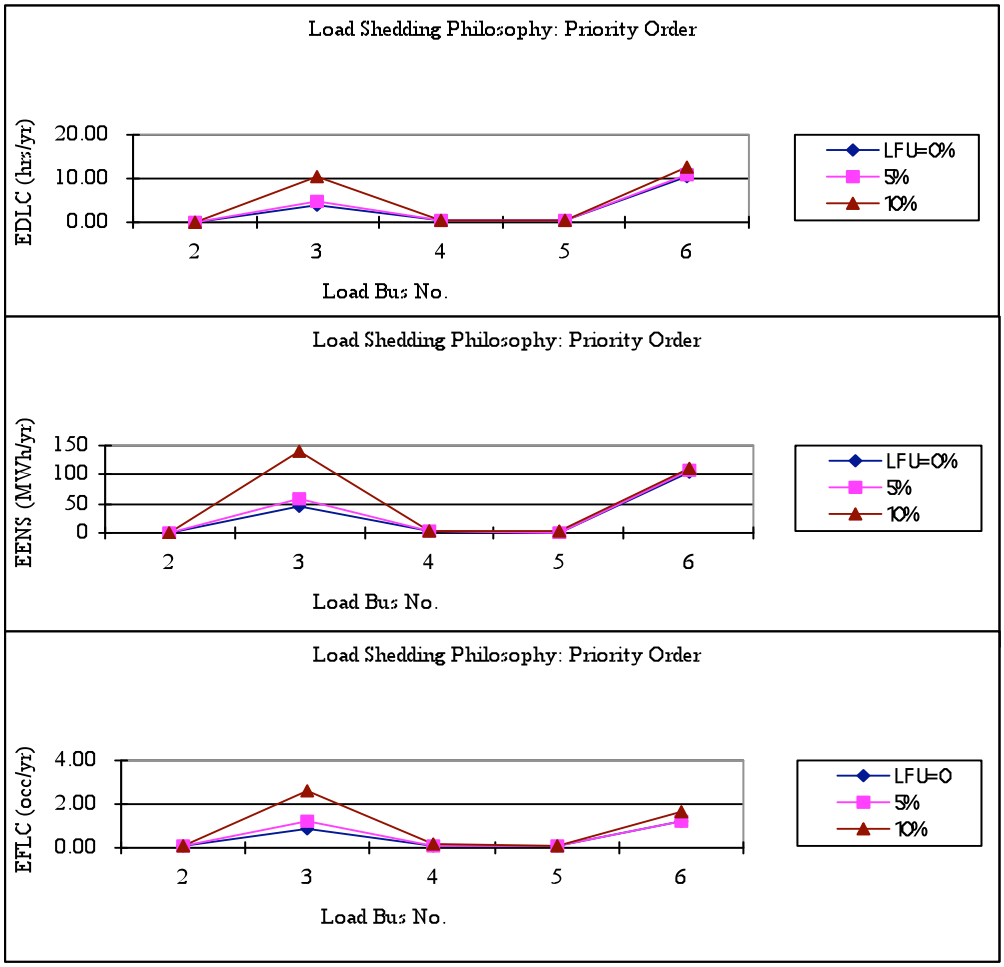

Figure 3.20: The load bus indices with LFU at HLII for the RBTS using the Priority Order criterion

It can be seen from Figure 3.20 that the reliability indices at bus #3 increase significantly compared to the ones when the Pass-I or Pass-II criterion is used as shown in Figures 3.18 and 3.19. The changes in the indices at bus #3 become more considerable with increase in the LFU. The indices at bus #6 increase slightly with increase in the LFU. The changes are slightly more observable than those in Figures 3.18 and 3.19. The changes in the indices for buses #2 and #4 decrease compared to

those in Figures 3.18. The LFU has very little effect on the indices at buses #2, #4 and #5 using the Priority Order criterion since these buses have large IEAR values.

The indices at bus #6 are a large proportion of the total system indices. The single transmission supply to bus #6 dominates the indices at bus #6 and masks the effects of LFU on the system indices and the indices at bus #6.

The load bus EDLC for the different load shedding polices at LFU of 0%, 5% and 10% are shown in Figure 3.21.

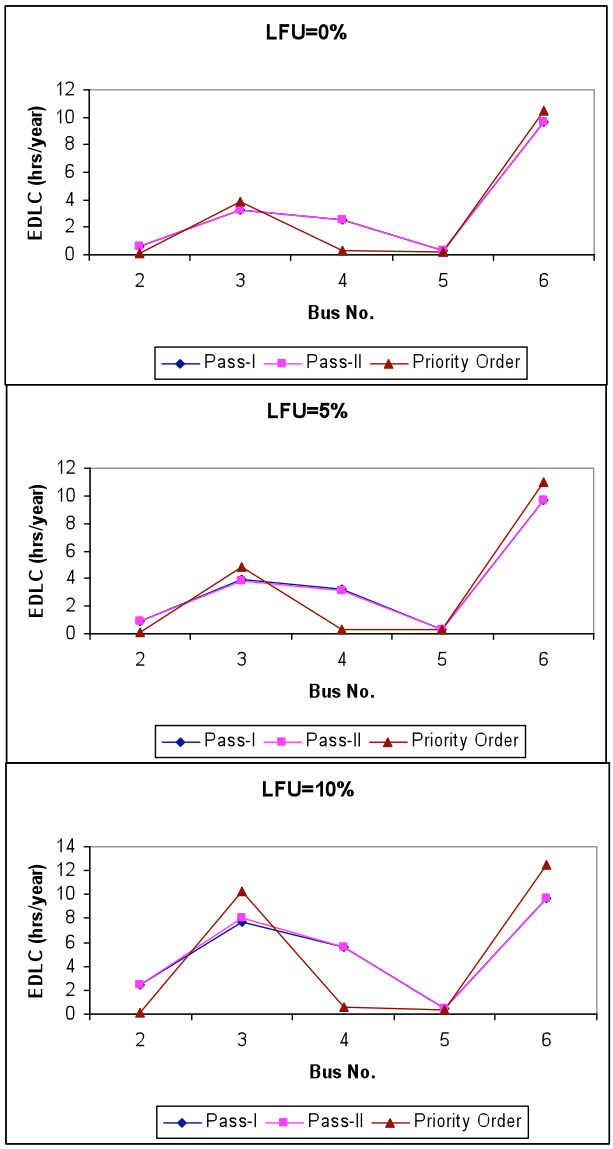

Figure 3.21: The EDLC for the RBTS with different load shedding philosophies

IEEE-RTS results

The load bus indices for the IEEE-RTS with different load shedding philosophies are shown in Figures 3.22 to 3.25.

It can be seen from Figure 3.22 that the increases in the load bus indices are larger when the indices are large. The LFU has larger effects on the buses that are less reliable compared to other buses.

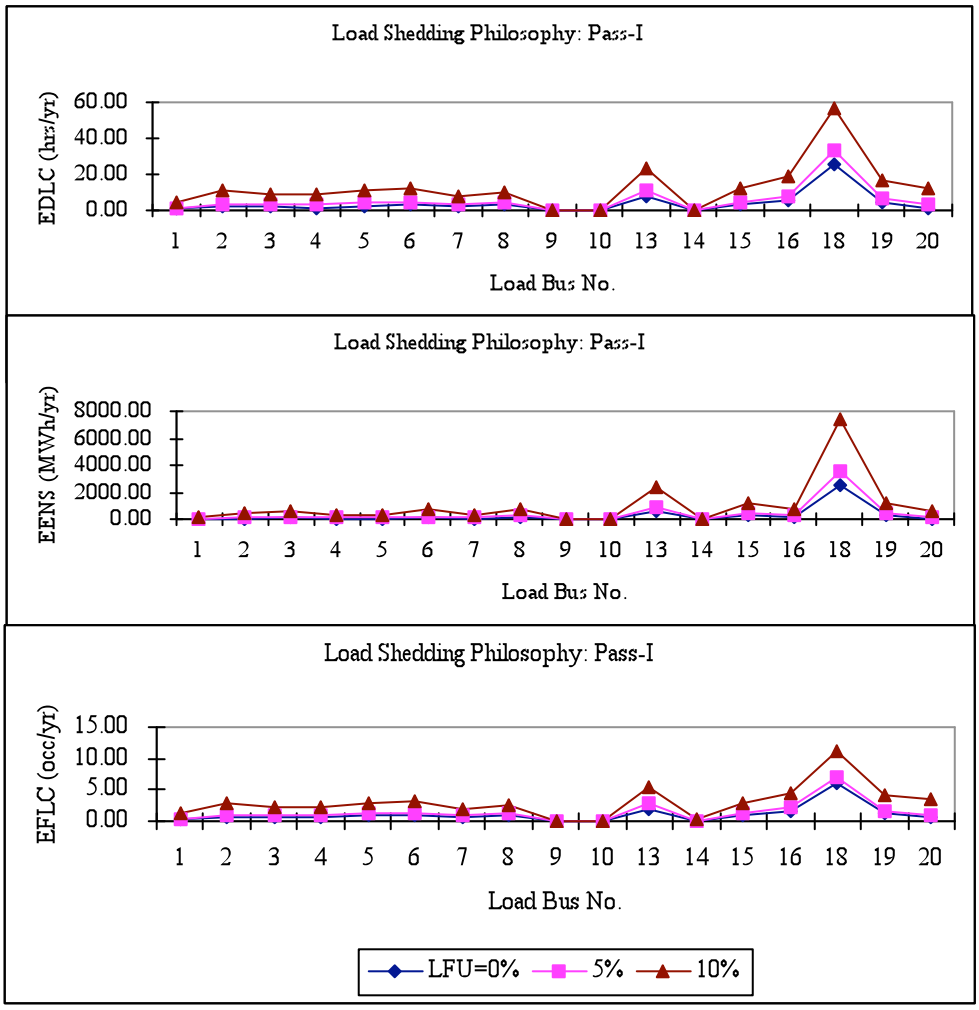

Figure 3.22: The IEEE-RTS load bus indices with LFU at HLII using the Pass-I criterion

Figure 3.23 shows the reliability indices for the IEEE-RTS when the Pass-II policy is used. It can be seen from this figure that the indices and the changes in the indices are similar to those in Figure 3.22. The reliability indices at most buses are close to those in Figure 3.22.

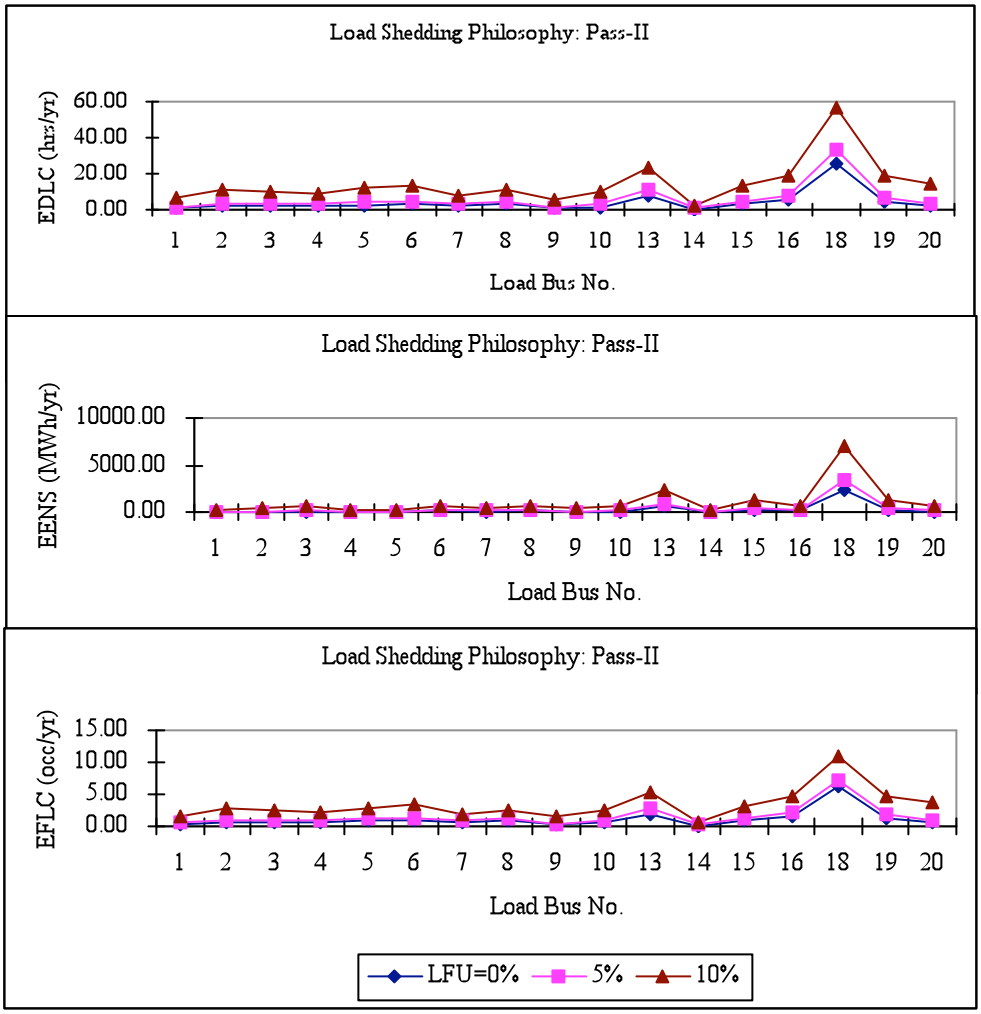

Figure 3.23: The IEEE-RTS load bus indices with LFU at HLII using the Pass-II criterion

Figure 3.24 shows the reliability indices when the Priority Order criterion is used. The buses in ascending IEAR value order are #9, #14, #19, #10, #18, #20, #3, #15, #6, #7, #16, #13, #2, #8, #1, #5, and #4. Loads at bus #9 are curtailed first, followed by loads at bus #14, then bus #19, etc. The load bus indices are quite different from those when the Pass-I or Pass-II criterion is used. It can be seen from Figure 3.24 that the reliability indices at buses #9, #14 and #19 are larger than those at other buses. The changes in the indices are similar, that is, the larger load bus indices increase more significantly with increase in the LFU.

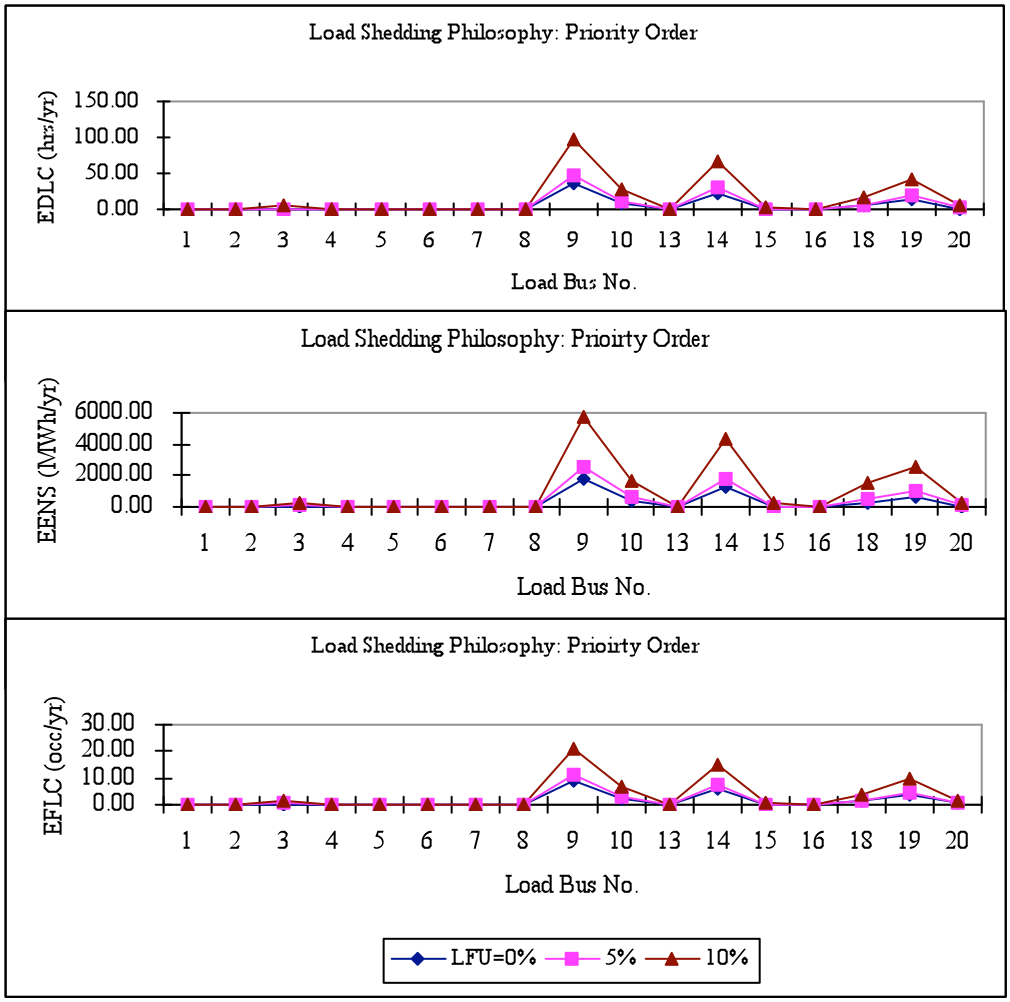

Figure 3.24: The IEEE-RTS load bus indices with various LFU at HLII using the Priority Order criterion

Generally, the load bus indices increase with increase in the LFU. The LFU has larger effects on less reliable buses when these load bus indices are not dominated by the transmission network configuration. If the reliability indices at some buses are mainly due to transmission deficiencies, the LFU may not have significant effects on the indices even if the indices at these buses are large.

The EDLC for the IEEE-RTS with different load shedding philosophies and LFU levels are shown in Figure 3.25.

It can be seen from Figure 3.25 that the load bus indices are similar for most load buses when the Pass-I or Pass-II criterion is used. This is mainly due to the fact that the IEEE-RTS is a transmission strong system. The EDLC at buses #9 and #10 are slightly

different when the Pass-I or Pass-II policy is used. The difference increases when the LFU increases. The changes in the load bus indices are significant when the Priority Order criterion is used. It can be seen from Figure 3.25 that buses #9, #14 and #19 have the largest EDLC compared to the other buses when the Priority Order policy is used, while buses #18 and #13 have the largest EDLC when the Pass-I or Pass-II policies are applied.

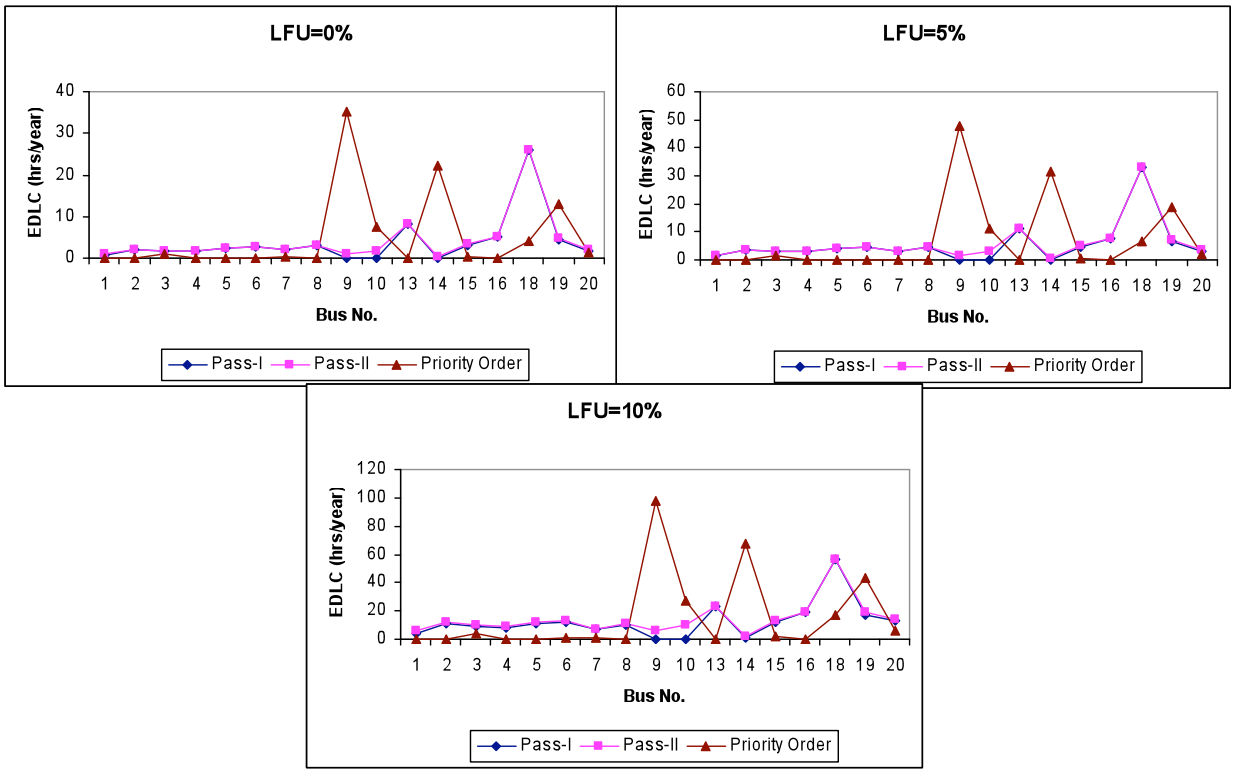

Figure 3.25: The EDLC for the IEEE-RTS with LFU and different load shedding philosophies

System indices give an overall appraisal, but sometimes factors such as the generation composition, the transmission network configuration and the load shedding philosophy mask what is actually happening. Additional information can be obtained by examining the load bus indices at different LFU.

3.5. Effects of Bus Load Correlation on HLII Reliability Evaluation

The bus load correlation is considered to be 100% dependent in Section 3.4. The bus load correlation can have significant effects on the system reliability. In this study,

the Pass-II criterion is used as the load shedding philosophy. Different bus load correlations are considered for both the RBTS and the IEEE-RTS.

The following three levels of bus load correlation for the RBTS and the IEEE-RTS are designated as Case A, Case B and Case C.

Case A: The bus loads are 100% dependent.

Case B: The bus loads are partially correlated as shown in Tables 3.9 and 3.10 for the RBTS and the IEEE-RTS respectively.

Case C: The bus loads are 100% independent.

Table 3.9: Case B bus load correlation for the RBTS

Bus No.	2	3	4	5	6
2	1	0	0	0	0
3	0	1	0.8	0	0
4	0	0.8	1	0	0
5	0	0	0	1	0.8
6	0	0	0	0.8	1

Table 3.10: Case B bus load correlation for the IEEE-RTS

Voltage Level	138 kV	230 kV
138 kV	0.8	0.2
230 kV	0.2	0.4

3.5.1. Effects on the HLII system indices

RBTS results

The system indices for the RBTS with different load bus correlation and LFU are shown in Table 3.11.

Table 3.11: The system indices for the RBTS Cases A, B and C with LFU

	LFU=5%				LFU= 10%			
Cases	PLC	EDLC (hrs/yr)	EENS (MWh/yr)	EFLC (occ/yr)	PLC	EDLC (hrs/yr)	EENS (MWh/yr)	EFLC (occ/yr)
A	0.001640	14.38	168.80	2.02	0.002200	19.25	248.19	3.25
B	0.001570	13.74	157.10	1.85	0.001710	14.94	178.02	2.17
C	0.001590	13.92	156.89	1.83	0.001690	14.76	174.73	2.13

The system indices for the RBTS are also shown in Figure 3.26. It can be seen that the EDLC, EENS and EFLC index profiles are similar for the three bus load

correlation conditions. When the bus loads are 100% dependent, the indices are the largest for the same LFU. When the bus loads are independent, the indices are the smallest. The differences in the indices between cases A and B are larger than those between cases B and C. This is because the bus loads in Case B are not strongly correlated.

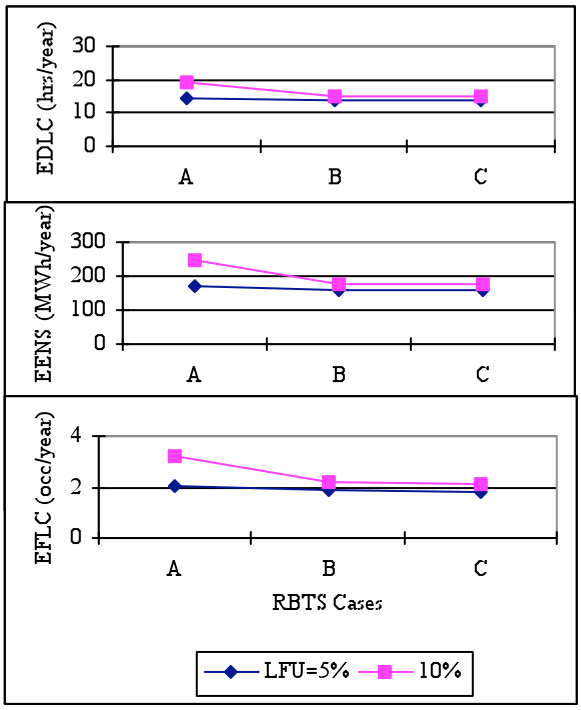

Figure 3.26: The system indices for the RBTS Cases A, B and C with LFU

IEEE-RTS results

The system indices for the IEEE-RTS are shown in Table 3.12. The EDLC, EENS and EFLC for the IEEE-RTS Cases A, B and C are also shown in Figure 3.27.

Table 3.12: The system indices for the IEEE-RTS Cases A, B and C with LFU

	LFU=5%				LFU=10%			
Cases	PLC	EDLC (hrs/yr)	EENS (MWh/yr)	EFLC (occ/yr)	PLC	EDLC (hrs/yr)	EENS (MWh/yr)	EFLC (occ/yr)
A	0.005523	48.43	6717.65	11.44	0.011500	100.76	17545.91	21.13
B	0.004490	39.33	5434.86	9.67	0.006010	52.65	8990.87	12.08
C	0.004170	36.55	4710.05	9.18	0.004470	39.20	5544.23	9.58

It can be seen from Table 3.12 and Figure 3.27 that the system indices increase when the bus loads become more correlated. It can be seen from Table 3.12 that when

the loads are 100% independent, the reliability indices when the uncertainty is 10% are smaller than those when the uncertainty is 5% and the bus load correlation is 100% dependent.

It can also be seen that when the LFU is larger, the bus load correlation has larger effects on the system indices. There is a big decrease in the indices from Case A to Case B when the LFU is 10%. The decrease in the indices from Case B to Case C is relatively small. The general effects of bus load correlation on the system indices are similar for the RBTS and the IEEE-RTS.

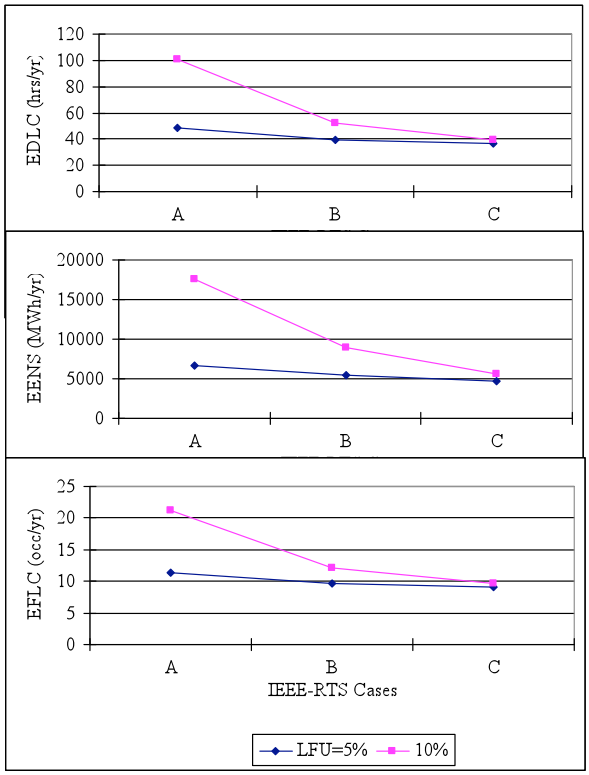

Figure 3.27: The system indices for the IEEE-RTS Cases A, B and C with LFU

3.5.2. Effects on the HLII load point indices

RBTS results

The load bus indices for the RBTS Cases A, B and C with various LFU using different load shedding policies are shown in the following figures.

Figure 3.28 shows the load bus indices when the Pass-I criterion is used. It can be seen from this figure that when the bus loads become more dependent, the LFU has more effect on the load bus indices. When the bus loads are 100% dependent as in Case

A, the indices increase considerably. The differences in the load bus indices are larger between Cases A, B and C when the LFU is 10% than those when the LFU is 5%. For buses #2, #5 and #6, the indices remain almost unchanged for the three cases under the 5% and 10% LFU conditions.

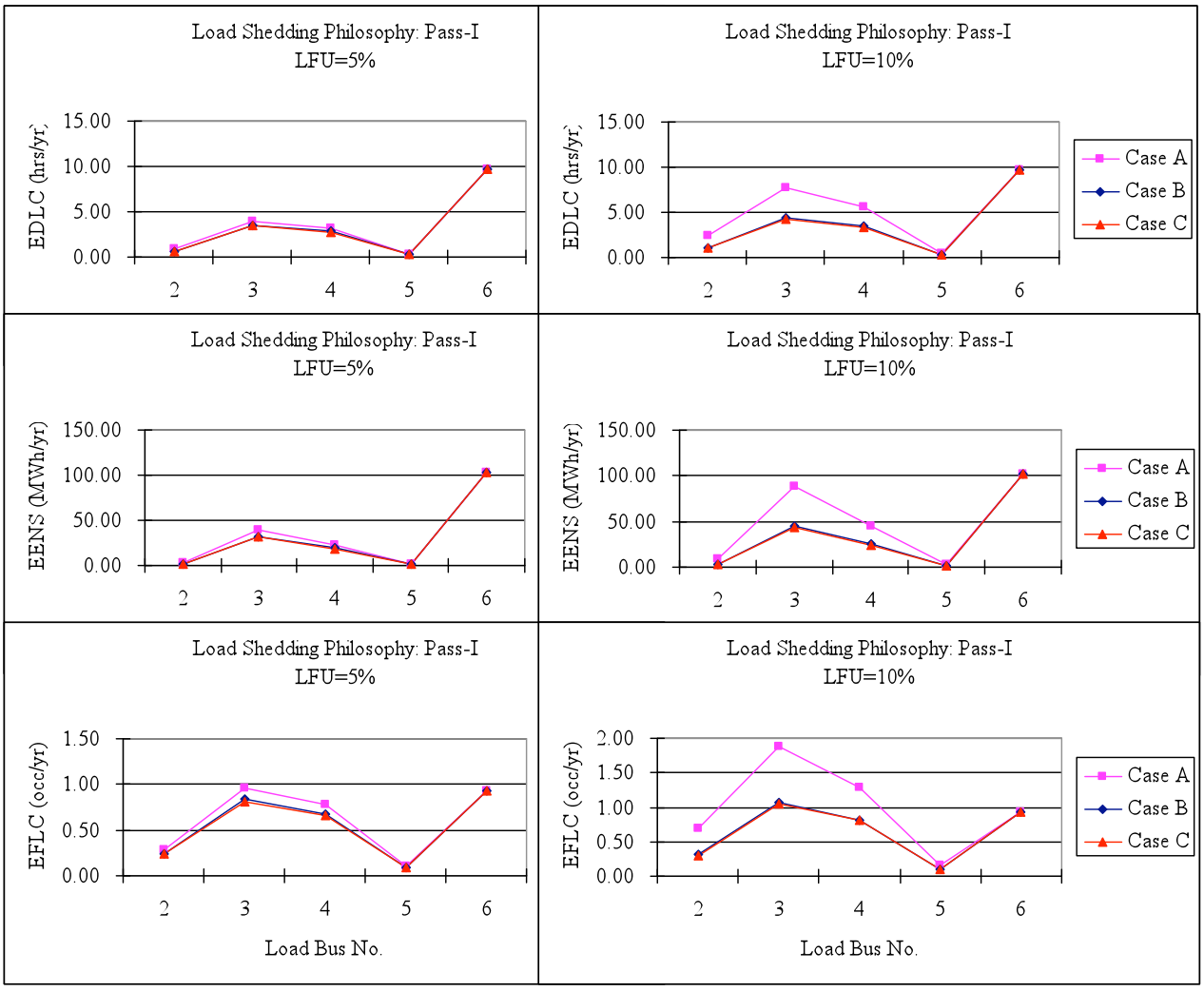

Figure 3.28: The load bus indices for the RBTS cases with LFU, using the Pass-I criterion

The load bus indices when the Pass-II criterion is used are similar to the Pass-I results. Figure 3.29 only shows the EDLC of each load bus. Figure 3.30 shows the load bus indices for the RBTS cases using the Priority Order load shedding policy. When the Priority Order criterion is used, the load bus indices change only slightly with bus load correlation when the LFU is 5%. When the LFU increases to 10%, the indices at bus 3 change significantly for Cases A and B.

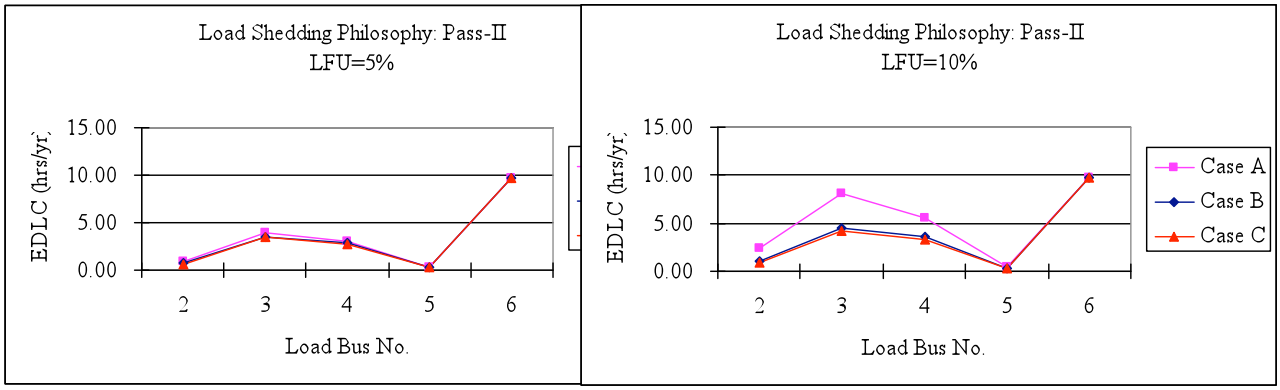

Figure 3.29: The EDLC for the RBTS cases with LFU, using the Pass-II criterion

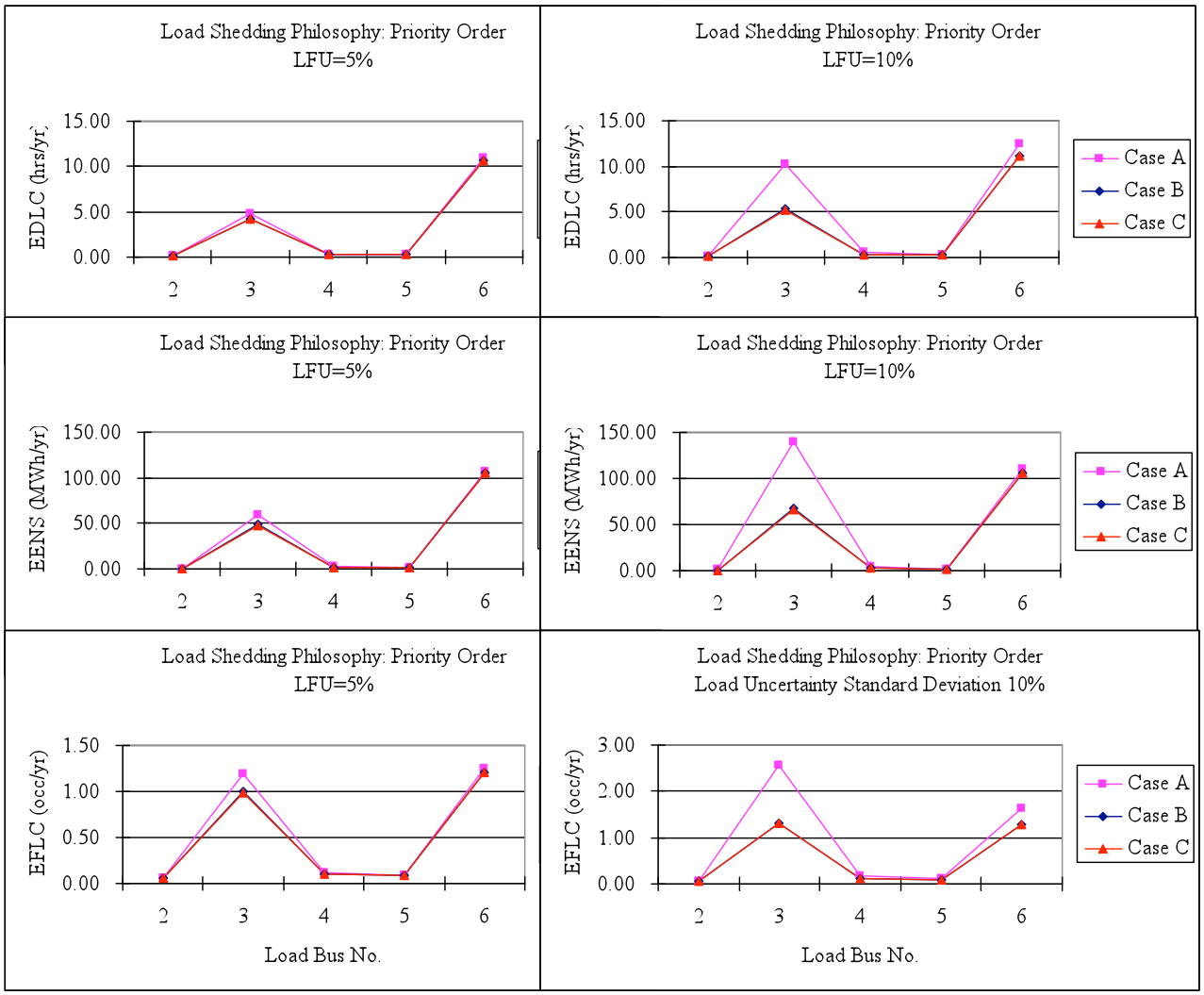

Figure 3.30: The load bus indices for the RBTS cases with LFU using the Priority Order criterion

IEEE-RTS results

The load bus indices for the IEEE-RTS with different bus load correlation when the LFU is 5% are shown in Figure 3.31. It can be seen from Figure 3.31 that the load bus indices do not change significantly in this situation. An LFU of 5% creates only small changes in the total system indices as shown in Figure 3.27. Buses #13 and #18, at which the indices are larger than at the other buses, are more affected by bus load correlation than the other buses.

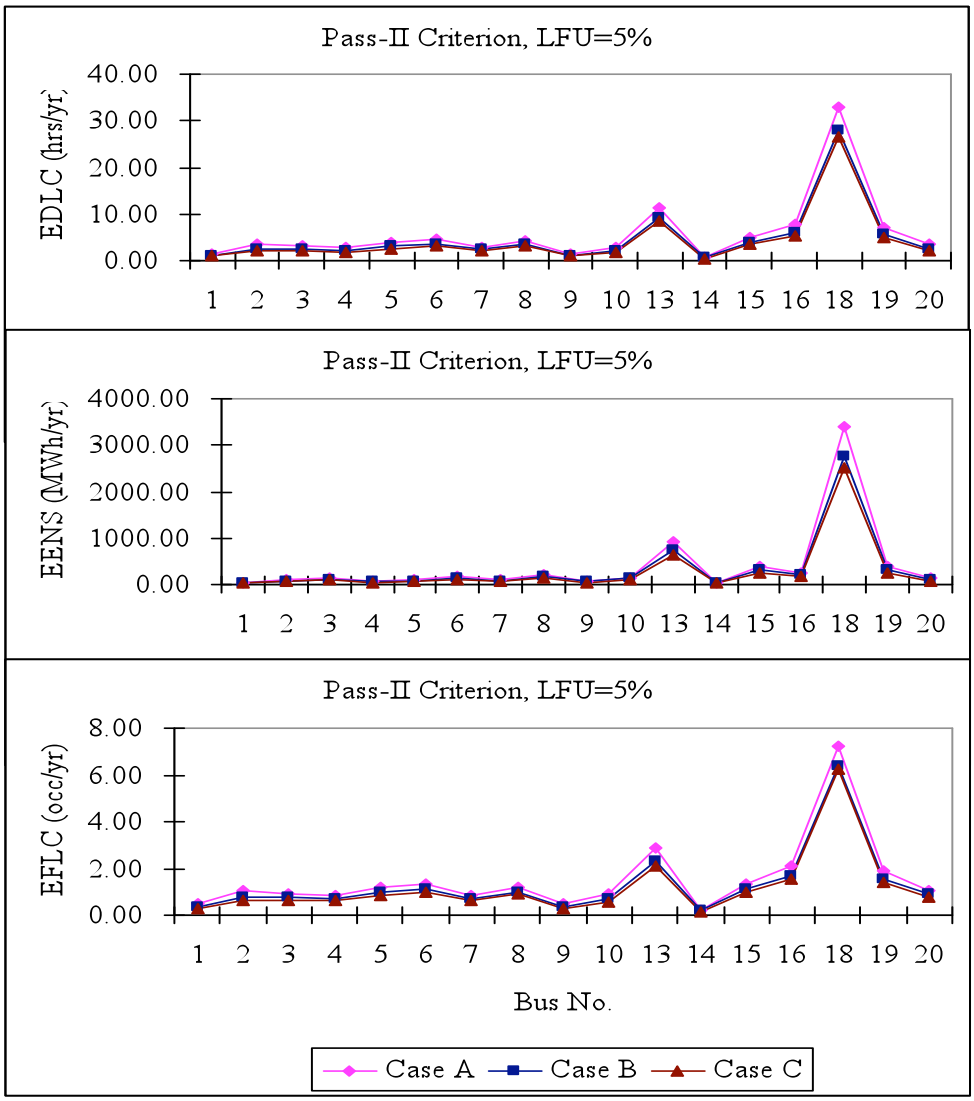

Figure 3.31: The load bus indices for the IEEE-RTS Cases A, B and C, LFU=5%, using the Pass-II criterion

The load bus indices when the LFU is 10% are shown in Figure 3.32. It can be seen that in this case, the differences between the indices are more considerable than those with an LFU of 5%.

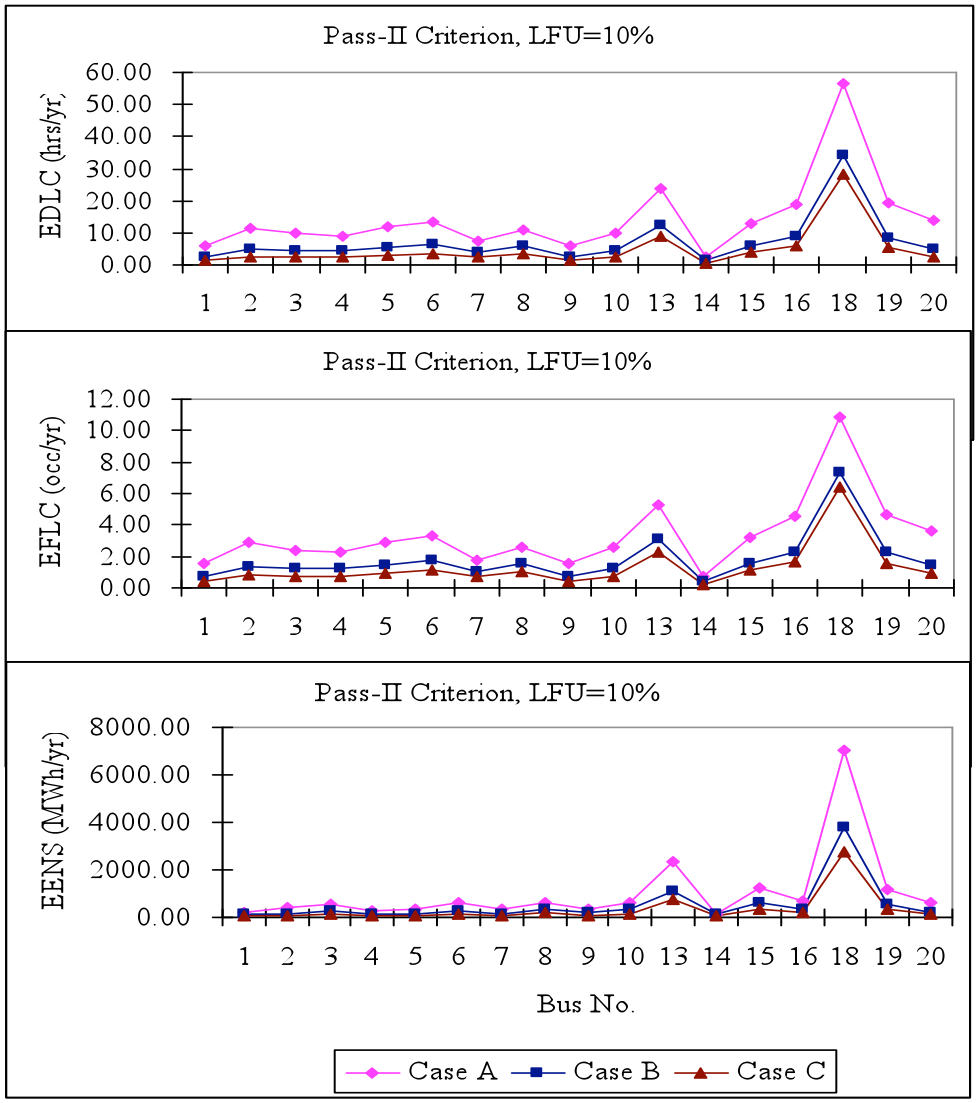

Figure 3.32: The load bus indices for the IEEE-RTS Cases A, B and C, LFU=10%, using the Pass-II criterion

Bus load correlation affects both the system indices and the load bus indices. The stronger the correlation between buses, the more considerable are the effects on the reliability indices. The effects of bus load correlation on system indices and load bus indices increase when the LFU increases. The bus load correlation affects the indices at each load bus differently as load bus indices are also affected by the composite system

network configuration. The impacts of bus load correlation on the load bus indices also change with the load shedding philosophy.

3.6. Effects of Load Forecast Uncertainty on HLII Reliability Evaluation with Different Network Configurations

In this study, the RBTS and the IEEE-RTS were modified to create generation deficient or transmission deficient systems and the effects of the LFU and bus load correlation on different network configurations are examined. The Pass-II policy was used.

3.6.1. Study Cases

RBTS Cases

The original RBTS system was modified and is designated as Cases 1 to 4 in Table 3.13.

Table 3.13: The modified RBTS Cases

Cases	Modifications of the RBTS
Case 1	RRBTS described in Chapter 2
Case 2	Add 1*20 MW units at bus #1 to Case 1
Case 3	Add 3*20 MW units at bus #1 to Case 1
Case 4	Add line 11 between buses #1 and #3 to Case 3

IEEE-RTS Cases

The original IEEE-RTS has a strong transmission network and a weak generation system. The IEEE-RTS was modified as follows to examine the effects of LFU on reliability indices with different network configurations. The different cases are shown in Table 3.14.

Table 3.14: The modified IEEE-RTS Cases

Cases	Modifications of the IEEE-RTS
Case 1	Double the generation at buses #16, #18, #21, #22 and #23, a total of 12 units are added. The total installed capacity is 5320 MW. The peak load is 4132.13 MW, which is 1.5 times of the original value.
Case 2	Case 1, Change the transfer capacity of all the transmission lines to 70% of their original values.

3.6.2. RRBTS Results

The system indices at a peak load of 179.28 MW are shown in Table 3.15. A comparison of the results in Tables 3.3 with Table 3.15 shows that the reliability indices decrease significantly when a line is added between buses #5 and #6. The increase in the reliability indices for the original and reinforced RBTS cases at a peak load of 179.28 MW with increase in LFU when the load correlations are considered to be 100% dependent are shown in Table 3.16.

It can be seen from Table 3.16 that the increases in the reliability indices are slightly larger in the RRBTS at LFU of 5% and 10% even though the reliability indices for the RRBTS are much smaller than those of the RBTS. The original RBTS has a transmission deficiency, as load bus #6 is supplied by a single line. The load bus indices at bus #6 are a large portion of the total system indices for the original RBTS. The bus #6 indices are mainly determined by the failure of transmission line #9. The LFU does not significantly affect the indices at bus #6. When a line is added between buses #5 and #6, the transmission system becomes relatively strong. The effect of transmission failure does not dominate the load bus indices at bus #6 as in the original RBTS. The LFU affects the resulting indices at bus #6 in the RRBTS more and therefore causes a larger increase in the total system indices.

Table 3.15: The system indices for the RRBTS with LFU, peak load = 179.28 MW

	0%	LFU=5%			LFU=10%		
Indices		Case A	Case B	Case C	Case A	Case B	Case C
EDLC (hrs/yr)	3.66	4.70	4.08	3.96	10.51	5.44	4.95
EENS (MWh/yr)	44.91	61.05	50.60	48.42	148.53	72.85	64.62
EFLC (occ/yr)	0.81	1.12	0.94	0.91	2.60	1.30	1.18
ECOST (k$/yr)	188.31	246.44	208.99	201.07	537.21	285.05	258.52

Table 3.16: The increase in the system indices for the RBTS and the RRBTS with LFU, peak load =179.28 MW

	RBTS			RRBTS		
LFU	EDLC Increase (hrs/yr)	EENS Increase (MWh/yr)	EFLC Increase (occ/yr)	EDLC Increase (hrs/yr)	EENS Increase (MWh/yr)	EFLC Increase (occ/yr)
0	0	0	0	0	0	0
5%	1.02	15.88	0.30	1.03	16.13	0.31
10%	5.90	95.27	1.52	6.85	103.62	1.79

The system indices for the RRBTS when the peak load is 188.24 MW and 197.21 MW are shown in Tables 3.17 and 3.18 respectively.

Table 3.17: The system indices for the RRBTS with LFU, peak load = 188.24 MW

	LFU=0%	LFU=5%			LFU=10%		
Indices		Case A	Case B	Case C	Case A	Case B	Case C
EDLC (hrs/yr)	7.43	9.72	8.13	8.02	23.04	11.83	10.77
EENS (MWh/yr)	100.91	135.84	112.15	110.21	356.24	166.64	152.24
EFLC (occ/yr)	1.81	2.41	1.94	1.91	5.41	2.91	2.68
ECOST (k$/yr)	398.80	518.53	437.19	431.36	1206.51	610.61	565.78

It can be seen from Tables 3.15, 3.17 and 3.18 that the reliability indices increase significantly with increase in the peak load. The increase in the reliability indices also becomes more significant with increase in the LFU.

Table 3.18: The system indices for the RRBTS with LFU, peak load = 197.21 MW

	LFU=0%	LFU=5%			LFU=10%		
Indices		Case A	Case B	Case C	Case A	Case B	Case C
EDLC (hrs/yr)	14.98	21.81	16.73	16.47	44.83	24.98	23.33
EENS (MWh/yr)	216.02	312.02	243.31	238.06	746.35	365.17	338.42
EFLC (occ/yr)	3.21	5.70	4.11	4.03	9.84	6.27	5.89
ECOST (k$/yr)	814.36	1120.96	901.18	883.85	2433.02	1271.02	1193.64

Figure 3.33 shows the increase in the EDLC (hrs/yr) for the RRBTS considering LFU compared with that of the RRBTS at the LFU of 0%. Cases A, B and C represent 100% dependent, partially correlated and 100% independent load correlations as in Section 3.5.

It can be seen from Figure 3.33 that when the peak load increases, the LFU has more effect on the system reliability indices. Case A affects the system indices the most while Case C affects them the least for the same LFU and at the same peak load level.

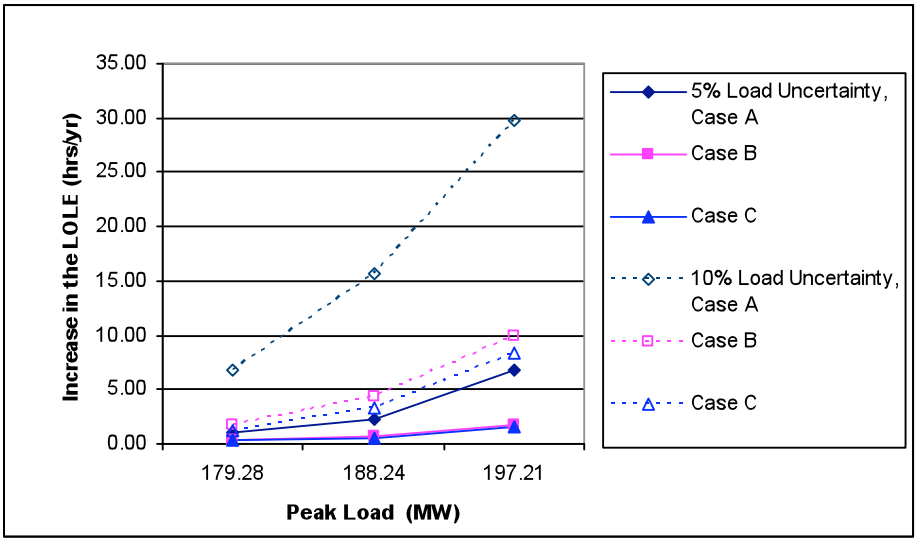

Figure 3.33: Increase in the EDLC for the RRBTS considering LFU and bus load correlation

Generation deficient systems

The RRBTS becomes generation deficient when the peak load is 197.21 MW. An additional 20 MW unit is added to bus #1 in Case 2. The system in Case 2 has adequate generation at this load level. The bus load correlation is considered to be 100% dependent. The reliability indices for the RRBTS are shown in Table 3.15. The indices for the RBTS Case 2 are shown in Table 3.19.

Table 3.19: The system indices for RBTS Case 2 with LFU, peak load = 197.21 MW

Indices	LFU		
	0%	5%	10%
EDLC (hrs/yr)	4.35	5.92	12.00
EENS (MWh/yr)	47.49	71.79	179.66
EFLC (occ/yr)	1.22	1.60	3.01
ECOST (k$/yr)	184.18	255.64	568.15

It can be seen that the reliability indices decrease in the RBTS Case 2 because of the added generating unit. The increases in the system indices with increase in the LFU for the two systems are shown in Table 3.20.

It can be seen from Table 3.20 that the increases in the system indices are larger for the generation deficient system. The LFU has a significant effect in a generation

deficient system when the system indices are not dominated by a specific generator or transmission deficiency.

Table 3.20: The increase in the system indices for the RRBTS and RBTS Case 2 with LFU, peak load = 197.21 MW

	RBTS Case 2			RRBTS (Generation deficient)		
LFU	EDLC Increase (hrs/yr)	EENS Increase (MWh/yr)	EFLC Increase (occ/yr)	EDLC Increase (hrs/yr)	EENS Increase (MWh/yr)	EFLC Increase (occ/yr)
0	0	0	0	0	0	0
5%	1.58	24.30	0.38	6.83	96.00	2.49
10%	7.66	132.18	1.80	29.85	530.33	6.63

Transmission deficient systems

The peak load was increased by 20% for the configuration in RBTS Case 3. The peak load is now 215.14 MW and the total installed capacity is 300 MW. There is 84.86 MW of capacity reserve. The system has considerable generation but the transmission system is under considerable stress. The utilization of Lines #1 and #6 is approximately 85% of the line rating at the system peak load condition. Failure of one of these parallel lines will cause overload on the other line, which may cause load curtailment. RBTS Case 3 is a transmission deficient system. A line is added between buses #1 and #3 in RBTS Case 4 which alleviates the stress faced by lines #1 and #6.

The reliability indices for RBTS Cases 3 and 4 are shown in Table 3.21. The reliability indices drop significantly from RBTS Case 3 to Case 4 because of the added transmission line between buses #1 and #3.

Table 3.21: The system indices for RBTS Cases 3 and 4 with LFU, peak load = 215.14 MW

Indices	RBTS Case 4			RBTS Case 3 (transmission deficient)		
	0%	5%	10%	0%	5%	10%
EDLC (hrs/yr)	0.33	0.51	1.78	6.93	7.18	8.76
EENS (MWh/yr)	3.96	6.60	27.30	72.81	90.90	149.00
EFLC (occ/yr)	0.10	0.16	0.52	1.79	1.73	2.06
ECOST (k$/yr)	15.43	23.90	81.77	199.52	251.50	420.29

The increase in the system indices due to the consideration of LFU for RBTS Cases 3 and 4 are shown in Table 3.22.

Table 3.22: The increases in the system indices for RBTS Cases 3 and 4 with LFU, peak load = 215.14 MW

LFU	RBTS Case 4			RBTS Case 3 (transmission deficient)		
	EDLC Increase (hrs/yr)	EENS Increase (MWh/yr)	EFLC Increase (occ/yr)	EDLC Increase (hrs/yr)	EENS Increase (MWh/yr)	EFLC Increase (occ/yr)
0%	0	0	0	0	0	0
5%	0.18	2.64	0.06	0.26	18.09	-0.06
10%	1.45	23.34	0.42	1.83	76.19	0.26

The increases in the system indices for Case 4 are smaller than for Case 3. The LFU has larger effects on a transmission deficient system than on a transmission sufficient system as long as the system indices are not dominated by a specific transmission deficiency.

The LFU has different effects on the system reliability indices of different network configurations. Generally, LFU has more significant effects on the reliability indices when the system is generation deficient or transmission deficient. In some cases, if the deficiency itself is a main cause of load curtailment, then the effects of LFU on the reliability indices can be masked. It can be seen from the results for the original RBTS and RRBTS that the increases in the reliability indices are larger in the RRBTS than in the RBTS even though the RRBTS is a more reliable system than the RBTS.

3.6.3. IEEE-RTS Results

Generation deficient system

The original IEEE-RTS is a generation deficient system and the reliability indices for the IEEE-RTS with changing LFU are shown in Table 3.4. The reliability indices for the IEEE-RTS Case 1 (Table 3.14) with LFU are shown in Table 3.23. The peak load is 4132.13 MW and the bus load correlation is considered to be 100% dependent.

Table 3.23: The IEEE-RTS Case 1 system indices with LFU, peak load = 4132.13 MW

Indices	LFU		
	0%	5%	10%
EDLC (hrs/yr)	13.49	20.32	50.28
EENS (MWh/yr)	3363.28	5355.40	16672.29
EFLC (occ/yr)	3.83	5.46	12.16
ECOST (k$/yr)	10354.31	15269.59	42177.25

This system has considerable reserve generating capacity and the system reliability indices are considerably lower than those shown in Table 3.4 for the basic IEEE-RTS. When the LFU is 0% and 5%, the EDLC and EFLC are less than half the IEEE-RTS values. When the LFU is 10%, the EDLC and EFLC for the IEEE-RTS Case 1 are approximately half of those in the original case. The EENS does not decrease as much as the EDLC and EFLC.

The increases in the reliability indices for the two systems attributable to LFU are shown in Table 3.24.

Table 3.24: The reliability index increases for the IEEE-RTS and IEEE-RTS Case 1 with LFU, peak load = 4132.13 MW

	IEEE-RTS Case 1			Original IEEE-RTS		
LFU	EDLC Increase (hrs/yr)	EENS Increase (MWh/yr)	EFLC Increase (occ/yr)	EDLC Increase (hrs/yr)	EENS Increase (MWh/yr)	EFLC Increase (occ/yr)
0	0	0	0	0	0	0
5%	6.83	1992.12	1.63	13.04	2369.22	2.43
10%	36.79	13309.01	8.33	64.80	12463.57	12.24

It can be seen from this table that the increases in the reliability indices for the original IEEE-RTS are larger than those for the modified IEEE-RTS. This is because the original system is generation deficient and the LFU creates more stress on this system than on the modified system.

Transmission deficient systems

In Case 2, the load carrying capabilities of the transmission lines in the IEEE-RTS Case 1 are changed to 70% of their original values. The transmission system in the IEEE-RTS Case 2 is now weak. The load correlation is considered to be 100%.The

reliability indices for the IEEE-RTS Case 2 at a peak load of 4132.13 MW with different LFU are shown in Table 3.25.

Table 3.25: The IEEE-RTS Case 2 reliability indices with LFU, peak load = 4132.13 MW

Indices	LFU	
	0%	5%
EDLC (hrs/yr)	48.18	55.63
EENS (MWh/yr)	12655.20	15377.36
EFLC (occ/yr)	11.24	12.71
ECOST (k$/yr)	40711.53	47617.54

The system reliability indices for the IEEE-RTS Case 2 are considerably higher than those of the IEEE-RTS Case 1 because of the deficient transmission system.

The increases in the reliability indices attributable to LFU for the two systems are shown in Table 3.26.

Table 3.26: The increase in the system indices for the IEEE-RTS Cases 1 and 2 with LFU, peak load = 4132.13 MW

	IEEE-RTS Case 2			IEEE-RTS Case 1		
LFU	EDLC Increase (hrs/yr)	EENS Increase (MWh/yr)	EFLC Increase (occ/yr)	EDLC Increase (hrs/yr)	EENS Increase (MWh/yr)	EFLC Increase (occ/yr)
0%	0	0	0	0	0	0
5%	7.45	2722.16	1.47	6.83	1992.12	1.63

It can be seen that the increases in the EDLC and EENS are larger for the IEEE-RTS Case 2 than for Case 1. The increase in the EFLC in the IEEE-RTS Case 2 is smaller than in Case 1. The IEEE-RTS Case 1 is considerably more reliable than the IEEE-RTS Case 2 as shown by the relative EDLC and EENS values. The impact on the EFLC due to LFU is diminished when the duration of load curtailment increases significantly in the IEEE-RTS Case 2 analysis. The LFU has a more significant effect on the reliability indices of generation or transmission deficient systems than on balanced systems.

3.7. Conclusion

The reliability of an electric power system decreases with increase in the LFU. The effect of LFU on HLI and HLII indices are different. The relative index changes at HLI are larger than those at HLII for the RBTS. In the IEEE-RTS, the HLII indices change more than the HLI indices do with increase in the LFU. The reliability index probability distributions are also affected by LFU. The standard deviations and the ranges of the reliability index probability distributions increase with increasing LFU. The LFU creates considerable variability in the system reliability performance.

In general, the load bus indices increase with increase in LFU. The LFU tends to have a relatively large effect on less reliable buses whose reliability indices are not dominated by the transmission network configuration. If the reliability indices at some buses are mainly due to a transmission deficiency, the LFU might not have a significant effect on the indices even when the indices at these buses are large. System indices provide an overall appraisal but sometimes factors such as generating unit conditions, transmission network topology and bus load curtailment strategies mask what is actually happening inside the system. In this case, bus indices can provide some interesting and valuable insight.

Bus load correlation affects both the system indices and the load bus indices. The stronger the correlation between buses, the more considerable are the effects on the reliability indices. The effects of bus load correlation on system indices and load bus indices increase when the LFU increases. Bus load correlation affects the individual load bus indices in different ways as the load bus indices are also influenced by the composite system network configuration and the load curtailment strategy. Different load shedding philosophies do not significantly affect the system reliability indices determined under different degrees of load bus correlation. The impacts of load correlation on load bus indices can vary considerably, however, with changes in the load shedding philosophy. The load bus indices at bus #6 in the RBTS do not change significantly with LFU and bus load correlation when the Pass-I, Pass-II and Priority Order load shedding criteria are used.

Generally, the LFU has a larger effect on generation or/and transmission deficient systems than on systems with strong generation and transmission networks.

Exceptions can occur when the system indices are dominated by a particular generation or transmission deficiency, in which case, the effects of LFU may be masked.

CHAPTER 4

EFFECTS OF WIND POWER

4.1. Introduction

Wind is regarded as an important alternative to traditional electric power generating sources as it is clean and does not diminish with use. The continuous development of wind energy technologies since the 1980's has resulted in wind turbines with high availability at a relatively low price [48]. Wind energy is one of the lowest-priced renewable energy technologies available today. The interest in the utilization of wind power as a renewable energy source has been increasing considerably worldwide for the last two decades due to the enhanced public awareness of the environment.

There are a number of utility and governmental initiatives. One of these is an energy policy known as the Renewable Portfolio Standard (RPS) [100]. The RPS is a flexible, market-driven policy. Acceptance of the RPS is a commitment to produce a specified percentage of the total power generated from renewable sources by a certain date. Most of this renewable energy will come from wind as other renewable sources are not as suitable for bulk power generation at this time. The total installed wind capacity in Canada is now approximately 1.5 GW, which is about 1% of the total electric power generation. The Canadian Wind Energy Association (CanWEA) has committed itself to a specific target of 10,000 MW of wind power capacity by 2010, which requires an annual growth rate of 60% [49]. Many US states and Canadian provinces have agreed to generate between 5% to 25% of their electrical power from renewable energy sources by 2010-2015.

The integration of renewable energy sources and particularly wind power into existing electric power systems dominated by conventional generating sources introduces many technical and business challenges for the next generation of power systems. The major challenge in using wind as a source of power is that the wind is intermittent and is not always available when the electric power is needed, which is

quite different from the characteristics of the more conventional energy sources. Increasing penetration of wind power introduces significant impacts on power system reliability, and security analyses become more uncertain due to the unpredictable nature of wind power. One important technical challenge is to incorporate wind power reliability considerations in the reliability assessment techniques presently used by electric power utilities to assess the adequacy of the overall generating capacity to serve the future load requirements. The development of comprehensive reliability evaluation techniques will become even more important as wind power penetration levels continue to increase in the near future.

A large number of studies incorporating wind power in generating system reliability evaluation (Hierarchical Level I (HLI)) assessment have been conducted [47, 102, 107]. Relatively little work has been done on composite generation and transmission system (Hierarchical Level II (HLII)) reliability assessment incorporating wind power and particularly in the well-being framework [101]. The following research is focused on examining the impacts of wind power on system reliability in HLII well-being analysis. The interactive effects of wind power and LFU on system reliability are also shown. Planning studies incorporating wind power are performed and the system reinforcement alternatives are compared using reliability cost/worth analysis in the well-being framework. The HLI and RapHL-II programs were modified to incorporate wind in the well-being analysis framework. The RBTS and the IEEE-RTS are used as study systems and the conventional system reliability indices, load point indices and well-being indices are used to illustrate the effects of wind energy and the interactive effects of wind power and LFU on system reliability.

4.2. Methodology to Incorporate Wind power

The sequential Monte Carlo simulation method as described in Chapter 2 is used for the HLI and HLII reliability evaluation. The methods used to incorporate wind power in the simulation process and to perform the well-being analysis are described in this section.

4.2.1. Methodology

A wind energy conversion system (WECS) model consists of two main parts, the wind speed model and the wind turbine generator (WTG) model [102, 103]. The time varying wind speed can be predicted using an autoregressive moving average (ARMA) time series. The nonlinear relationship between the power output of the WTG and the wind speed can be described by the operating parameters of the WTG. Three commonly used parameters are the cut-in, rated and cut-out wind speeds. The power produced by a wind turbine generator (WTG) at a particular site is highly dependent on the wind regime at that location.

Appropriate wind speed data are therefore essential elements in the creation of a suitable WTG model. The actual data for a site or a statistical representation created from the actual data can be used in the model. A site located at Regina in Saskatchewan, Canada has a wind speed mean and standard deviation of 19.52 km/h and 10.99 km/h respectively. The hourly mean and standard deviation of wind speeds from an 8-year database (1996 to 2003) for this location were obtained from Environment Canada. An optimal Auto-Regressive Moving Average Model (ARMA) time series model, ARMA (4,3), was built using these data [104] as shown in Equation (4.1).

$$\begin{aligned} y_t &= 0.9336y_{t-1} + 0.4506y_{t-2} - 0.5545y_{t-3} + 0.1110y_{t-4} \\ &\quad +\alpha_t - 0.2033\alpha_{t-1} - 0.4684\alpha_{t-2} + 0.2301\alpha_{t-3} \end{aligned} \tag{4.1}$$

$$\alpha_t \in NID(0, 0.409423^2)$$

The simulated wind speed SW_t can be calculated from Equation (4.2) using the wind speed time series model.

$$SW_t = \mu_t + \sigma_t * y_t \tag{4.2}$$

where

μ_t: the mean observed wind speed at hour t;

σ_t: the standard deviation of the observed wind speed at hour t;

$\{\alpha_t\}$ is a normal white noise process with zero mean and the variance 0.409423^2.

The mean and standard deviation of the wind speed at the Swift Current site are 19.46 km/h and 9.7 km/h respectively. The ARMA (4,3) model for the Swift Current site and the parameters are shown in Equation (4.3):

$$y_t = 1.1772y_{t-1} + 0.1001y_{t-2} - 0.3572y_{t-3} + 0.0379y_{t-4} + \alpha_t - 0.5030\alpha_{t-1} - 0.2924\alpha_{t-2} + 0.1317\alpha_{t-3} \quad (4.3)$$

$$\alpha_t \in NID(0, 0.524760^2)$$

The ARMA(3,2) model for Saskatoon site are shown in Equation (4.4):

$$y_t = 1.5047y_{t-1} - 0.6635y_{t-2} + 0.1150y_{t-3} + \alpha_t - 0.8263\alpha_{t-1} + 0.2250\alpha_{t-2} \quad (4.4)$$

$$\alpha_t \in NID(0, 0.447423^2)$$

The nonlinear relationship between the power output and the wind speed is shown in Figure 4.1.

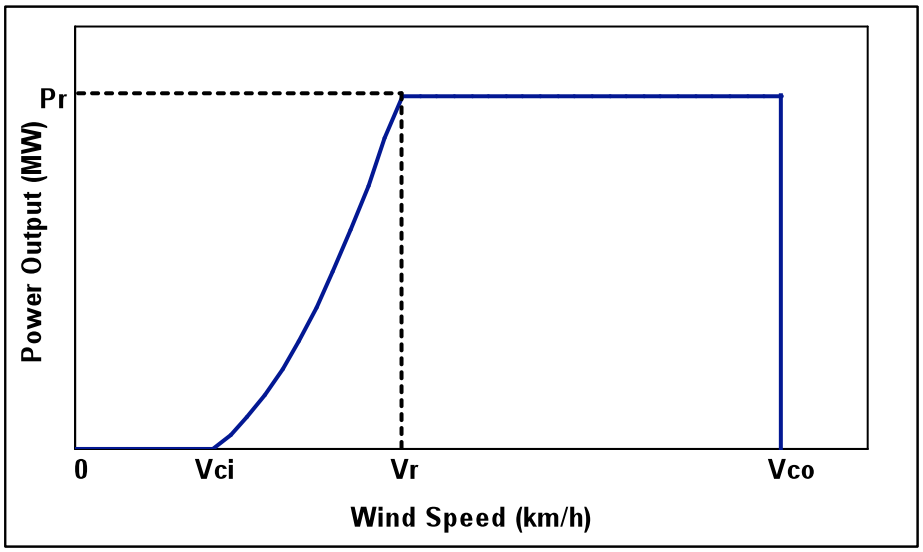

Figure 4.1: Wind turbine generator power curve

The hourly power output can be calculated from the obtained wind speed using Equation (4.5).

$$P(SW_t) = \begin{cases} 0 & 0 \le SW_t < V_{ct} \\ (A + B * SW_t + C * SW_t^2) * P_r & V_{ci} \le SW_t < V_r \\ P_r & V_r \le SW_t < V_{co} \\ 0 & SW_t \ge V_{co} \end{cases} \quad (4.5)$$

where V_{ci}, V_r and V_{co} are the cut-in, rated and cut-out speed respectively.

P_r is the rated power output of the wind turbine generator.

The constant A, B and C are as shown in Equation (4.6) [104].

$$A = \frac{1}{(V_{ci} - V_r)^2} \left\{ V_{ci}(V_{ci} + V_r) - 4V_{ci}V_r \left[\frac{V_{ci} + V_r}{2V_r} \right]^3 \right\}$$

$$B = \frac{1}{(V_{ci} - V_r)^2}\left\{4(V_{ci} + V_r)\left[\frac{V_{ci} + V_r}{2V_r}\right]^3 - (3V_{ci} + V_r)\right\}$$

$$C = \frac{1}{(V_{ci} - V_r)^2}\left\{2 - 4\left[\frac{V_{ci} + V_r}{2V_r}\right]^3\right\} \quad (4.6)$$

4.2.2. Wind speed correlation considerations

Section 4.2.1 briefly describes the simulation of wind power output using an ARMA model. When more than one wind site is considered, the effect of wind speed correlation between wind farms should be included. It is a reasonable assumption that wind speeds are independent when the distance between the wind sites are very large. When the wind farms are in close proximity, there will be different degrees of wind speed correlation. The technique used in this research to correlate wind speed time series in wind speed simulation models is presented in this section.

The wind speed correlation between two wind sites can be calculated using the cross-correlation index [105, 106] R_{xy} as in Equation (4.7).

$$R_{xy} = \frac{\frac{1}{n}\sum_{i=1}^{n}(x_i - \mu_x)(y_i - \mu_y)}{\sigma_x \sigma_y} \quad (4.7)$$

Where

R_{xy}: the cross-correlation coefficient,

x_i and y_i: the elements of the first and second wind speed time series,

μ_x and μ_y: the mean values of the first and second wind speed time series,

σ_x and σ_y: are the standard deviations of the first and second wind speed time series,

n: the number of points in the time series.

The wind speed time series is calculated using the auto-regressive moving average (ARMA) time series model described in Section 4.2.1. The ARMA model includes two parts, the auto-regressive (AR) and the moving average (MA) segments. The AR segment involves lagged terms in the time series, which are wind speeds from previous hours. The MA segment involves lagged terms in the noise or residuals, which

are random, independent and normally distributed. The wind speed correlation between multiple wind sites can be adjusted by selecting appropriate seeds for the random numbers used in the MA model.

If the wind speed time series for two wind sites are simulated from a single random number seed at the same time, the wind speed time series at the two wind sites will be highly correlated. If the wind speed time series for the two wind sites are produced using two independent random number seeds, the simulated wind speeds will be uncorrelated. Highly independent and highly dependent wind speeds at various locations can be generated using this procedure. The level of correlation between two or more wind sites can be adjusted by selecting random number seeds as mentioned earlier. Assume there are two wind sites A and B and the correlation coefficient between the two wind sites is "C". Let the random number seed for wind site A be "X" and the uniformly distributed random numbers be X_i. The task now is to determine an initiating value (seed) at each hour for the second wind site B so that the wind speed correlation coefficient between the two wind sites A and B is "C". The initiating value (seed) at each hour for wind site B is a proportional value of the uniformly distributed X_i at each hour (mX_i). A trial process can be used to determine a suitable "m" that results in a correlation of "C".

The process used to incorporate the simulation of wind power output and the wind speed correlation between multiple wind farms in the analysis software is presented in the following section.

4.2.3. Modification of the HLI and HLII programs

The process to incorporate wind power and wind speed correlation considerations in the HLI and HLII reliability evaluation programs are shown in Figure 4.2 using a block diagram. The simulation of the wind speed and the wind power output are added to the simulation process right after Step 2 in Figure 2.1.

Well-being analysis for a system with wind power is similar to the procedure shown in Figure 2.2.

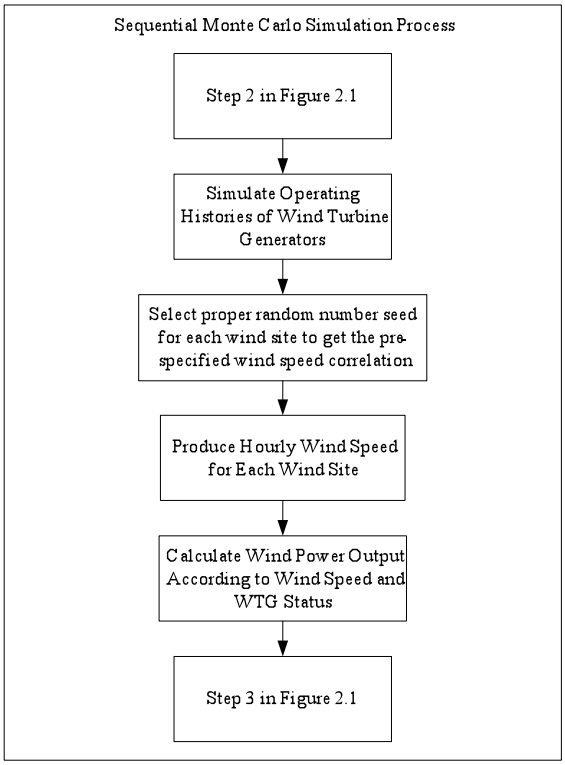

Figure 4.2: Block diagrams to incorporate wind power in the HLI and HLII sequential simulation program

The difference is in the selection of the largest generating unit capacity. When there are wind turbine generators (WTG) in the system, all the WTG at one wind site are considered as one unit as each WTG at a given wind site can lose its generation at the same time due to the wind speed condition. The HLI and HLII programs were modified accordingly and applied to the RBTS and the IEEE-RTS to investigate the effects of wind power on HLI and HLII reliability evaluation and the results are shown in the following sections. The studies are extended to examine the impacts on reliability indices and reliability cost worth assessments in the HLII security constrained framework due to wind power injecttions in a bulk electric system.

4.3.Effects of Wind Power Additions on HLI Reliability Evaluation

Wind power behaves quite differently from conventional generating units in that it is highly dependent on the site wind regime. Wind power has different effects on system reliability compared to those of the conventional generating units. The modified

HLI program was applied to the RBTS and the effects of wind power on HLI reliability indices are illustrated in the following.

The original load model is used for the RBTS at a peak load of 185 MW. Various amounts of wind power are added to the RBTS and the added wind capacity is considered to be either completely dependent or fully independent. The site wind regimes for each wind farm addition are completely correlated when the site wind regimes are dependent and there is zero correlation when the site wind regimes are independent. These conditions may not exist in an actual system and there will be some degree of cross-correlation between the site wind regimes. The dependent and independent conditions provide boundary values that clearly indicate the effects of site wind speed correlation. The Regina wind site data is used in this study. The sampling size for the RBTS is 40,000 years.

4.3.1. Effects of wind power addition on HLI reliability indices

The LOLE and the LOEE for the RBTS with wind capacity additions from one 10 MW to five 10 MW injections [107] are illustrated pictorially in Figure 4.3.

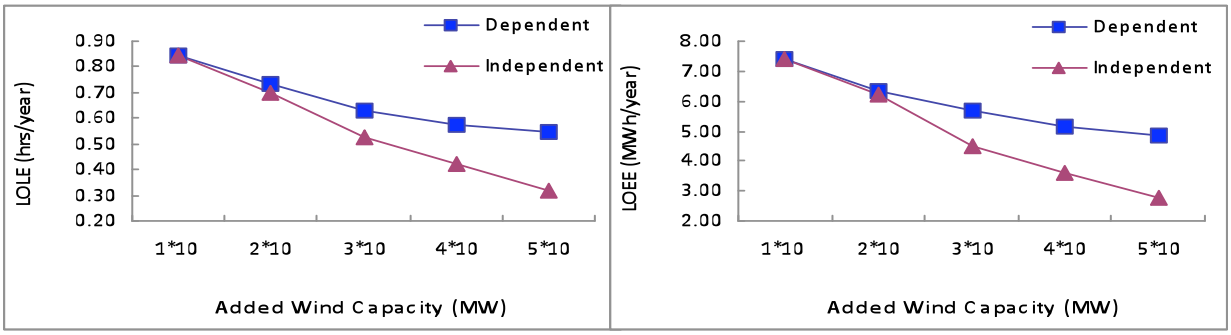

Figure 4.3: The RBTS LOLE and LOEE with successive wind power additions

The LOLE and LOEE for the RBTS at HLI are 1.09 hrs/yr and 9.85 MWh/yr respectively as shown in Table 2.3. It can be seen from Figure 4.3 that the LOLE and LOEE decrease with increase in the wind power. The LOLE and LOEE are significantly lower when the 10 MW wind sites are independent than when they are dependent. When the wind regimes are dependent, the LOLE and LOEE decrease significantly with the addition of the first and second 10 MW wind farm. The reduction in risk decreases considerably as the third, fourth and fifth 10 MW wind farms are added. The system risk

becomes saturated when the wind power additions reach a certain level. This is not the case when the site wind regimes are independent. Saturation will occur but at much higher wind power levels. The LOLE and LOEE graphs are very similar in form. The system reliability benefits associated with wind capacity additions are the highest when the site wind regimes are independent, and decrease as the degree of site wind regime correlation increases.

4.3.2. Increases in peak load carrying capability due to adding wind power to the RBTS

The addition of wind power provides the system with the ability to satisfy a higher peak load while maintaining the system reliability criterion. The following studies examine the RBTS reliability indices with various wind power additions at different peak load levels with dependent and independent site wind regimes. The increase in the peak load carrying capability (IPLCC) attributable to each wind capacity addition is illustrated.

The RBTS LOEE as a function of the peak load with successive wind power additions are shown in Figure 4.4 assuming dependent or independent site wind regimes. The LOLE at each peak load level with increase in the wind capacity changes similarly to that of the LOEE and is not shown here.

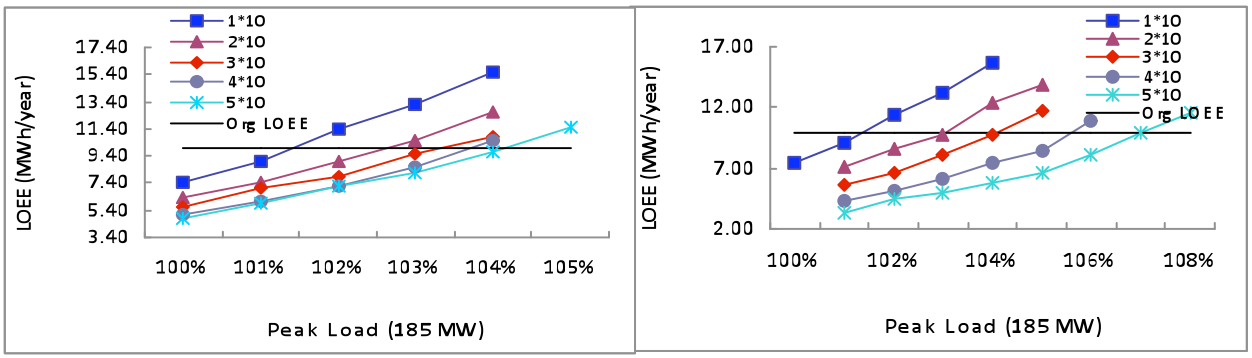

(Dependent site wind regimes) (Independent site wind regimes)

Figure 4.4: The RBTS LOEE as a function of the peak load with successive wind power additions

The LOEE at each peak load level decreases with increase in the wind capacity and increases with increase in the peak load for each wind power capacity condition

considering dependent or independent site wind regimes. The horizontal lines in Figure 4.4 are the criterion LOEE for the RBTS prior to adding wind power of 9.8531 MWh/yr given in Table 2.3. Figure 4.4 shows that the separation (IPLCC) between the individual risk profiles decreases as 10 MW increments of wind power are added when the wind regimes are dependent. The separation between the individual risk profiles with the successive wind power addition is relatively constant when the wind regimes are independent, which indicates that the system risk is not yet saturated due to the added wind power.

Figure 4.5 shows the RBTS IPLCC attributable to each wind capacity addition based on the LOLE and LOEE criterion risk levels. The IPLCC of each added wind farm decreases as additional wind capacity is added when the site wind regimes are dependent. When the wind regimes are independent, the IPLCC for each wind capacity addition tends to decrease slightly. There is an obvious exception, however, where the IPLCC of the third wind site capacity addition is smaller than the values for the fourth and fifth additions.

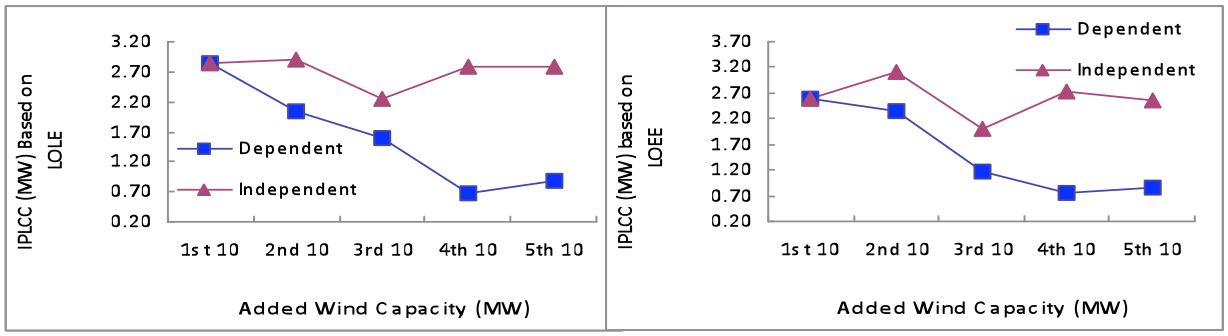

Figure 4.5: The RBTS IPLCC as a function of the added capacity based on LOLE and LOEE

The RBTS IPLCC associated with successive wind power additions tends to decrease with each addition. The decrease in the IPLCC is relatively insignificant for independent wind regimes, but as shown in Figure 4.5, can be substantial for dependent wind regime situations.

The IPLCC associated with a wind capacity addition is the increase in load carrying capability that can be attributed to this addition. The IPLCC is therefore the wind farm Capacity Credit (CC). The values used to plot Figure 4.5 are given in Tables

4.1 and 4.2 as a percentage of the added capacity, These tables also show the Capacity Credit associated with the aggregate wind capacity added to the system.

Tables 4.1 and 4.2 show that the capacity credit directly associated with each added increment of wind power decreases significantly when the site wind regimes are dependent. This situation could occur when multiple wind farms are located in close proximity to each other or when a single wind farm is expanded by adding more wind capacity. The incremental capacity credit is relatively constant when the site wind speeds are independent.

Table 4.1: The RBTS Wind Capacity Credit (CC) with sequential wind power additions based on the LOLE

Wind Capacity (MW)	Wind Regimes		Wind Capacity (MW)	Wind Regimes	
	Dependent	Independent		Dependent	Independent
	CC(%)	CC(%)		CC(%)	CC(%)
0	0	0	0	0	0
1*10	28.58	28.58	10	28.58	28.58
2*10	20.44	28.92	20	24.51	28.75
3*10	16.06	22.63	30	21.69	26.71
4*10	6.79	27.78	40	17.97	26.98
5*10	8.92	27.79	50	16.16	27.14

Table 4.2: The RBTS Wind Capacity Credit (CC) with sequential wind power additions based on the LOEE

Wind Capacity (MW)	Wind Regimes		Wind Capacity (MW)	Wind Regimes	
	Dependent	Independent		Dependent	Independent
	CC(%)	CC(%)		CC(%)	CC(%)
0	0	0	0	0	0
1*10	25.78	25.78	10	25.78	25.78
2*10	23.52	31.07	20	24.65	28.43
3*10	11.64	19.96	30	20.31	25.61
4*10	7.62	27.19	40	17.14	26.00
5*10	8.46	25.46	50	12.84	25.89

Tables 4.1 and 4.2 also show that the aggregate capacity credit associated with adding additional dependent wind site capacity decreases as the aggregated capacity increases. This is directly related to the saturation effect seen in Figure 4.3. The aggregated capacity credit remains relatively constant when the site wind regimes are independent. As noted earlier, the dependent and independent site wind regime results

provide lower and upper bound capacity credit limits. The results for similar studies including wind farm correlation will lie between these two bounds. A comparison of Tables 4.1 and 4.2 indicates that the wind capacity credit values obtained using the LOLE and LOEE criterion risk levels are very similar. The aggregated capacity credit, which contains a smoothing effect by successively averaging the incremental contributions, is lower when the LOEE values are used.

Similar studies have been done by adding one to five 10 MW conventional generating units to the RBTS. The RBTS IPLCC based on the LOLE and LOEE are shown in Figure 4.6. The IPLCC for each 10 MW generating capacity addition is approximately 11 MW, which is higher than the actual unit capacity. This is because the added units are much smaller than the capacity of the largest unit (40 MW) in the RBTS and therefore have a small positive effect on the overall system reliability. There is very little difference between the IPLCC values obtained using the LOLE and LOEE indices. It can be seen that the relationship between the IPLCC and the aggregate added capacity is almost linear.

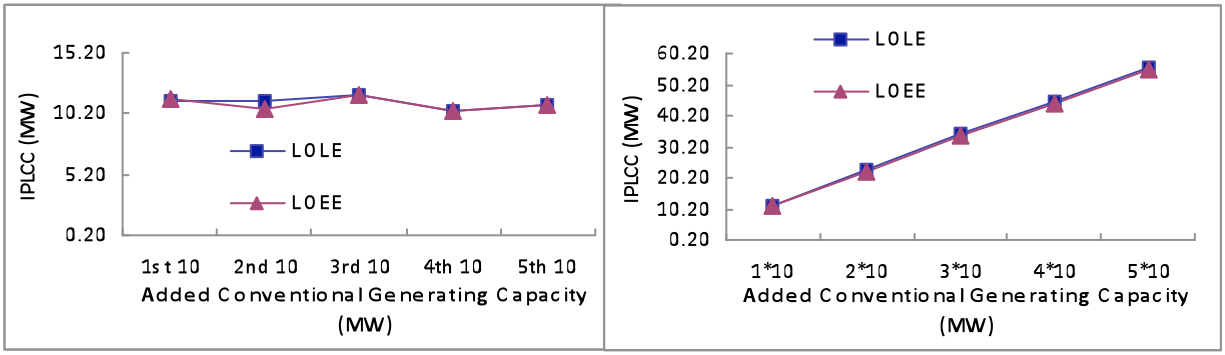

(individual added conventional capacity) (aggregated added conventional capacity)

Figure 4.6: The RBTS IPLCC as a function of the added conventional capacity based on the LOLE and LOEE

Similar studies have been done on the IEEE-RTS by adding wind power and conventional generating capacity. The capacity credit values of the wind power added to the IEEE-RTS are different from those of the RBTS. The results also indicate that there is saturation in the effects of wind power on system reliability with the increase in the wind penetration level. System reliability can be improved by adding generating capacity. The actual benefits are dependent on a number of factors that include the

composition of the existing generating system and the type of units to be added. As shown in Section 4.3.1 and 4.3.2, the effects on the system reliability and the resulting reliability benefits of adding conventional generating units and wind generated capacity are quite different. The capacity credit values shown in Tables 4.1 and 4.2 are therefore system and data specific. The capacity credit attributable to the addition of wind power to a system is fundamentally different to that associated with the addition of conventional generating capacity. This is largely due to the fact that power systems are usually designed to minimize the likelihood of multiple generating unit failures and that conventional generating unit outages are therefore considered to be independent events. The power output of each wind turbine generator in a wind farm, however, is dependent and directly linked to the wind speed at the site and there will be no power output from the farm if the wind speed drops below the cut-in speed. This relationship extends to the power output from dependent wind farms. The studies clearly indicate the effects of dependent and independent wind site regimes. The considerable difference between the capacity credit and benefits associated with dependent and independent site wind regimes clearly indicates the need to determine and incorporate the correlation between the existing and proposed wind farms as utilities and governments pursue higher wind penetration levels.

4.4. Effects of Wind Power on Conventional HLII Reliability Evaluation

In Section 4.3, the HLI indices for the RBTS with wind power addition considering dependent and independent wind speed regimes are investigated. The studies provide boundary values for the effects of wind speed correlation. The effects of wind speed correlation on HLII reliability evaluation are examined in this section.

4.4.1. Effects of wind speed correlation on HLII reliability evaluation

Two 20 MW wind farms using the Regina and Swift Current wind data were added to the RBTS and the RRBTS at bus #4 and the two study systems are designated as RBTSW and RRBTSW. Wind speed correlation levels of 0.94, 0.75, 0.48, 0.25 and 0.05 are considered. A wind speed correlation of 0.94 indicates that the wind speeds for the two sites are basically dependent and a correlation of 0.05 indicates that the wind speeds are basically independent. The modified load model is used in these studies.

The RapHL-II program was used to perform the analysis. The Pass-II criterion was used as the load shedding philosophy. The sampling size is 8,000 years and the resulting coefficient of variation is less than 4%.

Effects on HLII reliability indices

The HLII reliability indices for the RBTSW with wind addition when the wind speeds are dependent or independent are shown in Table 4.3.

Table 4.3: HLII indices for the RBTSW at various wind speed correlation levels

Correlation Levels	EDLC (hrs/yr)	EENS (MWh/yr)	EFLC (occ/yr)
0.94	11.70	130.14	1.53
0.05	11.35	125.58	1.46
Decrease in the reliability indices from Correlation of 0.94 to 0.05	0.35	4.56	0.07

It can be seen from Table 4.3 that the reliability indices for the two wind speed correlation levels are quite close. The relative decreases in the EDLC, EENS and EFLC are 2.99%, 3.50% and 4.80% respectively when the correlation decreases from 0.94 to 0.05, which indicates that wind speed correlation does not significantly affect the reliability indices for the RBTSW.

The HLII reliability indices for the RRBTSW at various wind speed correlation levels are shown in Table 4.4.

Table 4.4: HLII indices for the RRBTSW with wind speed correlation

Correlation Levels	LOLP	EDLC (hrs/yr)	EENS (MWh/yr)	EFLC (occ/yr)
0.94	0.000228	2.00	22.56	0.64
0.75	0.000220	1.92	21.38	0.62
0.48	0.000209	1.83	20.11	0.59
0.25	0.000191	1.68	18.37	0.56
0.05	0.000189	1.66	18.18	0.54
Decrease in the reliability indices from Correlation of 0.94 to 0.05	0.000039	0.34	4.38	0.10

It can be seen by comparing Tables 4.3 and 4.4 that the decreases in the reliability indices from a correlation level of 0.94 to 0.05 for the RRBTSW are similar to those for the RBTSW. The relative decreases in the EDLC, EENS and EFLC when the

correlation decreases from 0.94 to 0.05 of 16.95%, 19.42% and 14.98% respectively for the RRBTSW are considerably larger than the ones for the RBTSW. The transmission network is reinforced in the RRBTS by adding one line between buses #5 and #6. The reliability indices for the RRBTS are not dominated by the transmission deficiency in the RBTS. Although the absolute values of the decreases in the reliability indices are similar, wind speed correlation has more a significant effect on the system reliability in the RRBTSW than in the RBTSW. Wind speed correlation can have considerable effects on the system reliability at HLII when the system reliability is not dominated by transmission deficiencies.

Effects on load carrying capability

The effective load carrying capability (ELCC) at HLII with wind turbine generating unit additions can be determined in a similar manner to that used earlier at HLI. Different reliability indices have different responses to wind capacity additions. The wind speed correlation levels can also affect the load carrying capability. The RRBTSW is used in this study. The EDLC and EFLC for the RRBTS at a peak load of 179.28 MW are 3.66 (hrs/yr) and 0.81 (occ/yr) respectively. The EDLC and EFLC for the RRBTSW at different peak load levels considering wind speed correlation are shown in Table 4.5.

Table 4.5: HLII reliability indices for RRBTSW at various peak load levels

Peak Load (MW)	Wind Speed Dependent		Wind Speed Independent	
	EDLC (hrs/yr)	EFLC (occ/yr)	EDLC (hrs/yr)	EFLC (occ/yr)
179.28	2.00	0.64	1.66	0.54
181.07	2.32	0.73	1.93	0.62
182.88	2.68	0.85	2.25	0.70
184.71	3.11	0.98	2.63	0.82
186.56	3.60	1.15	3.05	0.95
188.43	4.17	1.32	3.53	1.10
190.31	4.81	1.52	4.09	1.26
192.21	5.54	1.74	4.72	1.45

The ELCC with respect to the EDLC and EFLC with the addition of two 20 MW wind farms when wind speeds are dependent or independent are shown in Figures 4.7 and 4.8. The criterion values in Figures 4.7 and 4.8 are the EDLC and EFLC for the RRBTS at the peak load of 179.28 MW respectively.

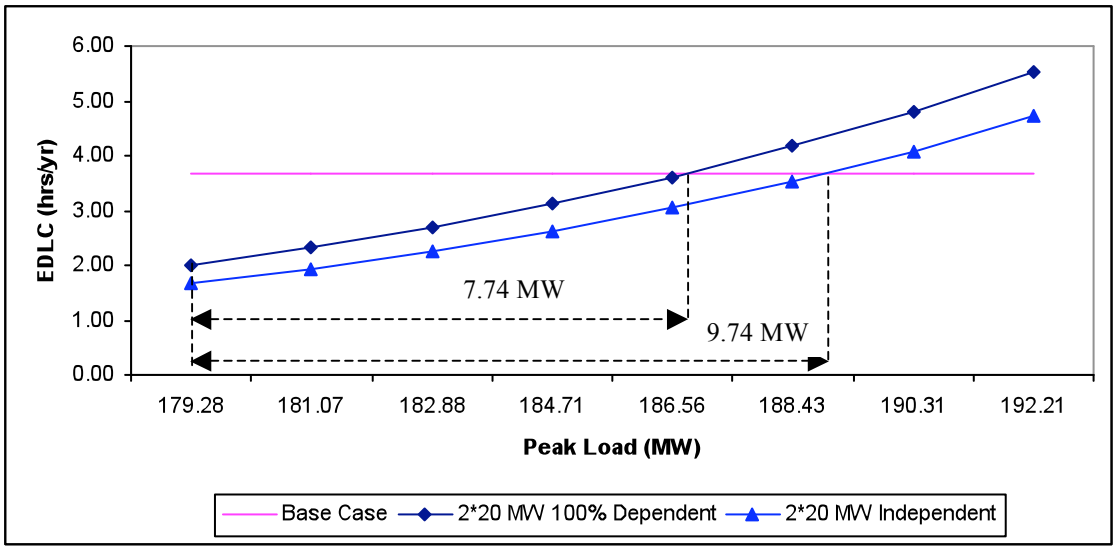

Figure 4.7: The ELCC based on the EDLC for the RRBTSW considering wind speed correlation

Figure 4.7 shows that the ELCC based on the EDLC is 7.74 MW when the two wind sites are dependent. When the wind speeds are independent, the ELCC increases to 9.74 MW. In Figure 4.8, the ELCC based on the EFLC are 3.08 MW and 5.25 MW when the wind speeds are dependent or independent respectively. The ELCC increases with decrease in the wind speed correlation. The ELCC based on the EDLC is quite different from that obtained using the EFLC.

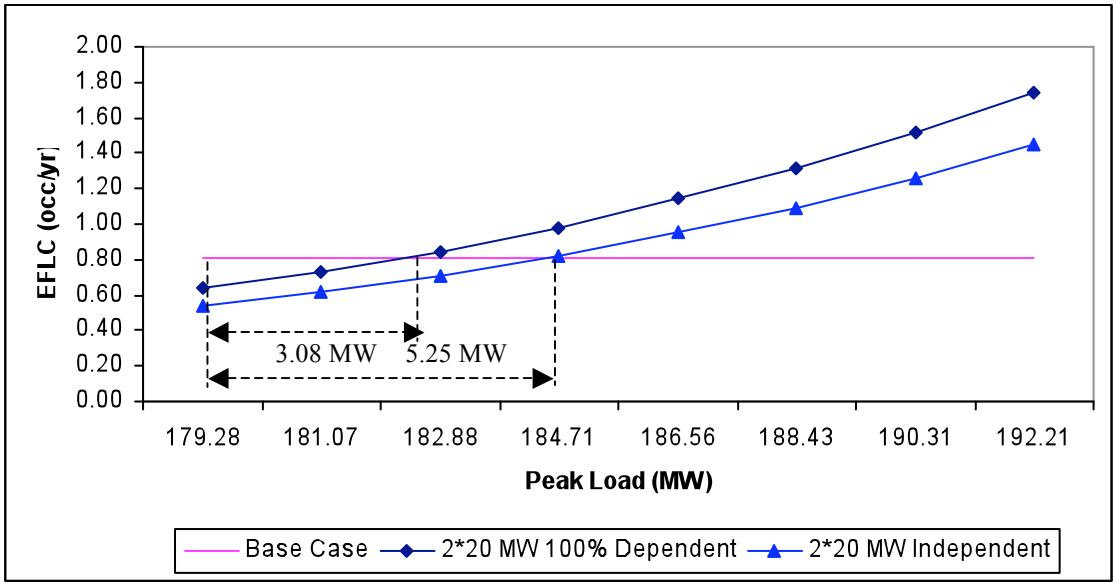

Figure 4.8: The ELCC based on the EFLC for the RRBTSW considering wind speed correlation

The ELCC based on the EDLC and EFLC obtained using the composite system reliability evaluation are smaller than those determined in the HLI reliability evaluation. In HLII studies, transmission network contingencies are included, which tend to counteract improvements in the system reliability created by adding wind capacity.

4.4.2. Interactive effects of wind and LFU on conventional HLII reliability evaluation

The effects of LFU (LFU) on HLII reliability evaluation are presented in Chapter 3. The interactive effects of LFU and wind addition on the system reliability at HLII are shown in this section. Bus load correlation is considered to be 100% dependent. The RapHL-II program was applied to the RBTS with different wind power injection options and the modified load model was used. The sampling size in this study is 8,000 years and the Pass-II criterion is used as the load shedding philosophy.

Effects on HLII reliability indices

The reliability indices for the RBTS with wind power injections at various LFU levels are shown in Figure 4.9. It can be seen from this figure that the reliability indices for each wind condition increase with increase in the LFU. At each LFU level, the reliability indices decrease with increasing wind capacity. The indices are the lowest when the two wind additions are independent.

It can also be seen from Figure 4.9 that the separations between the 0 MW and 1*20 MW wind addition risk profiles are larger than those between the 1*20 MW and 2*20 MW dependent wind addition profile. This indicates that the first 20 MW of wind addition provides more benefit in improving the system reliability than the second added wind farm if the two wind site speeds are dependent. This is consistent with the comments made in Section 4.3.2 when the reliability evaluation is conducted at HLI.

Figure 4.10 shows the increases in the EDLC and EENS attributable to the specific LFU for each wind addition case. It can be seen from Figure 4.10 that the EDLC and EENS increases are smaller when the wind power is added compared to the values when there is no wind addition. This indicates that wind power is able to counteract the effects of LFU on the system reliability indices.

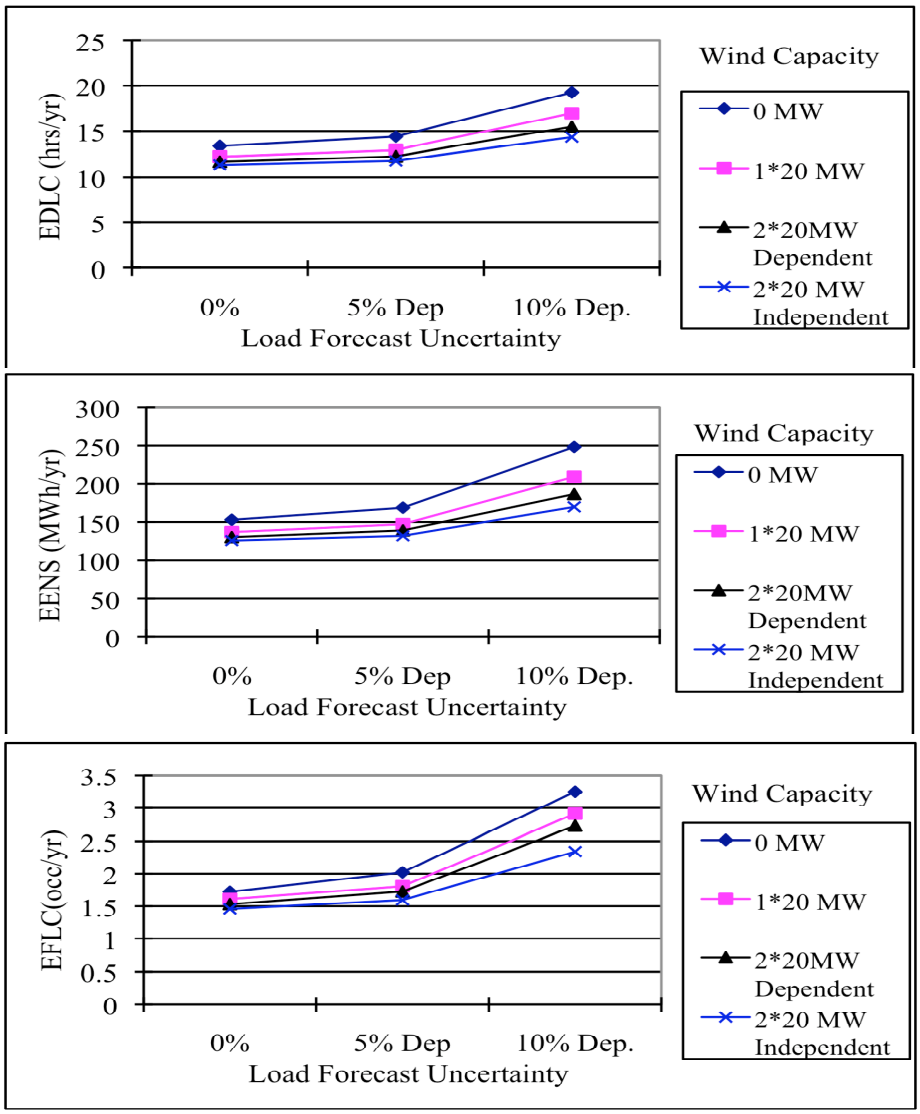

Figure 4.9: The system indices versus LFU for the RBTS with different wind injection options

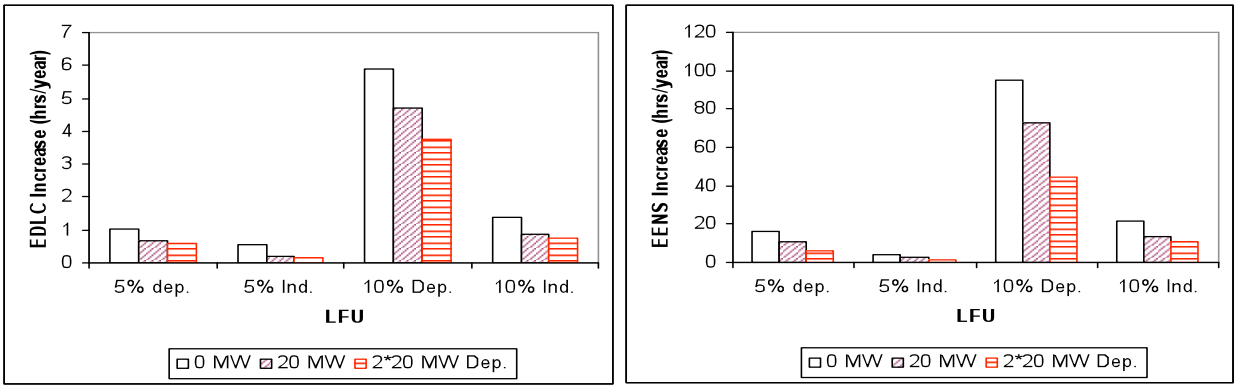

Figure 4.10: The increase in the EDLC and EENS attributable to the LFU with different wind injection options

Interactive effects of wind addition and LFU on load carrying capability

The reliability indices for the RBTS when LFU is considered without wind power injection at the peak load of 179.28 MW are shown in Table 3.3.

The RBTS with two 20 MW wind farms added at bus #4 is designated as the RBTSW earlier in this chapter. The reliability indices for the RBTSW with dependent and independent wind speeds for changing peak loads at an LFU of 5% are shown in Table 4.6.

Table 4.6: HLII reliability indices for the RBTSW at an LFU of 5%

Peak	Wind Speed Dependent			Wind Speed Independent		
Load	EDLC	EENS	EFLC	EDLC	EENS	EFLC
(MW)	(hrs/yr)	(MWh/yr)	(occ/yr)	(hrs/yr)	(MWh/yr)	(occ/yr)
179.28	12.28	139.02	1.73	11.80	131.88	1.60
181.07	12.70	146.39	1.87	12.19	139.14	1.69
182.88	13.16	153.59	2.00	12.68	146.93	1.84
184.71	13.74	162.08	2.18	13.10	154.16	1.98
186.56	14.38	172.68	2.40	13.69	163.04	2.15
188.43	15.18	185.12	2.65	14.36	173.19	2.36
190.31	16.11	199.76	2.92	15.17	186.77	2.61

The ELCC based on the EDLC, EENS and EFLC for the RBTSW are shown in Figures 4.11 to 4.13. It can be seen that the ELCC based on the EDLC is 7.29 MW when the wind speeds at the two sites are 100% dependent. When the wind speeds are 100 % independent, the ELCC is 9.20 MW.

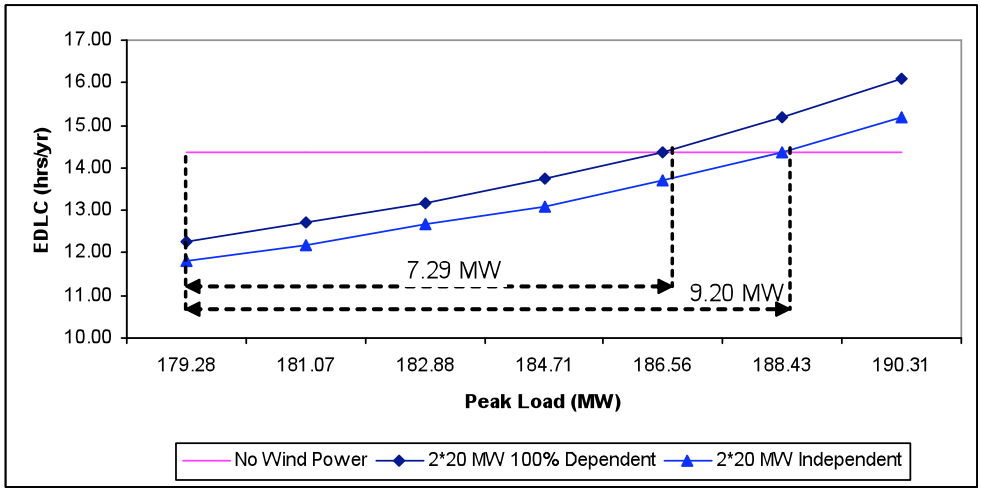

Figure 4.11: The ELCC based on the EDLC for the RBTSW with different wind speed correlations, LFU = 5%.

The ELCC based on the EENS in Figure 4.12 are 6.60 MW and 8.34 MW for the dependent and independent wind speed cases respectively. The ELCC based on the EENS is smaller than that based on the EDLC.

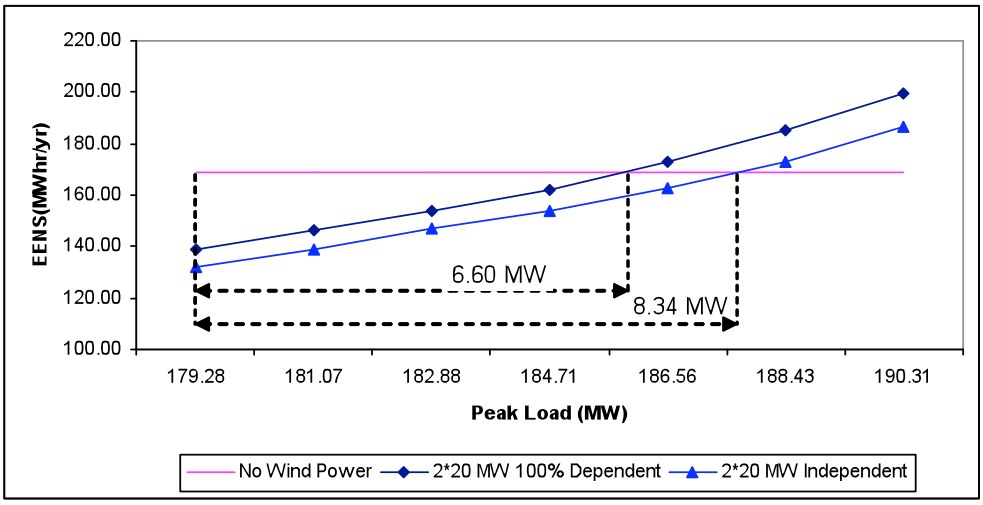

Figure 4.12: The ELCC based on the EENS for the RBTSW with different wind speed correlations, LFU=5%

Figure 4.13 shows the ELCC based on EFLC for the RBTSW. The ELCC for the dependent and independent wind cases are 3.85 MW and 5.90 MW respectively.

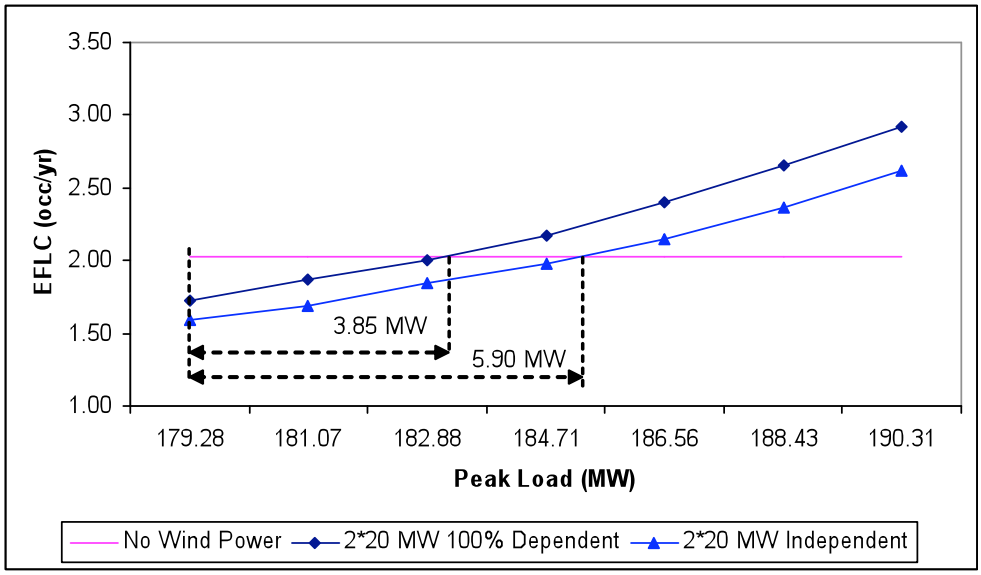

Figure 4.13: The ELCC based on the EFLC for the RBTSW with different wind speed correlations, LFU = 5%

The ELCC based on the EFLC is considerably smaller than when based on the EDLC and EENS. This is due to the highly variable nature of wind power. The EFLC

index does not improve as much with wind power as the EDLC and the EENS indices do.

The reliability indices and the ELCC based on the EDLC, EENS and EFLC for the RBTSW with changing peak loads at the LFU of 10% are shown in Figures 4.14 to 4.16 respectively.

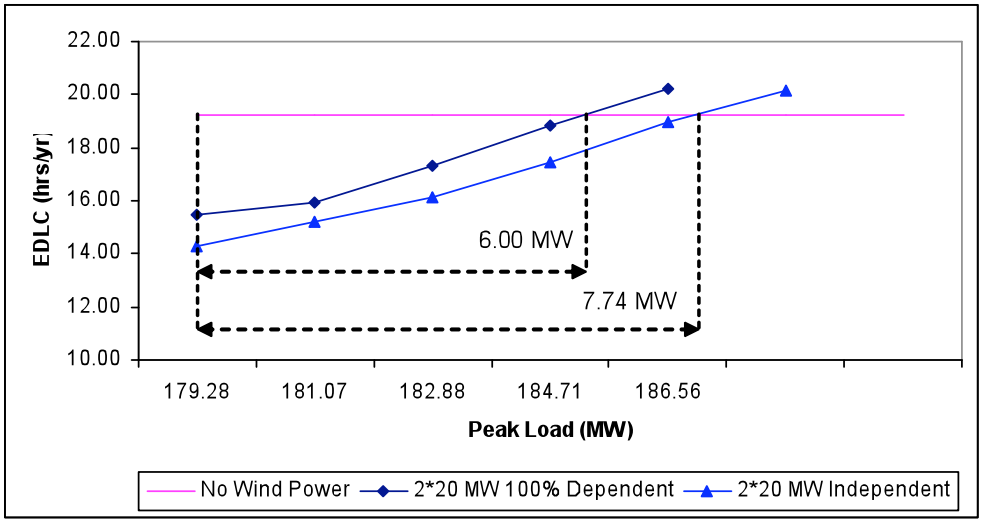

Figure 4.14: The ELCC based on the EDLC for the RBTSW with different wind speed correlations, LFU=10%

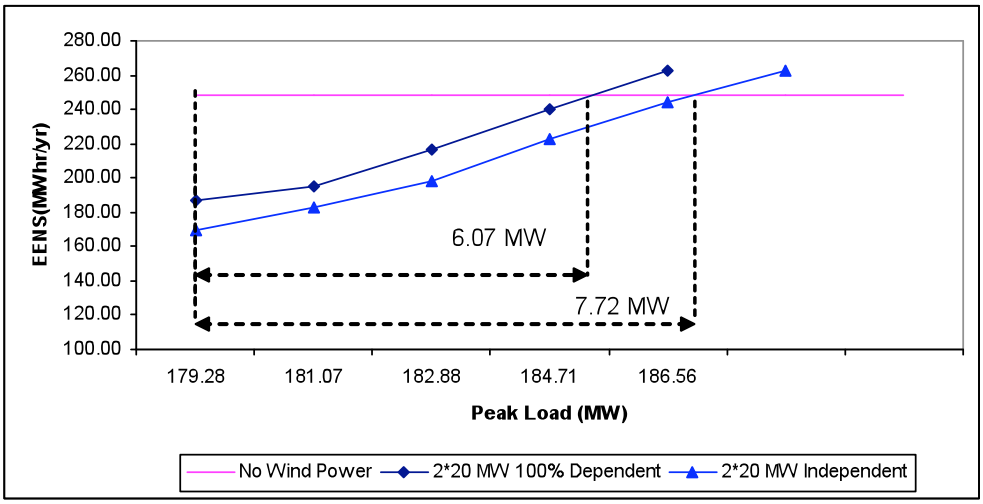

Figure 4.15: The ELCC based on the EENS for the RBTSW with different wind speed correlations, LFU=10%

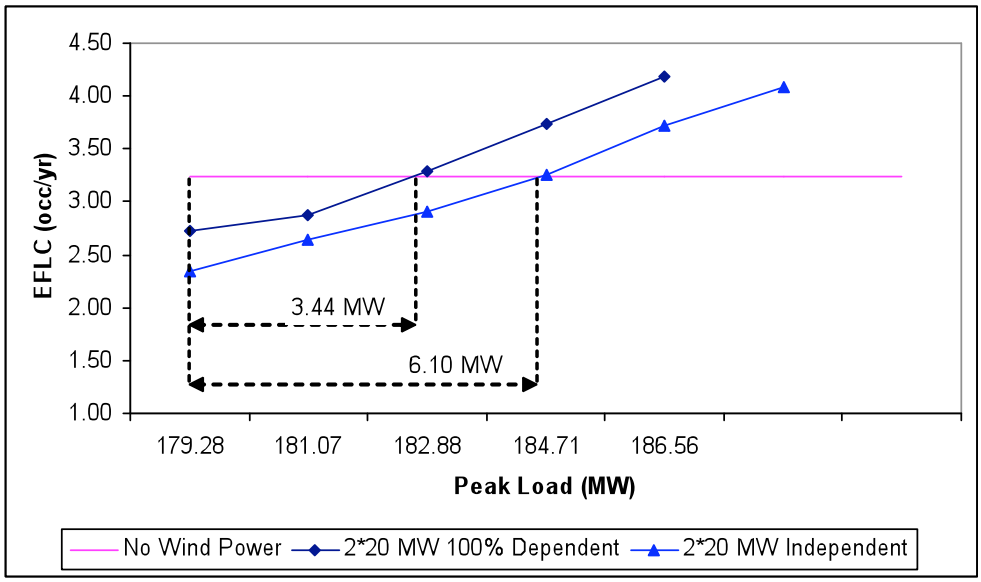

Figure 4.16: The ELCC based on the EFLC for the RBTSW with different wind speed correlations, LFU = 10%

It can be seen that the ELCC based on the EDLC and the EENS are quite close, while the ELCC corresponding to the EFLC is smaller. It can be seen by comparing Figures 4.11 to 4.13 with Figures 4.14 to 4.16, that the ELCC decreases with increase in the LFU for the ELCC obtained using the EDLC, EENS and EFLC when the reliability indices at an LFU of 0% are used as the criterion.

The ELCC associated with wind power addition and varying LFU can be compared with that attributable to the addition of conventional generating capacity. This is illustrated in the following study, where a 5.5 MW conventional combustion turbine unit (CTU) unit is added to the RBTS. The wind site speeds for the RBTSW are considered to be 75% correlated. The bus load correlation is considered to be 100% dependent. The 5.5 MW capacity of the CTU is required to keep the EDLC approximately the same as that for the RBTSW at the peak load of 179.28 MW when the LFU is 0%.

Figure 4.17 shows the EDLC for the RBTS with the two different generation addition options at LFU of 0%, 5% and 10%. The ELCC based on the EDLC are also indicated. It can be seen from Figure 4.17 that when the EDLC at each LFU level is used as the EDLC criterion, the calculated ELCC decreases with increase in the LFU for both the CTU added system and the wind added system. The added conventional unit

provides a slightly larger improvement in system reliability at a LFU of 0% at each peak load level. The EDLC difference between the two systems increase with increase in the peak load. The EDLC for the system with wind addition and CTU become closer at the LFU of 5% than those at the LFU of 0%. The EDLC for the wind added system are smaller than those for the CTU added system at the LFU of 10% at some peak load levels, which indicates that the wind power can counteract the effects of the LFU more than the CTU can.

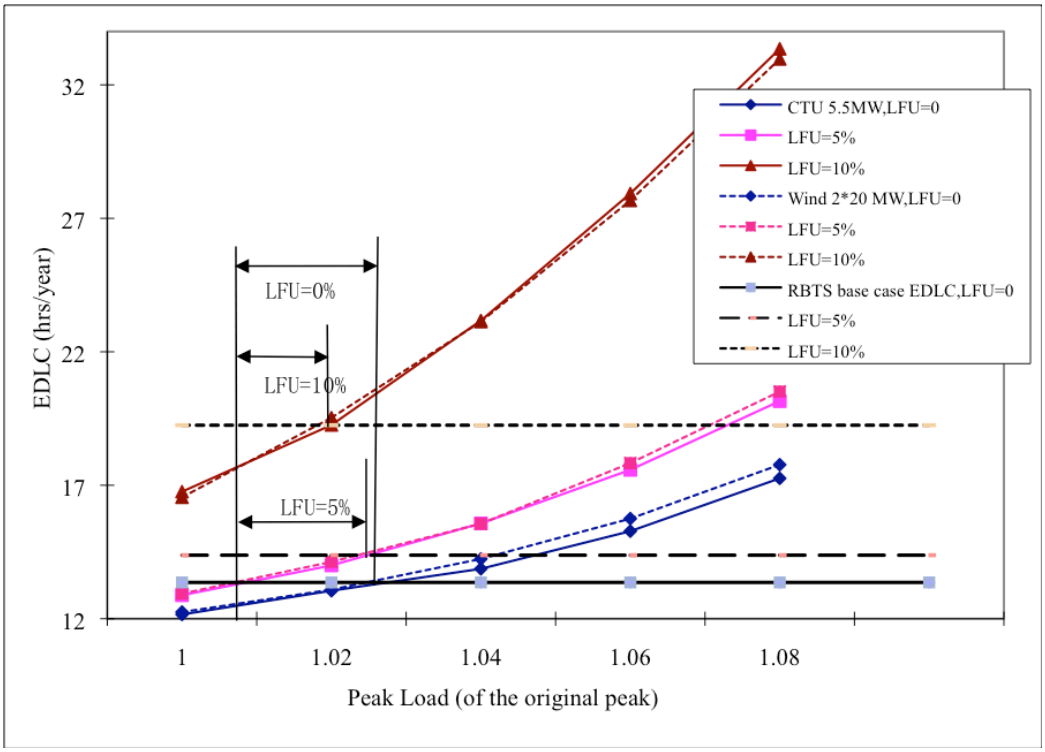

Figure 4.17: The EDLC for the RBTS with different LFU and generation unit addition options

4.5. Effects of Wind power on the HLII Well-being Analysis Framework

The RBTS does not satisfy the N-1 criterion and the RRBTS is used in the well-being analysis. The effects of wind power addition on reliability indices and well-being indices are examined. The RapHL-II program with well-being analysis was applied to the RRBTS and the Pass-II policy was used as the load shedding philosophy. The sample size is 10,000 years.

4.5.1. Effects of wind power additions

Effects on HLII system indices

The reliability indices for the RRBTS with different wind additions using the Regina wind speed data are shown in Table 4.7. It can be seen that the reliability indices decrease with increase in the wind power addition and the incremental benefits decrease with increasing wind power.

Table 4.7: Reliability indices for the RRBTS with different wind additions

Wind Addition (MW)	EDLC (hrs/yr)	EENS (MWh/yr)	EFLC (occ/yr)
0	3.88	46.95	0.84
10	2.99	34.36	0.74
20	2.45	28.06	0.68
30	2.15	24.42	0.64
40	1.94	22.07	0.61

Effects on HLII well-being indices

The well-being indices for the RRBTS with different wind additions are shown in Tables 4.8 to 4.10.

Table 4.8: The system probability in hrs/yr of each state for the RRBTS with different wind additions

	Wind Addition (MW)				
State	0	10	20	30	40
Healthy	8558.91	8564.36	8583.58	8599.13	8610.17
Marginal	173.21	168.64	149.97	134.72	123.90
At Risk	3.88	2.99	2.45	2.15	1.94

The “At Risk” values in Table 4.8 are the EDLC values given in Table 4.7. It can be seen that the time spent in the healthy state increases and the time spent in the marginal state decreases as the system reliability improves with the added wind power.

Table 4.9 shows the system frequency of each state with different wind injections. The system frequency for each state is also shown in Figure 4.18.

It can be seen that the frequencies of the healthy state and the marginal state are relatively close compared to that of the at risk state. The marginal state frequency is slightly larger than that of the healthy state. The frequencies of the three states tend to

decrease with increase in the added wind power. The frequencies of the healthy and marginal states when the wind injection increases from 10 MW to 20 MW remain almost unchanged. The frequency could increase due to the highly variable nature of wind power. The addition of the wind power to the system, however, causes the system frequency to decrease.

Table 4.9: The system frequency in occ/yr of each state for the RRBTS with different wind additions

	Wind Addition (MW)				
State	0	10	20	30	40
Healthy	33.38	32.75	32.83	31.65	30.75
Marginal	34.14	33.44	33.46	32.25	31.31
At Risk	0.84	0.74	0.68	0.64	0.61

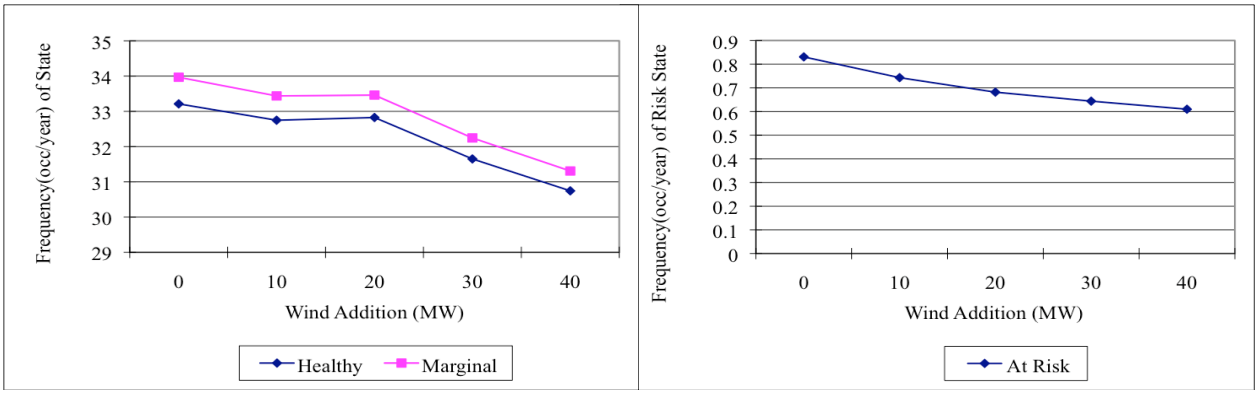

Figure 4.18: The system frequency of each state for the RRBTS with different wind additions

Table 4.10 and Figure 4.19 show the average residence duration in each state for the RRBTS. The system is quite reliable and the average residence duration in the healthy state is considerably larger than in the marginal and the at risk states.

Table 4.10: The average residence duration in hrs/occ of each state for the RRBTS with different wind additions

	Wind Addition (MW)				
State	0	10	20	30	40
Healthy	257.73	261.52	261.49	271.69	280.05
Marginal	5.08	5.04	4.48	4.18	3.96
At Risk	4.56	4.03	3.60	3.34	3.17

It can be seen that the healthy state average duration increases with increase in the wind power addition. This is to be expected, as the healthy state probability increases and the frequency decreases. The average residence duration decreases for the marginal and at risk states. The probability and frequency of these two states with increase in the wind power both decrease, but the probability decreases faster which leads to a decrease in the average duration.

In a general sense, the addition of wind power improves the system reliability. The healthy state probability increases with increasing wind power, while the marginal and at risk state probabilities decrease. The frequency of each state generally drops slightly with an increase in the added wind power. The decrease is due to the generating capacity contribution of the added wind power counteracted by the intermittent nature of the wind.

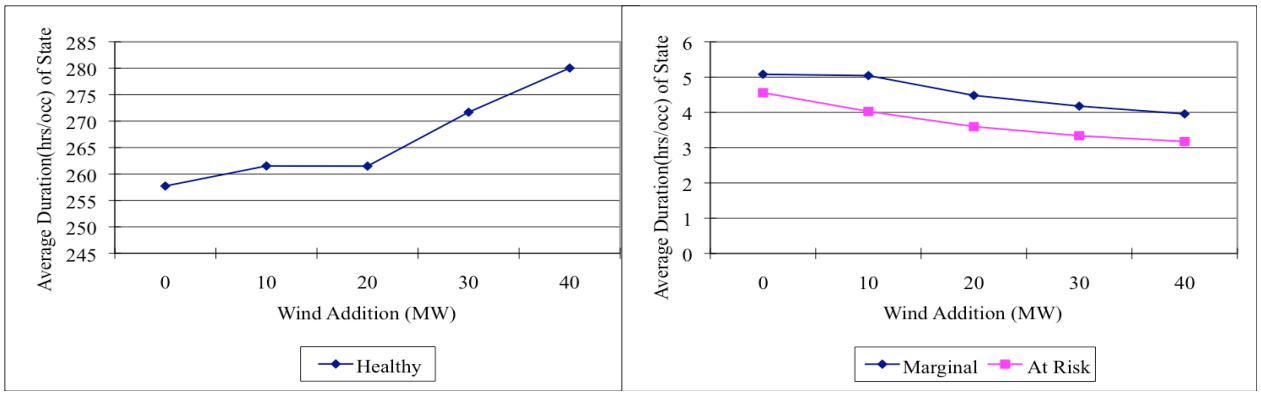

Figure 4.19: The average residence duration of each state for the RRBTS with different wind additions

4.5.2. Effects of wind power on a wind replaced conventional generating unit system in the HLII well-being analysis framework

The fundamental effects of wind power on the well-being indices tend to be masked in the analyses in Section 4.5.1 as the system capacity increases with the addition of the wind power and the system becomes more reliable. This is examined in the following analyses using two equivalent wind capacity systems designated as WRRBTS-1 and WRRBTS-2.

WRRBTS-1: The WRRBTS-1 is the RRBTS with a 5 MW generating unit removed and replaced by 20 MW of wind power at bus #4. The addition of 20 MW of

wind power with this wind regime is required to maintain the EDLC criterion risk when a 5 MW unit is removed.

WRRBTS-2: The WRRBTS-2 is the RRBTS with a 10 MW unit removed and replaced by 65 MW of wind power to meet the EDLC criterion risk.

The wind power required to maintain reliability equivalence is obviously dependent on the wind regime at the wind site and the connection point in the transmission system. This latter aspect is not a factor in this case as bus #4 is close to the load center and the southern transmission is relatively strong. The required wind capacity at a given wind regime is, however, dependent on the system reliability criterion used in the evaluation, and therefore dependent on the system peak load level.

The Regina wind regime described in Section 4.2.1 is used in the analyses and the reliability indices for the three study systems at the peak load of 179.28 MW are shown in Table 4.11.

Table 4.11: The HLII system indices for the three study systems

System	EDLC (hrs/yr)	EENS (MWh/yr)	EFLC (occ/yr)
RRBTS	3.88	46.95	0.84
WRRBTS-1	3.87	46.87	1.04
WRRBTS-2	3.89	49.72	1.32

The RRBTS, WRRBTS-1 and WRRBTS-2 are equivalent in the sense that they have the same level of adequacy expressed by the EDLC at the peak load level of 179.28 MW. The EENS are slightly different for the three systems and the LOLF for the WRRBTS-1 and WRRBTS-2 are larger than that of the RRBTS. This indicates that the required wind power would be different if the EENS or the EFLC is used as the criterion.

The reliability indices for the RRBTS, WRRBTS-1 and the WRRBTS-2 for a range of peak loads are shown in Tables 4.12, 4.13 and 4.14 respectively. It can be seen by comparing Table 4.12 with Table 4.14 that the EENS values for the WRRBTS-2 are larger than those of the RRBTS. The EDLC and EENS for the WRRBTS-1 are close to those of the RRBTS as shown in Tables 4.12 and 4.13. This is because the wind power in the WRRBTS-1 is less than that in the WRRBTS-2 and therefore does not have as much effect on the energy supply. The EFLC index for the RRBTS is the smallest and

that of the WRRBTS-2 is the largest at each peak load level due to the intermittent nature of the added wind power.

Table 4.12: The HLII system indices for the RRBTS with changing peak loads

Peak Load (MW)	EDLC (hrs/yr)	EENS (MWh/yr)	EFLC (occ/yr)
125.30 (70%)	0.02	0.22	0.01
134.46 (75%)	0.05	0.47	0.01
143.42 (80%)	0.09	1.03	0.02
152.39 (85%)	0.27	2.65	0.06
161.35 (90%)	0.53	6.34	0.12
170.32 (95%)	1.64	17.12	0.53
179.28 (100%)	3.88	46.95	0.84
188.24 (105%)	7.75	104.38	1.90
197.21 (110%)	15.78	223.39	3.34
206.17 (115%)	31.86	453.60	10.29
215.14 (120%)	80.05	1079.26	21.11

Table 4.13: The HLII system indices for the WRRBTS-1 with changing peak loads

Peak Load (MW)	EDLC (hrs/yr)	EENS (MWh/yr)	EFLC (occ/yr)
125.30 (70%)	0.03	0.19	0.01
134.46 (75%)	0.05	0.44	0.01
143.42 (80%)	0.11	1.03	0.03
152.39 (85%)	0.26	2.70	0.07
161.35 (90%)	0.60	6.56	0.21
170.32 (95%)	1.85	18.88	0.53
179.28 (100%)	3.87	46.87	1.04
188.24 (105%)	7.93	105.01	2.12
197.21 (110%)	15.01	217.94	3.77
206.17 (115%)	34.86	471.59	11.11
215.14 (120%)	79.38	1094.07	20.16

Table 4.14: The HLII system indices for the WRRBTS-2 with changing peak loads

Peak Load (MW)	EDLC (hrs/yr)	EENS (MWh/yr)	EFLC (occ/yr)
125.30 (70%)	0.04	0.35	0.01
134.46 (75%)	0.07	0.70	0.02
143.42 (80%)	0.14	1.52	0.04
152.39 (85%)	0.26	3.21	0.09
161.35 (90%)	0.83	8.30	0.31
170.32 (95%)	1.95	22.43	0.62
179.28 (100%)	3.89	49.72	1.32
188.24 (105%)	7.76	109.37	2.23
197.21 (110%)	15.58	221.31	5.87
206.17 (115%)	39.63	515.14	13.04
215.14 (120%)	75.33	1113.24	22.82

The EDLC for the RRBTS, WRRBTS-1 and WRRBTS-2 are shown pictorially in Figure 4.20. The EDLC for the RRBTS, WRRBTS-1 and WRRBTS-2 are very close for the peak load levels from 95%, to 105%. When the peak load level increases or decreases further, the systems are no longer equivalent.

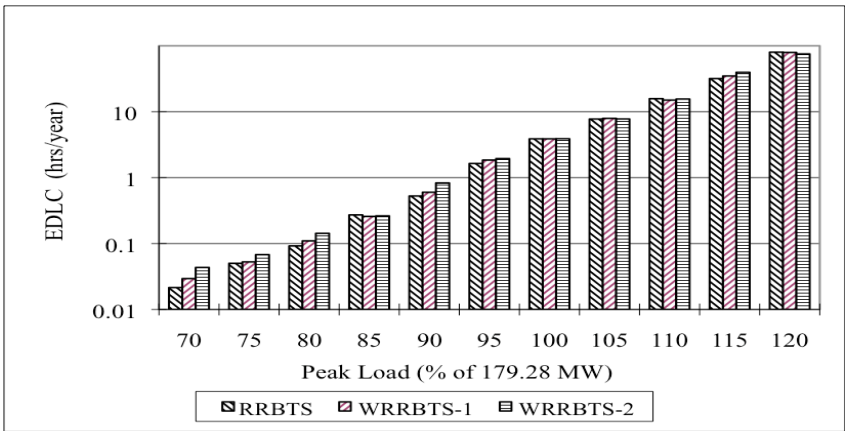

Figure 4.20: The EDLC for the RRBTS, WRRBTS-1 and WRRBTS-2 versus peak load

It can be seen from Figure 4.20 that when the peak load is less than 95% of the base peak load of 179.28 MW, the EDLC is larger for the larger wind injected system. In general, the EDLC is smaller for systems with larger wind injections when the peak load is larger than the peak load level at which the systems are equivalent. The replacement of a conventional unit with wind power changes the system capacity outage probability table (COPT) [2]. The derated states associated with the added wind power widen the range of the COPT. The probability when the available capacity is low or high increases and probabilities in the middle decrease. When the peak load increases, the high available capacity in the system with wind is able to supply the large load values, which causes the EDLC to decrease. When the peak load decreases, the middle part of the COPT has larger effects on the EDLC and the EDLC increases. There is an exception at the peak load of 206.17 MW, which is 115% of the original peak load. The EDLC increases with increase in the wind power addition. This is because at this peak load level, when the RRBTS loses the largest unit of 40MW, the available capacity is 200 MW which is smaller than the peak load. The loss of the largest unit has a larger effect on the EDLC than the injection of wind power.

The EENS of the RRBTS, WRRBTS-1 and WRRBTS-2 are shown in Figure 4.21. The EENS varies differently from the EDLC with changes in the peak load. The

EENS for the WRRBTS-1 is closer to that of the RRBTS than that of the WRRBTS-2. It can be seen from Tables 4.14 to 4.16 that when the peak load is smaller than 105% of the base peak load, the EENS is larger for the systems with wind additions. The EENS is higher when the wind capacity is a relatively larger fraction of the total installed capacity. The difference in the EENS, however, decreases with increasing peak load. When the peak load reaches a certain value, the EENS for the systems with wind are smaller than for systems with no wind.

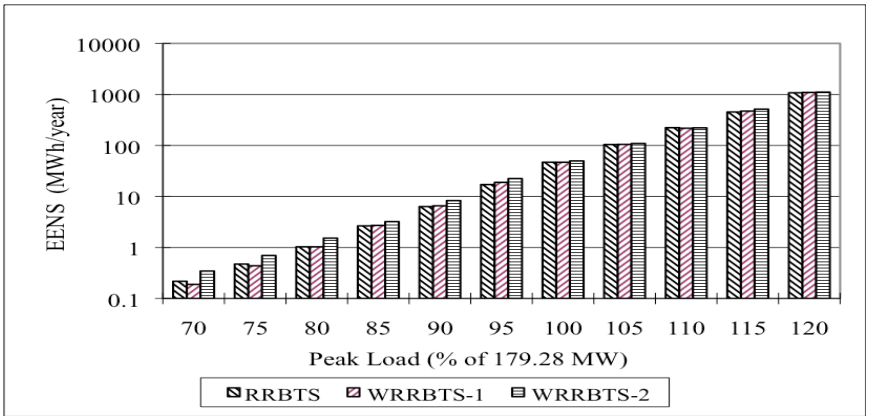

Figure 4.21: The EENS for the RRBTS, WRRBTS-1 and WRRBTS-2 versus peak load

The well-being indices for the RRBTS, WRRBTS-1 and WRRBTS-2 are shown in Tables 4.15 to 4.17.

Table 4.15: The system probability in hrs/yr of each operating state for the different systems

State	Systems		
	RRBTS	WRRBTS-1	WRRBTS-2
Healthy	8558.91	8528.76	8551.45
Marginal	173.21	203.37	180.67
At Risk	3.88	3.87	3.89

The healthy state probability indicates the amount of time that the system spends in the state in which the deterministic (N-1) criterion is satisfied. The marginal state indicates the time in which the system resides in the state in which the criterion is not satisfied but there is no actual load curtailment. The healthy state probabilities for the WRRBTS-1 and WRRBTS-2 are smaller than that of the RRBTS, while the marginal state probability of the WRRBTS-1 and WRRBTS-2 are larger than that of the RRBTS.

This table shows that while the at risk state probabilities (EDLC) are very close, the healthy and marginal state probabilities are different for the three systems.

The system frequencies of the operating states for the three systems are shown in Table 4.16. It can be seen that the frequencies of the three states are larger for the WRRBTS-1 and WRRBTS-2 than for the RRBTS. This indicates that the replacement of conventional generating units with wind turbine generators causes more state transitions due to the intermittent performance of wind power. The WRRBTS-2 has a larger proportion of wind power than the WRRBTS-1 and therefore the intermittent performance of wind power has a larger effect on the operating state frequencies of the three states for the WRRBTS-1 as shown in Table 4.16.

Table 4.16: The system frequency in occ/yr of each operating state for the different systems

State	Systems		
	RRBTS	WRRBTS-1	WRRBTS-2
Healthy	33.38	42.88	47.52
Marginal	34.14	43.86	48.75
At Risk	0.84	1.04	1.32

Table 4.17 shows the average duration of each operating state for the RRBTS, WRRBTS-1 and WRRBTS-2.

Table 4.17: The average residence duration in hrs/occ of each operating state for the different systems

State	Systems		
	RRBTS	WRRBTS-1	WRRBTS-2
Healthy	256.44	198.90	179.96
Marginal	5.07	4.64	3.71
At Risk	4.61	3.72	2.95

The average duration of each state decreases because the frequency of each state increases with increase in the wind capacity. The marginal state probability also increases but the marginal state frequency increases more than the probability and therefore the marginal state average duration decreases.

When a conventional generating unit is replaced by wind power to maintain the system reliability at a certain level, the well-being indices change. In general, the system transitions between states increase because of the intermittent characteristics of wind power. The healthy state probability decreases and marginal state probability increases. The frequency of each state increases due to the injection of the wind power. The effects of wind power on the system operating state probabilities and state frequencies increase as the proportion of wind capacity to the total installed capacity increases. The average residence duration of each state changes correspondingly.

The system probability of the healthy state for the three systems with changing peak loads is shown in Figure 4.22. The healthy state probability profiles are divided into two segments in this figure in order to show the separation between the three systems profiles at the 179.28 MW peak load level.

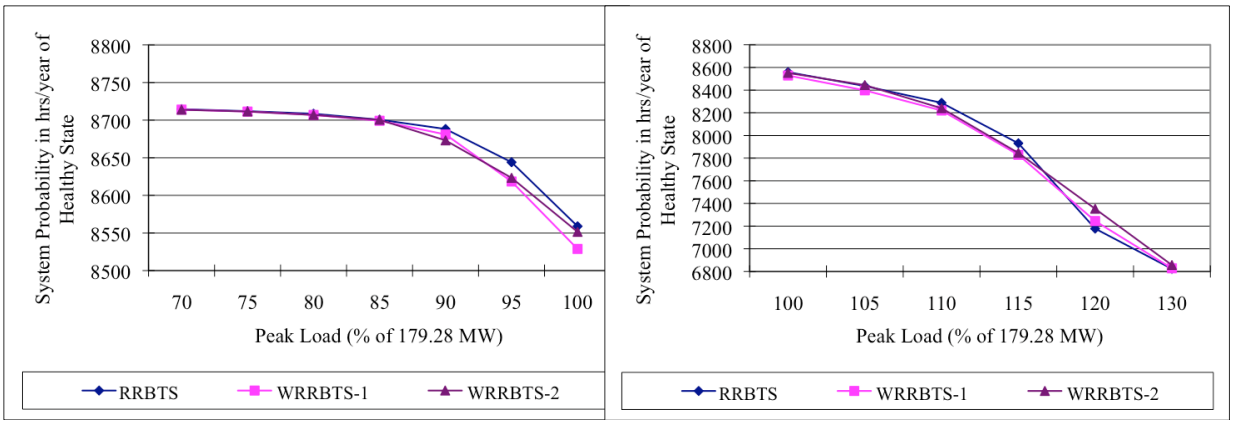

Figure 4.22: The probability of the healthy state with changing peak loads for the three systems

It can be seen that the healthy state probabilities for the three systems are very close at low peak load levels. The healthy state probability in hrs/yr moves towards 8736 (hrs/yr) when the peak load decreases. The difference in the healthy state probability increases when the peak load increases. The RRBTS healthy state probability is slightly larger when the peak load is less than 179.28 MW, followed by the WRRBTS-1 and the WRRBTS-2. The system probability of the at risk state is the same as the EDLC for the various cases and is shown earlier in Tables 4.12 to 4.14.

The probability of the marginal state for the three systems is shown in Figure 4.23. It can be seen from Figure 4.23 that the probabilities of the marginal state for the

three systems move towards zero when the peak load decreases. The differences in the marginal state probabilities for the different systems become more observable with increasing peak load. When the peak load reaches a certain level, the differences decreases again.

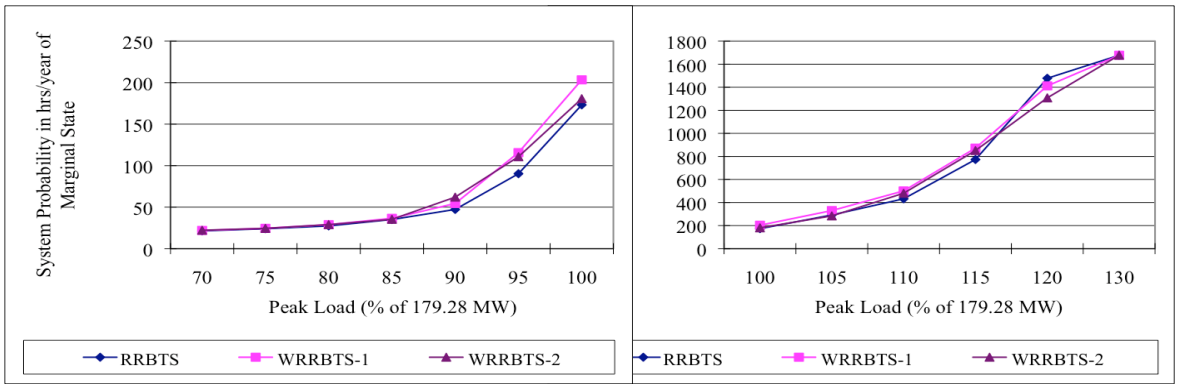

Figure 4.23: The probability of the marginal state with changing peak loads for the three systems

The system frequencies of the healthy and marginal states for the three systems are shown in Figures 4.24 and 4.25 respectively. It can be seen that the system frequencies for both the healthy and marginal states increase with increase in the peak load. The average residence duration of the healthy state for the three systems are shown in Figure 4.26. It can be seen that the average duration decreases quickly with increase in the peak load. The differences in the average duration for the three systems is larger when the peak load is lower. As the peak load continues to increase, the duration of the healthy state drops to the limiting value of 0 hrs/occ.

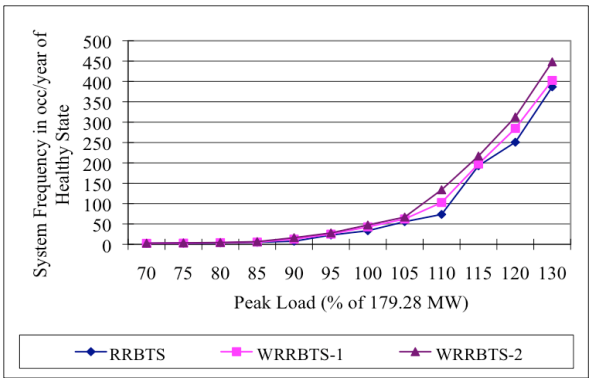

Figure 4.24: The frequency of the healthy state with peak load for the three systems

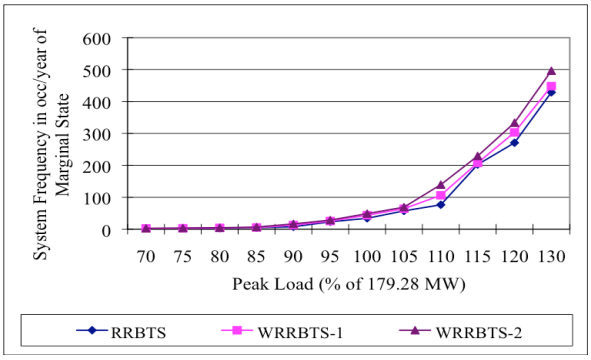

Figure 4.25: The frequency of the marginal state with peak load for the three systems

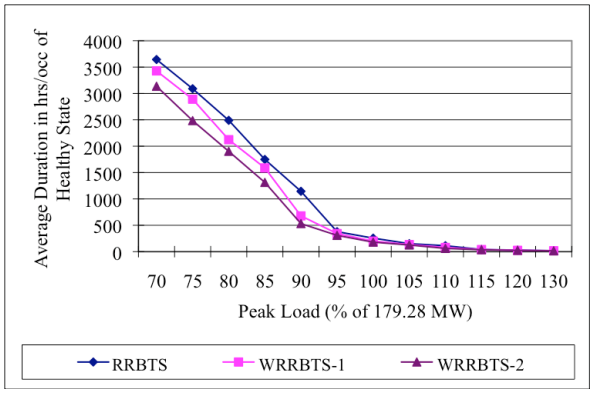

Figure 4.26: The average duration of the healthy state with peak load for the three systems

Figures 4.27 and 4.28 show the average residence durations of the marginal and at risk states for the three systems respectively. It can be seen from these two figures that the average durations of the marginal and at risk states for the RRBTS are larger than those of the WRRBTS-1 and the WRRBTS-2 for most peak load levels. The larger the wind addition, the smaller is the average duration. This is because the frequency of each state increases when the wind injection increases. The average durations in the marginal and at risk states for the three systems are close, however, at some peak load levels such as the peak loads of 95% and 115%. This could be because the system performance is dominated at these peak load levels by the generation composition of the conventional generating units, which masks the effects of the wind power additions.

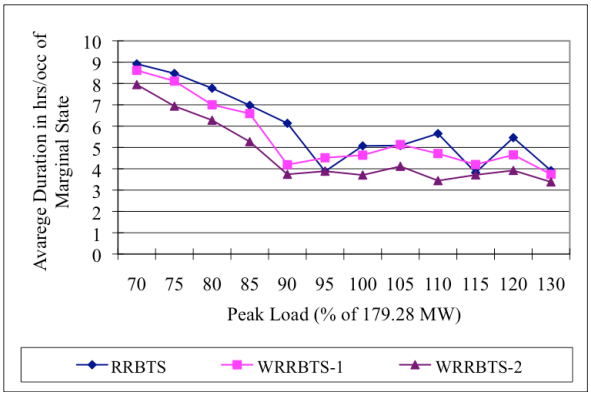

Figure 4.27: The average duration of the marginal state with peak load for the three systems

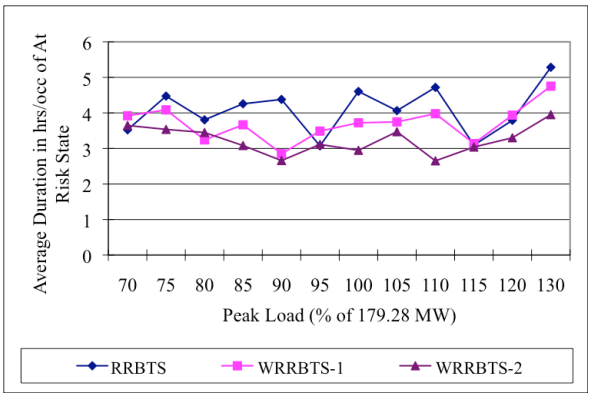

Figure 4.28: The average duration of the at risk state with peak load for the three systems

4.5.3. Interactive effects of wind power and load forecast uncertainty in the well-being analysis framework

Effects on the HLII reliability indices

The RRBTS, WRRBTS-1 and WRRBTS-2 are used in the analyses. The reliability indices for the three systems are shown in Tables 4.18 to 4.20.

Table 4.18: The HLII system indices for the RRBTS with LFU

LFU	EDLC (hrs/yr)	EENS (MWh/yr)	EFLC (occ/yr)
0	3.88	46.95	0.84
5%	4.88	61.70	1.17
10%	10.36	147.03	2.53

Table 4.19: The HLII system indices for the WRRBTS-1 with LFU

LFU	EDLC (hrs/yr)	EENS (MWh/yr)	EFLC (occ/yr)
0	3.87	46.87	1.04
5%	4.84	62.66	1.30
10%	10.92	135.17	2.92

Table 4.20: The HLII system indices for the WRRBTS-2 with LFU

LFU	EDLC (hrs/yr)	EENS (MWh/yr)	EFLC (occ/yr)
0	3.89	49.72	1.32
5%	4.45	64.21	1.52
10%	9.31	151.12	3.17

It can be seen that the EDLC and EENS in Tables 4.19 and 4.20 are slightly different from those in Table 4.18. The EFLC in Tables 4.19 and 4.20 are much larger than those in Table 4.18. This is due to the replacement of the conventional generation unit with wind power. The intermittent nature of wind power causes an increase in the frequency of load curtailment. The WRRBTS-2 has a larger proportion of wind power and therefore has a larger EFLC.

It can be seen that the EDLC for the WRRBTS-1 is slightly less than that of the RRBTS when the LFU is 5%. This shows that the added wind power counteracts the effects of the LFU on the EDLC. The installed capacity of the wind power is 20 MW for the WRRBTS-1, which is four times the capacity of the removed conventional generating unit. In this case, the produced wind power is able to complement some of the larger loads introduced by LFU. When the LFU is 10%, it can be seen that the EDLC for the RRBTS is slightly smaller than for the WRRBTS-1. This indicates that the added wind power is not able to counteract the effects of the LFU on the EDLC when the LFU increases to a certain level. The capacity of the removed unit is 10 MW and the added wind power is 65 MW in the WRRBTS-2. The replacement ratio in this case is 6.5, which is larger than that in the WRRBTS-1. The EDLC for the WRRBTS-2 is less than that of the RRBTS and the WRRBTS-1 at LFU of 5% and 10%. This indicates that the WRRBTS-2 is able to counteract the effect of the LFU more than in the WRRBTS-1 due to the larger wind replacement ratio.

Effects on the HLII well-being indices

Tables 4.21-4.23 show the system probability, frequency and average duration of each operating state with various LFU for the RRBTS.

Table 4.21: The system probability in hrs/yr of each state for the RRBTS with LFU at HLII

State	LFU		
	0	5%	10%
Healthy	8558.91	8536.04	8448.48
Marginal	173.21	195.08	277.15
At Risk	3.88	4.88	10.36

It can be seen from Table 4.21 that the probability of the healthy state drops with increase in the LFU and the probabilities of the marginal and at risk states increase. The system is not only more likely to spend more time in the marginal state where the N-1 criterion is no longer satisfied, but also more likely to go into the at risk state.

Table 4.22: The system frequency in occ/yr of each state for the RRBTS with LFU at HLII

State	LFU		
	0	5%	10%
Healthy	33.38	37.96	54.44
Marginal	34.14	39.04	56.76
At Risk	0.84	1.17	2.53

Table 4.22 shows the system frequency of each operating state for the RRBTS. The frequency of the marginal state is larger than that of the healthy state because there are more transitions between the marginal and at risk states than between the healthy and at risk states. The frequency of the at risk state is relatively small because the system is quite reliable and most of the time there is no violation of the operating constraints. The state transitions are mainly between the healthy and marginal states.

Table 4.23 shows the average duration of each operating state versus the LFU. It can be seen that the average duration of the healthy state is much larger than the average duration of the other two states. The average duration in the marginal state is relatively close to that in the at risk state.

Table 4.23: Average duration in hrs/occ of each state for the RRBTS with LFU at HLII

State	LFU		
	0	5%	10%
Healthy	256.44	224.86	155.18
Marginal	5.07	5.00	4.88
At Risk	4.61	4.18	4.09

It can also be seen that the decrease in the healthy state is the largest and the decrease in the marginal state is the smallest. The average durations of the healthy, marginal and at risk states decrease with increase in the LFU due to the more frequent transitions between states. Even though the probabilities of the marginal and at risk states increase with increase in the LFU, the average durations decrease as the increases in the frequencies of these two states are higher than the respective increases in the state probabilities.

Tables 4.24-4.26 show the system operating state probabilities, frequencies and durations for the WRRBTS-1.

Table 4.24: The system probability in hrs/yr of each state for the WRRBTS-1 with LFU at HLII

State	LFU		
	0	5%	10%
Healthy	8528.76	8508.80	8410.68
Marginal	203.37	222.37	314.41
At Risk	3.87	4.84	10.92

It can be seen from Table 4.24 that the system probability of the healthy state decreases with increase in the LFU, while those of the marginal state and at risk state increase. The increase is larger when the LFU changes from 5% to 10% than that from 0 to 5%. This is similar to that of the RRBTS.

The frequencies of the three operating states shown in Table 4.25 increase with increase in the LFU as in the RRBTS case. The average duration of the healthy state decreases and that of the at risk state increases with increase in the LFU. The average duration of the marginal state, however, changes differently from that of the RRBTS.

Table 4.25: The system frequency in occ/yr of each state for the WRRBTS-1 with LFU at HLII

State	LFU		
	0	5%	10%
Healthy	42.88	45.22	63.71
Marginal	43.86	46.43	66.44
At Risk	1.04	1.30	2.92

Table 4.26: The average duration in hrs/occ of each state for the WRRBTS-1 with LFU at HLII

State	LFU		
	0	5%	10%
Healthy	198.90	188.17	132.02
Marginal	4.64	4.79	4.73
At Risk	3.72	3.71	3.74

Tables 4.27 to 4.29 show the well-being indices for the WRRBTS-2 at HLII with changing LFU. The changes in the well-being indices are similar to those in Tables 4.22 to 4.24 for the WRRBTS-1. The LFU affects both the reliability indices and the well-being indices. In general, the system becomes less reliable and less secure as the LFU increases.

Table 4.27: The system probability in hrs/yr of each state for the WRRBTS-2 with LFU at HLII

	LFU		
State	0	5%	10%
Healthy	8551.45	8547.81	8468.84
Marginal	180.67	183.75	257.86
At Risk	3.89	4.45	9.31

Table 4.28: The system frequency in occ/yr of each state for the WRRBTS-2 with LFU at HLII

	LFU		
State	0	5%	10%
Healthy	47.52	50.53	69.97
Marginal	48.75	51.94	72.92
At Risk	1.32	1.52	3.17

Table 4.29: The average duration in hrs/occ of each state for the WRRBTS-2 with LFU at HLII

	LFU		
State	0	5%	10%
Healthy	179.96	169.18	121.04
Marginal	3.71	3.54	3.54
At Risk	2.95	2.93	2.94

The system probabilities for the three operating states for the RRBTS and the WRRBTS-1 are shown graphically in Figure 4.29.

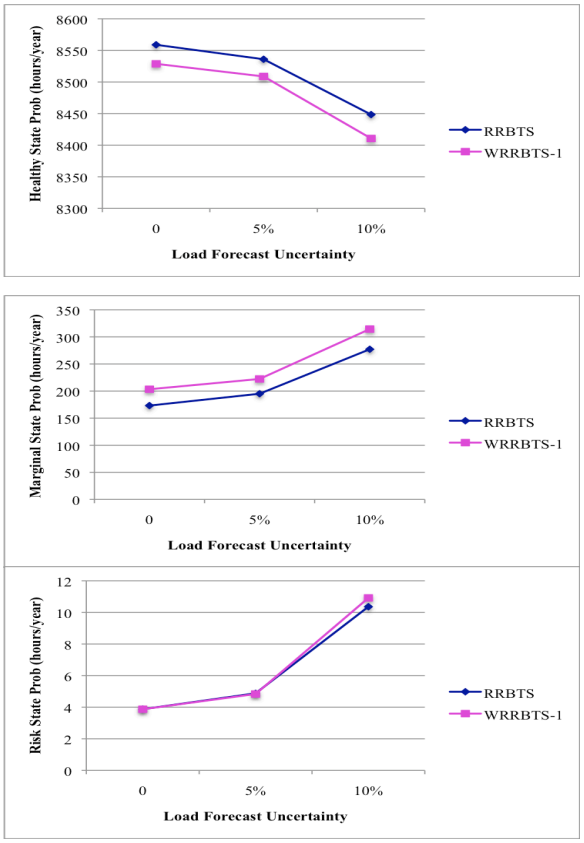

Figure 4.29: The system probabilities of the three operating states for the RRBTS and the WRRBTS-1 with LFU

This figure illustrates the differences in the well-being indices for the two systems and how the indices vary with increase in LFU. It can be seen from Figure 4.29 that the at risk state probabilities (EDLC) for the two systems are relatively close to each other over the LFU range considered. The healthy state probability for the RRBTS is larger than that for the WRRBTS-1 at each LFU level and the opposite is true for the

marginal state. The differences in the healthy state and marginal state probabilities for the two systems are relatively constant with increase in the LFU.

The frequencies of the three operating states for the two systems are shown in Figure 4.30 where it can be seen that the operating state frequencies of the WRRBTS-1 are larger than those of the RRBTS at each LFU level. The differences in the two frequencies for each operating state vary when the LFU changes. The frequency differences in the healthy, marginal and at risk states are the smallest at the LFU of 5%. This shows that replacing a conventional generating unit with wind power tends to counteract the effects of LFU on the system and the transitions between the states decrease. When the LFU continues to increase, the difference becomes larger.

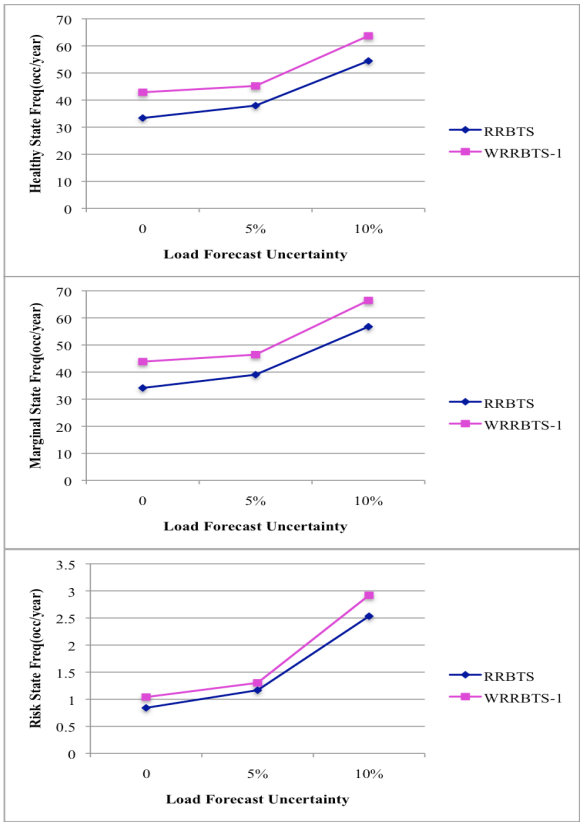

Figure 4.30: The system frequencies of the three operating states for the RRBTS and the WRRBTS-1 with LFU.

The average durations of the three operating states are shown in Figure 4.31. Figure 4.31 shows that the average duration in each state for the two systems responds quite differently with LFU. The average duration is determined by the system probability and system frequency. It can be seen in the figures that the difference in the

healthy state probability between the two systems decreases with increase in the LFU. The average duration of the marginal state for the RRBTS decreases with increasing LFU, while that of the WRRBTS-1 increases with the LFU of 0% to 5%, then decreases with the LFU of 5% to 10%. The at risk state average duration for the RRBTS and WRRBTS-1 decreases and increases respectively with increase in the LFU. The average durations of all the operating states for the WRRBTS-1 are smaller than those for the RRBTS due to the intermittent behaviour of the added wind power.

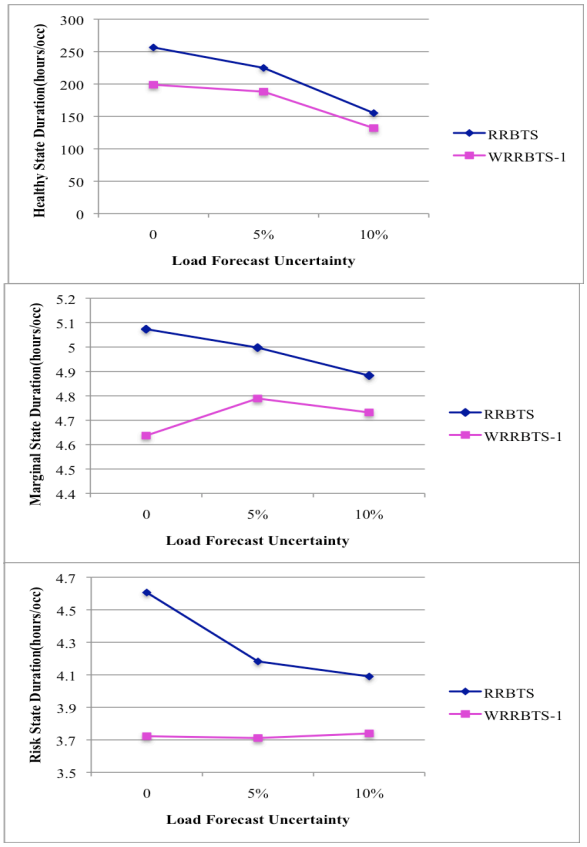

Figure 4.31: The average durations of the three operating states for the RRBTS and the WRRBTS-1 with LFU

4.5.4. Effects of wind power in the well-being analysis framework for the IEEE-RTS

The RRBTS is a relatively small system developed for teaching and research purposes. In order to examine the well-being effects associated with wind power on a larger system, similar studies were conducted on the IEEE-RTS and a wind modified system designated as the IEEE-WRTS. The IEEE-RTS is wind modified by removing a 50 MW unit and replacing it with 205 MW wind capacity at bus #1 to maintain the

EDLC at the peak load of 2754.75 MW. The modified system is designated as the IEEE-WRTS.

Effects on the HLII reliability indices

The reliability indices for the IEEE-RTS and the IEEE-WRTS with changing peak loads are shown in Tables 4.30 and 4.31 respectively. The EDLC for the IEEE-RTS and the IEEE-WRTS at different peak load levels are also illustrated pictorially in Figure 4.32.

The EDLC are slightly smaller for the IEEE-RTS than those of the IEEE-WRTS when the peak load is less than 100%. When the peak load is larger than 100%, the EDLC for the IEEE-WRTS are smaller than the those for the IEEE-RTS. This is similar to the results for the RRBTS. The EDLC for the IEEE-RTS and the IEEE-WRTS compare quite closely at the different peak load levels due to the fact that the wind injection is a smaller percentage of the total capacity than in the WRRBTS-1 and WRRBTS-2.

Table 4.30: The HLII system indices for the IEEE-RTS with peak load

Peak Load	EDLC (hrs/yr)	EENS (MWh/yr)	EFLC (occ/yr)
85%	1.58	153.51	0.46
90%	4.65	510.59	1.26
95%	13.32	1566.91	3.47
(100%)	35.70	4510.17	9.13
105%	82.31	11824.06	18.56
110%	173.50	27491.92	39.20
115%	355.21	60357.34	77.37

Table 4.31: The HLII system indices for the IEEE-WRTS with peak load

Peak Load (MW)	EDLC (hrs/yr)	EENS (MWh/yr)	EFLC (occ/yr)
85%	1.59	148.68	0.51
90%	4.77	516.37	1.43
95%	13.53	1598.06	3.86
(100%)	35.45	4550.81	9.46
105%	80.47	11681.07	20.15
110%	184.10	30998.12	42.85
115%	346.22	59231.64	78.22

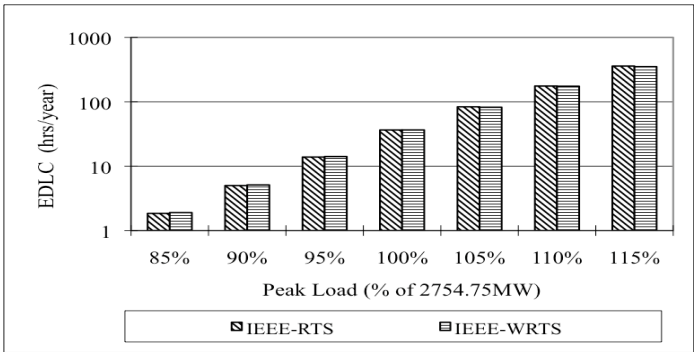

Figure 4.32: The EDLC for the IEEE-RTS and IEEE-WRTS versus peak load.

Effects on the HLII well-being indices

The well-being indices for the IEEE-RTS and the IEEE-WRTS are shown in Table 4.32. The healthy state probability of the IEEE-WRTS is smaller than that of the IEEE-RTS and agree with the situation for the RRBTS and the WRRBTS-1 or WRRBTS-2. The frequencies of the three states are larger for the IEEE-WRTS due to the intermittent nature of the added wind power. The added wind power in the IEEE-WRTS has similar effects on the well-being indices as in the WRRBTS-1 and WRRBTS-2. The effects are, however, not exactly the same as the IEEE-RTS is a less reliable system than the RRBTS.

Table 4.32: Well-being indices for the IEEE-RTS and IEEE-WRTS.

State	IEEE-RTS			IEEE-WRTS		
	Probability	Frequency	Duration	Probability	Frequency	Duration
Healthy	8274.03	95.75	86.41	8224.40	104.32	78.84
Marginal	425.50	102.53	4.15	475.09	112.14	4.24
At Risk	36.47	9.14	3.99	36.51	9.47	3.86

Interactive effects of wind power and LFU

The well-being indices for the IEEE-RTS and the IEEE-WRTS with various LFU are shown in Tables 4.33 to 4.35.

Table 4.33: The system probability in hrs/yr of each state for the IEEE-RTS and the IEEE-WRTS with LFU at HLII

State	IEEE-RTS			IEEE-WRTS		
	0	5%	10%	0	5%	10%
Healthy	8274.03	8181.83	7997.59	8224.40	8129.98	7983.78
Marginal	425.50	505.25	636.21	475.09	555.72	657.52
At Risk	36.47	48.92	102.20	36.51	50.29	94.70

Table 4.34: The system frequency in occ/yr of each state for the IEEE-RTS and the IEEE-WRTS with LFU at HLII

State	IEEE-RTS			IEEE-WRTS		
	0	5%	10%	0	5%	10%
Healthy	95.75	105.69	125.66	104.32	117.91	132.31
Marginal	102.53	114.82	141.90	112.14	128.56	149.81
At Risk	9.14	11.65	21.59	9.47	12.85	21.83

Table 4.35: The average duration in hrs/occ of each state for the IEEE-RTS and the IEEE-WRTS with LFU at HLII

State	IEEE-RTS			IEEE-WRTS		
	0	5%	10%	0	5%	10%
Healthy	86.41	77.41	63.64	78.84	68.95	60.34
Marginal	4.15	4.40	4.48	4.24	4.32	4.39
At Risk	3.99	4.20	4.73	3.86	3.92	4.34

It can be seen from Table 4.33 that the healthy and marginal state probabilities with increase in the LFU for the IEEE-RTS and the IEEE-WRTS behave in a similar manner to those for the RRBTS and the WRRBTS-1. The at risk state probabilities for the IEEE-RTS and the IEEE-WRTS are relatively close for the three LFU compared to the healthy and marginal state probabilities. The at risk state probability for the IEEE-WRTS is slightly larger than that of the IEEE-RTS at the LFU level of 5% and smaller at 10%. This is different from that in the RRBTS and the WRRBTS-1. This is because the RRBTS and the IEEE-RTS are at different reliability levels and act differently when the interactive effects of wind power and LFU on the indices are considered.

The system frequency of each state for the IEEE-WRTS shown in Table 4.34 are larger than those for the IEEE-RTS at each LFU level as in the RRBTS and the WRRBTS-1 analyses.

The average duration of each state for the IEEE-RTS and the IEEE-WRTS change correspondingly to the changes in the system probability and frequency.

The different degrees of LFU not only changes the system reliability indices, but also the well-being indices. When a conventional generating unit is replaced by a specific amount of wind power to maintain the system reliability, the reliability indices of systems with larger wind penetration are smaller than those of systems with lower

wind penetration when LFU is considered. The added wind power is able to counteract the effects of the LFU on the system reliability indices to some extent.

The healthy state probability decreases with increase in the LFU. In systems in which different wind replacement options are used to maintain the reliability indices, the more reliable the system is, the higher is the probability of the healthy state, and the lower is the probability of the marginal state. The frequency of each state increases with increase in the wind power penetration and LFU. The intermittent nature of the wind power creates more transitions between states. When the LFU increases, higher peak loads occur more often during the simulation process, which causes the system to transit between states more often.

4.6. Planning Studies Incorporating Wind Power and Load Forecast Uncertainty

4.6.1. Planning studies

The interactive effects of adding wind power to a system and the existence of LFU is illustrated using a selected series of wind power additions to the IEEE-MRTS. This system is the IEEE-RTS Case 1 described in Section 3.6.2. The IEEE-MRTS was modified by adding two 240 MW wind farms located at different buses. The modified study systems are as follows.

IEEE-WMRTS1: 240 MW WECS are connected to bus #1 and #8 both through two transmission lines.

IEEE-WMRTS2: 240 MW WECS are connected to bus #1 and #13 both through two transmission lines.

IEEE-WMRTS3: 240 MW WECS are connected to bus #1 and #18 both through two transmission lines.

IEEE-WMRTS4: 240 MW WECS are connected to bus #8 and #13 both through two transmission lines.

IEEE-WMRTS5: 240 MW WECS are connected to bus #8 and #18 both through two transmission lines.

IEEE-WMRTS6: 240 MW WECS are connected to bus #13 and #18 both through two transmission lines.

System reliability indices for the different wind addition options

The Regina and Swift Current wind data are used and wind speed correlations of 0%, 75% and 100% between the two wind sites are considered. The load shedding philosophy used is the Pass-I policy. The reliability indices for the six study systems are shown in Table 4.36.

Table 4.36: The system indices for the IEEE-WMRTS with different wind speed correlations

Reliability Indices	IEEE-WMRTS1			IEEE-WMRTS2		
	Wind Speed Correlation			Wind Speed Correlation		
	0%	75%	100%	0%	75%	100%
EFLC (occ/yr)	2.63	2.84	2.88	2.82	3.01	3.05
EDLC (hrs/yr)	7.53	7.97	8.08	8.32	8.74	8.90
ECOST(M$/yr)	4.877	5.27	5.36	5.75	5.98	6.03
DPUI (sys. mins)	22.29	24.20	24.67	25.67	26.82	27.11
Reliability Indices	IEEE-WMRTS3			IEEE-WMRTS4		
	Wind Speed Correlation			Wind Speed Correlation		
	0%	75%	100%	0%	75%	100%
EFLC (occ/yr)	3.28	3.38	3.40	2.64	2.83	2.86
EDLC (hrs/yr)	9.62	9.95	10.11	8.38	8.79	8.93
ECOST(M$/yr)	6.30	6.47	6.47	6.19	6.23	6.39
DPUI (sys. mins)	28.26	29.10	29.09	27.82	27.91	28.77
Reliability Indices	IEEE-WMRTS5			IEEE-WMRTS6		
	Wind Speed Correlation			Wind Speed Correlation		
	0%	75%	100%	0%	75%	100%
EFLC (occ/yr)	3.25	3.32	3.38	3.50	3.59	3.61
EDLC (hrs/yr)	9.99	10.46	10.51	10.96	11.26	11.45
ECOST(M$/yr)	6.58	6.80	6.77	8.04	8.06	8.22
DPUI (sys. mins)	30.30	31.36	31.26	36.56	36.59	37.57

It can be seen from Table 4.36 that the delivery point unavailability index (DPUI) and the EDLC for the IEEE-WMRTS1 are the smallest, followed by those of the IEEE-WMRTS2 and IEEE-WMRTS4. The EFLC for the IEEE-WMRTS1 and IEEE-WMRTS4 are similar and are smaller than those of the other cases. The IEEE-WMRTS1 with the two 240 MW WECS added to buses #1 and #8 provides a larger improvement in the system reliability than does the other study systems. This is mainly because the northern part of the IEEE-MRTS has most of the generating capacity and it is more efficient to add generating capacity directly to the southern portion to relieve the stress

on the transmission network associated with transmitting power from the northern part to the southern part.

It can also be seen from Table 4.36 that the reliability indices for the six study systems increase with increase in the wind speed correlation between the two WECS. When the two WECS are connected to two buses that are in relatively close proximity, the changes in the wind speed correlation have slightly more effect on the system reliability indices than when the WECS are connected to two buses that are widely separated. The transmission network tends to mask the effects of wind speed correlation on the system reliability.

Effects on the reliability indices of the various reinforcement alternatives considering LFU

The IEEE-WMRTS1 and IEEE-WMRTS2 are used in the following studies. The wind speed correlation between the two wind sites is considered to be 75%.

Line #23 (connecting buses #14 and #16), line #6 (connecting buses #3 and #9) and line #28 (connecting buses #16 and #17) in the IEEE-WMRTS1 and IEEE-WMRTS2 have the largest overload times in the previous studies. The transmission networks in the two systems are reinforced as follows.

Alt. 1: Add a line between buses #14 and #16.

Alt. 2: Add a line between buses #3 and #9.

Alt. 3: Add a line between buses #16 and #17.

The reliability indices for the IEEE-WMRTS1 and IEEE-WMRTS2 with the different reinforcement alternatives are shown in Table 4.37.

Table 4.37: The system indices for the IEEE-WMRTS1 and IEEE-WMRTS2 with the three reinforcement alternatives

Reliability Indices	IEEE-WMRTS1			IEEE-WMRTS2		
	Alt. 1	Alt. 2	Alt. 3	Alt. 1	Alt. 2	Alt. 3
EFLC (occ/yr)	2.56	2.56	2.66	2.67	2.66	2.91
EDLC (hrs/yr)	7.45	6.74	7.74	8.07	7.15	8.66
ECOST(M$/yr)	4.12	3.56	5.45	4.67	4.11	5.94
DPUI (sys. mins)	19.03	16.70	24.56	21.28	18.98	26.29

It can be seen from Table 4.37 that Alt. 2 provides the highest improvement in the system reliability compared to Alt. 1 and Alt. 3 for both the IEEE-WMRTS1 and IEEE-WMRTS2 when LFU is not considered.

The LFU of 5% and 10% with 100% dependent bus load correlation were added to the study. The reliability indices for the IEEE-WMRTS1 and IEEE-WMRTS2 are shown in Table 4.38.

Table 4.38: The system indices for the IEEE-WMRTS1 and IEEE-WMRTS2 with the three reinforcement alternatives considering LFU

Reliability Indices	IEEE-WMRTS1					
	LFU = 5%			LFU = 10%		
	Alt. 1	Alt. 2	Alt. 3	Alt. 1	Alt. 2	Alt. 3
EFLC (occ/yr)	3.82	3.79	3.84	8.47	9.78	9.41
EDLC (hrs/yr)	11.73	11.05	11.91	29.33	33.86	33.59
ECOST(M$/yr)	6.67	6.38	8.17	18.99	24.98	24.50
DPUI (sys. mins)	31.69	30.81	38.17	92.92	117.85	119.07
Reliability Indices	IEEE-WMRTS2					
	LFU = 5%			LFU = 10%		
	Alt. 1	Alt. 2	Alt. 3	Alt. 1	Alt. 2	Alt. 3
EFLC (occ/yr)	3.89	3.92	4.02	9.37	9.47	9.67
EDLC (hrs/yr)	12.38	11.44	12.41	33.49	32.92	34.89
ECOST(M$/yr)	7.54	6.91	8.32	23.63	24.48	26.94
DPUI (sys. mins)	35.50	32.83	38.25	114.59	118.38	129.25

The EDLC and DPUI for the IEEE-WMRTS1 are also shown in Figures 4.33 and 4.34 respectively. It can be seen that the reliability indices for Alt. 1 and Alt. 2 are quite close when the LFU is 5% but the indices for Alt. 2 are still slightly smaller than those for the Alt. 1. The indices for Alt. 2 are larger than those for Alt. 1 when the LFU is 10%.

When there is no LFU, the transmission network moving power from north to south is under less stress and the addition of a line between buses #3 and #9 (Alt. 2) improves a system reliability considerably since the major problem is in the southern segment. When LFU is considered, the transmission network transmitting power from the northern part to the southern part is under more stress and the line between buses #14 and #16 experiences the largest overload time. The addition of a line between buses

#14 and #16 (Alt. 1) improves the system reliability more than Alt. 2 does. The optimum reinforcement options change when different conditions such as LFU are considered.

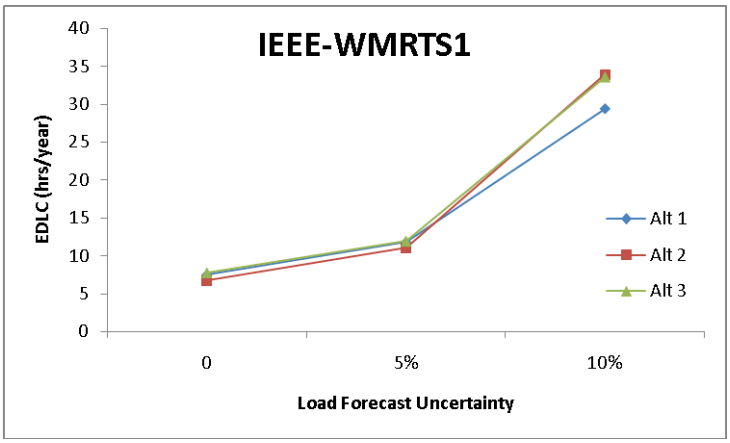

Figure 4.33: The EDLC for the IEEE-WMRTS1 reinforcement alternatives with LFU

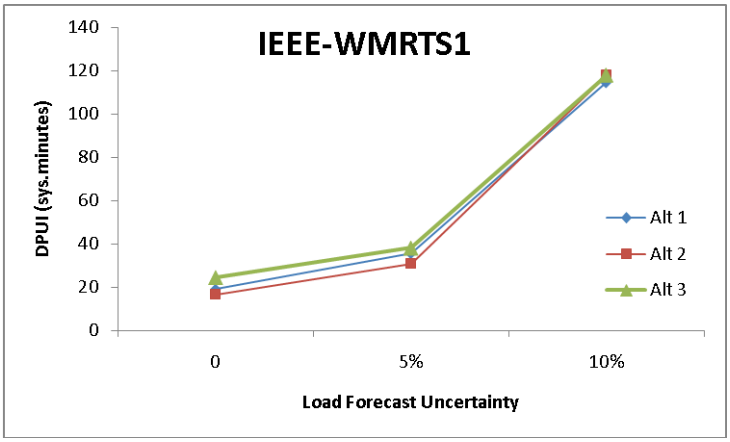

Figure 4.34: The DPUI for the IEEE-WMRTS1 reinforcement alternatives with LFU

4.6.2. Reliability cost/worth studies for different system reinforcement alternatives

A reliability cost/worth study was used to perform economic analyses of the tranmission reinforcement alternatives. The ECOST defined in Chapter 2 is the expected cost associated with load curtailments and is usually used in a conventional adequacy evaluation. The Total Cost (TOC) is the summation of the ECOST and the utility cost. The utility cost includes the capital cost and the operating and maintenance costs. Operating cost in the form of production costs were not inluded in this evaluation. The maintenance cost is included in the capital cost. The Annual Capital Payment (ACP) is the annual payment on a project from the beginning of the construction year through the useful lifetime of this project calculated as in [22]. A balance between the investment

capital cost related to improving the system reliability and the benefits associated with the improvement is created by minimizing the TOC using reliability cost/worth assessment.

The following studies show the reliability indices for the IEEE-MRTS with different wind addition and transmission network reinforcement options. The study systems and system reinforcement alternatives are as follows. The system reinforcement alternatvies are presented and utilized in the research in [22]. This thesis is focused on the impacts of LFU on these alternatives in terms of the ECOST and the TOC. The LFU of 0%, 5% and 10% are considered.

IEEE-WMRTS7: Two 240 MW WECS were added to the system at a new bus #25 and connected to bus #1 through two transmission lines. The system is reinforced as follows [22].

Case 1: Add a line between buses #1 and #2.

Case 2: Add a line between buses #1 and #3.

Case 3: Add a line between buses #1 and #4.

Case 4: Add one line between buses #1 and #3 and another line between buses #3 and #9.

Case 5: Add one line between buses #1 and #4 and another line between buses #4 and #9.

IEEE-WMRTS8: Two 240 MW WECS were added to the system through bus #25 and connected to different buses each through one transmission line. The reinforcement alternatives are as follows.

Case 6: Construct lines between buses #25 and #1 and between buses #25 and #3.

Case 7: Add a line between buses #3 and #9 based on Case 6.

Case 8: Construct lines between buses #25 and #1 and between buses #25 and #4.

Case 9: Add a line between buses #4 and #9 based on Case 8.

Case 10: Construct lines between buses #25 and #3 and between buses #25 and #4.

Case 11: Add one line between buses #4 and #9 based on Case 10.

The reliability indices for the 11 cases when LFU is not considered are shown in Table 4.39. It can be seen from this table that Case 11 has the smallest ECOST when the LFU is 0%. Table 4.40 shows the reliability indices for the IEEE-WMRTS Cases 1 to 11 considering the LFU. The bus load correlation is considered to be 100% dependent in this study.

Table 4.39: The system indices for the IEEE-WMRTS with different transmission network reinforcement alternatives

Cases	EFLC (occ/yr)	EDLC (hrs/yr)	ECOST (M$/yr)	DPUI (sys. mins)
Case 1	2.90	8.25	5.31	24.10
Case 2	4.12	9.58	4.83	21.20
Case 3	3.17	8.59	5.73	25.64
Case 4	3.63	8.54	4.34	19.43
Case 5	3.01	7.88	4.67	20.83
Case 6	2.88	7.52	4.29	19.47
Case 7	2.61	6.94	3.60	16.73
Case 8	2.82	7.75	4.91	22.37
Case 9	2.56	6.94	4.15	19.08
Case 10	2.64	6.55	3.26	15.28
Case 11	2.40	6.13	3.05	14.52

Table 4.40: The system indices for the IEEE-WMRTS with different transmission network reinforcement alternatives considering LFU

Cases	LFU = 5%				LFU = 10%			
	EFLC (occ/yr)	EDLC (hrs/yr)	ECOST (M$/yr)	DPUI (sys. mins)	EFLC (occ/yr)	EDLC (hrs/yr)	ECOST (M$/yr)	DPUI (sys. mins)
Case 1	4.16	12.79	8.41	39.29	9.25	31.89	23.61	114.03
Case 2	5.35	13.82	7.63	34.94	11.30	36.31	25.07	120.16
Case 3	4.31	12.57	8.31	38.38	10.30	35.83	26.77	128.50
Case 4	4.88	12.59	6.87	31.86	10.21	32.28	21.23	101.82
Case 5	4.17	11.95	7.48	34.85	9.21	31.34	22.37	107.74
Case 6	4.04	11.40	6.66	31.25	9.28	31.78	22.32	108.59
Case 7	3.82	11.19	6.37	30.47	9.37	31.86	22.00	107.07
Case 8	3.97	11.86	7.56	35.48	9.23	32.33	23.79	114.44
Case 9	3.73	11.19	7.05	33.23	9.12	31.63	22.33	108.09
Case 10	3.77	10.48	5.83	27.91	9.27	31.57	22.27	108.65
Case 11	3.52	9.88	5.34	25.74	9.33	32.26	22.48	110.17

It can be seen that the reliability indices increase significantly when the LFU increases. The order of the reliability indices for each case changes with increased LFU.

The ECOST for the IEEE-WMRTS cases are also shown pictorially in Figure 4.35. When the LFU is 0% and 5%, Case 11 has the smallest ECOST. When the LFU increases to 10%, Case 4 becomes the best reinforcement alternative in terms of the ECOST.

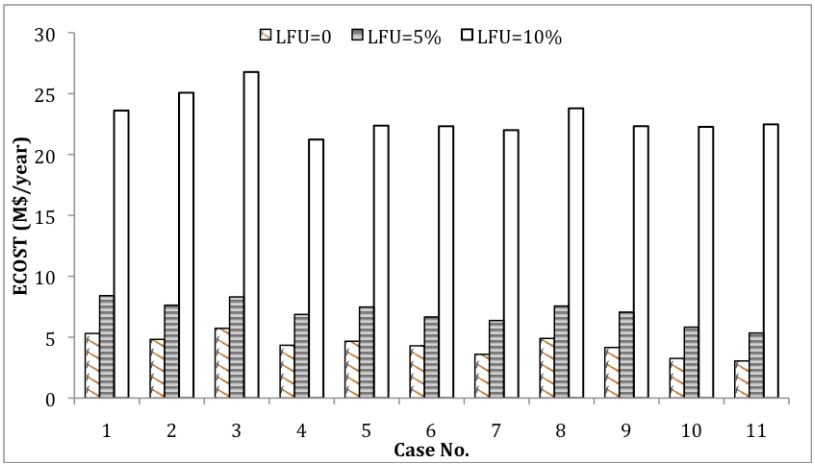

Figure 4.35: The ECOST of the IEEE-WMRTS cases with LFU

Table 4.41 shows the annual capital payment (ACP), the ECOST and the total cost (TOC) for the eleven IEEE-WMRTS cases. The TOC for each case with various LFU is also shown in Figure 4.36 and 4.37. It can be seen that Case 10 has the smallest TOC at an LFU of 0%. Case 10 and Case 6 have the smallest TOC respectively at the LFU of 5% and 10%.

Table 4.41: The ACP, ECOST and TOC for the IEEE-WMRTS cases with LFU

Cases		LFU = 0%.		LFU = 5%.		LFU = 10%.	
	ACP (M$/yr)	ECOST (M$/yr)	TOC (M$/yr)	ECOST (M$/yr)	TOC (M$/yr)	ECOST (M$/yr)	TOC (M$/yr)
Case 1	1.06	5.31	6.37	8.41	9.47	23.61	24.67
Case 2	3.10	4.83	7.92	7.63	10.73	25.07	28.17
Case 3	1.27	5.73	7.00	8.31	9.58	26.77	28.04
Case 4	4.86	4.34	9.20	6.87	11.74	21.23	26.09
Case 5	2.82	4.67	7.49	7.48	10.30	22.37	25.19
Case 6	2.11	4.29	6.41	6.66	8.77	22.32	24.44
Case 7	3.87	3.60	7.47	6.37	10.24	22.00	25.88
Case 8	2.11	4.91	7.02	7.56	9.67	23.79	25.91
Case 9	3.66	4.15	7.82	7.05	10.71	22.33	25.99
Case 10	2.82	3.26	6.08	5.83	8.64	22.27	25.09
Case 11	4.37	3.05	7.41	5.34	9.71	22.48	26.84

Figure 4.37 shows the TOC sorted in ascending order using the TOC when the LFU is 0%. It can be seen that the TOC when the LFU is 5% and 10% are not in ascending order. The incorporation of LFU in the analysis can affect the selection of the optimum reinforcement alternative.

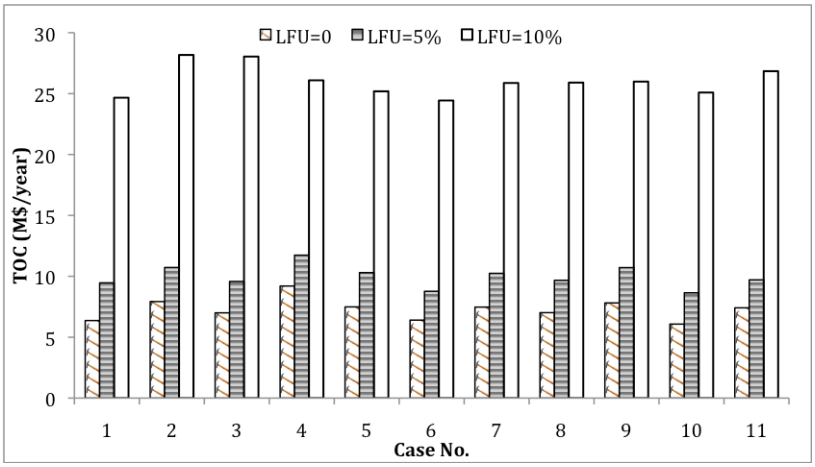

Figure 4.36: The TOC for the IEEE-WMRTS cases with LFU

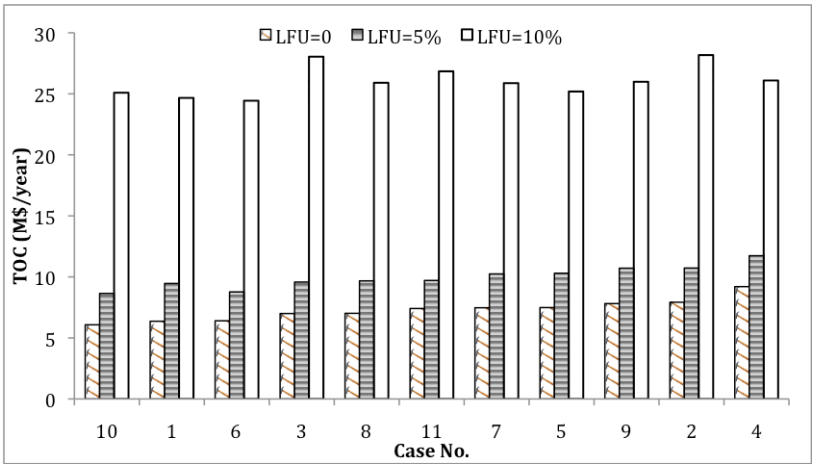

Figure 4.37: The TOC based on the ascending order at a LFU of 0% for the IEEE-WMRTS cases with LFU

4.6.3. Reliability cost/worth study for different system reinforcement alternatives incorporating security cost

Methodology to calculate security cost

Power system security depends on the manner in which a power system is operated and is defined as the ability of the system to withstand unexpected failures and

continue operating without interruption of supply to the consumers [108]. The failure of a single element of a power system does not have a wide impact under normal conditions. In some cases, however, the failure may trigger a sequence of events leading to partial or total collapse of the power system. Frequency collapse, cascading thermal overloads, transient instability, voltage instability and hidden failures such as malfunctions of protection systems are some of the mechanisms that can cause power systems to collapse [108].

It is impossible to eliminate all the failures in the system and a power system can never be totally secure. Different actions can be taken to improve the security of a power system. These measures can be categorized based on their cost or based on the time when they are implemented. In a cost-based classification, the cost of the measures that affect the flow of reactive power such as adjusting the transformer taps, or the voltage set-points of generators and SVCs is almost negligible. These measures, however, are often ineffective or insufficient to correct a security problem. The active power controls normally involve buying energy from more expensive generators, which creates an increase in the generation cost. Security considerations always impose a limit on the amount of power that can be transferred and often requires a generation dispatch that is not the most economic one. In the timing-based classification, there are preventive, corrective and desperate actions [108, 109]. Preventive actions can be considered for all contingencies and since an outage or disturbances can occur at any time, preventive measures can be very costly. Corrective actions are taken to react to an unanticipated event and the costs are lower because they are only implemented when actually needed. Corrective actions have a lower effectiveness when voltage or transient instability is a problem. Corrective load shedding provides a reasonably fast way to reduce active power flows in a weak power system. Desperate actions are used when preventive and corrective measures are not sufficient to solve the problem. These actions are aimed at saving the system from shedding significant amounts of load and to stop the spread of the disturbance.

Bulk Electric System (BES) reliability assessment has two basic aspects designated as system adequacy and system security. Power system security in BES is generally focused on the operation of the system in different operating states designated

as normal, alert, emergency and extreme emergency states [16-18, 110]. Transient (dynamic) and steady-state (static) are two forms of security analysis. Static security analysis involves the determination of whether there is a secure operating point for the perturbed power system after the dynamic oscillations have damped out. The traditional deterministic criterion known as the N-1 criterion is utilized in BES static security assessment. The well-being approach uses the deterministic criterion as the degree of steady state security in the system at any point in time by quantifying the likelihood of residing in the healthy and marginal states.

System well-being can be categorized into the three states of healthy, marginal and at risk as shown in Figure 1.3. In the healthy (secure) state, there is sufficient generation and transmission capacity to serve the total system demand and to meet the N-1 criterion. The system is operating without violation in the marginal (insecure) state, but there is not enough margin to satisfy the pre-defined deterministic criterion. In the at risk state, system operating constraints are violated and load may be curtailed.

Security costs are associated with a wide range of situations. This is an extremely complex problem to study in detail and is outside the scope of this research. The security cost considered in this research is simply related to the cost of the corrective actions involving active power control that can be used to bring the system from the marginal state back into the healthy state. The responding energy needed and the costs associated with this energy can be estimated as follows.

$$Resp.\quad Energy = \sum_{i=1}^{N}\sum_{j=1}^{8760}(TL_j - (AC_{ij} - C_{Lij}))/N \tag{4.8}$$

$$Security\quad Cost = \sum_{i=1}^{N}\sum_{j=1}^{8760}(P_j * (TL_j - (AC_{ij} - C_{Lij})))/N \tag{4.9}$$

where :

Resp. Energy is the responding energy required.

Security Cost is the cost related to the corrective actions required to bring the system from the marginal state back into the healthy state.

i is the sampling year

j is the hour in a year when the total generating capacity minus the largest unit is less than the total load.

TL_j is the total system load at hour j

AC_{ij} is the total available generating capacity at hour j of year i

C_{Lij} is the largest unit capacity at hour j of year i

N is the sample size.

P_j is the price of the energy at hour j.

The price in the power market varies and is time dependent. A constant energy cost of $80/MWh is assumed in this research to illustrate the concept.

Security cost for the RRBTS in the well-being analysis framework

The RRBTS is used in the well-being analysis in this section. The LFU and the peak load of the RRBTS are varied to examine their effects on the security cost.

The annual system energy requirement based on the load profile is 991,104 MWh at a peak load of 179.28 MW. Table 4.42 shows the responding energy needed to bring the system from the marginal state to the healthy state, the cost related to these corrective actions and the average cost of each occurrence of the marginal state with various LFU.

Table 4.42 shows that the security cost is relatively high due to the corrective actions required to keep the system operating in a secure state. The responding energy required to bring the system from the marginal state to the healthy state increases with increase in the LFU and the security costs increase accordingly. The average duration of the marginal state and the active power required to move the system from the marginal state to the healthy state also increase. The average security cost increases with increase in the LFU.

Table 4.42: The responding energy, security cost and average security cost for the RRBTS with LFU

LFU	Energy (MWh/yr)	Security cost ($/yr)	Average Security cost ($/occ)
0%	1752.89	140225.30	3511.92
5%	2140.08	171200.40	4067.96
10%	5547.16	443690.20	7403.21

Table 4.43 shows the responding energy required to bring the system from the marginal to the healthy state, the cost related to the action and the average cost at each occurrence of the marginal state as a function of the peak load.

Table 4.43: The responding energy, security cost and average cost for the RRBTS with various peak loads

Peak Load (%)	Energy (MWh/yr)	Security Cost ($/yr)	Average Security Cost ($/occ)
100	1752.89	140225.30	3511.92
101	2020.24	161732.70	3801.05
102	2314.59	185050.30	3965.98
103	2636.58	210790.20	4059.52
104	2987.63	238916.10	4161.62
105	3367.06	269695.10	4303.02
106	3779.24	302427.20	4632.80

It can be seen from Table 4.43 that the security cost and average security cost increase with increase in the peak load as the system is operating under more insecure conditions.

Studies on the IEEE-MRTS considering security cost

A series of studies were conducted to examine the economic effects associated with adding specific transmission lines to the wind assisted IEEE-MRTS with LFU.

The IEEE-MRTS, Case 1, Case 2, Case 4, Case 6 and Case 10 were studied using well-being analysis. Table 4.44 shows the HLII well-being indices for the IEEE-MRTS with LFU.

Table 4.44: HLII Well-being indices for the IEEE-MRTS with LFU

State	LFU = 0%		
	Probability (hrs/yr)	Frequency (occ/yr)	Average Duration (hrs/occ)
Healthy	5949.72	342.09	17.39
Marginal	2772.43	345.85	8.02
At Risk	13.85	4.04	3.43
State	LFU = 5%		
	Probability (hrs/yr)	Frequency (occ/yr)	Average Duration (hrs/occ)
Healthy	6082.37	320.59	18.97
Marginal	2632.50	326.29	8.07
At Risk	21.13	5.97	3.54
State	LFU = 10%		
	Probability (hrs/yr)	Frequency (occ/yr)	Average Duration (hrs/occ)
Healthy	6485.48	268.64	24.14
Marginal	2200.53	279.48	7.87
At Risk	49.99	12.75	3.92

It can be seen that the healthy and at risk state probabilities increase with increase in the LFU, while the marginal state probability decreases at this peak load level. The healthy, marginal state frequencies decrease with increase in the LFU, while the at risk state frequency increases with increase in the LFU. This indicates that the transitions between the healthy and marginal states decrease. The average durations of the healthy and the at risk states increase with increase in the LFU. The marginal state average duration increases slightly with LFU of 0% to LFU of 5%, then decrease from LFU of 5% to 10%. The LFU have different effects on the well-being indices for systems with different generation compositions, transmission network configurations and load levels.

The well-being indices for the IEEE-WMRTS7 Cases 1, 2 and 4 are shown in Tables 4.45, 4.46 and 4.47 respectively.

Table 4.45: HLII Well-being indices for the IEEE-WMRTS7 Case 1 with LFU

State	LFU = 0%		
	Probability (hrs/yr)	Frequency (occ/yr)	Average Duration (hrs/occ)
Healthy	6671.52	351.83	18.96
Marginal	2056.23	354.48	5.80
At Risk	8.25	2.90	2.84
State	LFU = 5%		
	Probability (hrs/yr)	Frequency (occ/yr)	Average Duration (hrs/occ)
Healthy	6713.71	323.08	20.78
Marginal	2009.49	326.99	6.15
At Risk	12.79	4.16	3.07

Table 4.46: HLII Well-being indices for the IEEE-WMRTS7 Case 2 with LFU

State	LFU = 0%		
	Probability (hrs/yr)	Frequency (occ/yr)	Average Duration (hrs/occ)
Healthy	6073.23	399.50	15.20
Marginal	2653.19	403.25	6.58
At Risk	9.58	4.12	2.33
State	LFU = 5%		
	Probability (hrs/yr)	Frequency (occ/yr)	Average Duration (hrs/occ)
Healthy	6100.55	376.65	16.20
Marginal	2621.64	381.70	6.87
At Risk	13.82	5.35	2.58

It can be seen from Table 4.45 that the healthy, marginal and at risk state probabilities, frequencies and durations for the IEEE-WMRTS7 Cases 1, and 4 change in a similar manner to those in the IEEE-MRTS. The probability of the healthy state for the IEEE-WMRTS Case 1 is larger than that for the IEEE-MRTS due to the addition of wind power, whereas the marginal and at risk state probabilities are smaller. The frequencies of the three states for the IEEE-WMRTS Case 1 are larger than those for the IEEE-MRTS due to the intermittent nature of wind power.

It is noted that the probabilities of the healthy state and at risk state increase with increase in the LFU, while the marginal state probability decreases. This is mainly because the higher peak loads associated with the LFU make the system reside longer in the at risk state and the lower peak loads make the system reside longer in the healthy state at this forecast peak load level when the LFU increases. The marginal state probability therefore decreases. The frequencies of the healthy and marginal states also decrease with LFU. When the forecast peak load changes, the changes in the well-being indices may be different from those at this specified peak load.

Table 4.47: HLII Well-being indices for the IEEE-WMRTS7 Case 4 with LFU

State	LFU = 0%		
	Probability (hrs/yr)	Frequency (occ/yr)	Average Duration (hrs/occ)
Healthy	6074.62	398.32	15.25
Marginal	2652.85	401.68	6.60
At Risk	8.54	3.63	2.35
State	LFU = 5%		
	Probability (hrs/yr)	Frequency (occ/yr)	Average Duration (hrs/occ)
Healthy	6140.44	372.79	16.47
Marginal	2582.97	377.38	6.84
At Risk	12.59	4.88	2.58

The well-being indices for the IEEE-WMRTS8 Case 6 and 10 at various LFU are shown in Tables 4.48 and 4.49 respectively.

Table 4.48: HLII Well-being indices for the IEEE- WMRTS8 Case 6 with LFU

State	LFU = 0%		
	Probability (hrs/yr)	Frequency (occ/yr)	Average Duration (hrs/occ)
Healthy	6327.15	368.33	17.18
Marginal	2401.34	371.00	6.47
At Risk	7.52	2.88	2.61
State	LFU = 5%		
	Probability (hrs/yr)	Frequency (occ/yr)	Average Duration (hrs/occ)
Healthy	6338.35	341.58	18.56
Marginal	2386.27	345.36	6.91
At Risk	11.40	4.04	2.82
State	LFU = 10%		
	Probability (hrs/yr)	Frequency (occ/yr)	Average Duration (hrs/occ)
Healthy	6454.39	304.31	21.21
Marginal	2249.83	312.50	7.20
At Risk	31.78	9.28	3.42

Table 4.49: HLII Well-being indices for the IEEE-WMRTS8 Case 10 with LFU

State	LFU = 0%		
	Probability (hrs/yr)	Frequency (occ/yr)	Average Duration (hrs/occ)
Healthy	6465.55	347.83	18.59
Marginal	2263.90	350.28	6.46
At Risk	6.55	2.64	2.48
State	LFU = 5%		
	Probability (hrs/yr)	Frequency (occ/yr)	Average Duration (hrs/occ)
Healthy	6458.39	317.02	20.37
Marginal	2267.14	320.76	7.07
At Risk	10.48	3.77	2.78
State	LFU = 10%		
	Probability (hrs/yr)	Frequency (occ/yr)	Average Duration (hrs/occ)
Healthy	6566.70	276.10	23.78
Marginal	2137.74	285.44	7.49
At Risk	31.57	9.27	3.41

It can be seen from Tables 4.49 and 4.45 that the at risk state probability for Case 10 is the smaller than that for Case 1, which indicates that Case 10 is more reliable than Case 1. The healthy state probability for Case 10 is, however, less than that for Case 1, which implies that Case 10 resides for a shorter time in the healthy state. A more reliable system is not necessarily a more secure system in terms of the healthy state probability. The well-being indices with increasing LFU for the IEEE-WMRTS8 Case 6

and Case 10 change in the same manner as those for the IEEE-WMRTS7 Case 1, Case 2 and Case 4.

The energy required to bring the system from the marginal state to the healthy state and the related security cost for the IEEE-WMRTS Cases 1, 2, 4, 6 and 10 at LFU of 0% and 5% are shown in Table 4.50 and Figure 4.38.

Table 4.50: Responding energy and security cost for the IEEE-WMRTS Cases with LFU

Cases	LFU = 0 %.		LFU = 5 %.	
	Energy (MWh/yr)	Security Cost (M$/yr)	Energy (MWh/yr)	Security Cost (M$/yr)
Case 1	5696.98	0.4558	8537.03	0.6830
Case 2	5696.29	0.4557	8604.81	0.6884
Case 4	5702.18	0.4562	8392.02	0.6714
Case 6	5703.78	0.4563	8323.44	0.6659
Case 10	5704.29	0.4563	8389.51	0.6712

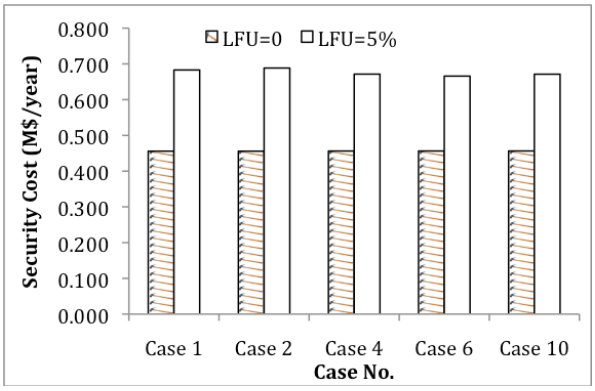

Figure 4.38: The security cost for the IEEE-WMRTS cases with LFU

It can be seen that the responding energy required and the security cost compare quite closely for these five cases at the LFU of 0%. The difference in the energy required and the related security cost vary slightly at the LFU of 5%. This is because the responding energy to bring the system from the marginal state to the healthy state is only required when the available system generating capacity minus the largest generating unit is less than the total system load. This is mainly determined by the generation composition and the load profile. The different additions to the transmission configuration do not significantly affect the responding energy and the associated security cost. The generation compositions of the IEEE-WMRTS cases are the same and only the transmission networks are different, and therefore, the security costs of these

cases are relatively close to each other. The transmission network is under more stress at the LFU of 5% and has a larger effect on the responding energy and the security cost.

The LFU has a large effect on the security cost in the IEEE-WMRTS cases as can be seen in Table 4.50 and Figure 4.38. The security cost increases by approximately 50% when the LFU increases from 0% to 5%. The marginal state probability decreases with increasing LFU for the IEEE-WMRTS cases. This is because the increase in the LFU causes the system peak load to move either lower or higher. The lower loads associated with LFU make the system reside in the healthy state longer and the marginal state shorter. The higher loads have the opposite effect. The marginal state probability decreases because the effects of the lower loads dominate the healthy state and marginal state probabilities in this specific system. The higher loads make the responding energy at the marginal state duration higher which exceeds the effects on the responding energy at the lower loads. The responding energy and the security cost increases with LFU even though the marginal state probability decreases.

The ECOST, TOC, which is the summation of the ECOST and the ACP, and the TOC+Security Cost are shown in Table 4.51.

Table 4.51: The ECOST, TOC and TOC+Security Cost for the IEEE-WMRTS Cases with LFU

Cases	LFU = 0 %			LFU = 5 %		
	ECOST (M$/yr)	TOC (M$/yr)	TOC+Security Cost (M$/yr)	ECOST (M$/yr)	TOC (M$/yr)	TOC+Security Cost (M$/yr)
Case 1	5.309	6.366	6.822	8.408	9.465	10.148
Case 2	4.825	7.924	8.380	7.627	10.726	11.414
Case 4	4.340	9.201	9.657	6.874	11.735	12.406
Case 6	4.293	6.406	6.862	6.660	8.773	9.439
Case 10	3.260	6.078	6.534	5.826	8.644	9.315

Figures 4.39 and 4.40 show the TOC and the TOC+Security Cost for the IEEE-WMRTS cases at LFU of 0% and 5% respectively. It can be seen from Figures 4.39 and 4.40 that the inclusion of the security cost does not change the order of the TOC since the security costs for the different IEEE-WMRTS cases compare closely. The concept of security cost provides an estimate of the overall annual expected cost related to active

power control in the marginal state. The security cost could change the order of the total cost when the peak load changes or different system reinforcement alternatives are considered.

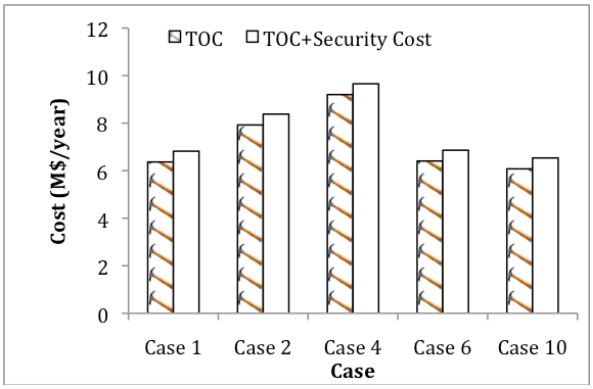

Figure 4.39: The TOC and TOC+Security Cost for the IEEE-WMRTS at the LFU of 0%

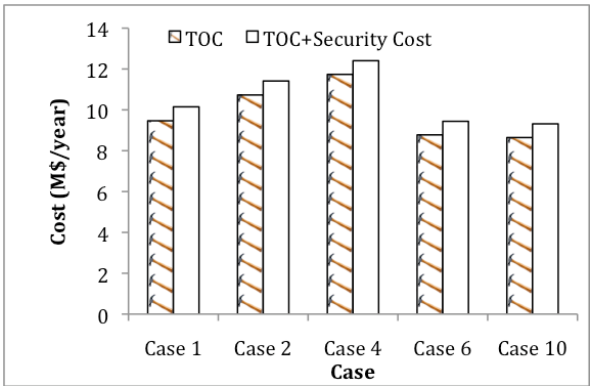

Figure 4.40: The TOC and TOC+Security Cost for the IEEE-WMRTS at the LFU of 5%

4.7. Conclusion

This chapter illustrates the technique used to add wind power in HLI and HLII reliability assessment. The sequential MCS technique permits a wide range of factors to be considered in a study and provides an excellent approach to include the correlation between the wind speed and the load in the analysis. The approach used in this research also facilitates the inclusion of the correlation between different wind sites in HLI and HLII analysis.

The results presented in this chapter clearly illustrate the effects in HLI generating capacity adequacy assessment of dependence and independence in site wind speeds and the capacity credit attributable under these conditions. The capacity credit attributable to the addition of wind power to a system is fundamentally different to that

associated with the addition of conventional generating capacity. The conventional generating unit outages are considered to be independent events. The power output of each wind turbine generator in a wind farm, however, is dependent and directly linked to the wind speed at the site. The capacity credit associated with each added increment of wind power deceases significantly when the site wind speeds are dependent and is relatively constant when the site wind speeds are independent. This clearly indicates the need to determine and incorporate the correlation between the existing and proposed wind farms as utilities and governments pursue higher wind penetration levels.

The HLI studies on the effects of wind speed correlation are extended to HLII analysis in this chapter. The ELCC based on the HLII EDLC and EFLC obtained are smaller than those determined in the HLI reliability evaluation. In HLII studies, transmission network contingencies are included, which tend to counteract improvements in the system reliability created by adding wind capacity. The LFU concepts introduced in Chapter 3 are extended to wind assisted composite system analysis in this chapter. The results show that the calculated ELCC decreases with increase in the LFU for the wind added system.

The research described in this chapter examines the impacts of wind power addition using the well-being framework including LFU considerations. The well-being indices are affected by the addition of wind power. The healthy state probability increases with increase in wind power in the system, while the marginal and at risk state probabilities decrease. In general, the frequency of each operating state decreases slightly with increase in the wind capacity. The decrease is due to the generating capacity contribution of the added wind power counteracted by the intermittent nature of the wind.

System reliability is improved by the addition of any suitable form of generating capacity, including wind power. When a conventional unit is replaced with an equivalent amount of wind power to maintain the EDLC or the EENS, the EFLC in the wind power added system will be larger than that of the original system due to the intermittent behaviour of wind power. When the system peak load changes, the EDLC and EENS equivalencies no longer apply but the difference may be acceptable for small load changes. Even though the EDLC for the equivalent system with wind is the same as

in the original system, the healthy state probability is smaller and the marginal state probability is larger for the wind assisted system. This indicates that the equivalent capacity system is more likely to transfer to the at risk state than the original system. The state frequencies increase considerably for the equivalent system, which indicates that there are more transitions between states. The operating state frequencies increase as more conventional generating capacity is replaced. The average duration of an operating state is determined by the probability and frequency of the state. When wind power is introduced in a system, the frequency increases more than the probability does and the average duration of each operating state decreases.

In general, system reliability indices increase with increase in LFU. The effects of LFU on the well-being indices are different for the original system and a system with wind replacing conventional generation. The difference in the at risk state probability at each LFU level for the two systems is relatively small. This is not the case for the healthy and marginal states. The replacement of conventional generating units with wind power tends to counteract the effect of LFU on the system reliability due to the multi-state output levels associated with the added wind power and the increase in the frequency is mitigated at low LFU levels. The operating state frequencies increase as the LFU increases.

The well-being approach provides the opportunity to integrate an accepted deterministic criterion into a probabilistic framework and to quantify the likelihood of operating in the marginal state. The increased cost associated with operating in the marginal state is incorporated in the economic analyses associated with system expansion planning including wind power and LFU in this chapter. This approach is illustrated using a series of case studies on the IEEE-WRTS. The results show that the optimum reinforcement option may change by recognizing LFU. The security cost did not affect the order of the total costs for the different transmission reinforcement alternatives applied to the IEEE-WMRTS. The incorporation of a security cost could change the selection of the optimum option when different system configurations or operating conditions are considered.

CHAPTER 5
EFFECTS OF DEMAND SIDE MANAGEMENT

5.1. Introduction

Demand side management (DSM) refers to initiatives that can be implemented by an electric power utility to encourage consumers to adopt energy efficient practices that are beneficial from both customer and system viewpoints [57-63]. Demand side management includes a wide range of techniques and objectives, one of which is load shaping or management (LM). A variety of LM techniques such as peak clipping, valley filling, load shifting, energy conservation etc have been proposed and studied. The benefits of implementing DSM include improving energy efficiency, system reliability and security, reducing capital and operating costs, transmission network congestion and the reduction of environmental damage and customer cost [55, 56, 65-69].

Demand for electricity continues to increase throughout the world due to industrial load growth and increases in population. The infrastructure investments required to meet the increasing demand are expected to be very expensive. Power utilities are also faced with an increasing awareness of environment conditions [64, 111]. Existing and new DSM programs will therefore play an important practical role in meeting the challenges faced by electric power utility companies.

References 64-69, 111, and 112 indicate some of the work that has been published on the effects of DSM on various aspects of power system reliability. These publications cover a wide range of issues and applications. The studies show that both the system and load point reliability indices can be impacted and improved by implementing DSM activities and that these improvements can be quantified using a probabilistic approach. The primary focus of this research is on the effects of selected DSM programs on the load point and system reliability indices of a bulk electric power system in the well-being analysis framework.

Different DSM initiatives such as peak clipping, load shifting, residential load sector load shifting and wind power added as distributed generation are examined in this

chapter. A DSM program was developed to modify the load model and create the required input data for the sequential Monte Carlo simulation program. The modifications to the RapHL-II program are also described.

Both the RBTS and the IEEE-RTS are used in this study. A modified load model with load sector compositions are used in this research. The basic load shape at each load point and for the system can be modified using different DSM activities. This research examines the effects on both systems of peak load clipping and load shifting using a valley filling approach. The analyses are extended to study load additions during the low load periods such as those which could occur due to charging electric vehicles. The effects of wind power injection or conventional generation in the form of local distributed generations are also considered. The conventional bulk electric system reliability indices [2], Expected Duration of Load Curtailment (EDLC), Expected Frequency of Load Curtailment (EFLC), Expected Energy Not Supplied (EENS), Expected Cost (ECOST) are used to illustrate the reliability effects of DSM.

5.2. Incorporating Demand Side Management in HLII Reliability Evaluation

The modified load model described in Chapter 2 is used in this research. As noted in Chapter 2, the aggregate load at each bus was decomposed into customer sector loads, and each load point in the RBTS and the IEEE-RTS is then composed of a number of customer sectors. The load model at a bus is obtained by summing the customer load sector data at that bus. There are seven customer load sectors: Residential, Commercial, Industrial, Government, Office, Large Users and Agricultural. The peak load for the RBTS and the IEEE-RTS is 179.28 MW and 2754.75 MW respectively.

The activities designated as peak clipping, load shifting, off-peak load addition and wind power addition as distributed generation are described in the following.

5.2.1. Methodology

Peak clipping and valley filling modeling

Peak clipping limits the peak load to a pre-specified peak value P. Peak clipping by itself is an extreme measure. The results, however, clearly show the impact of this portion of the load profile on the system and load point reliability indices. Valley filling or load shifting transfers all or part of the energy not supplied during the peak hours to

the off-peak hours if possible [65, 66]. The modified load is calculated using Equation 5.1.

$$\overline{L(t)} = \begin{cases} P & t \in \Omega \\ L(t) + A & t \in \Psi \end{cases} \tag{5.1}$$

where,

$$A = a\left[\frac{\sum_{t \in \Omega} (L(t) - P)}{N}\right] \tag{5.2}$$

$L(t)$: basic load model

$\overline{L(t)}$: modified load model,

Ψ: set of off-peak hours during which the energy is recovered,

Ω: set of on-peak hours during which the energy is reduced,

A : MW load added to each off-peak hour of Ψ.

N : number of off peak hours in Ψ.

a: the percentage of the energy reduced during on-peak hours that is recovered during off-peak hours.

In this research, the on-peak and off-peak hours are determined by the pre-specified peak load and the valley load values respectively. The energy reduced during a day is shifted to the immediately following off-peak hours.

The peak clipping and valley filling procedures can be applied to the entire bus load or a particular load sector such as the residential load component. When a is zero, the reduced energy at the peak hours is not shifted to the off-peak hours and the procedure becomes peak clipping. When a is larger than zero, a part or all the energy reduced at the peak hours is shifted to the off-peak hours and the procedure is designated as load shifting.

Off-peak load addition

In this case, the load is modified using Equation (5.3).

$$\overline{L(t)} = \begin{cases} VL & t \in \Psi \\ L(t) & t \in others \end{cases} \tag{5.3}$$

where

VL : the pre-specified minimum load,

Ψ : when the $L(t)$ is smaller than the pre-specified VL.

In this study, Ψ is determined by the bus load and the pre-specified minimum load. Peak clipping, valley filling and off-peak load addition can be applied at all buses, to a specific bus or a specific customer load sector.

Distributed generation

Distributed generation involves the use of small-scale power generation technologies located in the distribution networks. The application of distributed generation can result in lower costs, reduced emissions, reduced losses in the BES, improve the system reliability and expand customer energy options. Both conventional and renewable energy can be used as a source of distributed generation. Wind is an important energy source and is regarded as an important alternative to traditional electric power generating units [47], particularly in the area of distributed generation.

When conventional generation or wind power is added as distributed generation, the load at the buses where the distributed generation is added is modified using Equation (5.4).

$$\overline{L(t)} = \begin{cases} L(t) - P(t), when & P(t) \le L(t) \\ 0, \quad when & P(t) > L(t) \end{cases} \tag{5.4}$$

where

$P(t)$: Power output of the distributed generation at hour t.

It is assumed that the primary purpose of the distributed generation is to serve the customer load in the load network. Additional energy not required in the local network is transmitted to the grid. Distributed generation in the form of conventional generation is simulated as in [22, 73] and wind power is simulated using the concepts described in Chapter 4.

5.2.2. Programs and results

A DSM program was developed to perform the DSM initiatives stated in Section 5.2.1 and the RapHL-II program was modified to read the output load data from the DSM program and to incorporate wind power or conventional generation as distributed generation. The focus in this research is on the effects of the DSM initiatives and

distributed generation on the BES load point and system reliability. The modifications to the RapHL-II program to include the DSM output and incorporate distributed generation are illustrated in Figure 5.1. Steps 1, 2 and 3 in Figure 5.1 are described in Section 2.2 and shown in Figure 2.1.

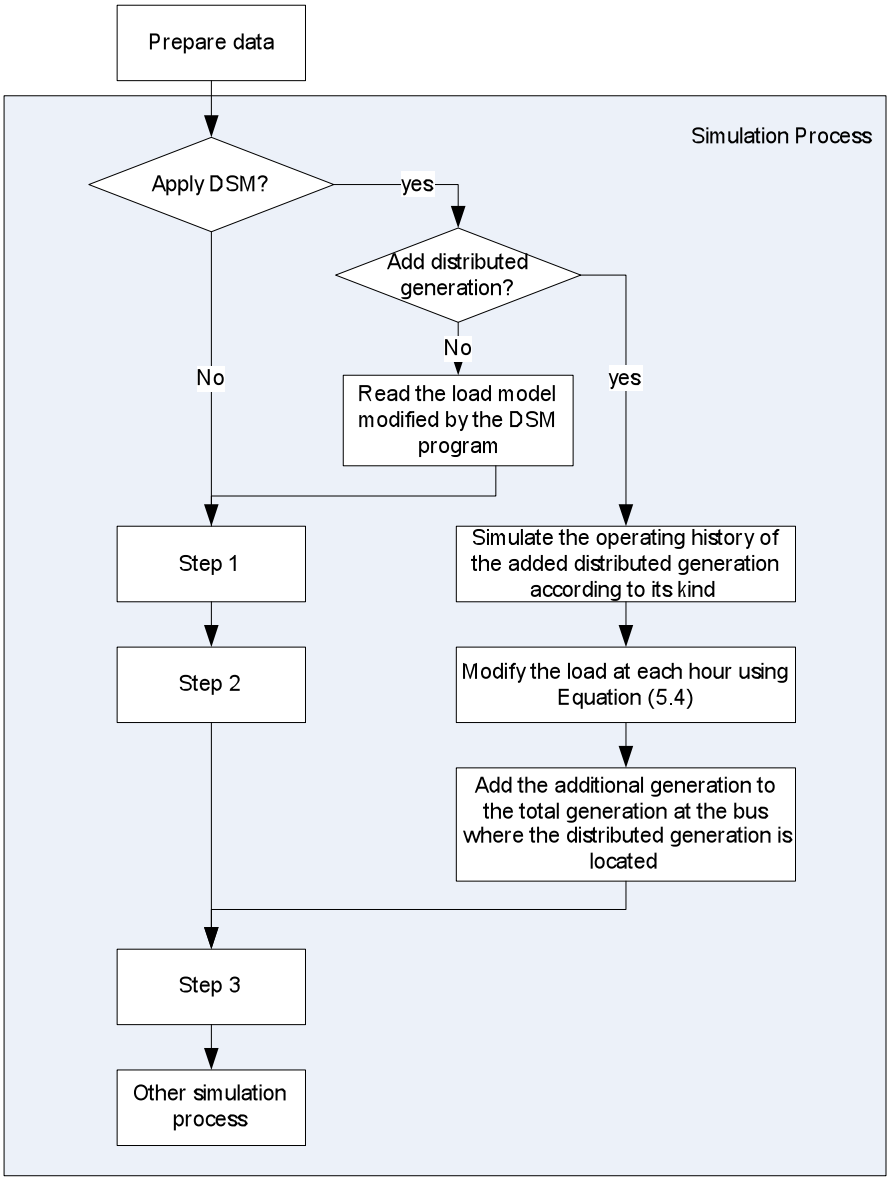

Figure 5.1: The process to incorporate DSM in sequential Monte Carlo simulation

The DSM program was applied to the modified load models for the RBTS and the IEEE-RTS described in Chapter 2. There are seven customer load sectors in both systems. The load models are composed of one or more sector loads and therefore the

bus loads are based on the sector load compositions at each bus. Each bus therefore has a unique load model.

The different DSM programs applied to the RBTS and the IEEE-RTS in this research are shown in Table 5.1. In this table, peak clipping, load shifting, residential load shifting and load addition are designated as PC, LS, Res-LS and LA respectively. The DSM initiative designated as PC80 indicates that the load at each bus is clipped at 80% of the original annual peak load for that bus. The DSM initiative designated as LA20 indicates that load will be added during the off-peak hours. The modified load at any hour during this period is not allowed to exceed 20% of the annual peak load for that bus. The additional load was assumed to be added only to the residential sector load as noted in Table 5.1.

Table 5.1: The DSM programs used in this research

DSM	Applied to	Pre-specified Peak (percent of the original peak)	Pre-specified Valley (percent of the original peak)	Energy Recover Percentage %
PC80	Bus load at all buses or one bus	80	-	0
PC85		85	-	0
PC90		90	-	0
LS80		80	50	100
LS85		85	50	100
LS90		90	50	100
Res-LS80	Residential load sector at all buses	80	50	100
Res-LS85		85	50	100
Res-LS90		90	50	100
LA20	Load addition on residential load sector at all buses	-	20	-
LA40		-	40	-
LA60		-	60	-

A particular 48-hour load profile at bus #3 of the RBTS with the application of various DSM programs is shown in Figure 5.2. The DSM programs were applied to all buses in the RBTS in this case.

It can be seen from these profiles that with peak clipping, the loads higher than the pre-specified peak are clipped. The lower the pre-specified peak load, the more energy is reduced. When load shifting is applied, the reduced energy in the on-peak hours is moved to the immediately following off-peak hours. The lower the pre-

specified peak load, the more energy is shifted from on-peak hours to off-peak hours. When load shifting is applied only to the residential load sector, the change in the bus load is not significant. When load addition is applied, the load at the off-peak hours increases. More load is added to the off-peak hours as the pre-specified minimum load increases.

Figure 5.3 shows the 48-hour residential sector load data with residential load shifting and load addition. In the residential load shifting application, the residential load is reduced at the on-peak hours and moved to the off-peak hours according to the residential load curve. The change is relatively small compared to the bus load.

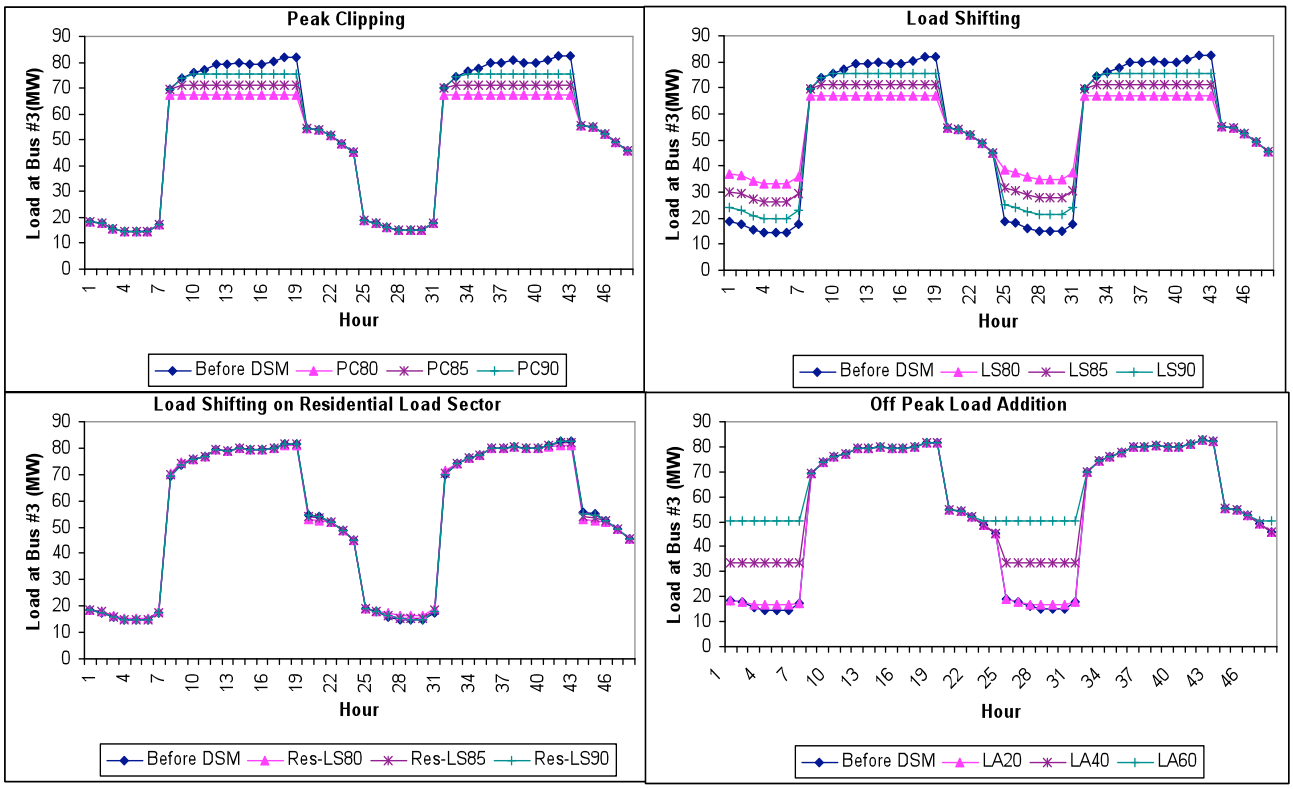

Figure 5.2: A 48-hour load profile at bus #3 of the RBTS with various DSM programs

When load addition is applied, the load is added in the valley portion of the residential load. It can be seen that the residential load shape changes significantly. As noted earlier, these additions could occur due to new requirements, such as charging the batteries of electric cars. The peak of the modified load when the pre-specified minimum load is 60% of the bus load is much higher than the original peak of the residential load sector at bus #3.

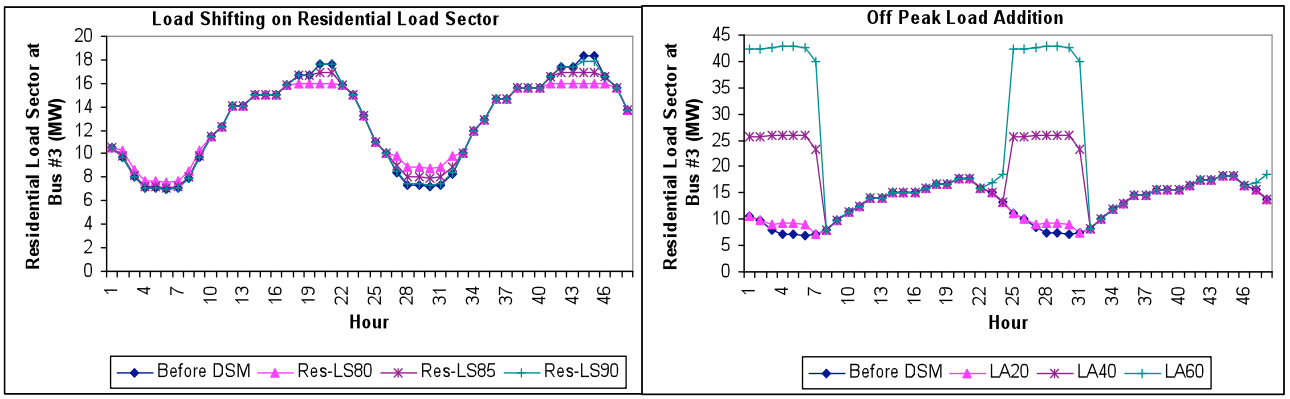

Figure 5.3: A 48-hour residential load profile at bus #3 of the RBTS with various DSM programs

A 48-hour system load profile created by summing the bus loads for the RBTS with the various DSM programs are shown in Figure 5.4.

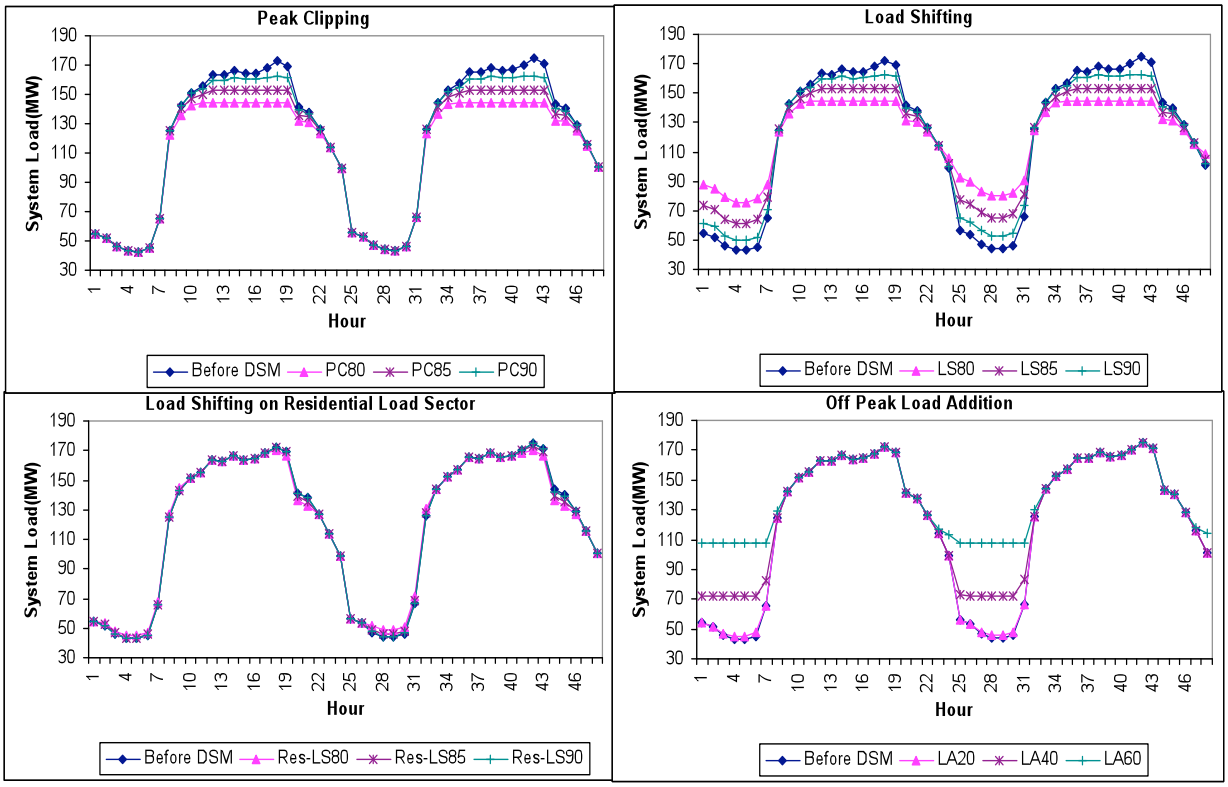

Figure 5.4: A 48-hour system load profile of the RBTS with various DSM programs

The DSM programs are applied to all buses in the system. The system load shape is slightly different from that of the load at bus #3 but the general changes in the system load profile with the application of the DSM programs are similar.

The load profile at bus #18 after applying the various DSM programs on the IEEE-RTS is shown in Figure 5.5. It can be seen from Figure 5.5 that the 48-hour load profile of bus #18 in the IEEE-RTS changes in a similar manner to that of bus #3 in the RBTS with the application of the various DSM programs. The 48-hour residential load sector data at bus #18 with residential load shifting and the off-peak load addition applications are shown in Figure 5.6.

It can be seen that the load shapes for the RBTS and the IEEE-RTS are slightly different, while the residential load profiles for the two systems with the residential load shifting or off-peak load addition are relatively similar but with different magnitudes.

It can be seen from the above results that the load models at different buses are changed significantly by applying the DSM initiatives. The effects of the DSM programs on system reliability are expected to be significant and are examined in the following using the DSM model in HLII reliability evaluation using the well-being framework.

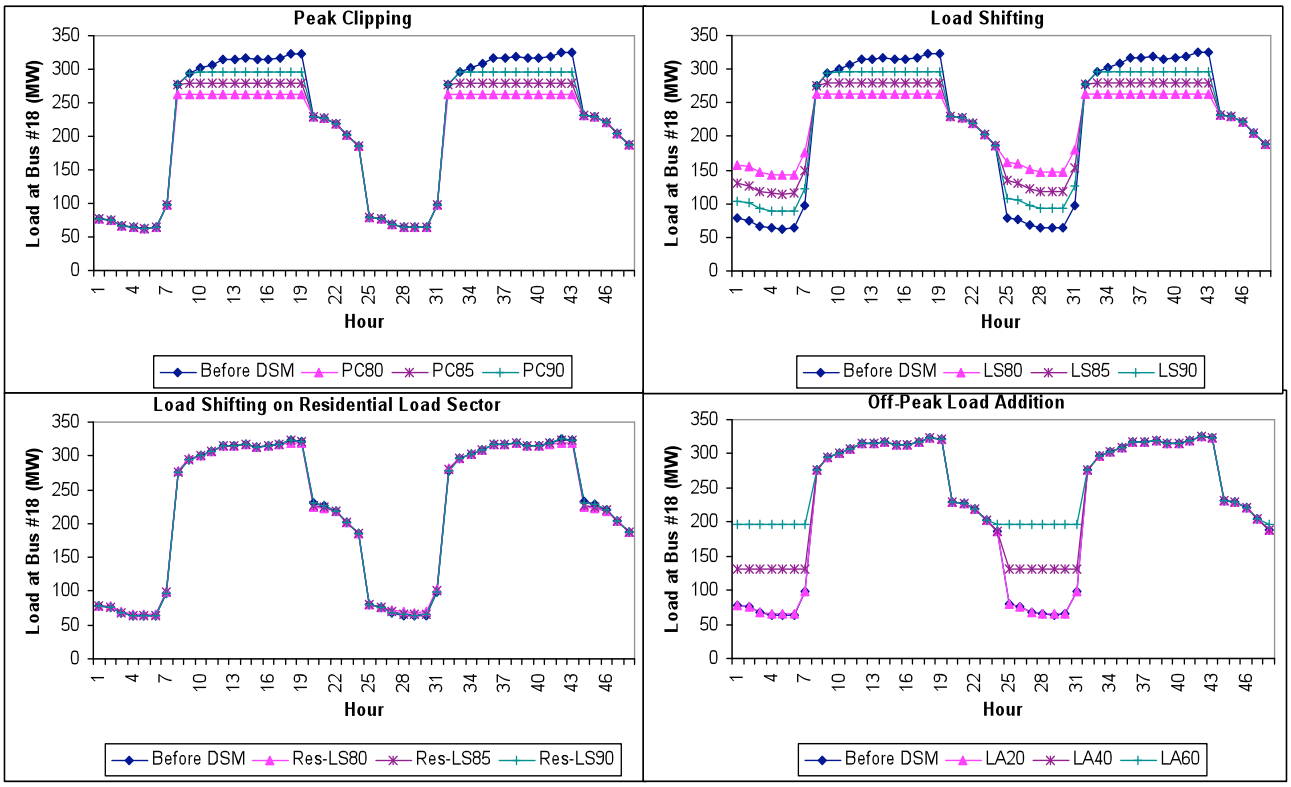

Figure 5.5: A 48-hour load profile at bus #18 of the IEEE-RTS with the various DSM programs

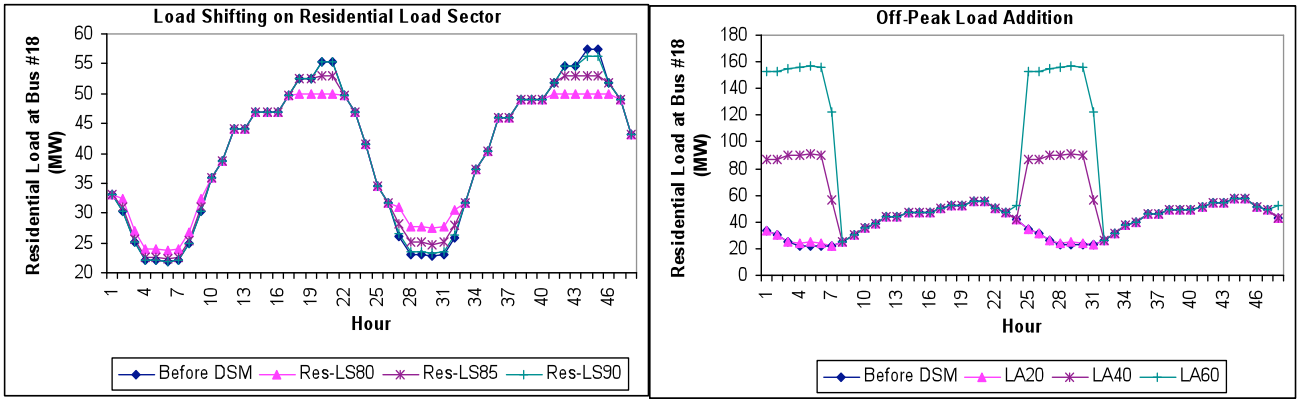

Figure 5.6: A 48-hour residential load profile at bus #18 of the IEEE-RTS with the various DSM programs

5.3. Effects of Peak Clipping in the Well-being Analysis Framework

The RapHL-II program was applied to the RRBTS and the IEEE-RTS with the sampling sizes of 8,000 and 4,000 years respectively. The Pass-I policy was used as the load shedding philosophy throughout this chapter.

5.3.1. RRBTS Results

The system reliability indices for the RRBTS when peak clipping was applied to all buses with changes in the pre-specified peak load are shown in Table 5.2.

Table 5.2: HLII system reliability indices for the RRBTS with peak clipping

DSM	EDLC (hrs/yr)	EENS (MWh/yr)	EFLC (occ/yr)	ECOST (k$/yr)
PC80	0.60	5.68	0.09	30.62
PC85	0.86	11.57	0.14	53.06
PC90	3.02	26.11	0.63	118.84
Base Case	3.92	47.58	0.85	200.83

It can be seen from Table 5.2 that the EDLC, EENS, EFLC and ECOST increase significantly with increase in the pre-specified peak load. The EENS when PC80 is applied is about one ninth of that of the Base Case. System reliability can be improved considerably by applying peak clipping. The load bus indices for buses #2 to #6 are shown in Figure 5.7.

It can be seen clearly in Figure 5.7 that the load point indices increases with increase in the pre-specified peak load. The changes in the reliability indices between

the base case and PC90 are more significant than between the other cases. The change is relatively insignificant between PC85 and PC80 where the pre-specified peak load decreases from 85% to 80%. This indicates that the change in the reliability indices becomes insignificant when the pre-specified peak load decreases to a certain level. The changes in the reliability indices at buses #3, #4 and #2 are larger than those at buses #5 and #6. This indicates that peak clipping has larger effects on buses with higher reliability indices. The changes in the EFLC with peak clipping are similar to those in the EDLC. The changes in EENS are similar to those of the ECOST as the ECOST is determined by the EENS and the IEAR.

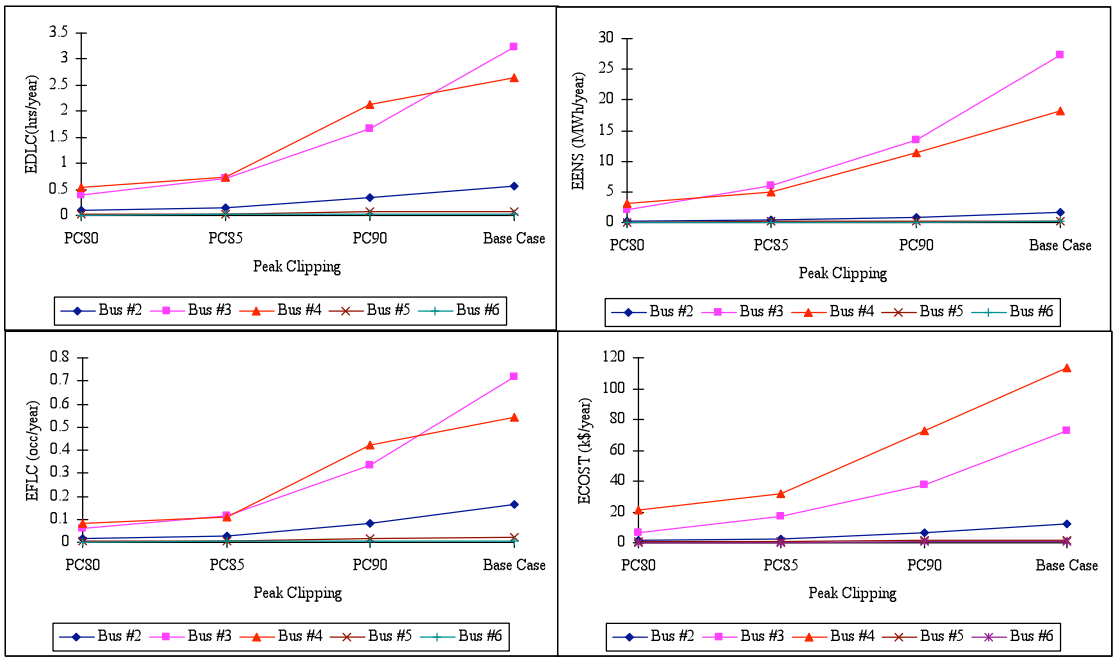

Figure 5.7: The load point indices for the RRBTS with peak clipping

The changes in the reliability indices with the peak clipping measures are different at different buses even though the same DSM measure is applied at each bus. Buses #3 and #4 have larger reliability indices than the other buses as shown in Figure 5.7. The EDLC of bus #3 is larger than that of bus #4 for the base case and is smaller than that of bus #4 when PC90 is applied. This indicates that the PC90 has a larger effect on the EDLC of bus #3 than that of bus #4. When PC85 is applied, the EDLC of Buses #3 and #4 are relatively close and the bus #3 EDLC is smaller than that of bus #4 using PC80.

The EENS index at the lower reliability buses in the base case decrease more significantly than at the buses with higher reliability, which is similar to the changes in the EDLC. The EENS of bus #3 decreases faster than that of bus #4 with the decrease in the pre-specified peak load as shown in Figure 5.7. The EENS of bus #3 is larger than that of bus #4 at the pre-specified peak of 90% even though the EDLC of bus #3 is smaller. This is because bus #3 has a larger peak load and the load curtailed at each duration could be larger than that at bus #4.

The generation composition, transmission network and load profile all affect the reliability indices. Buses #3 and #4 compare closely in the RRBTS and the transmission network is not a dominant factor in the difference in the reliability indices. Bus #3 has a peak load of 85 MW as shown in Figure 2.5, which is the largest bus load, bus #4 has a peak load of 40 MW, which is the second largest. The application of peak clipping directly changes the load shape, and therefore, has larger effects on buses with higher loads.

The well-being indices for the RRBTS with the various peak clipping measures are shown in Tables 5.3 to 5.5.

Table 5.3: HLII system probability of each operating state for the RRBTS with peak clipping

DSM	Probability of (hrs/yr)		
	Healthy State	Marginal State	At Risk State
PC80	8701.73	33.67	0.60
PC85	8684.90	50.24	0.86
PC90	8580.68	152.30	3.02
Base Case	8541.58	190.50	3.92

Table 5.4: HLII system frequency of each operating state for the RRBTS with peak clipping

DSM	Frequency of (occ/yr)		
	Healthy State	Marginal State	At Risk State
PC80	5.12	5.20	0.09
PC85	8.14	8.26	0.14
PC90	30.95	31.54	0.63
Base Case	39.15	39.95	0.85

It can be seen that the healthy state probability increases with a decrease in the pre-specified peak, while the marginal and at risk state probabilities decrease. The system becomes more secure by applying peak clipping. The system frequency of each operating state decreases with a decrease in the pre-specified peak load, which indicates that there are less transitions between states. The system tends to stay longer in the healthy state and shorter in the marginal and at risk states. The average duration of each operating state increases as the pre-specified peak load decrease. Even though both the system probability and system frequency of the marginal state decreases, the average duration of the marginal state increases as the system frequency change is larger than that of the system probability.

Table 5.5: HLII average duration of each operating state for the RRBTS with peak clipping

DSM	Average Duration of (hrs/occ)		
	Healthy State	Marginal State	At Risk State
PC80	1700.18	6.47	6.37
PC85	1066.60	6.08	6.37
PC90	277.25	4.83	4.83
Base Case	218.19	4.77	4.59

The effects of peak clipping measures on the well-being indices are not only determined by the pre-specified peak load, but also by the original load profile. As can be seen from Tables 5.3 to 5.5, the well-being indices decrease the most from PC90 to PC85. The effects on the indices are system specific but in general, the changes in the well-being indices tend to decrease as the pre-specified peak load reaches to a certain level.

5.3.2. IEEE-RTS Results

Peak clipping was also applied to the IEEE-RTS and the HLII reliability indices are shown in Table 5.6. Table 5.7 shows the load point indices for the IEEE-RTS with the PC80 procedure.

Table 5.6 clearly shows the peak load effect on the system reliability indices. As noted earlier, peak clipping by itself is an extreme measure. The reduction in load at the

on-peak hours improves the system reliability dramatically and the ECOST decreases significantly.

Tables 2.10 and 5.7 show that the load point indices decrease significantly with peak clipping and that the impacts of peak clipping at the various buses are different.

Table 5.6: HLII system reliability indices for the IEEE-RTS with peak clipping

DSM	EDLC (hrs/yr)	EENS (MWh/yr)	EFLC (occ/yr)	ECOST (k$/yr)
PC80	3.09	315.57	0.60	1447.87
PC85	8.66	970.80	1.51	4207.70
PC90	19.95	2283.08	3.76	9626.71
Base Case	35.92	4514.39	9.29	19070.50

Table 5.7: HLII load point indices for the IEEE-RTS with the PC80 procedure

Bus No.	EDLC (hrs/yr)	EENS (MWh/yr)	EFLC (occ/yr)	ECOST (k$/yr)
1	0.02	0.68	0.01	5.42
2	0.08	1.66	0.02	11.12
3	0.11	4.39	0.02	23.56
4	0.09	1.38	0.02	11.90
5	0.14	2.63	0.03	21.78
6	0.17	4.78	0.04	28.96
7	0.37	3.88	0.16	24.87
8	0.20	8.16	0.03	52.19
9	0.00	0.38	0.00	1.13
10	0.02	1.88	0.00	8.16
13	0.78	47.07	0.12	283.83
14	0.03	1.00	0.01	3.31
15	0.21	13.81	0.04	61.31
16	0.37	10.07	0.06	56.77
18	2.57	191.00	0.38	779.95
19	0.42	22.45	0.07	71.76
20	0.01	0.36	0.00	1.83

The load point EENS for the IEEE-RTS with the various peak clipping procedures are shown in Figure 5.8. It can be seen from this figure that the changes in the EENS due to the various peak clipping procedures are larger for buses with large EENS as noted in the RRBTS study.

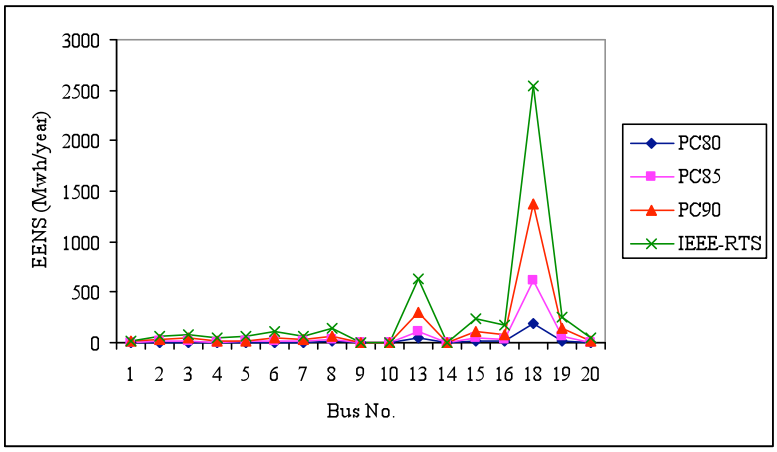

Figure 5.8: The load point EENS for the IEEE-RTS with the various peak clipping programs

As noted earlier, the peak clipping procedure is an extreme measure because it reduces the energy supplied to customers. The studies on peak clipping, however, clearly show how the system reliability can be affected and improved by applying this procedure.

5.4.Effects of Load Shifting on the Well-being Analysis Framework

Load shifting is a more practical process because it shifts customer energy usage from on-peak hours to off-peak hours instead of reducing power supply.

The load shifting procedures in Table 5.1 are used in this study. The off-peak hours in this study are the hours when the load is less than 50% of the original peak load at each bus. The load is shifted from the on-peak hours to the immediate off-peak hours of the day. Both the RRBTS and the IEEE-RTS are used in this research and the results are shown in the following.

5.4.1. Load shifting on all buses

RRBTS Results

The HLII system indices for the RRBTS when load shifting was applied to all bus loads with changes in the pre-specified peak load are shown in Table 5.8. Figure 5.9 shows the reliability index differences between peak clipping and load shifting for the RRBTS at the various pre-specified peak load levels.

Table 5.8: HLII system reliability indices for the RRBTS with load shifting

DSM	EDLC (hrs/yr)	EENS (MWh/yr)	EFLC (occ/yr)	ECOST (k$/yr)
LS80	0.60	5.81	0.09	31.33
LS85	0.87	11.65	0.14	53.40
LS90	3.02	26.21	0.63	119.31
Base Case	3.92	47.55	0.85	200.73

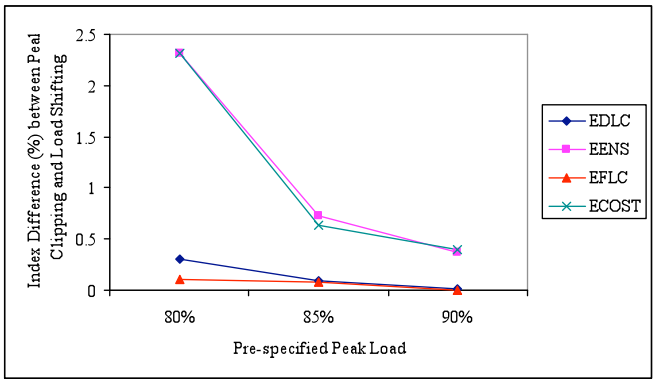

Figure 5.9: Differences in the reliability indices between peak clipping and load shifting for the RRBTS at the various pre-specified peak loads

It can be seen from Tables 5.2 and 5.9 that the reliability indices for the RRBTS when the peak clipping and load shifting procedures are applied are very close to each other at each pre-specified peak load level. It can be seen from Figure 5.9 that the differences in the reliability indices for the RRBTS using these two DSM measures are larger for the EENS and ECOST indices and smaller for the EDLC and EFLC. The largest difference is less than 2.5%. Load shifting is a more practical approach than direct load clipping and as shown in these studies, the increased load in the valleys in the profile does not create a significant decrease in the system reliability in the study system.

The load point EDLC and EENS for the RRBTS with peak clipping and load shifting are shown in Figure 5.10. As shown in Figure 5.9, the system EFLC change is similar to that in the EDLC and the ECOST change is similar to the EENS change. The EFLC and ECOST are not shown here.

It can be seen that both the load point EDLC and EENS for the RRBTS with peak clipping and load shifting compare closely. The EDLC at each load bus remains almost unchanged with the application of peak clipping and load shifting. It can be also

be seen from Figure 5.10 that the differences in the load bus EENS are a little larger than those in the load bus EDLC but are still very small. As shown in Figure 5.9, the differences in the system EENS expressed in percent are larger than those of the EDLC.

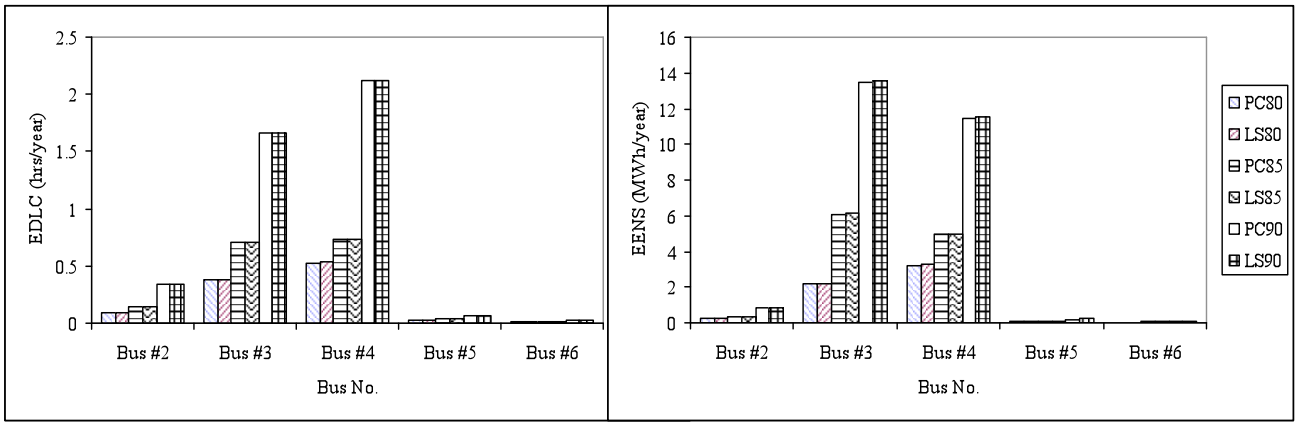

Figure 5.10: The load point EDLC and EENS for the RRBTS with the application of peak clipping and load shifting at the various pre-specified peak load

The differences in the EENS for the DSM measures at each pre-specified peak load divided by the EENS using peak clipping are shown in Figure 5.11. The EENS difference is less than 4%, which indicates that there is relatively little difference in the effects of peak clipping and load shifting in terms the system reliability improvement.

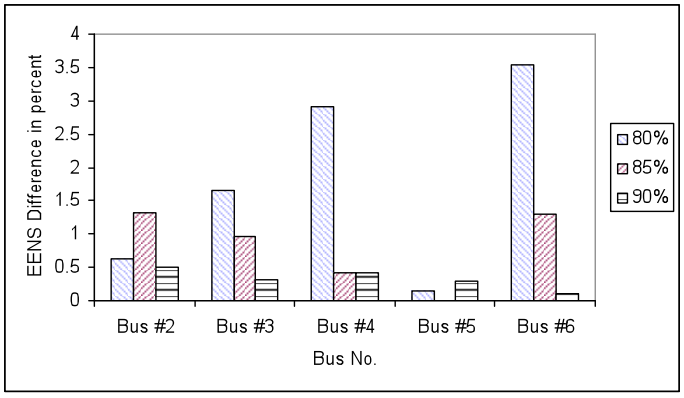

Figure 5.11: The difference in the load point EENS in percent for the RRBTS with the application of peak clipping and load shifting

The load point EENS changes differently at different buses and there is no specific pattern to the differences between peak clipping and load shifting with the pre-specified peak load. The load bus indices are determined by the generation composition, system transmission network, the load curtailment philosophy and the load profile at

each load bus. The effects on load point indices can be different even when the same DSM program is applied to each load bus.

The DLC and ENS distributions for the RRBTS with load shifting are shown in Figures 5.12 and 5.13.

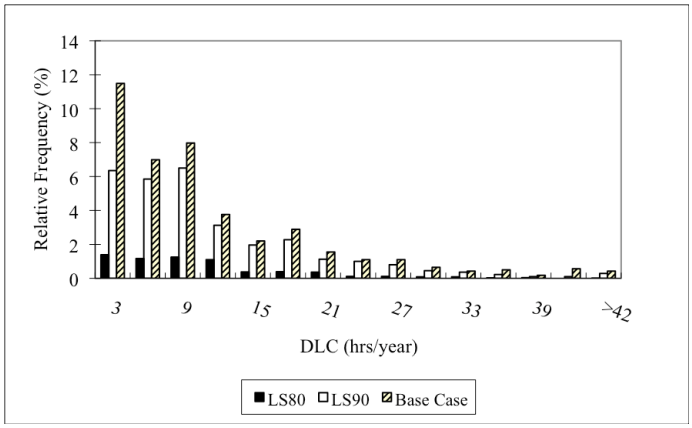

Figure 5.12: The DLC probability distribution for the RRBTS base case and the RRBTS with LS80 and LS90

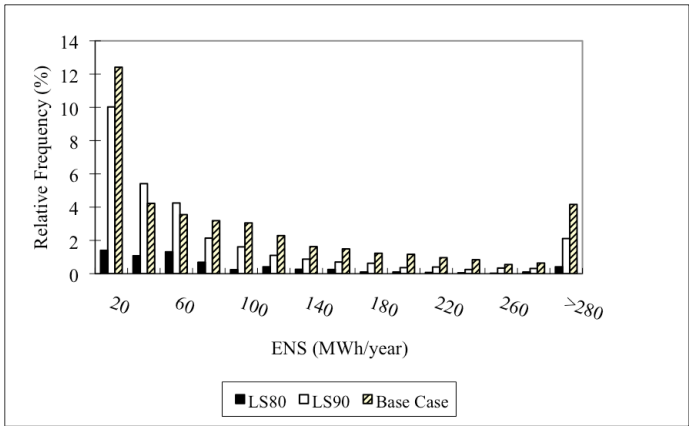

Figure 5.13: The ENS probability distribution for the RRBTS base case and the RRBTS with LS80 and LS90

The relative frequencies of encountering no load curtailment for the RRBTS with LS80, LS90 and the RRBTS base case are 58.64%, 69.49% and 93.50% respectively. The standard deviations of the DLC for the RRBTS with LS80, LS90 and the RRBTS base case are 3.01 hrs/yr, 6.67 hrs/yr and 7.60 hrs/yr respectively. The standard deviation and the range of the DLC decrease significantly when the load shifting procedures are applied. The relative frequency of each DLC class interval in Figure 5.12 for the RRBTS base case is considerably larger than that of the RRBTS with

LS80 or LS90. The ENS probability distributions for the RRBTS base case and the RRBTS with LS80 and LS90 show a similar pattern to the DLC distributions.

Tables 5.9 to 5.11 show the system probability, frequency and average duration of each operating state for the RRBTS. The well-being indices are close to those shown in Tables 5.3 to 5.5 when the peak clipping is applied. The changes are also similar but the values are slightly different. The energy shifted from on-peak hours to off-peak hours does not affect the well-being indices considerably.

Table 5.9: HLII system probability of each operating state for the RRBTS with load shifting

DSM	Probability of (hrs/yr)		
	Healthy State	Marginal State	At Risk State
LS80	8701.61	33.78	0.60
LS85	8684.86	50.28	0.87
LS90	8580.68	152.30	3.02
Base Case	8541.66	190.41	3.92

Table 5.10: HLII system frequency of each operating state for the RRBTS with load shifting

DSM	Frequency of (occ/yr)		
	Healthy State	Marginal State	At Risk State
LS80	5.13	5.22	0.09
LS85	8.15	8.27	0.14
LS90	30.95	31.54	0.63
Base Case	39.13	39.93	0.85

Table 5.11: HLII average duration of each operating state for the RRBTS with load shifting

DSM	Average Duration of (hrs/occ)		
	Healthy State	Marginal State	At Risk State
LS80	1695.23	6.48	6.38
LS85	1066.08	6.08	6.37
LS90	277.24	4.83	4.83
Base Case	218.30	4.77	4.59

IEEE-RTS Results

The results for the RRBTS show that there is not much difference in the system indices, load point indices and well-being indices when peak clipping or load shifting is

applied. The RRBTS is a relatively small reliable system. Similar studies were conducted on the IEEE-RTS which is a more practical system and the results are shown in the following.

The HLII system indices for the IEEE-RTS when the various load shifting measures are applied are shown in Table 5.12. It can be seen by comparing Tables 5.6 and 5.12 that the indices at the pre-specified peak load level when load shifting is applied are only slightly larger than those when peak clipping is applied for the IEEE-RTS. This indicates that the load reduced at the on-peak hours when added at the off-peak hours does not cause a significant decrease in system reliability. This is consistent with the conclusion drawn for the RRBTS. As shown in Figure 5.14, the reliability index differences in the IEEE-RTS using peak clipping and load shifting is less than 1%.

Table 5.12: HLII system reliability indices for the IEEE-RTS with load shifting

DSM	EDLC (hrs/yr)	EENS (MWh/yr)	EFLC (occ/yr)	ECOST (k$/yr)
LS80	3.12	317.81	0.60	1459.2
LS85	8.69	973.46	1.51	4222.6
LS90	19.96	2284.68	3.77	9633.5
Base Case	35.92	4514.39	9.29	19070.5

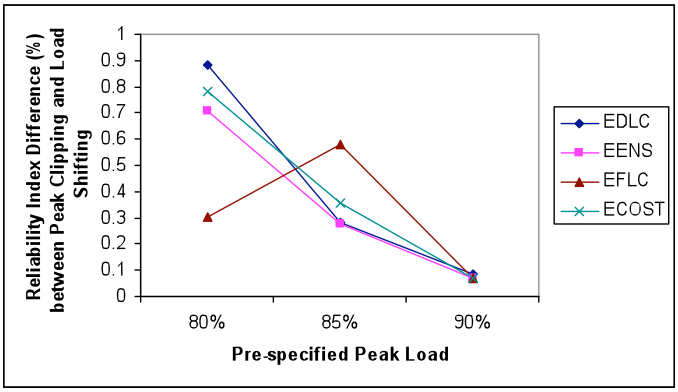

Figure 5.14: Differences in the reliability indices between peak clipping and load shifting for the IEEE-RTS at various pre-specified peak load

Table 5.13 shows the HLII load point indices with the LS80 procedure. A comparison of Table 5.7 and Table 5.13 shows that the load point indices for the IEEE-RTS with peak clipping are very close to those when load shifting is applied. The energy shifted from on-peak hours to off-peak hours does not significantly affect the load point indices in this case.

Table 5.13: The HLII IEEE-RTS load point indices with LS80

Bus No.	EDLC (hrs/yr)	EENS (MWh/yr)	EFLC (occ/yr)	ECOST (k$/yr)
1	0.03	0.70	0.01	5.6
2	0.08	1.67	0.02	11.2
3	0.11	4.44	0.02	23.8
4	0.10	1.41	0.02	12.2
5	0.14	2.66	0.03	22.0
6	0.17	4.84	0.04	29.4
7	0.36	3.92	0.16	25.0
8	0.20	8.24	0.03	52.7
9	0.00	0.40	0.00	1.2
10	0.02	1.93	0.00	8.3
13	0.78	47.42	0.12	287.1
14	0.03	1.00	0.01	3.3
15	0.21	13.86	0.04	61.6
16	0.37	10.13	0.06	57.1
18	2.60	192.26	0.39	784.9
19	0.43	22.56	0.07	72.0
20	0.01	0.36	0.00	1.8

The load point indices for the IEEE-RTS applying LS85 and LS90 are relatively close to those obtained by applying the corresponding peak clipping procedures and are not shown here. The load point EDLC and EENS at some selected buses with peak clipping and load shifting are shown in Figure 5.15.

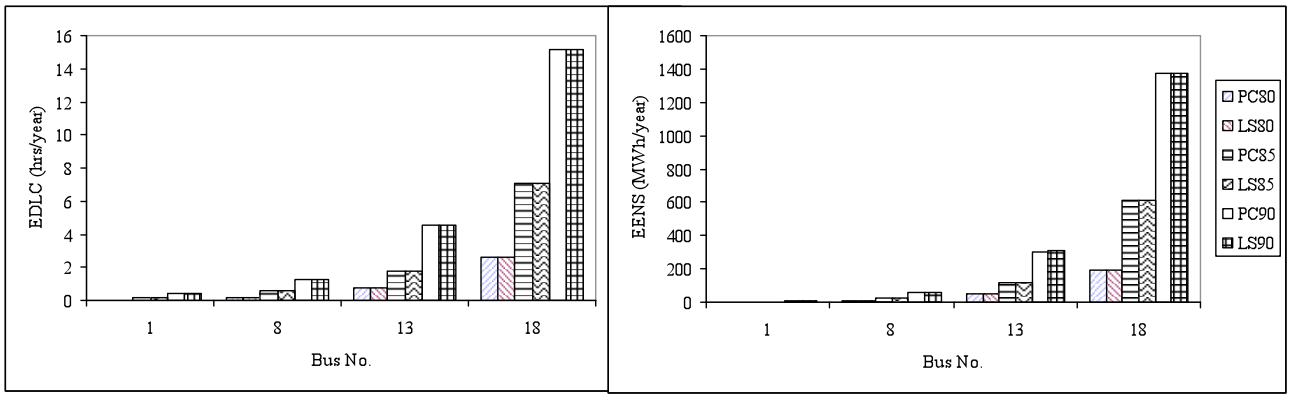

Figure 5.15: The load point EDLC and EENS for the IEEE-RTS with the application of peak clipping and load shifting at the various pre-specified peak loads

It can be seen from Figure 5.15 that the EDLC and EENS for the IEEE-RTS are similar when peak clipping or load shifting is applied at each pre-specified peak load level.

The DLC and ENS distributions for the IEEE-RTS with load shifting are shown in Figures 5.16 and 5.17.

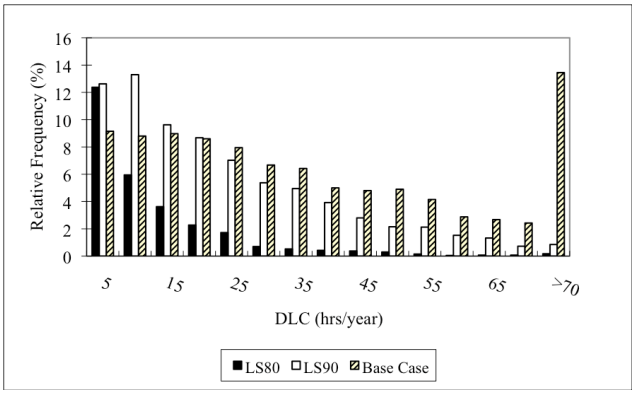

Figure 5.16: The DLC probability distribution for the IEEE-RTS base case and the RRBTS with LS80 and LS90

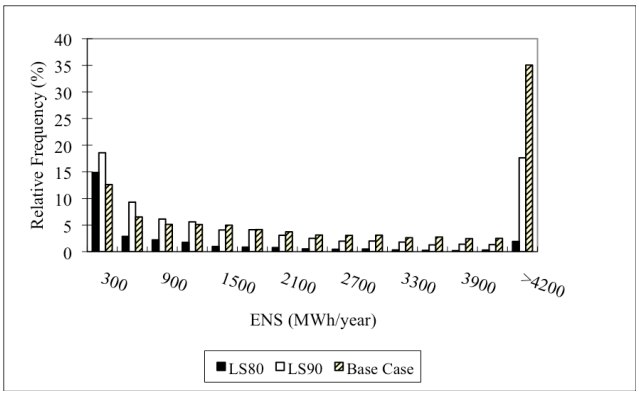

Figure 5.17: The ENS probability distribution for the IEEE-RTS base case and the RRBTS with LS80 and LS90

The relative frequencies of encountering no load curtailment for the IEEE-RTS with LS80, LS90 and the IEEE-RTS base case are 71.20%, 19.23% and 3.15% respectively. The standard deviations of the DLC for the IEEE-RTS with LS80, LS90 and the IEEE-RTS base case are 8.41 hrs/yr, 23.36 hrs/yr and 32.11 hrs/yr respectively. The standard deviation and the range of the DLC decrease significantly when the load shifting procedures are applied. The relative frequency of each interval for the IEEE-RTS with LS80 is smaller than those of the IEEE-RTS base case and the IEEE-RTS with LS90. The relative frequencies of the first 4 intervals for the IEEE-RTS with LS90 are larger than those for the IEEE-RTS base case. The relative frequencies of all the

other intervals for the IEEE-RTS with LS are smaller than those for the IEEE-RTS base case.

The ENS probability distributions have a similar form as the DLC distributions for the IEEE-RTS base case and the IEEE-RTS with LS80 and LS90.

The system well-being indices for the IEEE-RTS with various load shifting levels are shown in Tables 5.14 to 5.16.

Table 5.14: HLII system probability of each operating state for the IEEE-RTS with load shifting

DSM	Probability of (hrs/yr)		
	Healthy State	Marginal State	At Risk State
LS80	8590.18	142.70	3.12
LS85	8488.42	238.89	8.69
LS90	8353.83	362. 20	19.96
Base Case	8207.15	492.93	35.92

It can be seen from Table 5.14 that the health state probability increases with a decrease in the pre-specified peak load and the marginal state and at risk state probabilities decrease. The system tends to stay longer in the healthy state and shorter in the marginal and at risk states, which implies that the system is not only becoming more reliable with the utilization of load shifting, but also more secure.

Table 5.15 shows that the frequency of each operating state decreases with the application of DSM measures, which indicates fewer transitions between the three operating states.

Table 5.15: HLII system frequency of each operating state for the IEEE-RTS with load shifting

DSM	Frequency of (occ/yr)		
	Healthy State	Marginal State	At Risk State
LS80	23.99	24.34	0.60
LS85	38.73	39.85	1.51
LS90	62.81	65.76	3.77
Base Case	103.43	110.87	9.29

Table 5.16 shows that the average duration of the healthy state increases with decrease in the pre-specified peak load since the healthy state probability increases and the frequency decreases. The average durations of the marginal state and at risk state

changes are not as large as those of the health state and there are fluctuations in the marginal and at risk state average durations since both the probability and frequency decrease with decrease in the pre-specified peak load.

Table 5.16: HLII average duration of each operating state for the IEEE-RTS with load shifting

DSM	Average Duration of (hrs/occ)		
	Healthy State	Marginal State	At Risk State
LS80	358.14	5.86	5.23
LS85	219.15	5.99	5.74
LS90	132.99	5.51	5.30
Base Case	79.35	4.45	3.87

5.4.2. Effects on load carrying capability

The LS80, LS85 and LS90 procedures were applied to all buses in the RRBTS. A new load profile for each load bus was obtained as shown in Section 5.2.2.

Figure 5.18 shows the EDLC and EENS with changing peak load for the RRBTS with the various load shifting applications. The effective load carrying capability based on the EDLC and the EENS of the RRBTS with the application of load shifting measures are also shown. The EDLC and the EENS for the RRBTS base case at the peak load of 179.28 are used as the criterion values.

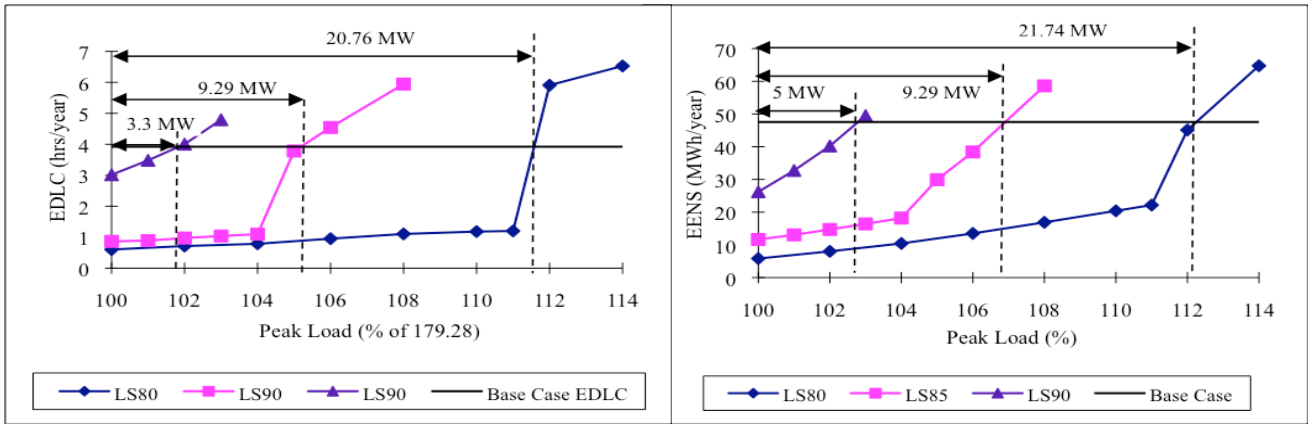

Figure 5.18: The EDLC and EENS versus peak load for the RRBTS with load shifting

It can be seen from Figure 5.18 that the reliability indices increase with increase in the peak load. When the LS80 procedure is applied, the EDLC increases slowly when

the peak load is less than 111% of the original value. The EDLC increases considerably when the peak load increases from 111% to 112% of the original value. When the LS85 procedure is applied, a big increase occurs when the peak load increases from 104% to 105%. This is due to the fact that when LS80 and LS85 are applied, the peak hour loads are flattened. When the peak load increases to a certain level, the flat top on the load profile causes the system to lose a large amount of load in the event of a significant disturbance. The EENS changes in a similar manner to the EDLC with increase in the peak load, but not quite as abruptly. The system ELCC increases as the pre-specified peak load in the load shifting procedure decreases. The ELCC values are similar for the EENS and EDLC criteria.

5.4.3. Load shifting on the residential load sector

The load shifting measure was applied to the residential load sector at all buses in order to modify the load profiles. In this case, the off-peak hours are those hours when the load is less than 50% of the peak.

RRBTS Results

The HLII system indices for the RRBTS when residential load shifting was applied to all buses with changes in the pre-specified peak load are shown in Table 5.17.

Table 5.17: HLII system reliability indices for the RRBTS with load shifting applied to the residential sector

DSM	EDLC (hrs/yr)	EENS (MWh/yr)	EFLC (occ/yr)	ECOST (k$/yr)
Res-LS80	3.84	43.56	0.83	188.58
Res-LS85	3.86	46.17	0.84	196.00
Res-LS90	3.91	47.36	0.85	200.01
Base Case	3.92	47.55	0.85	200.73

It can be seen that the reliability indices decrease with a decrease in the pre-specified peak load. The system reliability does not improve as much as when load shifting was applied to the bus load at all buses, as the residential sector takes only 23% to 47% of each bus load as shown in Table 2.1. The residential sector is only 23% of the load at bus #3, which has the largest peak load of 85 MW. As shown in Figure 5.2, when load shifting is only applied to the residential load sector, the total bus load changes only

slightly. It can also be seen from Table 5.17 that when the pre-specified peak is 80% of the residential sector load peak at each bus, the decrease in the ECOST is 12.15 k$/yr. The benefit in the ECOST will be larger for larger systems or for a system with a larger residential component.

The load point EDLC for the RRBTS with load shifting applied to the residential load sector at all buses are shown in Table 5.18. It can be seen from Table 5.18 that the changes in the load point EDLC are not as large as those when the DSM measures are applied to the total bus load.

Table 5.18: The EDLC (hrs/yr) at each bus for the RRBTS with load shifting applied to the residential sector

DSM	Res-LS80	Res-LS85	Res-LS90	Base Case
Bus #2	0.46	0.51	0.55	0.55
Bus #3	3.14	3.20	3.21	3.22
Bus #4	2.58	2.60	2.63	2.64
Bus #5	0.07	0.07	0.07	0.07
Bus #6	0.03	0.03	0.03	0.03

The decreases in the EENS and ECOST at each load bus of the RRBTS using residential sector load shifting compared to the base case values are shown pictorially in Figure 5.19.

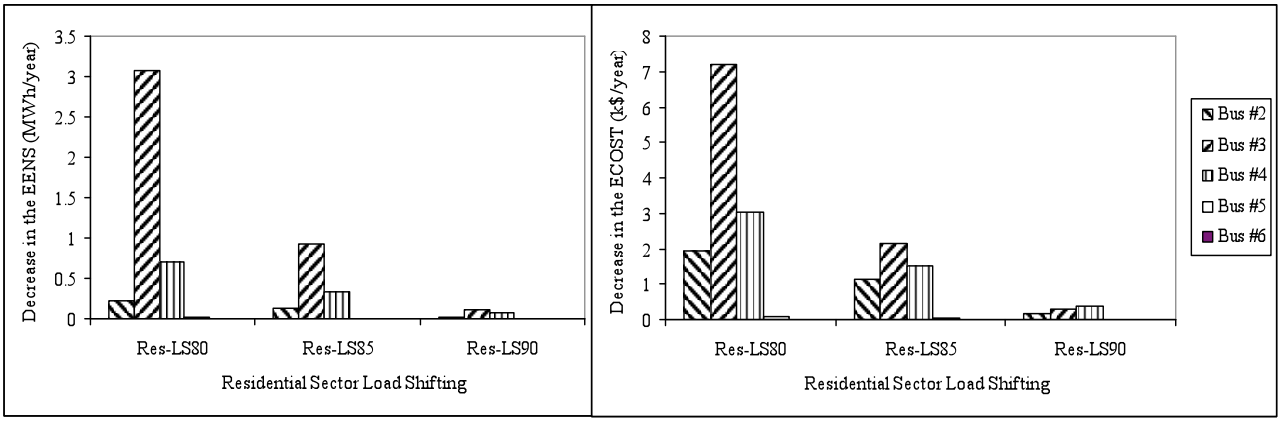

Figure 5.19: Decreases in the RRBTS load point EENS and ECOST with Res-LS procedures

As shown in Figure 5.19, the decrease in the EENS at bus #3 is the largest at each pre-specified peak load level. The decrease in the EENS at bus #4 is the second

largest followed by that at bus #2. bus #3 has the largest EENS, followed by bus #4, then bus #2 for the RRBTS base case, which indicates that the DSM procedures tend to have larger effects on lower reliability buses. The decreases in the load point ECOST are slightly different from those in the EENS as the ECOST is the product of the EENS and the IEAR.

The well-being indices for the RRBTS with the application of residential sector load shifting are shown in Tables 5.19 to 5.21. It can be seen from these tables that the changes are similar to those when load shifting is applied to the total bus load. The magnitudes of change are however quite different.

Table 5.19: HLII system probability of each operating state for the RRBTS with load shifting applied to the residential sector

DSM	Probability of (hrs/yr)		
	Healthy State	Marginal State	At Risk State
Res-LS80	8544.94	187.22	3.84
Res-LS85	8543.90	188.23	3.86
Res-LS90	8541.98	190.11	3.91
Base Case	8541.58	190.50	3.92

Table 5.20: HLII system frequency of each operating state for the RRBTS with load shifting applied to the residential sector.

DSM	Frequency of (occ/yr)		
	Healthy State	Marginal State	At Risk State
Res-LS80	37.55	38.32	0.83
Res-LS85	37.65	38.44	0.84
Res-LS90	38.80	39.60	0.85
Base Case	39.15	39.95	0.85

Table 5.21: HLII system average duration of each operating state for the RRBTS with residential sector load shifting

DSM	Average Duration of (hrs/occ)		
	Healthy State	Marginal State	At Risk State
Res-LS80	227.53	4.89	4.65
Res-LS85	226.94	4.90	4.59
Res-LS90	220.18	4.80	4.58
Base Case	218.19	4.77	4.59

The average duration of each healthy state for the RRBTS decreases, while the marginal and at risk state average duration fluctuates with an increase in the pre-specified peak load. The marginal and at risk state probabilities and frequencies increase with an increase in the pre-specified peak load. The average duration of these two states depends on the relative change in the probability and frequency.

IEEE-RTS Results

The HLII system indices for the IEEE-RTS with the various residential sector load shifting programs are shown in Table 5.22.

Table 5.22: HLII system reliability indices for the IEEE-RTS with residential sector load shifting

DSM	EDLC (hrs/yr)	EENS (MWh/yr)	EFLC (occ/yr)	ECOST (k$/yr)
Res-LS80	31.14	3849.60	7.45	16060.00
Res-LS85	34.70	4263.04	8.92	17915.50
Res-LS90	35.79	4479.92	9.25	18920.90
BASE CASE	35.92	4514.39	9.29	19070.50

Table 5.22 shows that the IEEE-RTS reliability indices decrease with a decrease in the pre-specified peak load with the application of load shifting on the residential load sector at all buses. As expected, the improvement is considerably less than when load shifting is applied to the entire bus load. The system indices for the IEEE-RTS when Res-LS90 is applied are very close to the base case values. The ECOST decreases by 3,010.5 k$/yr with Res-LS80. The decrease in the ECOST is much less than the 17,611.2 k$/yr with load shifting shown in Table 5.12. This is due to the fact that residential sector load shifting does not move as much energy at the on-peak hours as does the bus load shifting shown in Figure 5.5. The results substantiate the comment made earlier that while residential load shifting is an important initiative, this concept will have to be extended to other sectors in order to provide significant increases in load carrying capability and system reliability.

The load point indices for buses #1, #8, #13 and #18 at different pre-specified peak loads are shown in Table 5.23. It can be seen from Table 5.23 that the load point indices at these buses increase with an increase in the pre-specified peak load, but not as

significantly as when load shifting is applied to the whole bus load. The differences in the reliability indices when the pre-specified peak load increases is the smallest for bus #1, followed by bus #8, bus #13 to bus #18. This shows that load shifting in the residential load sector has larger effects on the lower reliability buses.

Table 5.23: HLII load point indices for the IEEE-RTS with residential sector load shifting

Bus No.	Res-LS80			
	EDLC (hrs/yr)	EENS (MWh/yr)	EFLC (occ/yr)	ECOST (k$/yr)
1	0.61	19.57	0.16	141.30
8	2.66	120.06	0.69	721.80
13	7.31	554.99	1.68	3037.00
18	23.42	2213.51	5.46	7773.60
Bus No.		Res-LS85		
1	0.67	21.63	0.19	156.90
8	2.93	138.68	0.80	829.40
13	7.79	608.74	1.87	3319.70
18	25.72	2426.50	6.16	8567.30
Bus No.		Res-LS90		
1	0.70	22.95	0.22	167.60
8	3.06	147.49	0.86	880.20
13	8.04	633.70	2.00	3456.10
18	26.23	2532.09	6.28	8957.40

The conventional reliability indices used in HLI and HLII analysis are expected values. These indices can be extended to describe the annual variation in each specific index. The reliability index probability distributions provide an additional dimension to conventional analysis using expected values and a more detailed appraisal of the system risk. Table 5.23 shows the Expected Duration of Load Curtailment (EDLC) and the Expected Energy not Supplied (EENS) with load shifting in the residential sector. The DLC is a random variable with an associated probability distribution. Figure 5.20 and 5.21 respectively show the DLC and ENS distributions with the various pre-specified peak loads. The standard deviations for the DLC distribution are 29.87 hrs/yr, 32.01 hrs/yr and 32.11 hrs/yr for the Res-LS80, Res-LS85 and Res-LS90 procedures and the IEEE-RTS base case respectively. The range of the DLC decreases slightly with a decrease in the pre-specified peak load.

Figure 5.20 shows that the zero DLC probability decreases with an increase in the pre-specified peak load. The last interval is the cumulative relative frequency of the DLC larger than 65 hrs/yr. It can be seen that the cumulative probability increases with an increase in the pre-specified peak load. The relative frequencies of the smaller DLC intervals at the pre-specified peak load of 80% are generally larger than in the other two cases, and are smaller at the larger DLC intervals as shown in Figure 5.20.

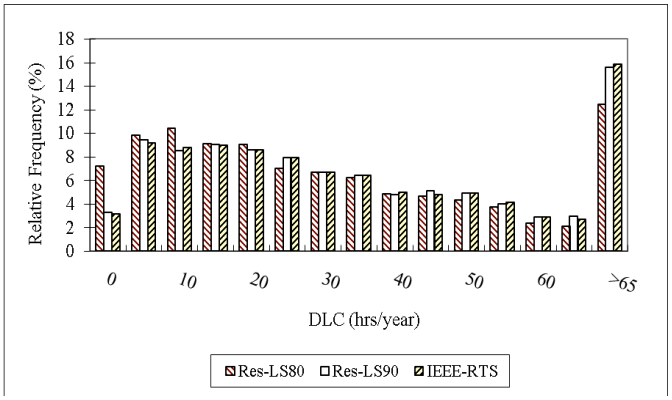

Figure 5.20: The IEEE-RTS DLC distribution with residential sector load shifting

Figure 5.21 shows the ENS distribution. The standard deviations of the ENS distribution are 5263.60 MWh/yr, 5722.10 MWh/yr and 5756.10 MWh/yr for Res-LS80, Res-LS85, Res-LS90 procedures and the IEEE-RTS base case respectively. The range of the ENS distribution also decreases with a decrease in the pre-specified peak load. It can be seen from Figure 5.21 that the effects of load shifting on the ENS distribution are similar to those on the DLC distribution.

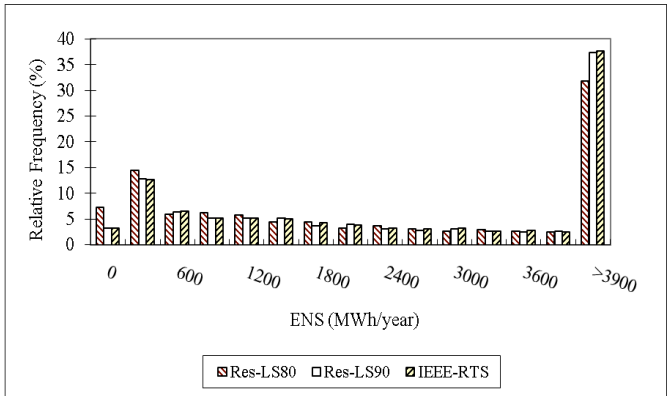

Figure 5.21: The IEEE-RTS ENS distribution with residential sector load shifting

Load shifting is a more practical demand side management program compared to the extreme process of peak clipping as it does not simply reduce power supply to customers. The impacts of load shifting on system reliability are close to those of peak clipping at the same pre-specified peak load levels.

5.4.4. Interactive effects of residential load shifting and LFU

In this section, load shifting is applied to the residential load sector and LFU is considered for the IEEE-RTS.

Table 5.24 shows the HLII system indices for the IEEE-RTS considering both load shifting and LFU. It can be seen from this table that the system indices increase considerably with an increase in the LFU.

Table 5.24: The IEEE-RTS system reliability indices with residential sector load shifting and LFU

LFU	Res-LS80			
	EDLC (hrs/yr)	EENS (MWh/yr)	EFLC (occ/yr)	ECOST (k$/yr)
0%	31.14	3849.60	7.45	16060.00
5%	44.04	6034.84	9.45	24235.80
10%	88.21	14736.11	17.40	55368.00
LFU	Res-LS90			
	EDLC (hrs/yr)	EENS (MWh/yr)	EFLC (occ/yr)	ECOST (k$/yr)
0%	35.79	4479.92	9.25	18920.90
5%	48.81	6800.08	11.51	27578.20
10%	99.47	16807.33	21.24	63438.80

The EDLC and EENS for the IEEE-RTS are also shown in Figure 5.22.

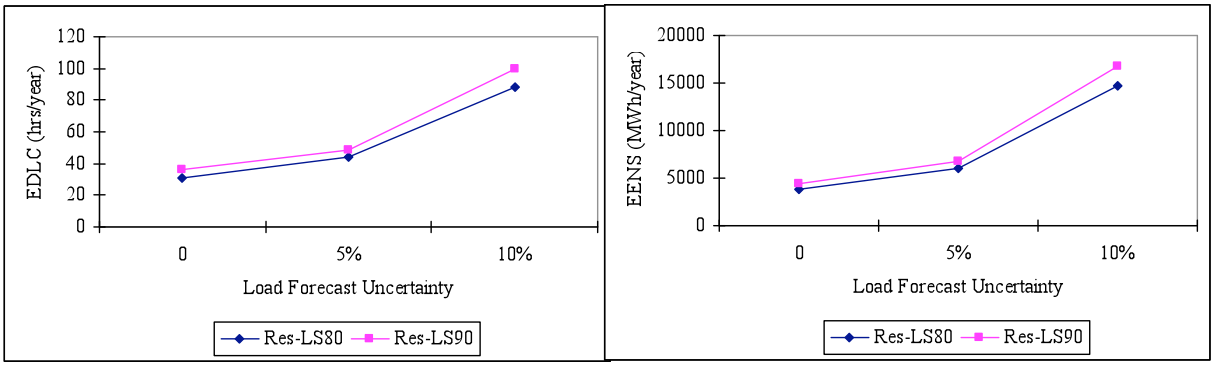

Figure 5.22: The IEEE-RTS EDLC and EENS with residential sector load shifting and LFU

It can be seen that the differences in the EDLC and EENS when these two load shifting measure were applied are smaller when the LFU is small. The differences are the largest when the LFU is 10%, which indicates that the load shifting in the residential load sector counteracts the effects of LFU on the system indices and reduces the inherent increase in the reliability indices.

5.5. Effects of Off-peak Load Addition in the Well-being Analysis Framework

The effects of off-peak load addition were examined at both the HLI and HLII levels. The off-peak load addition described in Section 5.2.2 is used to modify the load model.

5.5.1. Effects of load addition on HLI reliability evaluation

The system load can be formed by summing the load at each bus and used in the HLI simulation program. The 48-hour system load profiles for the RRBTS and the IEEE-RTS are similar and the 48-hour system load data for the IEEE-RTS with load addition are shown in Figure 5.23.

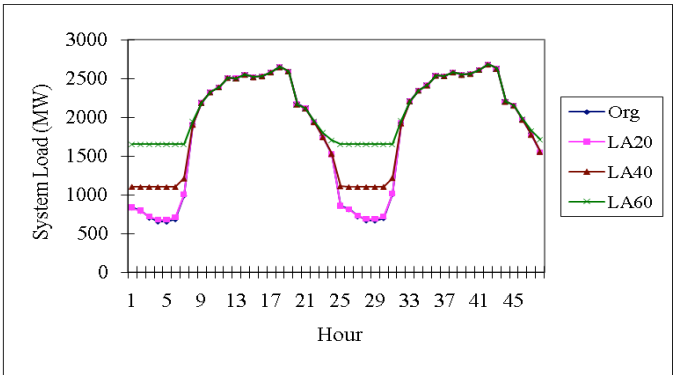

Figure 5.23: The 48-hour system load for the IEEE-RTS with load addition

RBTS Results

Table 5.25 shows the HLI reliability indices for the RBTS with the various load addition settings. It can be seen from Table 5.25 that the load addition at the off-peak hours does not significantly affect the HLI reliability indices. The fluctuation is due to the variations in the simulation.

Table 5.25: HLI system reliability indices for the RBTS with load addition

DSM	Added Energy (MWh)	LOLE (hrs/yr)	LOEE (MWh/yr)	EFLC (occ/yr)
LA20	3735.6	3.71	34.88	0.79
LA40	65606.1	3.78	35.91	0.80
LA60	167363.9	3.78	36.13	0.80
Base Case	0.00	3.74	35.30	0.80

The HLI well-being indices for the RBTS and the RBTS with LA60 are shown in Table 5.26.

Table 5.26: The HLI well-being indices for the RBTS and the RBTS with LA60

RBTS Base Case			
State	Probability (hrs/yr)	Frequency (occ/yr)	Average Duration (hrs/occ)
Healthy	8575.38	25.54	336.72
Marginal	132.95	26.28	5.07
At Risk	3.74	0.80	4.69
RBTS, LA60			
State	Probability (hrs/yr)	Frequency (occ/yr)	Average Duration (hrs/occ)
Healthy	8574.48	25.42	338.30
Marginal	133.81	26.16	5.13
At Risk	3.78	0.80	4.75

The well-being indices for the RBTS with LA20 and LA40 are not shown since the indices are very close. It can be seen from Table 5.26 that the well-being indices are also very close for the RBTS and the RBTS with LA60.

IEEE-RTS Results

The HLI reliability indices for the IEEE-RTS with various load addition settings are shown in Table 5.27.

Table 5.27: HLI system reliability indices for the IEEE-RTS with load addition

DSM	Added Energy (MWh)	LOLE (hrs/yr)	LOEE (MWh/yr)	EFLC (occ/yr)
LA20	62591.4	32.16	4033.48	8.45
LA40	996345.4	32.23	4052.60	8.43
LA60	2535103.6	32.58	4109.38	8.52
Base Case	0.0	32.15	4023.31	8.44

The HLI reliability indices do not change significantly with load addition at the off-peak hours. The changes in the reliability indices for the IEEE-RTS are larger than those for the RBTS as the IEEE-RTS is a larger system with a lower level of system reliability.

The HLI well-being indices for the IEEE-RTS are shown in Table 5.28. The well-being indices also remain almost unchanged with load addition at the off-peak hours.

Table 5.28: HLI well-being indices for the IEEE-RTS with load addition

IEEE-RTS Base Case			
State	Probability (hrs/yr)	Frequency (occ/yr)	Average Duration (hrs/occ)
Healthy	8348.17	75.44	110.97
Marginal	331.44	82.23	4.04
At Risk	32.46	8.49	3.84
IEEE-RTS, LA60			
State	Probability (hrs/yr)	Frequency (occ/yr)	Average Duration (hrs/occ)
Healthy	8344.25	75.46	110.88
Marginal	335.24	82.32	4.08
At Risk	32.58	8.52	3.83

The HLI reliability evaluation studies show that load addition at the off-peak hours does not significantly change the reliability and well-being indices for the two test systems and that these systems are able to provide more energy to the customers while maintaining the reliability to a certain level if the load addition is at the off-peak hours.

5.5.2. Effects of load addition on HLII reliability evaluation

The RapHL-II program was applied to the RRBTS and the IEEE-RTS in this study. The load addition procedures shown in Table 5.1 are used.

RRBTS Results

Table 5.29 shows the number of off-peak hours in a year when the loads are smaller than the specified minimum load and the energy in MWh added in the valley hours for the RRBTS. It can be seen that the off-peak hours increase significantly with an increase in the pre-specified minimum load. The load factor at bus #3 is 52.89%, 53.31%, 58.08% and 63.57% for the RRBTS base case, LA20, LA40 and LA60 procedures respectively.

Table 5.29: The number of off-peak hours in a year and the added energy for the RRBTS

Bus No.	Off-peak hours			Added Energy (MWh)		
	LA20	LA40	LA60	LA20	LA40	LA60
#2	4	2230	3481	0.11	3752.48	14928.58
#3	1822	2548	3825	3675.44	45327.11	93286.18
#4	0	1982	2546	0.00	5927.34	23469.89
#5	101	2357	4546	18.61	4319.06	17661.61
#6	386	2562	3890	41.47	6280.14	18017.68

The system reliability indices for the RRBTS with the various load additions are shown in Table 5.30. It can be seen that increasing the load in the tail of the load duration curve does not significantly change the system reliability. The total load energy of the RRBTS base case is 999,404.10 MWh. The added load for LA60 is about 16.75% of the RRBTS base case.

Table 5.30: HLII system reliability indices for the RRBTS with the load additions

DSM	Added Energy (MWh)	EDLC (hrs/yr)	EENS (MWh/yr)	EFLC (occ/yr)	ECOST (k$/yr)
LA20	3735.63	3.92	47.60	0.85	200.91
LA40	65606.13	3.92	48.19	0.85	203.42
LA60	167363.94	3.94	49.85	0.86	209.72
Base Case	0	3.92	47.58	0.85	200.83

The load point EDLC and EENS for the RRBTS and the RRBTS with LA60 are shown in Figure 5.24. It can be seen that the EDLC and EENS for the RRBTS with LA60 and the RRBTS base case are basically identical.

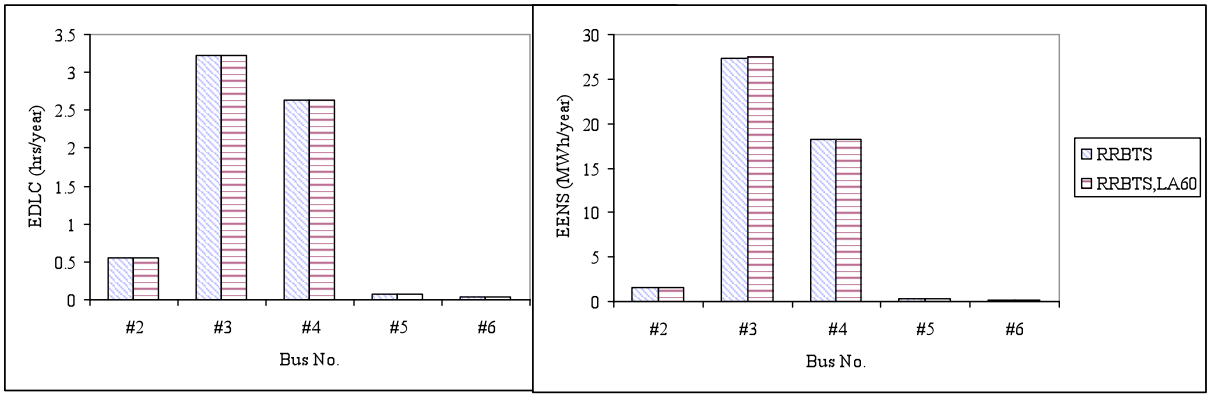

Figure 5.24: The load point EDLC and EENS for the RRBTS and RRBTS with LA60

The well-being indices for the RRBTS with various load additions are shown in Table 5.31. It can be seen from Table 5.31 that the system probability of the healthy state decreases with load addition compared to that of the base case. The marginal state and at risk state probabilities slightly increase. This indicates that load addition at the off-peak hours makes the system less secure. The frequency of each state slightly increases. The changes are, however, extremely small and can be considered to be negligible. Studies on the RRBTS show that the off-peak load additions considered do not significantly affect the system and load point reliability indices.

Table 5.31: HLII well-being indices for the RRBTS with load addition.

RRBTS Base Case			
State	Probability (hrs/yr)	Frequency (occ/yr)	Average Duration (hrs/occ)
Healthy	8541.66	39.13	218.30
Marginal	190.41	39.93	4.77
At Risk	3.92	0.85	4.59
RRBTS, LA60			
Bus No	Probability (hrs/yr)	Frequency (occ/yr)	Average Duration (hrs/occ)
Healthy	8539.89	39.15	218.13
Marginal	192.17	39.96	4.81
At Risk	3.94	0.86	4.60

IEEE-RTS Results

Similar studies were done on the IEEE-RTS to examine the effects of off-peak load addition on reliability indices in a larger power system.

The total load of the IEEE-RTS base case is 15,335,687.00 MWh. The added load is 2,535,103.63 MWh when the pre-specified minimum load is 60% of the original peak, which is about 16.53% of the total load for the IEEE-RTS base case.

The system reliability indices for the IEEE-RTS with load additions at the off-peak hours are shown in Table 5.32. It can be seen from this table that the HLII system reliability indices increase slightly with the increase in the load addition. The increases in the system indices are larger than those of the RRBT. This is due to the fact that the IEEE-RTS is not as reliable as the RRBTS and has larger indices.

Table 5.32: HLII system reliability indices for the IEEE-RTS with load addition.

DSM	Added Load (MWh)	EDLC (hrs/yr)	EENS (MWh/yr)	EFLC (occ/yr)	ECOST (k$/yr)
LA20	62591.41	35.96	4520.40	9.30	19092.68
LA40	996345.35	36.17	4538.95	9.30	19170.47
LA60	2535103.63	36.56	4622.74	9.29	19507.56
Base Case	0	35.92	4514.39	9.29	19070.46

Figure 5.25 shows the load point EDLC and EENS for the IEEE-RTS and the IEEE-RTS with LA60 at selected buses. It can be seen that the load point indices for the IEEE-RTS with load addition are slightly larger than those for the IEEE-RTS base case. The differences in the indices are larger than those in the RRBTS.

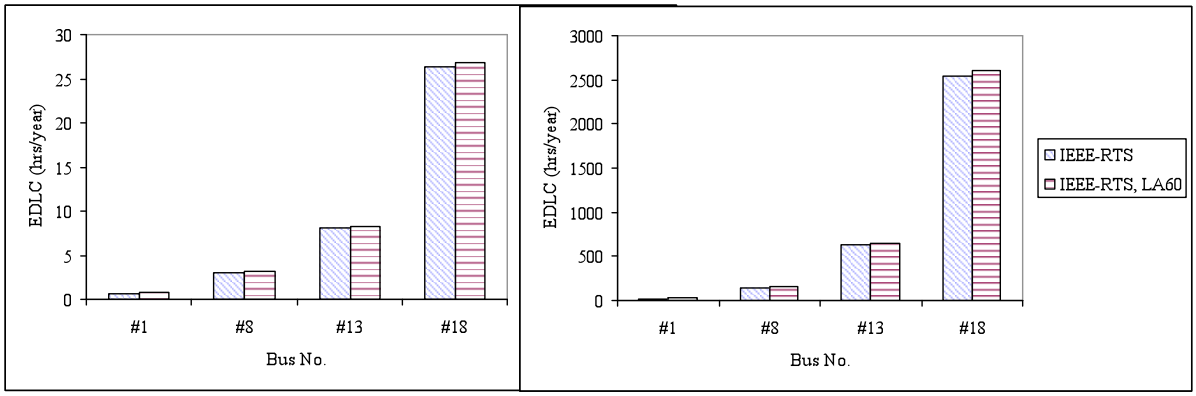

Figure 5.25: The load point EDLC and EENS for the IEEE-RTS and IEEE-RTS with LA60

Table 5.33 shows the HLII well-being indices for the IEEE-RTS base case and the IEEE-RTS with LA60.

Table 5.33: HLII well-being indices for the IEEE-RTS with load addition

IEEE-RTS Base Case			
State	Probability (hrs/yr)	Frequency (occ/yr)	Average Duration (hrs/occ)
Healthy	8207.15	103.43	79.35
Marginal	492.93	110.87	4.45
At Risk	35.92	9.29	3.87
IEEE-RTS, LA60			
Bus No.	Probability (hrs/yr)	Frequency (occ/yr)	Average Duration (hrs/occ)
Healthy	8179.98	101.52	80.58
Marginal	519.46	109.38	4.75
At Risk	36.56	9.29	3.94

It can be seen from Table 5.33 that the healthy state probability decreases with an increase in the added load, while the marginal and at risk state probabilities increase. This is similar to those found for the RRBTS. The system frequency of each state, however, changes differently. The system frequency of each state is smaller when LA60 is applied than the base case value. This is because when the minimum load increases to the pre-specified level it does not vary as much as the original load and the system remain longer in the load state.

The off-peak hour load addition does not affect the system reliability significantly at some load addition levels. In the case of the RBTS and the IEEE-RTS, even when the added load energy at the off-peak hour is approximately 16% of the original energy demand, the system reliability indices, load point indices and the well-being indices are not affected significantly. The effects of load addition are larger for the IEEE-RTS than those for the RRBTS as the IEEE-RTS is a less reliable system. The actual effects will differ for different systems and can be analyzed using the techniques developed in this research.

5.6. Effects of Distributed Generation in the Well-being Analysis Framework

Distributed generation (DG) includes a wide range of sources including co-generation and renewable energy sources and is installed in the distribution network to serve part or all of the local customer demand. Distributed generation allows customers to buy from or sell electricity to the electric power grid [57, 63, 113]. The implementation of DG helps reduce peak demand and dependency on the transmission system by strengthening the distribution system and can improve the efficiency of a power system. Large amounts of distributed generation, particularly wind generation, injected into a BES can create increased load uncertainty on the BES and introduce additional pressure on the bulk system due to the intermittent nature of wind power. The effects of wind power added as DG on BES reliability are illustrated in the following study.

5.6.1. Wind power added as distributed generation

The RapHL-II program was modified to incorporate distributed generation in reliability evaluation as described in Section 5.2.2. Conventional generation or wind

power connected to a bus in the form of distributed generation can be used to modify the BES load profile at that bus.

The RRBTS and the IEEE-RTS were modified by adding wind power or conventional generation as distributed generation. The sample size is 8,000 and 4,000 years for the RRBTS and the IEEE-RTS respectively. The Pass-I policy was used as the load shedding philosophy.

RRBTS Results

The distributed generation is assumed to be primarily intended to serve the loads at the local bus. Two situations are considered in this section. The first is that when the distributed generation exceeds the local load at a certain hour, the BES bus load at that hour is zero and the extra distributed generation is not transmitted to the grid. The second situation is where any distributed generation exceeding the local load is transmitted to the BES.

A 20 MW wind farm was added to the RRBTS at different buses. Any extra distributed generation is not transmitted to the BES in this case. The HLII system indices for the RRBTS with this wind addition are shown in Table 5.34. This table also shows the results for the RRBTS when the 20 MW wind is added as BES connected generation.

Table 5.34: HLII system reliability indices for the RRBTS with the 20 MW of wind added at different buses and extra generation not transmitted to the BES

Wind Capacity connected to bus	EDLC (hrs/yr)	EENS (MWh/yr)	EFLC (occ/yr)	ECOST (k$/yr)
#2	2.58	29.68	0.71	132.47
#3	2.54	28.81	0.70	131.08
#4	2.55	28.94	0.70	132.52
#5	2.54	28.74	0.69	128.82
#6	2.54	28.68	0.69	128.83
Added at bus #4 as BES connected generation	2.55	29.10	0.70	129.76

It can be seen from Table 5.34 that the reliability indices are relatively close to each other when the wind power is added as additional power or added as distributed generation to modify the load profile at the connected bus. The reliability indices are

slightly smaller when the wind power is added at buses #5 or #6 compared to those when the wind capacity is connected to other load buses. This is due to the fact that the system generation is installed at buses #1 and #2 which are far from buses #5 and #6. The RRBTS is a small system and the connection location of wind power does not create much difference in the reliability indices. This could be different in a larger system.

The HLII reliability indices for the RRBTS with wind power connected at different buses are shown in Table 5.35 for the second situation, in which any extra distributed generation is transmitted to the BES.

Table 5.35: HLII system reliability indices for the RRBTS with the 20 MW of wind power added at different buses and the extra capacity transmitted to the BES

Wind Capacity connected to bus	EDLC (hrs/yr)	EENS (MWh/yr)	EFLC (occ/yr)	ECOST (k$/yr)
#2	2.57	29.60	0.71	132.09
#3	2.54	28.75	0.70	130.39
#4	2.55	28.94	0.70	132.52
#5	2.53	28.34	0.69	127.18
#6	2.52	28.26	0.69	127.14

It can be seen that the reliability indices in Table 5.35 are slightly smaller than those in Table 5.34 as expected. The differences in this case are not large due to the fact that only 20 MW of wind power is added to the system. The wind power output in most hours is low and does not exceed the load at those hours. The extra wind energy that can be supplied to the BES grid is therefore relatively small.

The reliability indices for the RRBTS in the two situations compare closely. The load point indices and the well-being indices when the extra generation is transmitted to the system are shown in the following. Tables 5.36 to 5.39 show the individual load point EDLC, EENS, EFLC and ECOST for the RRBTS with the 20 MW wind farm connected to different buses as distributed generation.

It can be seen from Table 5.36 that the load point EDLC changes only slightly when the wind power is added at different buses. The system EDLC and the EDLC for each bus are smaller when the wind farm is connected to buses #5 or #6 compared to

that when the wind power is connected to other buses. This indicates that the system can obtain more benefit in terms of the EDLC when the distributed generation is located at buses that are far from the generation center. It can also be seen from Table 5.36 that the system benefit when the wind farm is added at either bus #5 or #6, are similar and the added distributed generation tends to have a larger effect on the indices at the bus where it is connected.

Table 5.36: The load bus EDLC (hrs/yr) for the RRBTS with the 20 MW wind power added as distributed generation at different buses

Bus No.	Wind Power Added at Bus				
	#2	#3	#4	#5	#6
#2	0.35	0.34	0.34	0.32	0.32
#3	2.00	1.95	2.04	1.93	1.93
#4	1.77	1.76	1.76	1.75	1.75
#5	0.06	0.06	0.05	0.05	0.05
#6	0.02	0.02	0.02	0.02	0.02

Table 5.37 shows the load point EENS for the RRBTS. The load point EENS values change slightly with the wind power connection point. The load point EENS changes differently from the EDLC with the wind power connection point. As shown in Table 5.37, the load point EENS at buses #2, #4, #5 or #6 are the lowest values when the wind farm is connected at these buses. This indicates that the wind power tends to have a larger effect on the bus where it is connected. The exception is the EENS at bus #3, which has its smallest value when the wind farm is added at bus #6. When the extra generation is not transmitted to the system, the EENS at bus #3 is the smallest when the wind power is connected to this bus. The wind power that exceeds the load at bus #6 can be transmitted to the BES and used to supply the demand at other buses.

Table 5.37: The load bus EENS (MWh/yr) for the RRBTS with the 20 MW wind power added as distributed generation at different buses

Bus No.	Wind Power Added at Bus				
	#2	#3	#4	#5	#6
#2	0.81	0.95	0.94	0.87	0.87
#3	16.68	15.76	16.72	15.72	15.68
#4	11.91	11.77	10.99	11.61	11.58
#5	0.21	0.20	0.20	0.16	0.20
#6	0.09	0.08	0.09	0.08	0.07

Table 5.37 also shows that the wind farm connection point affects the load bus EENS. The improvement in the load point EENS is higher when the wind farm is added to a bus that is far from the generation center. As shown in Table 5.37, the EENS at bus #2 is lower when the wind farm is connected to buses #5 and #6 than when the wind farm is connected to buses #3 and #4. The actual numerical differences in the respective indices in Table 5.37 are relatively small but these differences do indicate the system composition effects when using distributed generation at different locations in the system.

Table 5.38 shows the EFLC for the RRBTS with the 20 MW wind farm connected at different buses. The effects of the wind farm location on the EFLC are similar to those on the EDLC.

Table 5.38: The load bus EFLC (occ/yr) for the RRBTS with the 20 MW wind power added as distributed generation at different buses

Bus No.	Wind Power Added at Bus				
	#2	#3	#4	#5	#6
#2	0.1194	0.1110	0.1115	0.1088	0.1081
#3	0.5818	0.5703	0.5821	0.5704	0.5716
#4	0.4578	0.4499	0.4504	0.4520	0.4521
#5	0.0176	0.0164	0.0164	0.0153	0.0164
#6	0.0052	0.0051	0.0051	0.0054	0.0046

The effects of the wind farm location on the ECOST are similar to those on the EENS. There are slight differences as the duration of each interruption also affects the ECOST.

Table 5.39: The load bus ECOST (k$/yr) for the RRBTS with the 20 MW wind power added as distributed generation at different buses

Bus No.	Wind Power Added at Bus				
	#2	#3	#4	#5	#6
#2	6.92	7.54	7.53	6.98	6.98
#3	46.61	45.50	46.32	44.01	43.95
#4	76.58	75.46	76.77	74.55	74.40
#5	1.59	1.52	1.53	1.28	1.51
#6	0.39	0.36	0.37	0.35	0.31

The effects of the location of the wind power on system and load point indices are not very significant because the RRBTS is a generation and transmission sufficient system. In general, the added distributed generation tends to have larger effects on the load point indices at the bus to which it is connected. The reliability indices at those buses close to the bus where the wind power is connected will also improve.

Tables 5.40 to 5.42 show the system probability, frequency and average duration of each operating state for the RRBTS with the 20 MW wind farm added at different buses.

Table 5.40: HLII system probability of each operating state for the RRBTS with the 20 MW wind power added as distributed generation.

Wind power connected to bus #	Probability (hrs/yr)		
	Healthy State	Marginal State	At Risk State
#2	8599.47	133.96	2.57
#3	8605.93	127.53	2.54
#4	8604.59	128.86	2.55
#5	8609.69	123.79	2.53
#6	8609.87	123.61	2.52

Table 5.41: HLII system frequency of each operating state for the RRBTS with the 20 MW wind power added as distributed generation

Wind power connected to bus #	Frequency (occ/yr)		
	Healthy State	Marginal State	At Risk State
#2	35.11	35.75	0.71
#3	31.99	32.65	0.70
#4	32.23	32.88	0.70
#5	31.14	31.76	0.69
#6	31.02	31.64	0.69

It can be seen that the healthy state probability is the smallest when the wind capacity is added at bus #2, and largest at bus #6. This is similar to the effects of wind power location on the system reliability indices. The system frequency of each operating state is the smallest when the wind farm is added at bus #6 followed by the value at bus #5. The marginal state probability and frequency values in Tables 5.40 and 5.41 indicate that when the wind farm is connected at a load bus far from the generation center, the system well-being improves and the system becomes more secure. Even though bus #3

has the largest load, adding the wind farm at bus #3 does not provide the largest benefit. When the added wind power is relatively small compared to the load, the location of the wind power addition can have a major effect on the system reliability indices.

Table 5.42: HLII average duration of each operating state for the RRBTS with the 20 MW wind power added as distributed generation

Wind capacity connected to bus #	Average Duration (hrs/occ)		
	Healthy State	Marginal State	At Risk State
#2	244.90	3.75	3.63
#3	268.98	3.91	3.64
#4	267.01	3.92	3.64
#5	276.53	3.90	3.68
#6	277.57	3.91	3.67

IEEE-RTS Results

A 100 MW wind farm was added at bus #1 as distributed generation. The effects of the wind power on the system indices and load point indices are shown in the following.

Tables 5.43 and 5.44 show the system and load point reliability indices for the IEEE-RTS with the wind power added as distributed generation. It can be seen that the 100 MW of wind power improves the system reliability. It can be seen by comparing Tables 5.44 and 2.10 that the decrease in the EENS at bus #1 with the addition of the 100 MW of wind power divided by the base case EENS is 36.10%, which is the largest percentage change for all the load buses. This again indicates that adding wind power as distributed generation has a larger effect on the local bus.

Table 5.43: HLII system reliability indices for the IEEE-RTS with the 100 MW of wind power added as distributed generation

Cases	EDLC (hrs/yr)	EENS (MWh/yr)	EFLC (occ/yr)	ECOST (k$/yr)
Wind power connected to bus #1	29.26	3628.38	7.91	15390.85
Base Case	35.92	4514.39	9.29	19070.50

Table 5.44: HLII load point indices for the IEEE-RTS with the 100 MW of wind power added as distributed generation

Bus No.	EDLC (hrs/yr)	EENS (MWh/yr)	EFLC (occ/yr)	ECOST (k$/yr)
1	0.55	14.75	0.18	120.70
2	1.57	44.60	0.48	281.90
3	1.44	67.82	0.48	344.66
4	1.40	32.20	0.44	257.90
5	1.94	43.95	0.64	351.00
6	2.27	89.29	0.73	502.50
7	1.69	52.46	0.60	313.30
8	2.42	116.72	0.73	703.40
9	0.03	1.83	0.01	5.10
10	0.05	3.67	0.01	15.40
13	6.59	509.34	1.74	2798.90
14	0.09	4.54	0.03	13.60
15	2.46	187.22	0.72	734.70
16	4.28	139.94	1.27	751.50
18	21.65	2075.65	5.46	7406.20
19	3.58	207.95	0.98	617.40
20	1.06	36.54	0.48	172.80

5.6.2. Conventional generation added as distributed generation

Conventional generation was added to the RRBTS at each bus as distributed generation and extra generation is transmitted to the gird in the following studies.

Table 5.45 shows the reliability indices for the RRBTS when a conventional 5 MW unit was added at different buses in the system. It can be seen that the HLII system indices decrease with the 5 MW addition. The reliability indices are quite close to each other in each case.

Table 5.45: HLII system reliability indices for the RRBTS with the 5 MW conventional generation added as distributed generation at different buses

CG connected to bus	EDLC (hrs/yr)	EENS (MWh/yr)	EFLC (occ/yr)	ECOST (k$/yr)
#2	2.73	28.28	0.69	125.84
#3	2.67	27.33	0.66	124.15
#4	2.67	27.38	0.66	128.20
#5	2.67	27.25	0.66	120.55
#6	2.67	27.16	0.66	119.99

The load point EDLC and EENS for the RRBTS with the 5 MW conventional generation added as distributed generation are shown in Tables 5.46 and 5.47.

Table 5.46: The load bus EDLC (hrs/yr) for the RRBTS with the 5 MW conventional generation added as distributed generation at different buses

Bus No.	Conventional Generation Added at Bus				
	#2	#3	#4	#5	#6
#2	0.35	0.33	0.33	0.30	0.29
#3	1.93	1.86	2.00	1.85	1.85
#4	1.86	1.86	1.86	1.86	1.86
#5	0.06	0.06	0.06	0.06	0.06
#6	0.02	0.02	0.02	0.02	0.02

It can be seen from Table 5.46 that the EDLC for each bus are only slightly different when the distributed generation is added at different buses.

Table 5.47: The load bus EENS (MWh/yr) for the RRBTS with the 5 MW conventional generation added as distributed generation at different buses

Bus No.	Conventional Generation Added at Bus				
	#2	#3	#4	#5	#6
#2	0.65	0.92	0.90	0.80	0.80
#3	15.41	14.44	15.69	14.64	14.56
#4	11.92	11.69	10.50	11.58	11.55
#5	0.20	0.20	0.20	0.14	0.20
#6	0.10	0.09	0.09	0.09	0.06

It can be seen from Table 5.47 that the EENS at each bus is the smallest when the distributed generation is connected at this bus. This is mainly due to the fact that the added distributed generation is used to supply energy to the local load. This differs from when the 20 MW wind power was added, as shown in Table 5.37. When the capacity of the added distributed generation is smaller than the local load, the impact on the EENS at other buses will also be smaller. The effects of conventional generation as distributed generation on the well-being indices are very similar to those when wind power is added as distributed generation and are not shown here.

The effects of wind power or conventional generation added as distributed generation on system indices, load point indices and well-being indices are quite similar. Generation added at location far from the generation center provides more benefit. The

connection point of the distributed generation affects the indices and the distributed generation tends to have larger effects in terms of the EENS on the BES buses where the local generation is connected.

The RRBTS is a transmission strong system and the connection point of the distributed generation only slightly affects the system reliability indices. The RBTS is a transmission deficient system in that there is only one transmission line supplying the load at bus #6. A 5 MW of conventional generating capacity was added as distributed generation at different locations in the RBTS. The HLII system indices for the RBTS with conventional generating capacity are shown in Table 5.48.

Table 5.48: HLII system indices for the RBTS with the 5 MW conventional generation added as distributed generation at different buses

DG connected to bus	EDLC (hrs/yr)	EENS (MWh/yr)	EFLC (occ/yr)	ECOST (k$/yr)
No DG	13.59	156.15	1.76	621.90
#3	12.33	135.38	1.56	543.98
#6	10.38	88.65	1.73	451.39

It can be seen that the reliability indices decrease when the generation capacity is injected into the network at bus #3 or bus #6. The addition of generating capacity as distributed generation at bus #6 directly alleviates the impacts of the transmission deficiency on system reliability. The improvement in system reliability is higher when the capacity is added to the network at bus #6 than at bus #3.

Tables 5.49 and 5.50 show the HLII load point indices for the RBTS with the 5 MW of generation capacity added as distributed generation at different locations.

Table 5.49: HLII load point indices for the RBTS with the 5 MW conventional generation added as distributed generation at bus #3

Bus #	EDLC (hrs/yr)	EENS (MWh/yr)	EFLC (occ/yr)	ECOST (k$/yr)
2	0.36	0.92	0.12	7.11
3	2.03	15.81	0.62	46.23
4	2.03	12.56	0.50	78.29
5	0.25	1.10	0.10	7.97
6	9.71	105.03	0.92	404.38

Table 5.50: HLII system indices for the RBTS with the 5 MW conventional generation added as distributed generation at bus #6

Bus #	EDLC (hrs/yr)	EENS (MWh/yr)	EFLC (occ/yr)	ECOST (k$/yr)
2	0.29	0.79	0.08	6.13
3	2.00	15.94	0.59	43.54
4	2.00	12.37	0.47	77.21
5	0.23	1.10	0.08	7.85
6	7.72	58.48	1.09	316.65

The addition of conventional generation as distributed generation at bus #3 has only a slight effect on the load point indices at bus #6. The connection point of the distributed generation can have significant effects on the system and load point indices for systems with a deficient transmission network.

5.6.3. Increase in the peak load

The RRBTS with 20 MW of wind power addition as distributed generation was used in this study and the peak load of the RRBTS is increased to examine the IPLCC of the added wind power.

The EENS for the RRBTS with increase in the peak load is shown in Figure 5.26. The EENS is the largest when the wind capacity is added at bus #2 and smallest when the wind power is added at bus #6. The IPLCC of the added power is 4.92, 5.25, 5.19, 5.38 and 5.41 MW for the local addition at bus #2, #3, #4, #5 and #6 respectively.

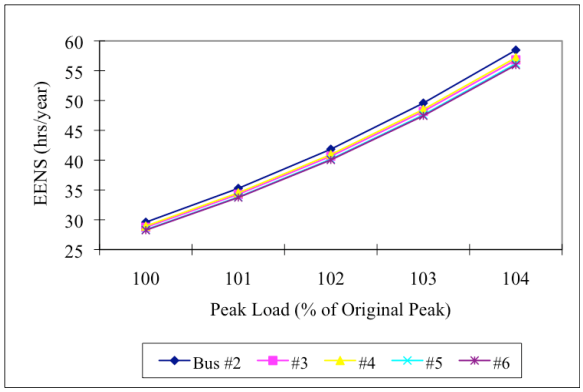

Figure 5.26: The EENS for the RRBTS with 20 MW of wind power added at different buses with increase in the peak load

The EENS of buses #2 and #3 for the RRBTS with the wind farm connected at different load buses versus peak load are shown in Figure 5.27. The load point EENS at buses #2 or #3 are the lowest when the wind farm is connected at this bus at these peak load levels. This is slightly different from that when the peak load is 100%, in which case the EENS of bus #3 is the smallest when the wind power is added at bus #6. This indicates that with an increase in the peak load, the added wind power has less chance of providing energy to the grid. The impact of the distributed generation on the reliability indices at other load buses becomes less significant when the capacity of the distributed generation is small or the load at this bus increases.

The EENS at the other buses changes similarly to that of bus #2 or #3 at these peak load levels and are not shown here.

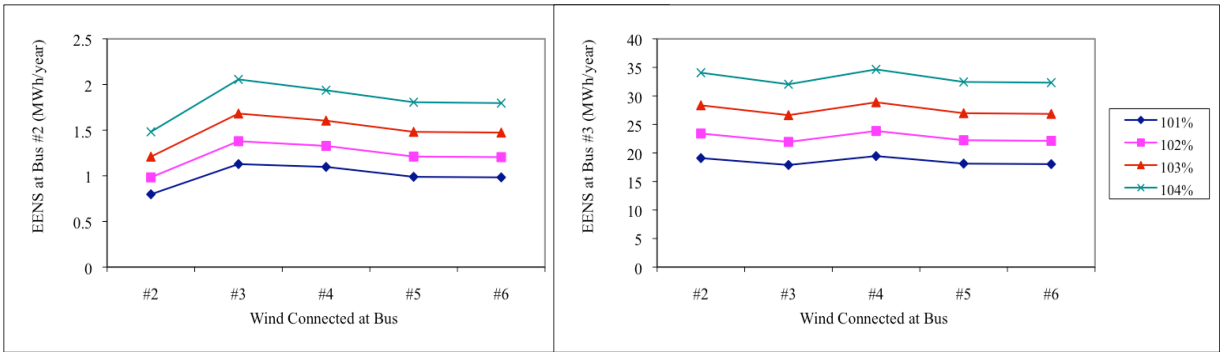

Figure 5.27: The EENS for the RRBTS with the 20 MW wind power added at different buses with increase in the peak load

Similar studies have been done when the conventional generation is added as distributed generation. The IPLCC based on the EENS of the added 5 MW unit is 5.11, 5.46, 5.44, 5.48 and 5.51 MW when the unit is added to bus #2, #3, #4, #5 and #6 respectively. The IPLCC does not change significantly with the connection location. The IPLCC is slightly larger than the capacity of the conventional generating unit because the largest unit in the system is 40 MW and the addition of a smaller unit improves the shape of the distribution in the generating capacity outage table. The reliability indices are quite close to each other at the original peak load with the addition of 20 MW wind power or a 5 MW conventional generating unit. The effects on the system reliability indices with increase in the peak load due to these two forms of

generation are different. In a general sense, adding wind power is similar to adding a relatively large unit with many derated states.

5.6.4. Interactive effects of distributed generation and LFU

In this section, the 20 MW wind power is added at bus #3 as distributed generation and wind power exceeding the local load is transmitted to the grid. The LFU of 0%, 5% and 10% are considered and the bus load correlation is 100% dependent. The system indices, load point indices and well-being indices are shown in the following.

The HLII system indices for the RRBTS are shown in Table 5.51. It can be seen that the system indices increase with an increase in the LFU in a similar manner to when the wind power is added to the BES.

Table 5.51: HLII system reliability indices for the RRBTS with the 20 MW of wind power added at bus #3 as distributed generation considering LFU

LFU	EDLC (hrs/yr)	EENS (MWh/yr)	EFLC (occ/yr)	ECOST (k$/yr)
0%	2.54	28.75	0.70	130.39
5%	3.18	38.60	0.90	166.44
10%	7.11	98.82	1.74	353.99

Tables 5.52 shows the load point indices for the RRBTS. It can be seen that the indices at each load bus increase with an increase in the LFU. The interactive effects of wind power and LFU are similar when the wind power is distributed generation or added directly to the BES.

The HLII system well-being indices for the RRBTS considering wind power as distributed generation and LFU are shown in Table 5.53.

Table 5.52: The load point indices for the RRBTS with the 20 MW of wind power added at bus #3 as distributed generation considering LFU

Bus No.	LFU		
	0%	5%	10%
		EDLC (hrs/yr)	
#2	0.34	0.46	1.56
#3	1.95	2.42	5.43
#4	1.76	2.11	4.07
#5	0.06	0.06	0.13
#6	0.02	0.02	0.04
Bus No.		EENS (MWh/yr)	
#2	0.95	1.35	5.52
#3	15.76	21.89	60.59
#4	11.77	14.20	32.04
#5	0.20	0.22	0.54
#6	0.08	0.06	0.13
Bus No.		EFLC (occ/yr)	
#2	0.11	0.13	0.43
#3	0.57	0.69	1.34
#4	0.45	0.50	0.91
#5	0.02	0.02	0.05
#6	0.01	0.01	0.02
Bus No.		ECOST (k$/yr)	
#2	7.54	10.05	35.83
#3	45.50	60.06	138.55
#4	75.46	86.59	175.30
#5	1.52	1.65	3.59
#6	0.36	0.39	0.72

5.6.5. Interactive effects of wind power and LFU considering load shifting

The Res-LS80 procedure was applied to the RRBTS with 20 MW of wind power added at bus #3 as distributed generation. The HLII system reliability indices for the RRBTS considering the Res-LS80 procedure and the LFU are shown in Table 5.54.

Table 5.53: HLII system well-being indices for the RRBTS with the 20 MW of wind power added at bus #3 as distributed generation considering LFU

State	LFU		
	0%	5%	10%
	System Probability of each Operating State		
Healthy	8605.93	8589.51	8519.15
Marginal	127.53	143.31	209.74
Risk	2.54	3.18	7.11
State	System Frequency of Each Operating State		
Healthy	31.99	34.45	42.18
Marginal	32.65	35.29	43.82
Risk	0.70	0.90	1.74
State	Average Duration of Each Operating State		
Healthy	268.98	249.35	201.97
Marginal	3.91	4.06	4.79
Risk	3.64	3.52	4.08

Table 5.54: HLII system reliability indices for the RRBTS with the 20 MW of wind power added at bus #3 as distributed generation considering LFU with Res-LS80

LFU	EDLC (hrs/yr)	EENS (MWh/yr)	EFLC (occ/yr)	ECOST (k$/yr)
0%	2.42	25.58	0.67	118.81
5%	2.97	35.27	0.78	151.31
10%	6.05	81.57	1.57	311.80

It can be seen by comparing Table 5.54 with Table 5.51 that the system indices drop at each LFU level due to the application of the Res-LS80 procedure. The EENS decrease due to the load shifting measure is 3.1706 MWh/yr and the ECOST decrease is 11.58 k$/yr at the LFU of 0%. The decrease in the EENS and ECOST in the RRBTS base case due to the application of load shifting is 4.02 MWh/yr and 12.25 k$/yr respectively as shown in Table 5.17. The absolute values of the decreases in the EENS and ECOST for the RRBTS with the wind power addition are slightly smaller than those for the RRBTS without the wind power addition. The relative decreases based on the values with no DSM application with added wind power are slightly larger than those for the RRBTS without wind power.

The EENS and ECOST for the RRBTS with wind power with or without applying the Res-LS80 procedure are also shown in Figures 5.28 and 5.29.

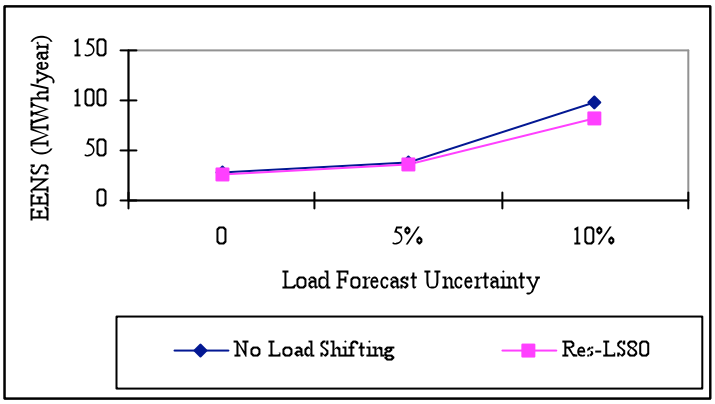

Figure 5.28: The EENS for the RRBTS with the 20 MW wind power addition with or without Res-LS80

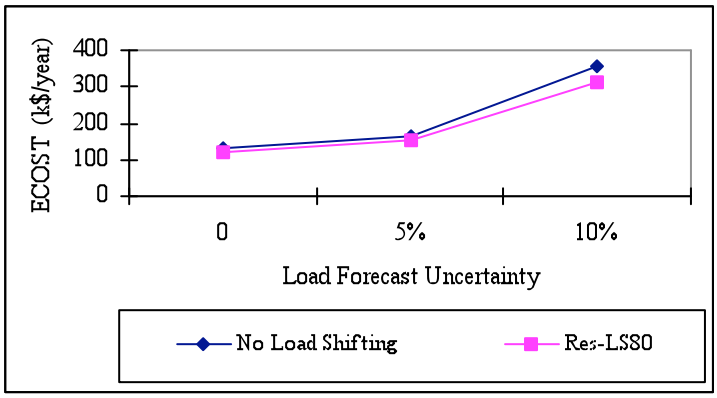

Figure 5.29: The ECOST for the RRBTS with the 20 MW wind power addition with or without Res-LS80

It can be seen from Figure 5.28 and 5.29 that the EENS and ECOST decrease due to the Res-LS80 procedure is relatively small at the LFU of 0% and 5% compared to that when the LFU is 10%. This indicates that load shifting on the residential load sector provides an observable improvement in system reliability when the LFU increases. It can also be seen from Figures 5.28 and 5.29 that the load shifting serves to decrease the increase in the EENS and ECOST due to LFU.

5.7. Conclusion

The DSM measures examined in this chapter improve the system reliability by modifying the load model. The system reliability indices, load point reliability indices

and the reliability index probability distributions are affected in different ways by the different DSM procedures. The system and load point indices decrease when DSM measures are applied and the system becomes more reliable and secure with the application of these measures.

Peak clipping has a major impact on the system reliability indices but is an extreme measure when applied by itself, and may not be practical as this reduces the electrical energy supplied to customers. System reliability can be improved considerably by applying peak clipping. The changes in the system reliability indices become insignificant when the pre-specified peak load decreases to a certain level. The generation composition, transmission network and load profile all affect the load point reliability indices. The changes in the reliability indices with the peak clipping measures are different at different buses even though the same measure is applied at each bus. Peak clipping has larger effects on buses with higher loads. The healthy state probability increases with a decrease in the pre-specified peak, while the marginal and at risk state probabilities decrease. The system frequency of each operating state decreases with a decrease in the pre-specified peak load indicating that there are fewer transitions between states. The system tends to stay longer in the healthy state and shorter in the marginal and at risk states. The system not only becomes more reliable with the utilization of peak clipping, but also more secure.

Load shifting results in a similar improvement in reliability and presents a practical opportunity to proceed with effective peak clipping. When the load shifting is applied, the energy clipped at peak hours will be filled in the valley hours. The load in the valley hours is still relatively low and the lower loads do not contribute significantly to the system reliability indices. Load shifting has a significant impact on the reliability index probability distributions. The relative frequency of encountering zero load curtailment increases with a decrease in the pre-specified peak load. The standard deviation and the range of the index probability distributions decrease significantly. The system ELCC increases as the pre-specified peak load in the load shifting procedure decreases. The ELCC values are similar for the EENS and EDLC indices. Load shifting on the residential load sector counteracts the effects of LFU on the system indices and reduces the inherent increase in the reliability indices. There is more improvement in

system reliability when the load shifting is applied to the bus load than when applied to a single customer load sector. This is expected as load shifting applied to the bus load results in more energy shifting. The residential load shifting is an important initiative, the concept, however, will have to be extended to other sectors in order to provide significant increases in load carrying capability and system reliability.

Valley filling with additional load due to new initiatives does not adversely affect the reliability at both the HLI and HLII at some load addition levels. In these cases, systems can provide more energy to the customers and maintain the reliability at a specified level. In the case of the RBTS and the IEEE-RTS, even when the load addition at the off-peak hour reaches 16% of the original load demand, the system reliability indices and load point indices are not affected significantly. The system probability of the healthy state decreases with load addition. The marginal state and at risk state probabilities slightly increase. This indicates that load addition at the off-peak hours makes the system less secure. The frequency of each state slightly increases. The changes are, however, extremely small and can be considered to be negligible. The actual effects will differ for different systems and can be analyzed using the techniques developed in this research.

Distributed generation sources such as wind power provide relief to the bulk system due to the addition of generation but can increase uncertainty due to their intermittent nature. The addition of wind power or conventional generation as distributed generation can improve the system and load point reliability indices in a similar manner to when the distributed generation is added to the BES with strong transmission networks. The distributed generation connection point affects both the system and the load point indices. The system can obtain more benefit when the distributed generation is located at buses that are far from the generation center. The effects of the location of the distributed generation on the system and load point indices are not very significant for a generation and transmission sufficient system. The connection point of the distributed generation can, however, have significant effects on the system and load point indices for systems with a deficient transmission network. In general, the added distributed generation tends to have larger effects on the load point indices at the bus to which it is connected. The reliability indices at those buses close to

the bus where the wind power is connected will also improve. The interactive effects of wind power and LFU are similar when wind power is added as distributed generation or added directly to the BES.

The research described in this chapter illustrates that the system reliability effects due to the specific DSM programs can be quantified and examined in terms of their reliability benefits. The studies in this chapter are focused on the reliability effects of DSM procedures in a bulk electric system and include wind power and LFU considerations. The numerical results in this chapter are obviously system and data specific. The general conclusions based on these results are, however, applicable to a wide range of electric power systems.

CHAPTER 6
SUMMARY AND CONCLUSIONS

Electric power systems are experiencing dramatic changes with respect to structure, operation and regulation and are facing increasing pressure due to environmental and societal constraints. Power system reliability is an important consideration in power system planning, design and operation particularly in the new competitive environment. A wide range of methods have been developed to perform power system reliability evaluation. The sequential Monte Carlo simulation technique can theoretically include all aspects and contingencies in a power system and can be used to produce an informative set of reliability indices. The development of computing power has made the simulation method a practical and viable tool for large system reliability assessment. This research is focused on bulk electric system reliability evaluation incorporating load forecast uncertainty, wind power and demand side management using the sequential Monte Carlo simulation technique.

The basic concepts of the sequential Monte Carlo simulation technique and the concept of the well-being analysis framework utilized in this research are discussed in Chapter 2. The load flow calculation techniques used in this research are briefly described. The formulation of various HLI and HLII system reliability indices and well-being indices and HLII load point indices are presented. Two existing programs utilizing sequential Monte Carlo simulation for HLI and HLII reliability evaluation are briefly introduced. The two study systems used throughout the thesis are presented together with a basic set of system, load point and well-being indices for each test system. The indices presented in this chapter are the base case values used in the following chapters to investigate the impacts of load forecast uncertainty, wind power and demand side management in HLII reliability evaluation.

Chapter 3 introduces the tabulating and sampling methods used to incorporate load forecast uncertainty in both the HLI and HLII reliability evaluation. A range of load forecast uncertainty levels and bus load correlation are considered. The effects of load forecast uncertainty on the HLI system indices and reliability index probability distributions are examined. The impacts of load forecast uncertainty on HLII system indices and index probability distributions are also studied considering changing peak loads. The effects of load forecast uncertainty on the HLII load point indices considering different load shedding philosophies are investigated. The impacts of bus load correlation in the bulk electric system reliability evaluation are also examined using the system and load point indices. The effects of load forecast uncertainty are also studied under different system generation and transmission network configurations.

The reliability of an electric power system decreases with increasing load forecast uncertainty. The effect of load forecast uncertainty on HLI and HLII system indices are different. The reliability index probability distributions are also affected by load forecast uncertainty. The standard deviations and the ranges of the reliability index probability distributions increase with increase in load forecast uncertainty. The load forecast uncertainty creates considerable variability in the system reliability performance.

Load bus indices generally increase with increase in load forecast uncertainty. Load forecast uncertainty tends to have a relatively large effect on less reliable buses whose reliability indices are not dominated by the transmission network configuration. If the reliability indices at some buses are mainly due to a transmission deficiency, the load forecast uncertainty may not have a significant effect on the indices even though the indices at these buses are large. Bus load correlation affects both the system indices and the load bus indices. The stronger the correlation between buses, the more considerable are the effects on the reliability indices. The effects of bus load correlation on system indices and load bus indices increase when the load forecast uncertainty increases. The effects on individual load bus indices are different as these indices are also influenced by the composite system network configuration and the load curtailment strategy. Different load shedding philosophies do not significantly affect the system

reliability indices determined under different degrees of load bus correlation. The impacts of bus load correlation on the bus indices can vary considerably, however, with different load shedding philosophies. System indices provide an overall appraisal but sometimes factors such as generating unit conditions, transmission network topology and bus load curtailment strategies mask what is actually happening in the system. In this case, load point indices can provide some interesting and valuable insight.

Generally, load forecast uncertainty has a larger effect on generation or/and transmission deficient systems than on systems with strong generation and transmission networks. Exceptions can occur when the system indices are dominated by a particular generation or transmission deficiency, in which case, the effects of load forecast uncertainty may be masked.

The method used to incorporate wind power in the reliability evaluation simulation process at HLI and HLII is presented in Chapter 4. Wind speed correlation between different wind sites is also considered. The sequential Monte Carlo simulation technique permits a wide range of factors to be considered in a study and provides an excellent approach to include the correlation between the wind speed and the load in the analysis. The effects of wind power addition in HLI generating capacity adequacy assessment considering dependent and independent site wind speeds are examined. The impacts of wind speed correlation in HLII reliability evaluation are investigated. The concepts of load forecast uncertainty introduced in Chapter 3 are extended in this chapter to examine the interactive effects of wind power and load forecast uncertainty on system reliability. Studies are also conducted in Chapter 4 to examine the impacts of wind power additions using the well-being framework including load forecast uncertainty considerations. Planning studies of wind assisted systems considering load forecast uncertainty are performed in the well-being analysis framework. The well-being approach provides the opportunity to integrate an accepted deterministic criterion into a probabilistic framework and to quantify the likelihood of operating in the marginal state. The increased cost associated with operating in the marginal state is incorporated in the economic analyses associated with system expansion planning including wind power and load forecast uncertainty in this chapter. Overall reliability cost/worth analyses

including marginal cost concepts are applied to select an optimal wind power injection strategy in a bulk electric system.

The results presented in Chapter 4 clearly illustrate the effects of dependence and independence in site wind speeds in HLI reliability assessment. The capacity credit attributable to a wind power addition to a system is fundamentally different to that associated with the addition of conventional generating capacity as conventional generating unit outages are considered to be independent events. The power output of each wind turbine generator in a wind farm, however, is dependent and directly linked to the wind speed at the site. The capacity credit associated with each added increment of wind power deceases significantly when the site wind speeds are dependent and is relatively constant when the site wind speeds are independent. This clearly indicates the need to determine and incorporate the degree of correlation between the existing and proposed wind farms, as utilities and governments pursue higher wind penetration levels. In HLII studies, the included transmission network contingencies tend to counteract improvements in the system reliability created by adding wind capacity. The ELCC based on the HLII EDLC and EFLC are smaller than those determined in a HLI reliability evaluation. The results also show that the calculated ELCC decreases with increases in the load forecast uncertainty for the wind added system.

System reliability is improved by adding any suitable form of generating capacity, including wind power. The well-being indices are also affected by wind power additions. The healthy state probability increases with an increase in wind power in the system, while the marginal and at risk state probabilities decrease. In general, the frequency of each operating state decreases slightly with an increase in the wind capacity. The decrease is due to the generating capacity contribution of the added wind power counteracted by the intermittent nature of the wind. When a conventional unit is replaced with an equivalent amount of wind power to maintain the EDLC or the EENS, the EFLC in the wind power added system will be larger than that of the original system due to the intermittent behaviour of wind power. Even though the EDLC for the equivalent system with wind is the same as in the original system, the healthy state probability is smaller and the marginal state probability is larger for the wind assisted

system. This indicates that the equivalent capacity system is more likely to transfer to the at risk state than the original system. The state frequencies increase considerably for the equivalent system, which indicates that there are more transitions between states. The operating state frequencies increase as more conventional generating capacity is replaced. When wind power is introduced in a system, the frequency increases more than the probability does and the average duration of each operating state decreases.

The effects of load forecast uncertainty on the well-being indices are different for the original system and a system with wind replacing conventional generation. The replacement of conventional generating units with wind power tends to counteract the effect of load forecast uncertainty on the system reliability due to the multi-state output levels associated with the added wind power and the increase in the frequency is mitigated at low load forecast uncertainty levels. The results in the system expansion planning applications show that the optimum reinforcement option may change by recognizing load forecast uncertainty. The security cost does not affect the order of the total costs for the different transmission reinforcement alternatives in the studies conducted in Chapter 4. The incorporation of a security cost could change the selection of the optimum option when different system configurations or operating conditions are considered.

Chapter 5 presents the inclusion of demand side management in the sequential Monte Carlo simulation process. The demand side management programs considered in this research are peak clipping, load shifting, valley filling and distributed generation. These DSM measures can be applied to all buses, a specified bus or a customer load sector. The effects of the various demand side management measures on system reliability are illustrated using the system, load point and well-being indices. The effects of load shifting on reliability index probability distributions are also investigated. The reliability effects of DSM procedures in a bulk electric system including wind power and load forecast uncertainty considerations are also investigated. The system reliability effects due to the specific DSM programs are quantified and examined in terms of their reliability benefits.

System reliability can be improved considerably by applying peak clipping. The changes in the reliability indices become insignificant when the pre-specified peak load decreases to a certain level. The generation composition, transmission network and load profile all affect the load point reliability indices. Peak clipping has larger effects on buses with higher loads. The healthy state probability increases with a decrease in the pre-specified peak, while the marginal and at risk state probabilities decrease. The system frequency of each operating state decreases with a decrease in the pre-specified peak load indicating that there are fewer transitions between states. The system tends to stay longer in the healthy state and shorter in the marginal and at risk states. The system not only becomes more reliable with the utilization of peak clipping, but also more secure. Peak clipping is an extreme measure and may not be acceptable as this procedure reduces the electrical energy supplied to customers.

Load shifting results in a similar improvement in reliability and presents a practical opportunity to proceed with effective peak clipping. When load shifting is applied, the energy clipped at peak hours is supplied in the valley hours. Load shifting has a significant impact on the reliability index probability distributions. The relative frequency of encountering zero load curtailment increases with a decrease in the pre-specified peak load. The standard deviation and the range of the index probability distributions decrease significantly. The system ELCC increases as the pre-specified peak load in the load shifting procedure decreases. Load shifting on the residential load sector counteracts the effects of load forecast uncertainty on the system indices and reduces the inherent increase in the reliability indices. There is more improvement in system reliability when the load shifting is applied to the entire bus load than when it is applied to a single customer load sector. Residential load shifting is an important initiative, but this concept will have to be extended to other sectors in order to provide significant increases in load carrying capability and system reliability.

Valley filling with additional load due to new initiatives does not adversely affect the reliability at both the HLI and HLII at some load addition levels. In these cases, systems can provide more energy to the customers and maintain the reliability at a specified level. The system probability of the healthy state decreases with load addition.

The marginal state and at risk state probabilities slightly increase. This indicates that load addition at the off-peak hours makes the system less secure. The frequency of each state increases slightly. The changes are, however, extremely small and can be considered to be negligible. The actual effects will differ for different systems and can be analyzed using the techniques developed in this research.

Distributed generation sources such as wind power provide relief to the bulk system due to the addition of generation but can increase uncertainty due to their intermittent nature. The addition of wind power or conventional generation as distributed generation can improve the system and load point reliability indices in a similar manner to when the distributed generation is added to a BES with a strong transmission network. The distributed generation connection point affects both the system and the load point indices. The system obtains more benefit when the distributed generation is located at buses that are far from the generation center. The effects of the location of the distributed generation on the system and load point indices are not very significant for a generation and transmission sufficient system. The connection point of the distributed generation can, however, have significant effects on the system and load point indices for systems with a deficient transmission network. In general, the added distributed generation tends to have maximum impact on the load point indices at the bus to which it is connected. The reliability indices at those buses close to the bus where the wind power is connected will also improve. The interactive effects of wind power and load forecast uncertainty are similar when wind power is added as distributed generation or added directly to the BES.

Monte Carlo simulation can be used to incorporate a wide range of factors in bulk electric system reliability evaluation. This thesis is focused on the incorporation of load forecast uncertainty, wind power and demand side management in bulk electric system reliability evaluation and in the well-being analysis framework using the sequential MCS technique. The numerical results in this thesis are system and data specific. The general conclusions based on the results and the methods used are, however, applicable to a wide range of electric power systems.

REFERENCES

[1] R. Billinton, R. N. Allan, “Power-System Reliability in Perspective”, IEE Journal on Electronics and Power, Vol. 30, No. 3, pp. 231-236, Mar. 1984.

[2] R. Billinton, R. N. Allan, *Reliability Evaluation of Power Systems*, second edition, Plenum Press, New York, 1996.

[3] R. Billinton, “Bibliography on the Application of Probability Methods in Power System Reliability Evaluation”, IEEE Transactions on Power Apparatus and Systems, Vol. PAS-91, No. 2, pp. 649-660, Mar. 1972.

[4] IEEE Subcommittee Report, “Bibliography on the Application of Probability Methods in Power System Reliability Evaluation 1971-1977”, IEEE Transactions on Power Apparatus and Systems, Vol. PAS-97, No. 6, pp. 2235-2242, Nov. 1978.

[5] R. N. Allan, R. Billinton, S. H. Lee, “Bibliography on the Application of Probability Methods in Power System Reliability Evaluation 1977-1982”, IEEE Transactions on Power Apparatus and Systems, Vol. PAS-103, No. 2, pp. 275-282, Feb. 1984.

[6] R. N. Allan, R. Billinton, S. M. Shahidehpour, C. Singh, “Bibliography on the Application of Probability Methods in Power System Reliability Evaluation 1982-1987”, IEEE Transactions on Power Systems, Vol. 3, No. 4, pp. 1555-1564, Nov. 1988.

[7] R. N. Allan, R. Billinton, A. M. Breipohl, and C. H. Grigg, “Bibliography on the Application of Probability Methods in Power System Reliability Evaluation: 1987-1991”, IEEE Transactions on Power Systems, Vol. 9, No. 1, pp. 41-49, Feb. 1994.

[8] R. N. Allan, R. Billinton, A. M. Breipohl, and C. H. Grigg, “Bibliography on the Application of Probability Methods in Power System Reliability Evaluation 1992-1996”, IEEE Transactions on Power Systems, Vol. 14, No. 1, pp. 51-57, Feb. 1999.

[9] R. Billinton, M. Fotuhi-Firuzabad, and L. Bertling, “Bibliography on the Application of Probability Methods in Power System Reliability Evaluation: 1996-1999”, IEEE Transactions on Power Systems, Vol. 16, No. 4, pp. 595-602, Nov. 2001.

[10] R. C. Bansal, T. S. Bhatti, and D. P. Kothari, "Discussion of "Bibliography on the Application of Probability Methods in Power System Reliability Evaluation"", IEEE Transactions on Power Systems, Vol. 17, No. 3, pp. 924, Aug. 2002.

[11] M. T. Schilling, R. Billinton, M.G. dos Santos, "Bibliography on Power Systems Probabilistic Security Analysis 1968-2008", International Journal of Emerging Electric Power Systems, Vol. 10, No. 3, Article 1, May 2009.

[12] R. Billinton, W. Li, *Reliability Assessment of Electric Power Systems Using Monte Carlo Methods*, Plenum Press, New York, 1994.

[13] R. Billinton, R. N. Allan, L. Salvaderi, *Applied Reliability Assessment in Electric Power Systems*, IEEE Press, New York, 1991.

[14] R. Billinton, "Criteria Used by Canadian Utilities in the Planning and Operation of Generating Capacity", IEEE Transactions on Power Systems, Vol. 3, No. 4, pp. 1488-1493, Nov. 1988.

[15] IEEE Working Group on Measurement Indices: C. C. Fong, R. Billinton, R. O. Gunderson, P. M. O'Neil, J. Raksani, A. W. Schneider Jr., and B. Silverstein, "Bulk System Reliability-Measurement and Indices", IEEE Transactions on Power Systems, Vol. 4, No. 3, pp. 829-835, Aug. 1989.

[16] L. H. Fink and K. Carlsen, "Operating Under Stress and Strain", IEEE Spectrum, pp 48-53, Mar. 1978.

[17] EPRI Final Report, "Composite System Reliability Evaluation: Phase I – Scoping Study", Tech Report EPRI EL-5290, Dec. 1987.

[18] R. Billinton and E. Khan, "A Security Based Approach to Composite Power System Reliability Evaluation", IEEE Transactions on Power Systems, Vol. 7, No. 1, pp 65-72, Feb. 1992.

[19] R. Billinton and G. Lian, "Composite Power System Health Analysis Using a Security Constrained Adequacy Evaluation Procedure", IEEE Transactions on Power Systems, Vol. 9, No. 2, pp 936-941, May 1994.

[20] A. M. L. da Silva, L. C. de Resende, L. A. da Fonseca Manso and R. Billinton, "Well-Being Analysis for Composite Generation and Transmission Systems", IEEE Transactions on Power Systems, Vol. 19, No. 4, pp. 1763-1770, Nov. 2004.

[21] S. A. S. Aboreshaid, *Composite Power System Well-being Analysis*, Ph.D. thesis, University of Saskatchewan, 1997.

[22] W. Wangdee, "Bulk Electric System Reliability Simulation and Application", Ph.D. thesis, University of Saskatchewan, 2005.

[23] R. Allan and R. Billinton, "Probabilistic Assessment of Power Systems", Proceedings of The IEEE, Vol. 88, No. 2, pp. 140-162, Feb. 2000.

[24] L. Salvaderi and R. Billinton, "A Comparison Between Two Fundamentally Different Approaches to Composite System Reliability Evaluation", IEEE Transactions on Power Apparatus and Systems, Vol. PAS-104, No. 12, pp. 3486-3492, Dec. 1985.

[25] R. Billinton and W. Li, "Hybrid Approach for Reliability Evaluation of Composite Generation and Transmission Systems Using Monte-Carlo Simulation and Enumeration Technique", IEE Proceedings-Generation, Transmission and Distribution, Vol. 138, No. 3, pp. 233-241, May 1991.

[26] M.E. Khan and R. Billinton, "A Hybrid Model for Quantifying Different Operating States of Composite Power Systems", IEEE Transactions on Power Systems, Vol. 7, No. 1, pp. 187-193, Feb. 1992.

[27] A. C. G. Melo, G. C. Oliveira, M. Morozowski Fo and M. V. F. Pereira "A Hybrid Algorithm for Monte Carlo/Enumeration Based Composite Reliability Evaluation", Third International Conference on Probabilistic Methods Applied to Electric Power Systems, pp. 70-74, Jul. 3-5, 1991.

[28] C. Singh and J. Mitra, "Composite System Reliability Evaluation using State Space Pruning", IEEE Transactions on Power Systems, Vol. 12, No. 1, pp. 471-479, Feb. 1997.

[29] W. Li and R. Bi1linton, "Effect of Bus Load Uncertainty and Correlation in Composite System Adequacy Evaluation", IEEE Transactions on Power Systems, Vol. 6, No. 4, pp. 1522-1529, Nov. 1991.

[30] E. G. Preston, W. M. Grady, and M. L. Baughman, "A New Planning Model for Assessing the Effects of Transmission Capacity Constraints on the Reliability of Generation Supply for Large Nonequivalenced Electric Networks", IEEE Transactions on Power Systems, Vol. 12, No. 3, pp. 1367-1373, Aug. 1997.

[31] T. X. Zhu, “A New Methodology of Analytical Formula Deduction and Sensitivity Analysis of EENS in Bulk Power System Reliability Assessment”, IEEE-PES Power Systems Conference and Exposition, pp. 825-831, Oct. 29, 2006.

[32] A. Sankarakrishnan and R. Billinton, “Effective Techniques for Reliability Worth Assessment in Composite Power System Networks using Monte Carlo Simulation”, IEEE Transactions on Power Systems, Vol. 11, No. 3, pp. 1255-1261, Aug. 1996.

[33] E. N. Dialynas, S. M. Megalokonomos and D. Agoris, “Reliability Cost Assessment of Power Transmission Networks using the Monte-Carlo Simulation Approach”, International Conference on Electric Utility Deregulation and Restructuring and Power Technologies, pp. 596-601, 4-7 Apr. 4-7, 2000.

[34] C. L. T. Borges, D. M. Falcao, J. C. O. Mello, and A. C. G. Melo, “Composite Reliability Evaluation by Sequential Monte Carlo Simulation on Parallel and Distributed Processing Environments”, IEEE Transactions on Power Systems, Vol. 16, No. 2, pp. 203-209, May 2001.

[35] A. Sankarakrishnan and R. Billinton, “Sequential Monte Carlo Simulation for Composite Power System Reliability Analysis with Time Varying Loads”, IEEE Transactions on Power Systems, Vol. 10, No. 3, pp. 1540-1545, Aug. 1995.

[36] A. C. G. Melo, M. V. F. Pereira and A. M. Leite da Silva, “Frequency and Duration Calculations in Composite Generation and Transmission Reliability Evaluation”, IEEE Transactions on Power Systems, Vol. 7, No. 2. pp. 469-476, May 1992.

[37] A. C. G. Melo, M. V. F. Pereira and A. M. Leite da Silva, “A Conditional Probability Approach to the Calculation of Frequency and Duration Indices in Composite Reliability Evaluation”, IEEE Transactions on Power Systems, Vol. 8, No. 3, pp. 1118-1125, Aug. 1993.

[38] J. M. S. Pinheiro, C. R. R. Dornellas, M. Th. Schilling, A. C. G. Melo, and J. C. O. Mello, “Probing the New IEEE Reliability Test System (RTS-96): HL-II Assessment”, IEEE Transactions on Power Systems, Vol. 13, No. 1, pp. 171-176, Feb. 1998.

[39] R. Billinton and W. Li, “Composite System Reliability Assessment using a Monte Carlo Approach”, Third International Conference on Probabilistic Methods Applied to Electric Power Systems, pp. 53-57, Jul. 3-5, 1991.

[40] G. C. Oliveira, M. V. F. Pereira, and S. H. F. Cunha, "A Technique for Reducing Computational Effort in Monte-Carlo Based Composite Reliability Evaluation", IEEE Transactions on Power Systems, Vol. 4. No. 4, pp. 1309-1315, Nov. 1989.

[41] M. V. F. Pereira, M. E. P. Macerira and L. M. V. G. Pinto, "Combining Analytical Models and Monte-Carlo Techniques in Probabilistic Power System Analysis", IEEE Transactions on Power Systems, Vol. 7, No. 1, pp. 265-272, Feb. 1992.

[42] A. Jonnavithula, "Composite System Reliability Evaluation Using Sequential Monte Carlo Simulation", Ph. D. Thesis, University of Saskatchewan, 1997.

[43] R. Billinton and W. Li, "A Monte-Carlo Method for Multi-Area Generation System Reliability Assessment", IEEE Transactions on Power Systems, Vol. 7, No. 4, pp. 1487-1492, Nov. 1992.

[44] W. Li and R. Billinton, "Incorporation and Effects of Different Supporting Policies in Multi-Area Generation System Reliability Assessment", IEEE Transactions on Power Systems, Vol. 8, No. 3, pp. 1061-1067, Aug. 1993.

[45] D. Zhai, A. M. Breipohl, F. N. Lee, and R. Adapa, "The Effect of Load Uncertainty on Unit Commitment Risk", IEEE Transactions on Power Systems, Vol. 9, No. 1, pp. 510-517, Feb. 1994.

[46] F. A. El-Sheikhi and R. Billinton, "Load Forecast Uncertainty Considerations in Generating Unit Preventive Maintenance Scheduling for Single Systems", Third International Conference on Probabilistic Methods Applied to Electric Power Systems, pp. 241-245, Jul. 3-5, 1991.

[47] R. Billinton, R. Karki, Y. Gao, P. Hu and D. Huang, "Wind Energy Considerations in Generating Capacity Adequacy Assessment", International Council on Large Electric Systems (CIGRE) 2007, Calgary, Canada.

[48] H. Bindner and P. Lundsager, "Integration of Wind Power in the Power System", IEEE 2002 28th Annual Conference of the Industrial Electronics Society, IECON 02, Vol. 4, pp. 3309 – 3316, Nov. 5-8, 2002.

[49] Canadian Electricity Association, "An Assessment of the Prospects for Wind Power Development in Canada", Dec. 2004, available at: http://www.canelect.ca/NEWSLETTERS/pdf/2734_web_doc_wind_eng.pdf

[50] Grid Connected Wind Power in China, available at: www.nrel.gov/docs/fy04osti/35789.pdf, Apr. 2004.

[51] R. Bakshl, "Wind Energy- The Indian Scenario", IEEE Power Engineering Society Winter Meeting, 2002, Vol. 1, pp. 344 - 345, Jan. 27-31, 2002.

[52] R. Karki and R. Billinton, "Cost-Effective Wind Energy Utilization for Reliable Power Supply", IEEE Transactions on Energy Conversion, Vol. 19, No. 2, pp. 435-440, June 2004.

[53] D. Lakhanpal, "Impacts of Demand-Side Management on Power System Adequacy and Costs", Master thesis, Department of Electrical Engineering, University of Saskatchewan, 1994.

[54] S. K. Adzanu, "Reliability Assessment of Non-utility Generation and Demand-side Management in Composite Power Systems", Ph.D. Thesis, University of Saskatchewan, 1998.

[55] J. N. Sheen, "Economic Profitability Analysis of Demand Side Management Program", Energy Conversion and Management, Vol. 46, No. 18-19, pp. 2919-2935, Nov. 2005.

[56] A. S. Malik, "Modelling and Economic Analysis of DSM Programs in Generation Planning", International Journal of Electrical Power and Energy Systems, Vol. 23, No. 5, pp.413-419, June 2001.

[57] F. Boshell, O. P. Veloza, "Review of Developed Demand Side Management Programs Including Different Concepts and Their Results", IEEE-PES Transmission and Distribution Conferences and Exposition, pp. 1-7, Aug. 13-15, 2008.

[58] C. W. Gellings, W. M. Smith, "Integrating Demand-side Management into Utility Planning", Proceedings of the IEEE, Vol. 77, No. 6, pp. 908-918, June 1989.

[59] C. W. Gellings, "The Concept of Demand-side Management for Electric Utilities", Proceedings of the IEEE, Vol. 73, No. 10, pp. 1468-1470, Oct. 1985.

[60] D. R. Limaye, "Implementation of Demand-side Management Programs", Proceedings of the IEEE, Vol. 73, No. 10, pp. 1503-1512, Oct. 1985.

[61] R. M. Delgado, "Demand-side Management Alternatives", Proceedings of the IEEE, Vol. 73, No. 10, pp. 1471-1488, Oct. 1985.

[62] S. Saini, “Conservation V. Generation: The Significance of Demand-Side Management (DSM), its Tools and Techniques”, Refocus, Vol. 5, No. 3, pp. 52-54, May/June 2004.

[63] Prepared by Charles River Associates, “Primer on Demand Side Management, Report for the World Bank”, Feb. 2005. Available at: http://siteresources.worldbank.org/INTENERGY/Resources/PrimeronDemand-SideManagement.pdf

[64] B. S. Reddy and J. K. Parikh, “Economic and Environmental Impacts of Demand Side Management Programs”, Energy Policy, Vol. 25, No. 3, pp. 349-356, Feb. 1997.

[65] M. Zhou, G. Li and P. Zhang, “Impact of Demand Side Management on Composite Generation and Transmission System Reliability”, IEEE-PES Power System Conference and Exposition, pp. 819-824, Oct. 29, 2006 – Nov. 1, 2006.

[66] M. Fotuhi-Firuzabad and R. Billinton, “Impact of Load Management on Composite System Reliability Evaluation Short-Term Operating Benefits”, IEEE Transactions on Power Systems, Vol. 15, No. 2, pp. 858-864, May 2000.

[67] T. S. Yau, W. M. Smith, R. G. Huff and H. L. Willis, “Demand-side Management Impact on the Transmission and Distribution System”, IEEE Transactions on Power Systems, Vol. 5, No. 2, pp. 506-512, May 1990.

[68] S. Rahman, Rinaldy, “An Efficient Load Model for Analyzing Demand Side Management Impacts”, IEEE Transactions on Power Systems, Vol. 8, No. 3, pp. 1219-1226, Aug. 1993.

[69] J. E. Runnels, “Impacts of Demand-side Management on T and D – Now and Tomorrow”, IEEE Transactions on Power Systems, Vol. 2, No. 3, pp. 724-729, Aug. 1987.

[70] Rachel Freeman MSc, “Managing Energy: Reducing Peak Load and Managing Risk with Demand Response and Demand Side Management”, Refocus, Vol. 6, No. 5, pp. 53-55, Sept.-Oct. 2005.

[71] M. V. F. Pereira and N. J. Balu, “Composite Generation/Transmission Reliability Evaluation”, Proceedings of the IEEE, Vol. 80, No. 4. pp. 470-491, Apr. 1992.

[72] A. M. da Silva, L. A. da Fonseca Manso, and G. J. Anders, "Composite Reliability Evaluation for Large-Scale Power Systems", IEEE Bologna Power Tech Conference Proceedings, Vol. 4, June 23-26, 2003.

[73] D. Huang, "Basic Considerations in Electrical Generating Capacity Adequacy Evaluation", Master Thesis, University of Saskatchewan, 2005.

[74] R. Y. Rubinstein, *Simulation and the Monte Carlo Method*, Wiley, New York, 1981.

[75] L. R. Ford, Jr. and D. R. Fulkerson, *Flows in Networks*, Princeton University Press, Princeton, New Jersey, 1962.

[76] R. L. Sullivan, *Power System Planning*, McGraw-Hill Book Company, New York, 1977.

[77] EPRI Report, "Transmission System Reliability Methods, Vol. 1: Mathematical Models, Computing Methods and Results", Technical Report EPRI EL-2126-V1, Power Technologies Inc., Schenectady, New York, Jul. 1982.

[78] B. Stott, "Review of Load-Flow Calculation Methods", Proceedings of the IEEE, Vol. 62, No. 7, pp. 916-929, Jul. 1974.

[79] B. Stott and O. Alsac, "Fast Decoupled Load Flow", IEEE Transactions on Power Apparatus and Systems, Vol. PAS-93, No. 3, pp. 859-869, May/June 1974.

[80] G. W. Stagg and A. H. EI-Abiad, *Computer Methods in Power System Analysis*, McGraw-Hill Book Company, New York, 1968.

[81] W. D. Stevenson, Jr., *Elements of Power System Analysis*, McGraw-Hill Book Company, New York, 1982.

[82] J. Sherman and W. J. Morrison, "Adjustment of an Inverse Matrix Corresponding to a Change in One Element of a Given Matrix", Annals of Mathematical Statistics, Vol. 21, No. 1, pp.124-127, 1950.

[83] M. E. Khan, "A Security Based Approach to Composite Power System Reliability Evaluation", Ph. D. Thesis, University of Saskatchewan, 1991.

[84] T. K. P. Medicherla, "Reliability Evaluation of Composite Generation and Transmission Systems", Ph.D. Thesis, University of Saskatchewan, 1978.

[85] D. G. Luenberger, *Linear and Nonlinear Programming*, 2nd Edition, Addison-Wesley, Reading, Massachusetts, 1984.

[86] A. J. Wood and B. F. Wollenberg, *Power Generation, operation and control*, 2nd Edition, J. Wiley & Sons, New York, 1996.

[87] V. A. Sposito, *Linear and Nonlinear Programming*, Iowa State University Press, Ames, Iowa, 1975.

[88] R. Billinton and R. Mo, "Deterministic/Probabilistic Contingency Evaluation in Composite Generation and Transmission Systems", IEEE-PES General Meeting, Vol. 2, pp. 2232-2237, Jun. 2004.

[89] R. Billinton, S. Aboreshaid and M. Fotuhi-Firuzabad, "Conceptual Framework for Composite Power System Health Analysis", Canadian Conference on Electrical and Computer Engineering 1996, Vol. 1, pp. 396-399, May 26-29, 1996.

[90] M. E. Khan, "Bulk Load Points Reliability Evaluation Using a Security Based Model", IEEE Transactions on Power Systems, Vol. 13, No. 2, pp. 456-463, May 1998.

[91] V. Brandwajn, "Efficient Bounding Method for Linear Contingency Analysis", IEEE Transactions on Power Systems, Vol. 3, No. 1, pp. 38-43, Feb. 1988.

[92] R. Billinton, S. Kumar, N. Chowdhury, K. Chu, K. Debnath, L. Goel, E. Khan, P. Kos, G. Nourbakhsh and J. Oteng-Adjei. "A Reliability Test System for Educational Purposes – Basic Data," IEEE Transactions on Power Systems, Vol. 4, No. 3, pp. 1238-1244, Aug. 1989.

[93] Reliability Test System Task Force of the IEEE Subcommittee on the Application of Probability Methods, "IEEE Reliability Test System," IEEE Transactions on Power Apparatus and Systems, Vol. PAS-98, No. 6, pp. 2047-2054, Nov. 1979.

[94] G. Verzhbinsky, H. Ruderman, M. Levine, "The LBL Residential Hourly and Peak Demand Model", LBL report #18698, Aug. 1984.

[95] R. N. Allan, R. Billinton and N. M. K. Abdel-Gawad, "The IEEE Reliability Test System - Extensions to and Evaluation of the Generating System", IEEE Transactions on Power Systems, Vol. 1 No. 4, pp. 1-7, Nov. 1986.

[96] R. Billinton and D. Huang, "Effects of Load Forecast Uncertainty on Bulk Electric System Reliability Evaluation", IEEE Transactions on Power Systems, Vol. 23, No. 2, pp. 418-425, May 2008.

[97] D. Huang and R. Billinton, "Load Forecast Uncertainty Considerations in Bulk Electric System Reliability Assessment", 40th North American Power Symposium, Sep. 28-30 2008, University of Calgary, Calgary, Canada.

[98] R. Billinton and D. Huang, "Aleatory and Epistemic Uncertainty Considerations in Power System Reliability Evaluation", 10th International Conference on Probabilistic Methods Applied to Power Systems, pp. 1-8, May 25-29 2008, Rincon, Puerto Rico.

[99] M. Abramovitz and I. A. Stegun, *Handbook of Mathematical Functions*, National Bureau of Standards, 1968.

[100] Renewable portfolio standard, Oct, 1997, available at : http://www.awea.org/policy/rpsbrief.html

[101] D. Huang, R. Billinton, "Effects of Wind Power on Bulk System Adequacy Evaluation using the Well-being Analysis Framework", IEEE Transactions on Power Systems, Vol. 24, No. 3, pp. 1232-1240, Aug. 2009.

[102] R. Billinton and G. Bai, "Generating Capacity Adequacy Associated with Wind Energy", IEEE Transactions on Energy Conversion, Vol. 19, No. 3., pp. 641-646, Sep. 2004.

[103] R. Billinton, H. Chen and R. Ghajar, "Time-Series Models for Reliability Evaluation of Power Systems including Wind Energy", Microelectronics and Reliability, Vol. 36, No. 9, pp. 1253-1261, Nov. 1996.

[104] P. Giorsetto and K. F. Utsurogi, "Development of a New Procedure for Reliability Modeling of Wind Turbine Generators", IEEE Transactions on Power Apparatus and Systems, Vol. PAS-102, No. 1, pp.134-143, Jan. 1983.

[105] B. Ernst, "Analysis of Wind Power Ancillary Service Characteristics with German 250 MW Wind Data", National Renewable Energy Laboratory, NREL Report No. TP-500-26969, Nov. 1999.

[106] H. Holttinen, "Hourly Wind Speed Variations in the Nordic Countries", Wind Energy, Vol. 8, No. 2, pp. 173-195, Apr./Jun. 2005.

[107] R. Billinton, D. Huang, “Wind Power Modeling and the Determination of Capacity Credit in an Electric Power System”, 18th Advances in Risk and Reliability Technology Symposium (AR2TS), Loughborough University, Apr. 2009.

[108] D. S. Kirschen, “Power System Security”, Power Engineering Journal, Vol. 16, No. 5, pp. 241-248, Oct. 2002.

[109] D. Wang and Y. Yu, “Dynamic Security Risk Assessment and Optimization of Power Transmission System”, 10th international conference on Probabilistic Methods Applied to Power Systems, May 25-29, 2008.

[110] W. Wangdee and R. Billinton, “Combined Adequacy and Static Security Considerations in Transmission System Reinforcement”, 10th international conference on Probabilistic Methods Applied to Power Systems, May 25-29, 2008.

[111] R. Billinton, D. Lakhanpal, ”Impacts of Demand-Side Management on Reliability Cost/Reliability Worth Analysis”, IEE Proceedings on Generation, Transmission and Distribution, Vol. 143, No. 3, pp. 225-231, May 1996.

[112] R. Azami, A. F. Fard, “Impact of Demand Response Programs on System and Nodal Reliability of a Deregulated Power System”, IEEE International Conference on Sustainable Energy Technologies, pp. 1262-1266, Nov. 24-27, 2008.

[113] A. Vojdani, “Smart Integration”, IEEE Power and Energy Magazine, Vol. 6, No. 6, pp. 71-79, Nov.-Dec. 2008.

APPENDIX A: BASIC SYSTEM DATA FOR THE RBTS AND THE IEEE-RTS

Tables A.1, A.2 and A.3 show the per unit bus data, line data and the generating unit reliability data for the RBTS. The base MVA is 100.

Table A.1: The bus data for the RBTS

Bus No.	Load (p.u.)		P_g	Q_{min}	Q_{max}	V_0	V_{min}	V_{max}
	Active	Reactive						
1	0.00	0	1.0	0.50	-0.4	1.05	0.97	1.05
2	0.20	0.07	1.2	0.75	-0.4	1.05	0.97	1.05
3	0.85	0.28	0.0	0.00	0.0	1.00	0.97	1.05
4	0.40	0.13	0.0	0.00	0.0	1.00	0.97	1.05
5	0.20	0.07	0.0	0.00	0.0	1.00	0.97	1.05
6	0.20	0.07	0.0	0.00	0.0	1.00	0.97	1.05

Table A.2: The line data for the RBTS

Line No.	Bus No		R	X	B/2	Current Rating (p.u.)	Failure Rate (occ/year)	Repair hours (hrs)
	from	to						
1	1	3	0.0342	0.1800	0.0106	0.85	1.50	10.00
2	2	4	0.1140	0.6000	0.0352	0.71	5.00	10.00
3	1	2	0.0912	0.4800	0.0282	0.71	4.00	10.00
4	3	4	0.0228	0.1200	0.0071	0.71	1.00	10.00
5	3	5	0.0228	0.1200	0.0071	0.71	1.00	10.00
6	1	3	0.0342	0.1800	0.0106	0.85	1.50	10.00
7	2	4	0.1140	0.6000	0.0352	0.71	5.00	10.00
8	4	5	0.0228	0.1200	0.0071	0.71	1.00	10.00
9	5	6	0.0228	0.1200	0.0071	0.71	1.00	10.00

Table A.3: The generating unit reliability data for the RBTS

Unit	Bus No.	Capacity (MW)	Failure Rate (occ/year)	Repair hours (hrs)
1	1	40.0	6.0	45.0
2	1	40.0	6.0	45.0
3	1	10.0	4.0	45.0
4	1	20.0	5.0	45.0
5	2	5.0	2.0	45.0
6	2	5.0	2.0	45.0
7	2	40.0	3.0	60.0
8	2	20.0	2.4	55.0
9	2	20.0	2.4	55.0
10	2	20.0	2.4	55.0
11	2	20.0	2.4	55.0

Tables A.4, A.5 and A.6 show the per unit bus data, line data and the generating unit reliability data for the IEEE-RTS respectively. The base MVA is also 100.

Table A.4: The bus data for the IEEE-RTS

Bus No.	Load (p.u.)		P_g	Q_{min}	Q_{max}	V_0	V_{min}
	Active	Reactive					
1	1.08	0.22	1.92	1.20	-0.75	0.95	1.05
2	0.97	0.20	1.92	1.20	-0.75	0.95	1.05
3	1.80	0.37	0.00	0.00	0.00	0.95	1.05
4	0.74	0.15	0.00	0.00	0.00	0.95	1.05
5	0.71	0.14	0.00	0.00	0.00	0.95	1.05
6	1.36	0.28	0.00	0.00	0.00	0.95	1.05
7	1.25	0.25	3.00	2.70	0.00	0.95	1.05
8	1.71	0.35	0.00	0.00	0.00	0.95	1.05
9	1.75	0.36	0.00	0.00	0.00	0.95	1.05
10	1.95	0.40	0.00	0.00	0.00	0.95	1.05
11	0.00	0.00	0.00	0.00	0.00	0.95	1.05
12	0.00	0.00	0.00	0.00	0.00	0.95	1.05
13	2.65	0.54	5.91	3.60	0.00	0.95	1.05
14	1.94	0.39	0.00	3.00	-0.75	0.95	1.05
15	3.17	0.64	2.15	1.65	-0.75	0.95	1.05
16	1.00	0.20	1.55	1.20	-0.75	0.95	1.05
17	0.00	0.00	0.00	0.00	0.00	0.95	1.05
18	3.33	0.68	4.00	3.00	-0.75	0.95	1.05
19	1.81	0.37	0.00	0.00	0.00	0.95	1.05
20	1.28	0.26	0.00	0.00	0.00	0.95	1.05
21	0.00	0.00	4.00	3.00	-0.75	0.95	1.05
22	0.00	0.00	3.00	1.45	-0.90	0.95	1.05
23	0.00	0.00	6.60	4.50	-0.75	0.95	1.05
24	0.00	0.00	0.00	0.00	0.00	0.95	1.05

Table A.5: The line data for the IEEE-RTS

Line No.	Bus No.		R	X	B/2	Current Rating (p.u.)	Failure Rate (occ/year)	Repair hours (hrs)
	From	To						
1	1	2	0.0260	0.0139	0.2306	1.93	0.24	16.00
2	1	3	0.0546	0.2112	0.0286	2.08	0.51	10.00
3	1	5	0.0218	0.0845	0.0115	2.08	0.33	10.00
4	2	4	0.0328	0.1267	0.0172	2.08	0.39	10.00
5	2	6	0.0497	0.1920	0.0260	2.08	0.39	10.00
6	3	9	0.0308	0.1190	0.0161	2.08	0.48	10.00
7	3	24	0.0023	0.0839	0.0000	5.10	0.02	768.00
8	4	9	0.0268	0.1037	0.0141	2.08	0.36	10.00
9	5	10	0.0228	0.0883	0.0120	2.08	0.34	10.00
10	6	10	0.0139	0.0605	1.2295	1.93	0.33	35.00
11	7	8	0.0159	0.0614	0.0166	2.08	0.30	10.00
12	8	9	0.0427	0.1651	0.0224	2.08	0.44	10.00
13	8	10	0.0427	0.1651	0.0224	2.08	0.44	10.00
14	9	11	0.0023	0.0839	0.0000	6.00	0.02	768.00
15	9	12	0.0023	0.0839	0.0000	6.00	0.02	768.00
16	10	11	0.0023	0.0839	0.0000	6.00	0.02	768.00
17	10	12	0.0023	0.0839	0.0000	6.00	0.02	768.00
18	11	13	0.0061	0.0476	0.0500	6.00	0.02	768.00
19	11	14	0.0054	0.0418	0.0440	6.00	0.39	11.00
20	12	13	0.0061	0.0476	0.0500	6.00	0.40	11.00
21	12	23	0.0124	0.0966	0.1015	6.00	0.52	11.00
22	13	23	0.0111	0.0865	0.0909	6.00	0.49	11.00
23	14	16	0.0050	0.0389	0.0409	6.00	0.38	11.00
24	15	16	0.0022	0.0173	0.0364	6.00	0.33	11.00
25	15	21	0.0063	0.0490	0.0515	6.00	0.41	11.00
26	15	21	0.0063	0.0490	0.0515	6.00	0.41	11.00
27	15	24	0.0067	0.0519	0.0546	6.00	0.41	11.00
28	16	17	0.0033	0.0259	0.0273	6.00	0.35	11.00
29	16	19	0.0030	0.0231	0.0243	6.00	0.34	11.00
30	17	18	0.0018	0.0144	0.0152	6.00	0.32	11.00
31	17	22	0.0135	0.1053	0.1106	6.00	0.54	11.00
32	18	21	0.0033	0.0259	0.0273	6.00	0.35	11.00
33	18	21	0.0033	0.0259	0.0273	6.00	0.35	11.00
34	19	20	0.0051	0.0396	0.0417	6.00	0.38	11.00
35	19	20	0.0051	0.0396	0.0417	6.00	0.38	11.00
36	20	23	0.0028	0.0216	0.0228	6.00	0.34	11.00
37	20	23	0.0028	0.0216	0.0228	6.00	0.34	11.00
38	21	22	0.0087	0.0678	0.0712	6.00	0.45	11.00

Table A.6: The generating unit reliability data for the IEEE-RTS

Unit	Bus No.	Capacity (MW)	Failure Rate (occ/year)	Repair hours (hrs)
1	22	50.0	4.42	20.00
2	22	50.0	4.42	20.00
3	22	50.0	4.42	20.00
4	22	50.0	4.42	20.00
5	22	50.0	4.42	20.00
6	22	50.0	4.42	20.00
7	15	12.0	2.98	60.00
8	15	12.0	2.98	60.00
9	15	12.0	2.98	60.00
10	15	12.0	2.98	60.00
11	15	12.0	2.98	60.00
12	15	155.0	9.13	40.00
13	7	100.0	7.30	50.00
14	7	100.0	7.30	50.00
15	7	100.0	7.30	50.00
16	13	197.0	9.22	50.00
17	13	197.0	9.22	50.00
18	13	197.0	9.22	50.00
19	1	20.0	19.47	50.00
20	1	20.0	19.47	50.00
21	1	76.0	4.47	40.00
22	1	76.0	4.47	40.00
23	2	20.0	9.13	50.00
24	2	20.0	9.13	50.00
25	2	76.0	4.47	40.00
26	2	76.0	4.47	40.00
27	23	155.0	9.13	40.00
28	23	155.0	9.13	40.00
29	23	350.0	7.62	100.00
30	18	400.0	7.96	150.00
31	21	400.0	7.96	150.00
32	16	155.0	9.13	40.00

APPENDIX B: CUSTOMER SECTOR LOAD DATA

The weekly residential sector allocation is shown in Table B.1.

Table B.1: Weekly Residential Sector Allocation

Week No.	Percentage Allocation	Week No.	Percentage Allocation
1	0.922	27	0.815
2	0.960	28	0.876
3	0.938	29	0.861
4	0.894	30	0.940
5	0.940	31	0.782
6	0.901	32	0.836
7	0.892	33	0.860
8	0.866	34	0.789
9	0.800	35	0.786
10	0.797	36	0.765
11	0.775	37	0.840
12	0.787	38	0.755
13	0.764	39	0.784
14	0.810	40	0.784
15	0.781	41	0.803
16	0.860	42	0.804
17	0.814	43	0.860
18	0.897	44	0.941
19	0.930	45	0.945
20	0.940	46	0.969
21	0.916	47	1.000
22	0.871	48	0.950
23	0.960	49	0.975
24	0.947	50	0.970
25	0.956	51	0.980
26	0.921	52	0.990

The daily and hourly percentage of the sector peak load for all sectors are shown in Table B.2 and B.3 respectively.

Table B.2: Daily percetnage of the sector peak load for all sectors.

Day	Res. (MW)	Com. (MW)	Ind. (MW)	Govt. & Inst. (MW)	Office & Building (MW)	Large User (MW)	Agri. (MW)
Monday	0.96	1.00	1.00	1.00	1.00	1.00	1.00
Tuesday	1.00	1.00	1.00	1.00	1.00	1.00	1.00
Wednesday	0.98	1.00	1.00	1.00	1.00	1.00	1.00
Thursday	0.96	1.00	1.00	1.00	1.00	1.00	1.00
Friday	0.97	1.00	1.00	1.00	1.00	1.00	1.00
Saturday	0.83	1.00	1.00	0.40	0.50	1.00	1.00
Sunday	0.81	1.00	1.00	0.30	0.40	1.00	1.00

Table B.3: Hourly percentage of the sector peak load for all sectors.

Hour No.	Res. Average Day	Res. Peak Winter	Res. Peak Summer	Average Com.	Peak Com.	Industrial
1	0.550	0.600	0.700	0.010	0.010	0.337
2	0.500	0.550	0.650	0.010	0.010	0.337
3	0.430	0.455	0.600	0.010	0.010	0.337
4	0.370	0.400	0.550	0.010	0.010	0.337
5	0.360	0.400	0.550	0.010	0.010	0.337
6	0.380	0.395	0.510	0.030	0.030	0.337
7	0.385	0.400	0.500	0.040	0.040	1.000
8	0.425	0.450	0.540	0.250	0.350	1.000
9	0.450	0.550	0.600	0.850	0.850	1.000
10	0.550	0.650	0.650	0.900	0.900	1.000
11	0.600	0.700	0.700	0.910	0.900	1.000
12	0.700	0.800	0.800	0.920	1.000	1.000
13	0.700	0.800	0.800	0.985	0.985	1.000
14	0.750	0.850	0.850	0.975	0.975	1.000
15	0.750	0.850	0.850	0.880	0.850	1.000
16	0.750	0.850	0.850	0.865	0.865	1.000
17	0.800	0.900	0.900	0.890	0.850	1.000
18	0.850	0.950	0.950	0.900	1.000	1.000
19	0.850	0.950	0.950	0.900	1.000	1.000
20	0.860	1.000	1.000	0.640	0.950	1.000
21	0.860	1.000	1.000	0.600	0.850	1.000
22	0.800	0.900	0.900	0.420	0.750	1.000
23	0.750	0.850	0.850	0.400	0.300	1.000
24	0.650	0.750	0.750	0.025	0.020	1.000

Table B.4: Hourly percentage of the sector peak load for all sectors (continued).

Hour No.	Govt. & Inst.	Peak Office & Building	Average Office & Building	Large User	Peak Agri.	Average Agri.
1	0.400	0.590	0.270	0.1037	0.010	0.001
2	0.400	0.590	0.410	0.1037	0.010	0.001
3	0.400	0.450	0.350	0.1037	0.010	0.001
4	0.400	0.420	0.400	0.1037	0.010	0.001
5	0.400	0.390	0.400	0.1037	0.010	0.001
6	0.600	0.410	0.300	0.1037	0.010	0.001
7	0.700	0.750	0.550	0.1037	0.100	0.020
8	0.750	0.770	0.650	1.0000	0.200	0.100
9	0.800	0.850	0.850	1.0000	0.600	0.400
10	0.850	0.840	0.800	1.0000	0.700	0.600
11	0.900	1.000	1.000	1.0000	0.750	0.650
12	0.920	1.000	1.000	1.0000	0.800	0.670
13	0.930	1.000	0.985	1.0000	0.770	0.650
14	0.960	1.000	0.975	1.0000	0.850	0.680
15	0.970	0.985	0.850	1.0000	1.000	0.690
16	0.970	0.975	0.865	1.0000	0.970	0.760
17	1.000	0.970	0.850	1.0000	0.950	0.810
18	0.980	0.965	0.900	1.0000	0.920	0.700
19	0.800	0.950	0.900	1.0000	0.900	0.500
20	0.750	0.950	0.680	0.5000	0.750	0.350
21	0.650	0.940	0.640	0.5000	0.550	0.300
22	0.500	0.920	0.420	0.5000	0.100	0.005
23	0.430	0.720	0.400	0.5000	0.020	0.004
24	0.120	0.520	0.025	0.5000	0.010	0.003

Where:

Res. Average Day = Average (Fall/Spring season) day for the residential sector

Res. Peak Winter = Peak Winter day for the residential sector

Res. Peak Summer = Peak Summer day for the residential sector

Average Com. = Average (Fall/Spring) day for the commercial sector

Peak Com. = Peak (Summer/Winter) day for the commercial sector

Industrial = Industrial for all seasons

Govt. & Inst. = Government & institutions for all seasons

Peak Office & Building = Peak (Summer/Winter) day for the Office Building sector

Average Office & Building = Average (Fall/Spring) day for the Office Building sector

Large User = Large Users for all seasons

Peak Agri. = Peak (Fall/Spring) day for the Agricultural sector

Average Agri. = Average (Summer/Winter) day for the Agricultural sector

Winter weeks = 1-8 & 44-52

Sprint / Fall weeks = 9-17 & 31-43

Summer weeks = 18-30